PATHOGENESIS OF HAEMATOGENOUS SPREAD IN *ACANTHAMOEBA CASTELLANII* INFECTIONS

JAMES EDWARDS-SMALLBONE, MA (Oxon).

Thesis submitted to the University of Nottingham for the degree of Doctor of Philosophy

December 2013

In Memoriam

Presented in memory of my mother Vanessa Edwards-Smallbone:

You are part of everything that I am and all that I have achieved. In losing you I have lost something of myself, but although we are parted I carry your love with me wherever I am. Thank you for your constant encouragement and for believing in me when I could not believe in myself; for every kindness and for all you have taught me.

This is for you, with my eternal love.

Dedication

This thesis is dedicated to my father Brian, my sister Rachel and my late grandmother Winifred with thanks for their constant love, support and understanding; and for giving me the courage to continue in the face of sorrow and adversity. I could not ask for a more wonderful family.

Abstract

Acanthamoeba castellanii is an amoeboid protozoan which causes opportunistic infections, including granulomatous encephalitis in immune-compromised patients. Haematogenous dissemination follows initial infection and the pathogen exhibits an ability to cross the blood-brain barrier (BBB).

In the bloodstream and at the site of BBB penetration in the brain microvasculature *A. castellanii* is exposed to host humoral immunity. Here, we have provided insights into *A. castellanii* pathogenesis and the identity of amoeba antigens participating in immune control. We have investigated the role circulating immunoglobulin plays in preventing penetration of the BBB, and whether trophozoites can alter the efficacy of the immune response. Furthermore we have extended previously published data, demonstrating that amoeba proteases can degrade all antibody classes including physiologically-derived antibody. Nonspecific binding of polyclonal antibody was also observed, and attributed to Fc-binding activity by trophozoites. Additionally, we have examined the binding dynamics of *A. castellanii* under physiological conditions. BBB disruption was shown to be not directly linked to binding, instead it is reliant on secreted proteases.

This study provides insights into mechanisms by which *A. castellanii* evades host immunity and crosses the BBB. This has the potential to enhance therapeutic strategies aimed at restoring essential disease prevention processes. In addition we have identified a number of amoeba antigens that are targets for the immune system and which may therefore be exploited through vaccination or immunotherapy.

Acknowledgements

This work was funded by an inter-departmental scholarship from the Schools of Biology, and Veterinary Medicine and Science, University of Nottingham; for whose support I am extremely grateful. I would also like to thank SVMS individually for additional financial and personal support during my studies.

At the risk of this resembling an Oscar speech, there are many people to whom I owe a debt of gratitude and without whom this thesis would not have been possible.

Firstly I would like to thank my supervisor Robin Flynn for excellent advice, support and encouragement. Thank you for stepping in to supervise me when I might otherwise have been left rudderless, and for every meeting, every draft comment and every pep talk since. Thanks for being a calming influence in times of stress and a motivational one when I lacked energy. Thank you also for your sympathy and understanding as well as reassurance when life got in the way of study. I always appreciated your dedication and humour and I hope I have been a good student (if an unexpected one!).

Thanks also to Naveed Khan and Richard Pleass who initiated the project and were of invaluable help in the first stages, and subsequently in preparing drafts and advising on experiments. Also for helping me to smooth out the initial wrinkles and soothe the early jitters! My thanks as well to the Pleass lab: Jaime, Dave, Dicky, JG and April who settled me in to the PhD life, and taught me the importance of regular pub trips.

To my fantastic flatmates and surrogate family: Jasmine, Narin and Rajiv. What would I have done without you? Thanks for being there for me through thick and thin, for encouragement and sympathy when things were looking bleak, and for sharing fun times and good laughs. The PhD road is a long one, and I'm privileged to have travelled it with you.

Thanks to my fellow Vet School-ers Katy, Mansi, Frank, Donna, Vydeki, Adam, Tim, Simon, and Nevi for innumerable lunches; for Friday evenings in The Anchor; and for listening to all my grumbling, my tedious facts, and my even more tedious jokes. If anything made the lab more like home than work, it was you!

A special thank-you as well to Mike, one of my oldest friends: a man who has been there, done that, got the T-shirt, and helped me on my own T-shirt quest! Thank you for reassurance, sympathy, and for telling me when I was just flat-out wrong! Our evenings in the Devon Dumpling were my refuge when it was all becoming too much.

And to my friends near and far who kept me going these past four years: the VLA crew, the Standard Seven, Chris and Rich, thank you. I am very fortunate to count you as my friends.

Finally, I would like to say a huge thank you to my family for their unending love and support. I would not have got far without you.

Table of Contents

List of Figures

List of Tables

List of Abbreviations

α	Alpha
β	Beta
γ	Gamma
Ω	Ohm
°	Degrees
aa	Amino acid
Ab	Antibody
ACM	*Acanthamoeba* conditioned medium
AGE	*Acanthamoeba* granulomatous encephalitis
AIDS	Acquired immune deficiency syndrome
AK	*Acanthamoeba* keratitis
AMP	Antimicrobial peptide
ANOVA	Analysis of variance
AP	Alkaline phosphatase
BBB	Blood-brain barrier
BLAST	Basic local alignment search tool
(H)BMEC	(Human) Brain microvascular endothelial cells

BSA	Bovine serum albumin
C	Celsius
CBF	Cerebral blood flow
CD	Cluster of differentiation
CNS	Central nervous system
cm	Centimetres
CO_2	Carbon dioxide
DAPI	4',6-diamidino-2-phenylindole
dd	Double-distilled
DMSO	Dimethyl sulfoxide
DTT	Dithiothreitol
ECM	Extracellular matrix
EF-1γ	Elongation factor 1-gamma
ELISA	Enzyme-linked immunosorbent assay
E/S	Excretory/secretory
EST	Expressed sequence tag
FACS	Fluorescence-activated cell sorting
FITC	Fluorescein isothiocyanate
FSC	Forward scatter

FcR	Fc receptor
g	gram
×g	Times gravity
ga	gauge
H_2O	Dihydrogen oxide (water)
HCl	Hydrochloric acid
HIV	Human immunodeficiency virus
HRP	Horseradish peroxidase
IL	Interleukin
ICAM	Intercellular adhesion molecule
IF	Immunofluorescence
IFN	Interferon
Ig	Immunoglobulin
(s)IgA	(secretory) Immunoglobulin alpha
IgE	Immunoglobulin epsilon
IgG	Immunoglobulin gamma
IgM	Immunoglobulin mu
kDa	Kilodalton
L	Litre

LDS	Lithium dodecyl sulphate
LDH	Lactate dehydrogenase
M	Mole
MBP	Mannose-binding protein
MHC	Major histocompatibility complex
ml	Millilitre
mM	Millimole
mm	Millimetre
ms	Millisecond
MS	Mass spectrometry
MS/MS	Tandem mass spectrometry
Mw	Molecular weight
NCBI	National Centre for Biotechnology Information
nM	Nanomole
nm	Nanometre
PAR	Protease activated receptor
PBS	Phosphate buffered saline
PBST	Phosphate buffered saline tween-20
PCR	Polymerase chain reaction

PEG	Polyethylene glycol
PfEMP1	*Plasmodium falciparum* erythrocyte membrane protein 1
PI3K	Phosphatidylinositide 3 kinase
PMSF	Phenylmethylsufonyl fluoride
PVDF	Polyvinylidine fluoride
RBC	Red blood cell
RNA	Ribonucleic acid
mRNA	Messenger ribonucleic acid
rRNA	Ribosomal ribonucleic acid
rpm	Revolutions per minute
s	Seconds
SD	Standard deviation
SDS	Sodium dodecyl sulphate
SDS-PAGE	Sodium dodecyl sulphate polyacrylamide gel electrophoresis
SEM	Standard error of the mean
SSC	Side scatter
Th	T-helper
TEER	Trans-endothelial electrical resistance
TGS	Tris glycine sodium dodecyl sulphate

TJ	Tight junction
TLR	Toll-like receptor
TNF	Tumour necrosis factor
TMB	Tetramethyl benzidine
TUNEL	Terminal deoxynucleotidyl transferase dUTP nick end labelling
U	Units
µg	Microgram
µl	Microliter
µM	Micromole
µm	Micrometre
V	Volts
w/v	Weight by volume
ZO	Zonula occludens

1. Introduction

1.1. Life Cycle

Acanthamoeba castellanii is a free-living amoeboid protozoan of soil and water environments. Isolation from a number of man-made environments including bottled water, ventilation, cooling and water systems has also been made (De Jonckheere, 1991). Trophozoites are typically 15-30µm in length and distinguishing morphological features include cytoplasm containing numerous large vacuoles and thin tapering pseudopodia termed acanthopodia (Figure 1.1). The free-living trophozoites divide by binary fission and are vegetative, predating a variety of bacterial species as well as smaller eukaryotes (Weekers et al., 1993, Gomez-Couso et al., 2007).

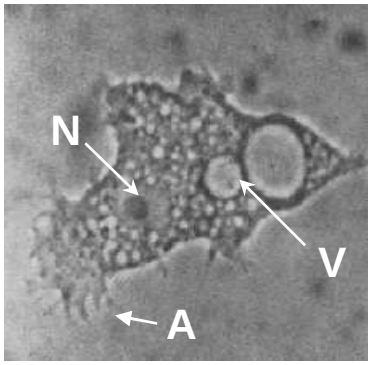

Figure 1.1 An *Acanthamoeba* trophozoite.

×4000 magnification. V = vacuole, A = acanthopodia, N = nucleus. Adapted from Culbertson *et al*., 1959.

Trophozoites can also encyst in response to hostile environmental conditions and cysts are highly resistant to lack of food, extremes in pH and temperatures, desiccation, and many available antimicrobials (Aksozek et al., 2002, Coulon et al., 2010). Morphologically the cyst is also highly

distinctive, having a double wall of which the inner part is smooth and rounded whilst the outer wall appears wrinkled (Pussard and Pons, 1977).

1.2. Classification

Acanthamoeba was first officially described by Castellani in 1930 and was subsequently placed into the genus *Hartmanella* (Culbertson et al., 1965a, Culbertson et al., 1965b). This group was revised soon afterward, and *Acanthamoeba* species were placed into their own genus. Classification thereafter followed the pattern suggested by Pussard and Pons who used cyst and other morphological characteristics to define relationships between species using a three group classification scheme (Pussard and Pons, 1977, Kong, 2009). Subsequently a robust genetic classification system, using 18S and 16S ribosomal RNA (rRNA) was developed (Daggett et al., 1985, Stothard et al., 1998, Schroeder et al., 2001, Kong, 2009). This yielded the current generally accepted scheme of fifteen genotypes (T1-T15) exhibiting at least 5% sequence divergence, with some basis for an additional genotype (T16) recently suggested (Goldschmidt et al., 2009, Corsaro and Venditti, 2010).

As well as the advantages of clarity and reliability, rRNA genotyping has illuminated genetic similarities between samples otherwise classed as separate species, particularly amongst clinical isolates. For the most part pathogenicity is confined to a small subset of genotypes, with T1 and T4 the dominant groups for both keratitis and granulomatous encephalitis (section

1.4 and 1.5) (Khan et al., 2002, Alsam et al., 2005b, Sissons et al., 2006a, Di Cave et al., 2009).

1.3. Emerging clinical importance

The first observations of *Acanthamoeba* pathogenicity were made by Culbertson, who identified the amoeba as a contaminant of mammalian tissue culture and subsequently demonstrated pathogenicity both *in vitro* and *in vivo* (Culbertson et al., 1958, Culbertson et al., 1959). Numerous case reports emerged in subsequent years (Jones et al., 1975, Martínez et al., 1977, Visvesvara et al., 1983, Blackman et al., 1984, Gardner et al., 1991) and *Acanthamoeba* species are now well-recognised to produce two distinct disease states, *Acanthamoeba* keratitis (AK) and *Acanthamoeba* granulomatous encephalitis (AGE). Whilst both diseases are rare, *Acanthamoeba* infections are being detected by clinicians with increasing frequency, especially as opportunistic infections of immunocompromised patients (Slater et al., 1994, Feingold et al., 1998, Steinberg et al., 2002, Tilak et al., 2008). This at-risk population is expanding as a result of increasing use of immune-suppressing therapies for cancer treatment and the worldwide HIV/AIDS pandemic (Friedland et al., 1992, Schwarzwald et al., 2003, Nachega et al., 2005).

1.4. *Acanthamoeba* Keratitis (AK)

AK is an infection of the cornea causing severe inflammation, intense pain and impaired vision and which is blinding if left untreated (Jones et al.,

1975, Awwad et al., 2007). Infection is initiated by trophozoite adhesion to corneal epithelium following which the infection develops as a ring infiltrate. In the latter stages of the disease amoebae invade the stromal layer, with the resulting opacity leading to loss of visual acuity and eventually blindness. Existing corneal damage is known to predispose to the condition and in addition more than 80% of AK infections are correlated with the use of contact lenses (Moore et al., 1985, Alizadeh et al., 2005, Gagnon and Walter, 2006). These risk factors are incorporated into experimental models of the disease, for example in work by van Klink *et al.* who used corneal abrasion and parasite-laden lenses to investigate AK in Chinese hamsters (van Klink et al., 1993). Nevertheless, a small subset of infections does not correlate with either risk factor (Barbeau, 2007, Ertabaklar et al., 2007).

Poor lens hygiene and inappropriate disinfection regimes are thought to contribute to infection risk by promoting the growth of bacteria on lenses onto which amoebae in turn adhere and proliferate. Trophozoites may also be accidentally inoculated directly onto lenses by exposure to contaminated water during swimming, washing with tap water or as a result of poor personal hygiene (Kaji et al., 2005, Bower et al., 2006, Niyadurupola and Illingworth, 2006). In epidemiological terms the infection is comparatively rare (Table 1.1), however the proportion of the population at increased risk of developing AK may rise as contact lenses continue to gain popularity for ophthalmic and recreational purposes (Moore et al., 1987, Lee et al., 2007).

Incidence rate (per 10,000 population)	Study Area	Reference
0.33	Hong Kong	(Stehr-Green et al., 1989)
0.05	Holland	(Stehr-Green et al., 1989)
0.01	USA	(Stehr-Green et al., 1989)
0.19	England	(Radford et al., 2002)
1.49	Scotland	(Lam et al., 2002)

Table 1.1 Incidence rates for *Acanthamoeba* keratitis

Per 10,000 head of population, various sources.

Diagnosis is typically reached by isolating amoebae from corneal biopsies and/or contact lens cases. PCR-based assays have been developed for rapid diagnosis however their use in clinical settings is limited by logistical and economic considerations. The high sensitivity and specificity of these assays however means that they are likely to see greater use in the future (Mathers et al., 2000, Yera et al., 2007). *In vivo* confocal microscopy may also be used but requires specialised equipment and appropriately trained staff and so is unlikely to enter routine use (Winchester et al., 1995). Standard treatment regimens are complex and prolonged, with a high intensity polyhexamethylene biguanide and propamidine isethionate therapy producing the most favourable outcomes without resorting to corneal transplant (Tien and Sheu, 1999, Gooi et al., 2008). Nevertheless complications such as bacterial and fungal co-infections and increased amoeba proliferation due to steroid anti-inflammatory treatments frequently prove detrimental to successful treatment (Rumelt et al., 2001, Rama et al.,

2003, Lorenzo-Morales et al., 2007). An additional difficulty is the parasite's ability to encyst, often prompted by initiation of treatment. This can cause an easing of symptoms only for the infection to re-emerge at a later date (Peterson et al., 1990). This is particularly apparent where keratoplasty has been attempted as the donor cornea may be re-infected by excysting amoebae. It is often the case that several transplants are necessary before the infection is finally eliminated (Peterson et al., 1990, Camposampiero et al., 2009).

1.5. Amoebic Granulomatous Encephalitis (AGE)

Whilst AK is a debilitating disease it is not the most severe manifestation of an *Acanthamoeba* infection. Amoebic granulomatous encephalitis (AGE) is an opportunistic infection mostly of immunocompromised patients, wherein amoebae enter neural tissue causing necrosis and severe encephalitis (Martínez et al., 1977, Di Gregorio et al., 1992). Evidence suggests that invasion occurs by one of two routes: either *Acanthamoeba* enter directly via the olfactory bulb and neuroepithelium, or the amoeba spreads haematogenously to brain microcapillaries (Martinez et al., 1975, Martínez et al., 1977). The initial route of entry for the latter has been suggested to be via cutaneous or pulmonary lesions with the latter probably resulting from the germination of inhaled cysts (May et al., 1992, Helton et al., 1993, Duarte et al., 2006, Walia et al., 2007). Trophozoites then disrupt the blood-brain barrier and enter the CNS (Culbertson et al., 1959, Kidney and Kim, 1998, Khan and Siddiqui, 2009)

Once amoebae reach the brain tissue the disease has a slow progression with neuronal damage inducing pro-inflammatory immune responses that lead to the formation of granulomas and haemorrhagic necrotic lesions (Martínez et al., 1977, Martínez et al., 1980). Symptoms include headache, fever, behavioural changes, aphasia, ataxia, vomiting, and seizures. These are common to a wide variety of unrelated neurological conditions however, frequently leading to slow or mis-diagnosis (Khan, 2007, Pemán et al., 2008, Bloch and Schuster, 2005).

Confirmation of AGE is achieved by isolation and *in vitro* culture of the parasite from cerebrospinal fluid (CSF), a method which may prove time consuming or inconclusive (Petry et al., 2006, Abd et al., 2009, da Rocha-Azevedo et al., 2009). There is evidence from AK infections that detection by PCR may improve diagnostic outcomes, however this method has yet to enter routine use for AGE (Yera et al., 2007, Thompson et al., 2008, Reddy et al., 2009). There is no recommended treatment, although early application of one or a combination of multiple drugs may improve prognosis e.g. ketoconazole, fluconazole, voriconazole, sulfadiazine, miltelfosine, amphotericin B, maxifloxacin, linezolid, meropenem azithromycin, or rifampin (Ofori-Kwakye et al., 1986, Seijo Martinez et al., 2000, Aichelburg et al., 2008, Sheng et al., 2009, Lackner et al., 2010) .

AGE is largely confined to patients with underlying immune suppression, due to co-infection (particularly HIV), chemotherapy treatment, primary immune deficiency or other underlying conditions which compromise immunity (Gardner et al., 1991, Uschuplich et al., 2004, MacLean et al., 2007). The immune-compromised condition of the patient, combined with

difficulties in diagnosis and therapy results in an alarmingly high mortality rate of around 90% (Bloch and Schuster, 2005, Khan, 2005). Fortunately the infection is very rare with case numbers in the low hundreds – in their 1997 review Martinez and Visvesvara give a figure of approximately 150 reported cases (Martinez and Visvesvara, 1997).

The scale of the problem may be underestimated by current measures however as a result of the aforementioned difficulties with diagnostics. This is especially the case in countries with poor access to primary healthcare and without thorough post-mortem procedures. Such countries often have large populations of HIV^+ individuals and this increases the likelihood of AGE cases remaining undiagnosed and untreated. The global at-risk population is also expanding due to the HIV/AIDS pandemic. In their 2011 global AIDS summary the World Health Organisation reported a population of 34 million people infected with HIV, increasing from 29.5 million in 2002 (WHO, 2011). Infection rates for AGE in areas with highest HIV incidence are unknown; however it seems likely that of the 1.7 million AIDS-associated deaths which occurred in 2011 a proportion are attributable to *Acanthamoeba* species

1.6. Immunity

The role played by the immune system in controlling *A. castellanii* infections is yet to be fully explored and is complicated by the existence of two distinct clinical syndromes occurring in settings of different immune competency. AGE is primarily a disease of immunocompromised patients

and disseminates haematogenously from an initial cutaneous, pulmonary or intranasal infection to primarily affect the brain. AK is confined solely to the eye, but does not require impaired immunity in order to initiate an infection. The immune environments that *A. castellanii* encounters in each disease therefore exhibit substantial differences; however it is worthwhile to explore the two diseases in parallel in order to gain an insight into potential protective immune mechanisms.

1.7. Innate immunity

1.7.1. Barriers to infection

Upon initial inoculation a combination of antimicrobial and physical defences prevent trophozoites from adhering to host cells. In the eye the greater proportion of corneal immunity is mediated by secretions from the tear glands and eyelids, distributed across the eye's surface by a pumping action created by the blink reflex (Niederkorn, 2002, Sack et al., 2001). Tear secretions are a complex mixture of peptides both nonspecific (lysozyme, lactoferrin, prostaglandins) and specific (secretory IgA) which combine with physical sweeping by the eyelids to form a strong barrier to infection (Alsam et al., 2008). In AK the use of contact lenses adds to infection risk as extended use induces hypoxia and a stress-related impairment of ocular immunity (Alizadeh et al., 2005, He et al., 1992). Additionally, infected contact lenses permit close contact to be maintained between trophozoites and corneal epithelial cells. This thins the tear film and protects amoebae from physical removal by eyelid sweeps.

The role played by antimicrobial peptides (AMP) in AGE is less clear due to the fact that both cutaneous and pulmonary infection routes have been reported in the literature (Steinberg et al., 2002, Duarte et al., 2006). Supporting evidence for the importance of AMP in mucosal defence against amoeba is also seen in a recent study which demonstrated that β-defensin-2 is produced by colonic epithelial cells in response to *Entamoeba histolytica* infection (Ayala-Sumuano et al., 2013). Specifically in *A. castellanii*, a study by Otri *et al.* using immortalised corneal epithelial cells showed upregulated expression of several genes involved in production of AMP upon infection. Elevated levels of mRNA coding for β-defensin-2, hepcidin, and RNase-7 were all seen (Otri et al., 2010). It is likely that similar AMP expression profiles are seen at all mucosal surfaces including the nasal, cutaneous and pulmonary epithelium. However this has yet to be empirically shown and the interaction between AMP and *A. castellanii* remains to be determined.

1.7.2. Complement

The complement cascade is one of the most important pathogen recognition and effector mechanisms of the innate immune system. Complement subunits present in the tear film and blood self-assemble on pathogen surfaces into complexes that prompt recognition and phagocytosis by phagocytes or else lyse pathogens directly by permeabilising the plasma membrane. Activation follows one of three pathways: the classical pathway, where complement is fixed in the presence of pathogen-specific antibody;

the alternative pathway, where complement subunits bind to pathogen surfaces directly; and the lectin pathway where pathogen surface glycoproteins activate the cascade.

A. culbertsoni, unspeciated T4 genotype, and unspeciated T6 genotype strains have been shown to activate serum complement via the alternative pathway (Ferrante and Rowan-Kelly, 1983, Pumidonming et al., 2011). Pumidonming *et al.* (2011) showed that binding of the C3 subunit which initiates the alternative pathway and C9 which is the final subunit to bind prior to formation of the membrane attack complex occurs when trophozoites were incubated with human serum. However there is conflicting evidence as to whether complement fixation leads to lysis of trophozoites in all cases. Some studies show that several strains are all lysed by human complement (Ferrante and Rowan-Kelly, 1983, Pumidonming et al., 2011) but differential susceptibility to complement lysis has been demonstrated by others (Toney and Marciano-Cabral, 1998). Complement resistance in this latter case correlated with strain virulence and is supported by evidence from the pathogenic amoebae *Naegleria fowleri* that virulent strains have greater resistance to lysis (Whiteman and Marciano-Cabral, 1987, Whiteman and Marciano-Cabral, 1989).

1.7.3. Pro-inflammatory cytokines

Pro-inflammatory cytokines govern and regulate many aspects of the immune response including proliferation and recruitment of lymphocytes and macrophage/neutrophil activation and trafficking. Both AK and AGE

are characterised by a vigorous inflammatory reaction, which is thought to be partly responsible for the observed pathology i.e. the characteristic eye reddening in AK and tissue oedema and encephalitis in AGE. Whilst this process is essential to clearing an infection, where inflammation is not resolved or correctly regulated the resulting tissue damage can make a major contribution to disease pathology (Mattana et al., 2002, Shin et al., 2001).

Studies characterising cytokine signalling in response to *A. castellanii* are sparse however data from corneal epithelial cells and stromal fibroblasts suggests TLR4 may play a role in pathogen detection leading to an increase in levels of IL-8, TNFα, and IFNβ (Ren et al., 2010, Ren and Wu, 2011). Additionally TNFα, IL-1α and IL-1β, whilst having no direct anti-amoebic activity in isolation are capable of enhancing killing of amoeba by brain-resident macrophages (microglia), and promoting further pro-inflammatory cytokine release (Benedetto et al., 2003, Benedetto and Auriault, 2002).

This process is likely to be phagocytosis-dependent as comparable anti-*A. castellanii* effects are not seen from macrophage-conditioned media (Hurt et al., 2003c). In addition, secretion of TNFα, IL-1α and IL-1β as well as IL-6 by macrophages increases when they are presented with trophozoites (Benedetto et al., 2003). This inflammatory mechanism is therefore self-reinforcing, and probably at least partially responsible for the excessive inflammation seen in disease.

1.7.4. Macrophages and Neutrophils

Macrophages and neutrophils are important effector arms of the innate immune system, and respond rapidly during *A. polyphaga* infections (Larkin and Easty, 1991). The most potent effects of these cells are seen when they have been primed with pro-inflammatory cytokines or ligands such as LPS (Benedetto et al., 2003). Naïve macrophages and especially neutrophils exhibit only low lytic activity. However, this effect is greatly enhanced by prior inoculation of experimental animals with amoeba antigens and greatest in the presence of active serum. This suggests that plasma components such as complement, cytokines and antibody interact with leukocytes to promote killing (Stewart et al., 1992, Marciano-Cabral and Toney, 1998).

This effect can also been seen in other free-living amoeba infections and there is a particular similarity to the macrophage and neutrophil response to *Naegleria fowleri*. In both cases neutrophils play a major role as demonstrated by studies in which specific neutrophil and macrophage depletion exacerbates infections (van Klink et al., 1996, Hurt et al., 2001, Hurt et al., 2003c). Activation of endogenous macrophages (specifically by IFNγ) results in significant lowering of AK incidence, and even nonspecific boosting of macrophage infiltration by latex beads has a protective effect (Clarke et al., 2006). Interestingly *Acanthamoeba* species demonstrate an ability to kill *in vitro* macrophage and microglia cultures (Marciano-Cabral and Toney, 1998, Harrison et al., 2010) and this suggests that amoeba/macrophage interactions are not unidirectional.

1.8. Acquired immunity

Acquired immunity is a crucial property of the mammalian immune system which combats pathogens and preserves immunological memory of past infections, so that a response can be initiated more rapidly and with greater magnitude during a subsequent infection by the same organism. It consists of two distinct but complementary mechanisms: cell-mediated responses governed and co-ordinated by T-lymphocytes; and humoral responses governed by antibody produced by B-lymphocytes and their specialised secretory derivatives plasma cells.

1.8.1. B cells and antibody

B-cells are one of two classes of lymphocytes which permit acquired immunity to infection. B-cells express a highly variable receptor which is structurally similar to antibody, and which is highly antigen-specific as a result of variable regions generated by somatic recombination. If a circulating B-cell encounters an antigen for which its receptor is specific it will proliferate in a process known as clonal expansion. This also requires a signal from $CD4^+$ T-helper (Th) cells specific to the same antigen and results in eventual differentiation into specialised antibody-secreting plasma cells. Antibody production dynamics are then modified in lymph structures called germinal centres to generate higher affinity molecules (affinity maturation) or to alter antibody class for specialised functions (class

switching). Differentiation into memory B-cells also occurs at this stage, permitting a more rapid and specific response to be raised in any future infection. Other than these general processes however, relatively little is known about the specifics of the B-cell response for either AK or AGE. The majority of previous studies have focused instead on the protective effect of antibody itself, or else used it as a marker of infection and the immune response.

A high proportion of healthy subjects have been shown to test positive for serum antibodies against *Acanthamoeba* species (Chappell et al., 2001, Brindley et al., 2009, Kiderlen et al., 2009). This is consistent with common exposure resulting from the organism's wide environmental distribution and also reflects the importance of antibody function in disease control, as patients from these studies were free from clinical disease.

Serum IgG levels are elevated in AK with no apparent effect on the outcome of infection and there appears to be limited translation of immunity between the systemic and mucosal response. This is shown by studies where corneal infection fails to stimulate humoral or cell-mediated immunity (Van Klink et al., 1997) and where systemic immunisation fails to protect against subsequent ocular challenge (Alizadeh et al., 1995). Mucosal immunisation produces better outcomes however; monoclonal IgA is shown to protect hamsters by passive transfer (Leher et al., 1999) and oral immunisation also demonstrates an IgA-mediated protective effect in pigs (Leher et al., 1998b). Interestingly, secretory (sIgA) levels in the cornea are lower in patients with keratitis (Alizadeh et al., 2001). However it is not clear at this stage whether lower sIgA levels occur as a result of parasite activity or whether an

underlying sIgA deficiency permits infections to establish. SIgA has been shown to prevent trophozoites from adhering to corneal epithelial cells, leading to immobilisation and destruction by leukocytes resident in the conjunctiva (Leher et al., 1998a, Campos-Rodríguez et al., 2004). However antibody cleavage has been demonstrated by *A. castellanii* isolates and so the efficacy of sIgA may not entirely depend on host factors (Na et al., 2002b).

The role of systemic antibody circulating in the blood is less well established. Anti-*Acanthamoeba* IgG and IgM antibody is found in surveys of healthy populations (Chappell et al., 2001, Kiderlen et al., 2009). However, anti-*Acanthamoeba* antibody has also been detected in serum from infected patients (Schuster et al., 2006), although in this particular study no isotype was given for the detected antibody. It is therefore unlikely that the presence of antibody alone is sufficient to grant total protection and this is supported by the inability of elevated serum IgG to affect the outcome of AK, as noted above (Alizadeh et al., 2001).

Where detected, serum antibody is of either the IgG or IgM class (Cursons et al., 1980, Alizadeh et al., 2001, Schuster et al., 2006). The IgG response has the greatest specificity and longest duration of all antibody responses and so its presence in serum of patients is further indication that antibody plays an important role in on-going control of the parasite. Since epitopes associated with previous infections are preserved in the bone marrow via long-lived memory B-cells this may also be an indication of repeated exposure to *Acanthamoeba* species generating a vigorous humoral response in response to subsequent pathogen challenge. The presence of IgM in

serum surveys supports this view (Cursons et al., 1980). This class is relatively less specific but is produced rapidly in response to an infection. Levels of serum IgM wane rapidly post-infection however and so the presence of IgM in serum generally represents a recent or on-going exposure. This reinforces the conception that individuals either undergo frequent short-lived *A. castellanii* infections or are constantly exposed to *A. castellanii* antigens, perhaps as a result of colonisation by cysts.

Previous investigators have attempted to take advantage of the antibody response to generate specific monoclonal antibody for therapeutic and diagnostic purposes. However many of the antibodies raised in these studies reacted mainly with the cyst stage, which is only weakly immunogenic (Turner et al., 2005). This reinforces the view that the on-going IgG responses detected in serum surveys may represent an immune response against cysts, and that the lower levels of antigen expression permit cysts to persist in host tissues. In support of this view the presence of cysts in the cornea is frequently asymptomatic (Camposampiero et al., 2009).

Where reactivity to trophozoites was shown, the precise role and targets of specific antibody and therefore relevance to known methods of pathogenesis was not consistently demonstrated (Fiori et al., 2006, Turner et al., 2005, Kennett et al., 1999). The presence of IgM in serum from both healthy and diseased patients indicates frequent infection and so this class is likely to have a major role to play in the response to trophozoites.

1.8.2. T-cells

T-lymphocytes are another important participant in the acquired immune response, and can be classified by expression of one of two cell surface molecules. $CD8^+$ T-cells are cytotoxic effector cells which target mostly intracellular pathogens by inducing apoptosis of infected cells. $CD4^+$ T-cells are described as 'helper' cells and perform two major functions: secretion of cytokines which influence inflammation and activate other immune cells; and aiding B-cell recognition of target antigens. T-cell antigen recognition is mediated by the T-cell receptor, which like B-cell receptors contains both conserved and variable regions. T-cells will not recognise free antigen however but instead respond only to antigen presented in consort with major histocompatibility complex (MHC) molecules of antigen-presenting cells. This ensures T-cell responses are sufficiently regulated and appropriate to the nature of the microbial threat. T-cell responses to infection by *Acanthamoeba* species have not been elucidated in great detail. Nevertheless because of the extracellular infection route it is likely that the T-cell response involves primarily $CD4^+$ cells. Understanding of T-cell responses to *A. castellanii* is still at an early stage however, and so the relative contributions of Th1, Th2 or Th17 pathways are yet to be definitively deduced. Evidence from a study by Tanaka *et al.* (1995) points towards Th1, as T-cells responsive to clinical *Acanthamoeba* isolates were of a $CD4^+/CD8^-$ phenotype with elevated IFNγ levels but low IL-4 production. This promotes a potent macrophage-activating phenotype, and macrophages have been shown to be important effector cells for destruction of trophozoites (see section 1.7.4).

Of significance to AGE, T-cells are amongst the cell types most depleted by artificial immune suppression and HIV infection. AIDS patients are at particular risk of acquiring AGE, so it is likely that T-cells have a critical role to play in preventing the disease. As $CD4^+$ T-cells have little antimicrobial activity of their own however, their significance lies in activation of effector mechanisms such as macrophages, neutrophils, and B-cell differentiation into plasma cells.

T-cells proliferate in response to amoebic antigens (Tanaka et al., 1994), and interestingly this response was greater to antigens derived from cysts rather than trophozoites (McClellan et al., 2002). This may indicate that cell-mediated immunity is preferentially activated in order to mount a response against cysts, however McClellan *et al.* also report that immunisation with trophozoites impairs subsequent cell-mediated responses to cysts. An additional layer of complexity is added by reports from Massilamany *et al.* which describe expression of mimicry epitopes in *A. castellanii* that generate cross-reactive T-cell responses (Massilamany et al., 2010, Massilamany et al., 2011). These responses were shown to generate autoimmunity in the CNS. It is not clear whether this mechanism contributes to the inflammation seen in AGE however these results demonstrate that there are likely to be underlying complexities to T-cell responses which are not yet appreciated.

1.9. Pathogenesis

1.9.1. Non-secreted factors

The importance of binding in the initiation of *Acanthamoeba* infections has been demonstrated in a variety of model systems, showing that when adhesion is blocked (primarily by exogenous mannose) the parasite's ability to kill corneal or endothelial host cells is reduced (Hurt et al., 2003b, Garate et al., 2006a, Morton et al., 1991). The involvement of mannose residues in binding was first tangentially demonstrated by Brown and colleagues who showed that carbohydrates were involved in phagocytosis by amoeba, a process in which binding is crucial (Brown et al., 1975). The specific involvement of the carbohydrates mannose and methyl-α-D-mannopyranoside was demonstrated by Morton *et al.* (1991) who showed that addition of these to culture media reduced trophozoite binding to corneal epithelial cells. Further investigation identified a specific mannose-binding protein (MBP) expressed on the cell surface which has subsequently been well characterised in several studies (Yang et al., 1997, Cao et al., 1998, Garate et al., 2004).

Addition of mannose or its derivatives prevents the occurrence of disease in several models, and taken with the widespread presence of mannose residues on a variety of cell types including corneal epithelium and brain endothelium this protein evidently has a major role to play in pathogenesis (Alsam et al., 2003, Hurt et al., 2003b, Garate et al., 2006a, Garate et al., 2006b). Some findings however suggest that adhesion to non-cellular structures such as extracellular matrix and inert surfaces is also MBP-

mediated and that this binding mechanism may therefore be non-specific (Gordon et al., 1993, Imbert-Bouyer et al., 2004). Nevertheless, some functional roles for MBP in pathogenesis have been partially elucidated and point to a direct role in cytotoxicity.

It is known that *A. castellanii* is capable of inducing apoptosis in a variety of cell types (Alizadeh et al., 1994, Shin et al., 2000, Zheng et al., 2004), a property it shares with major protozoan pathogens such as *T. brucei* and *P. falciparum* (Stiles et al., 2001, Stiles et al., 2004, Pino et al., 2005, Wilson et al., 2008). Hurt and colleagues observed secretion of a 133kDa protein (MIP-133) by trophozoites in response to addition of mannose or its derivatives (Hurt et al., 2003a, Hurt et al., 2003b). MIP-133 induced caspase-3 mediated apoptosis in both human and hamster corneal epithelium and also showed collagenase activity. Other apoptotic responses are also seen in response to *A. castellanii*; including alterations in cytosolic calcium, upregulation of genes involved in cell cycle arrest, and activation of phosphatidylinositol-3-kinase (Sissons et al., 2005, Taylor et al., 1995, Alizadeh et al., 1994, Mattana et al., 2001). However the relative contribution of each to cell death remains uncertain. The precise role of MBP in initiating these cellular events also remains undefined although the fact that addition of exogenous mannose can mitigate disease shows that some form of direct induction by MBP binding is likely.

Nevertheless MBP alone may not be sufficient to explain the entirety of contact-dependent interactions between host and pathogen, as low levels of binding are maintained even where amoebae have been treated with exogenous sugars (Imbert-Bouyer et al., 2004, Rocha-Azevedo et al.,

2009a). Supporting evidence for the involvement of additional binding factors in pathogenesis has been shown in work by Kennett *et al.* (1999). They describe a membrane-bound glycoprotein which when inhibited by binding of specific antibody caused reductions in the ability of amoebae to adhere to corneal epithelial cells. No competitive binding was observed between this antibody and mannan and so the authors concluded that this represents a protein distinct from MBP (Kennett et al., 1999). Any direct role for this molecule in pathogenesis was not characterised however and so it is possible that this represents a non-pathogenic adhesion mechanism. Alternatively host cell attachment may be mediated by more than one surface protein, and the fact that the adhesin described by Kennett *et al.* is a glycoprotein suggests that host carbohydrate-binding proteins could contribute to trophozoite adherence. There may also be many other molecules and molecular mechanisms involved in *A. castellanii* cytotoxicity which are yet to be described.

1.9.2. Secreted factors

Binding is evidently an important and possibly the limiting step in *A. castellanii* infections however taken alone it does not fully explain disease pathogenesis. Protease activity makes important contributions to pathogenesis in other protozoan pathogens such as *Entamoeba histolytica, Leishmania major, Trichomonas vaginalis* and *Trypanosoma cruzi* (Doyle et al., 2007, Kumar et al., 2012, Mahmoudzadeh-Niknam and McKerrow, 2004, Sommer et al., 2005) . Secreted proteases of *E. histolytica* in

particular make significant pathogenic contributions, having been shown to promote invasion by mucin cleavage (Moncada et al., 2003); and pathology by direct cellular damage (Lourenssen et al., 2010, Kumar et al., 2012). *Acanthamoeba* species secrete proteolytic enzymes both *in vitro* and *in vivo* (Serrano-Luna et al., 2006, Sissons et al., 2006a). Interestingly this trait is not restricted to pathogenic isolates but is common to many *Acanthamoeba* species. Levels of expression vary across species/genotypes however with the highest levels observed in pathogenic isolates (Hadas and Mazur, 1993, Khan et al., 2000b). *Acanthamoeba* secreted proteases are of several classes including serine, cysteine and metalloproteases (Alfieri et al., 2000, Alsam et al., 2005b). Of these, serine proteases appear to be the most intimately associated with disease as use of PMSF (a serine protease inhibitor) reduces pathogenicity *in vitro* (Alizadeh et al., 2008, Kim et al., 2006, Sissons et al., 2006a).

Broadly speaking, categories of activity demonstrated by *Acanthamoeba* secreted proteases include degradation of extracellular matrix (ECM), tight junctions, and immune system components (Na et al., 2002a). Serine and metalloproteases have been shown to break down components of the ECM, particularly collagen type I, type IV and fibronectin; and elastase activity has been similarly demonstrated (Ferrante and Bates, 1988, He et al., 1990, Mitro et al., 1994, Kong et al., 2000, Sissons et al., 2006a, Ferreira et al., 2009). It is likely that this enhances infectivity by facilitating invasion, both in the cornea and brain microvasculature, with a causal link between proteases in cell-free conditioned medium and concordant tissue damage having been established (He et al., 1990, Na et al., 2001). With particular

reference to AGE, serine proteases have been shown to target tight junctions leading to increased permeability of the blood-brain barrier and cell monolayer disruption (Sissons et al., 2006a, Alsam et al., 2003, Cho et al., 2000). Again there is a potential link with infectivity since, as previously discussed, crossing of the BBB is a prerequisite in establishment of AGE (Alsam et al., 2005b, Sissons et al., 2006a, Khan and Siddiqui, 2009).

1.10. The blood-brain barrier

Any discussion of pathogenesis during AGE is fundamentally incomplete without an appreciation of the structure and composition of the blood-brain barrier (BBB). In mammals the barrier is composed of three cell types: pericytes, astrocytes and endothelial cells, supported on a laminin basement membrane. Its primary purpose is to control the interaction between the brain and vasculature, restricting entry into the delicate neural tissues and preserving a dedicated neural microenvironment. Brain microvascular endothelial cells (BMEC) have historically received most research attention however astrocytes and pericytes are increasingly being recognised as having vital roles to play in the maintenance of barrier function. Many researchers are seeking to incorporate important contributions from these cell types into the working understanding of BBB function, and *in vitro* modelling.

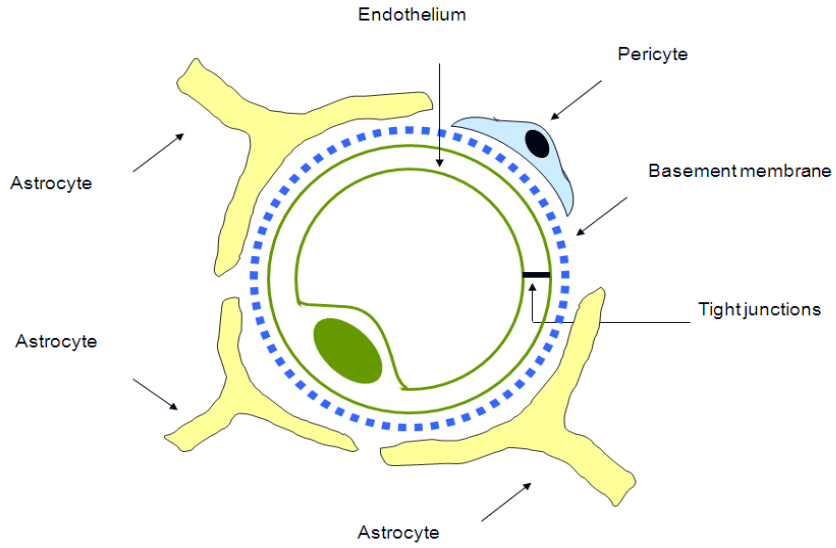

Figure 1.2 Cross-sectional diagram of the BBB

Reproduced from Khan (2007).

1.10.1. Cells of the BBB

BMECs may be considered to be the primary component of the BBB, forming the structure and lining of the blood vessels themselves and as such they are the main obstacle that any microorganism attempting to enter the CNS from the blood must first traverse. BMECs are highly specialised endothelial cells, expressing high levels of tight junction proteins such as occludin, claudin, and accessory proteins such as zonula occludens (ZO) (Watson et al., 1991, Hirase et al., 1997, Tsukita, 1998, Morita et al., 1999). As a result a highly impermeable barrier is formed and even small molecules are unable to diffuse across the BBB without active uptake or transport. This enables regulation of which cells and molecules move from the blood into the CNS and *vice versa*. BMEC monolayers in particular are impermeable even in comparison with other cell types which express tight junctions, such as epithelial cells (Milton and Knutson, 1990). BMECs have

also been shown to exhibit particularly high Trans-Endothelial Electrical Resistance (TEER), a common measure for the efficacy of barrier function. Typical TEER values *in vitro* vary according to culture technique. Static mono- and co-culture models fall in the range of 20-200Ω/cm^2 (Booth and Kim, 2012, Griep et al., 2012) however introduction of other parameters such as fluid flow can produce TEER in excess of 600Ω/cm^2 (Santaguida et al., 2006).

The barrier function of endothelial cells is further enhanced by the presence of other cell types which ensheath BMECs on the basal CNS surface, namely astrocytes and pericytes. Either the end-feet (astrocytes) or whole cell surface (pericytes) are in close proximity with the basement membrane on which BMECs sit, and there is a solid body of evidence suggesting that they are responsible for further regulating and enhancing barrier function (Hayashi et al., 1997, Armulik et al., 2010, Cantrill et al., 2012). Astrocytes in particular may have a dual effect in this regard, as both direct cellular contact and conditioned media from *in vitro* astrocyte cultures enhance BMEC TEER (Janzer and Raff, 1987, Siddharthan et al., 2007).

1.10.2. BBB *in vitro* models

BMECs, being the primary BBB component and site of the tight junctions which grant enhanced barrier function have been the main candidate for construction of *in vitro* models of the BBB. Primary human BMECs grow well in standard tissue culture environments, and to facilitate measurement of TEER or barrier-crossing assays transwell inserts are often used (Stins et

al., 1997, Alsam et al., 2005a, Grab et al., 2004). As the components of the BBB have become increasingly well understood so the models available to researchers have become more sophisticated. Co-culture models of astrocytes and BMECs have risen to prominence particularly in neurological research. These may be either simple mixed models or more elaborate methodologies which attempt to mimic structural aspects of astrocyte/BMEC interactions (Cucullo et al., 2002). It has been shown by Santaguida *et al.* and Siddarthan *et al.* for instance that the action of shear stress and blood flow rate has an impact on the integrity of the BBB (Santaguida et al., 2006, Siddharthan et al., 2007). In light of this the latest generation of BBB models now incorporate co-cultures under dynamic fluid flow (Booth and Kim, 2012, Griep et al., 2012, Prabhakarpandian et al., 2013). This is likely to lead researchers to the closest *in vitro* representation yet of BBB function.

1.10.3. The BBB in parasitic disease

The close binding of endothelial cells to one another is a highly effective physical barrier precluding access to the CNS, however a number of parasites are able to circumvent this barrier and produce neural infections. This may occur either by a transcellular pathway, where pathogens infect BMECs and emerge at the basal surface without disrupting cell-cell interaction; or a paracellular pathway, where disruption of cellular junctions permit parasites to traverse spaces between cells. Paracellular traversal is obligatory for large extracellular parasites due to physical size constraints.

A. castellanii for example is 15-30μm in size, not much smaller than a typical endothelial cell. As a result of this BBB traversal in these organisms is mediated by degradation of tight junction proteins by secreted proteases and direct cytotoxicity (Alsam et al., 2003, Kiderlen et al., 2006, Siddiqui et al., 2007, Khan and Siddiqui, 2009). Smaller pathogens such as *T. brucei* and *T. gondii* are not so restricted by size however and can exploit alternative mechanisms.

For example *T. gondii* disseminates through the host organism primarily by infection of phagocytes. This includes trafficking into the brain which has been demonstrated to depend on motility of infected leukocytes, namely monocytes and dendritic cells. These cells, infected with *T. gondii* are able to cross the blood-brain barrier and allow tachyzoites to infect neural cells (Courret et al., 2006). However the molecular mechanisms which underpin this process and any resemblance they bear to beneficial BBB traversal by uninfected phagocytes have not been fully elucidated. Conversely however, *T. gondii* is not intracellular at all stages of its lifecycle and this links with data which shows that free tachyzoites cluster around cellular borders and display tropism for tight junctions (Barragan and Sibley, 2002, Barragan et al., 2005). Transmigration assays performed in these studies demonstrated that traversal of epithelial monolayers occurred without disruption of barrier integrity or host cell lysis and this may imply that *T. gondii* can also cross the BBB by a paracellular route; however this process has yet to be observed in endothelial cell cultures. Transcellular crossing of the BBB is another possibility as tachyzoites are also capable of infecting endothelial

cells themselves, a process in which cell adhesion molecules such as ICAM1 may play a part (Lachenmaier et al., 2011).

T. brucei BBB traversal is a similarly complex process. Unlike *T. gondii, T. brucei* is extracellular at all stages of its lifecycle and thus the paracellular route is the most likely means of BBB traversal. This process has been shown to occur early in infection, prior to the mounting of an extensive inflammatory response and with little impairment of BBB function (Nikolskaia et al., 2006b, Frevert et al., 2012). Mulenga *et al.* (2001) showed that in a rat model of disease tight junctions were preserved during trypanosome crossing, with no reduction in immunostaining for occludin or ZO-1 (Mulenga et al., 2001). Grab *et al.* (2004) additionally showed that overall barrier function of BMEC was maintained as procyclic trypanosomes (non-infectious in mammals) were unable to traverse BMEC monolayers even in the presence of infectious trypomastigotes. The authors suggest that this indicates large-scale perturbations of the BBB do not occur. Nevertheless they also reported a reduction in TEER, indicating that BBB integrity was somewhat reduced. As with *T. gondii*, trypanosomes could also be visualised at cell junctions, further suggesting the importance of paracellular migration (Grab et al., 2004). Paracellular traversal is also enhanced by the ability of the parasite to induce apoptosis in BMEC, mediated through intracellular calcium alterations and Protease Activated Receptor (PAR) signalling (Nikolskaia et al., 2006a, Grab et al., 2009). Interestingly, exploiting paracellular traversal may not entirely explain BBB crossing as results from other experiments conducted by the same group show evidence for trypanosome entry into BMEC (Nikolskaia et al., 2006b).

Whether this represents transcellular crossing of the BBB however, or merely a dead-end entry event such as endocytosis to a lysosome has yet to be determined.

Perhaps the best studied interaction between a parasite and the BBB is in cerebral malaria. In contrast to *T. gondii* and *T. brucei*, breach of the BBB by *P. falciparum* is highly destructive, involving host cell death, tight junction loss and host inflammatory processes. Sequestration of parasitized erythrocytes in the brain microvasculature leads to occlusion of blood vessels and BBB dysfunction due to a combination of altered blood flow, tissue hypoxia, and cellular signalling responses. This latter process is mediated by host cellular adhesion molecules such as ICAM (also an important mediator of *T. gondii* and *T. brucei* BBB traversal) (Barragan et al., 2005, Girard et al., 2005). ICAM1 interacts with parasite proteins expressed by infected erythrocytes, for example PfEMP1 (Adams et al., 2000, Claessens et al., 2012). The result of this interaction is to activate the endothelium, leading to increased expression of adhesion molecules which in turn exacerbates further sequestration of infected RBC (Gray et al., 2003, Tripathi et al., 2006) .

The effects that this has on the BBB itself have been the subject of several independent studies, and are contributed to at least in part by the host immune response. For example increased pro-inflammatory cytokine expression, specifically TNFα and IL-1β, has been seen in tissue from cerebral malaria patients and was especially high in samples from the cerebellum (Brown et al., 1999b). Additionally, binding of infected erythrocytes has been shown to result in upregulation of apoptosis-related

genes including Bad and Bax, and activation of caspases (Pino et al., 2003). Loss or redistribution of tight junction markers occludin and ZO-1 have also been observed in brain sections from cerebral malaria patients (Brown et al., 1999a), alongside decreases in TEER induced by parasitized RBC (Tripathi et al., 2007).

1.11. Project Rationale and Aims

Pathophysiology of *Acanthamoeba* disease is mediated by multiple immune and pathogenic factors. However as a result of their low prevalence diseases caused by *A. castellanii* are not well understood despite their debilitating and life threatening consequences. Some pathogenic mechanisms have been partially characterised, however in many cases a full description is yet to be achieved. In particular haematogenous spread in AGE is an area which requires further study; both of BBB breakdown and pathology, and the role played by the immune system. Serum studies have illustrated common exposure across several populations and organisms from the *Acanthamoeba* genus are thought to be amongst the most numerous of free-living amoebae. It is thus an interesting question as to why and how infections with such devastating consequences arise from these otherwise adequately controlled microbes.

The ability of certain *Acanthamoeba* genotypes to sequester in the CNS following breach of the blood-brain barrier is of particular interest as an uncommon trait for many pathogens, but one which is shared with a number of parasites of considerable veterinary and medical importance; *P. falciparum, T. gondii,* and *T. brucei*. Within this context study of *A. castellanii* may also provide insights into broader mechanisms by which parasites cross the BBB, and the resultant consequences for infected patients.

Thus our aim is to investigate the haematogenous stage of AGE, and we have approached the question of how trophozoites survive during dissemination and breach the blood-brain barrier from two perspectives:

Firstly we focussed on the humoral immune response and the ways in which amoebae may evade antibody-mediated responses.

Secondly we investigated mechanisms of pathogenesis in an infection model of human brain microvasculature.

To facilitate this we immunised experimental animals and retrieved polyclonal antibody from hybridomas by *in vitro* fusion and culture techniques. Specific antibody was used to interrogate amoeba lysates to identify immune recognition targets, and tested for functional effects on adherence and cytotoxicity. Evasion mechanisms including cleavage of serum antibody and antibody inactivation via Fc-binding proteins were also investigated.

Additionally we addressed the issue of BBB breach using a dynamic flow system to improve modelling of the brain microvasculature *in vitro.* Current *in vitro* models of the BBB may not closely mimic the situation *in vivo* as measures of binding, cytotoxicity, and monolayer disruption are generally obtained from static 24-well plate cultures. This new model allowed us to investigate the relative importance of *A. castellanii* secreted and non-secreted virulence factors to BBB pathology in a physiologically relevant system.

2. Materials and Methods

2.1. Culture techniques

2.1.1. Acanthamoeba castellanii

A clinical isolate of *A. castellanii* belonging to the T4 genotype was obtained from the American Type Culture Collection (ATCC #50492). Amoebae were grown in 175cm^2 tissue culture flasks (Sarstedt, UK)[1] in autoclaved axenic peptone-yeast-glucose (PYG) medium comprising 0.75% w/v proteose peptone (Oxoid™, Thermo-Fisher Scientific, UK)[2], 0.75% w/v yeast extract[2], and 1.5% w/v glucose[2] in distilled water. Flasks were maintained in a humidified standard air incubator at 30°C. Every 3-5 days the growth medium was removed from culture flasks and replaced with fresh PYG. Under these conditions more than 90% of *A. castellanii* remained bound to the flask as trophozoites.

2.1.2. Human Brain Microvascular Endothelial Cells (HBMEC)

Primary Human Brain Microvascular Endothelial Cells (HBMEC) were obtained from Dr N.A. Khan and originated from individuals who had undergone neurosurgery at Johns Hopkins University School of Medicine (USA), as described by Khan and Siddiqui (2009). Isolation followed methods detailed by Alsam *et al.* (2003) and Stins *et al.* (1997). Purified cultures were obtained by fluorescence-activated cell sorting (FACS) and

[1] Sarstedt Ltd., Leicester, UK
[2] Thermo Fisher Scientific Ltd., Basingstoke, UK

tested positive for endothelial markers Factor-VIII, carbonic anhydrase IV and uptake of acetylated low density lipoprotein (Stins et al., 1997, Alsam et al., 2003, Khan and Siddiqui, 2009). HBMEC were maintained in 75cm^2 tissue culture flasks[1] in RPMI 1640 (Sigma-Aldrich, UK)[2] media supplemented with 100U/ml penicillin (Gibco®, Life Technologies, UK)[3], 100µg/ml streptomycin[3], 2mM L-glutamine[3], 1× minimum essential, 1mM sodium pyruvate[3], and 20% FBS[2], and were grown at 37°C with 5% CO_2. Under these conditions HBMEC have been shown to retain trans-endothelial electrical resistance (TEER) of >200mΩ and exhibit barrier function against bovine serum albumin (BSA) (Alsam et al., 2005a). Cells were used between passages 11-20 and retained normal growth characteristics until around the 20th passage. HBMEC were harvested by incubation with 5ml 10× Trypsin/EDTA[3] solution until cell monolayer detachment was observed at which point the Trypsin was inactivated by addition of 5ml complete culture medium and cells were collected by centrifugation at 1,000×g for 5 minutes.

2.1.3. Sp2/0 mouse myelomas

Sp2/0 murine myeloma cells were cultured in Dulbecco's modified Eagle's medium (DMEM)[3] plus 10% FBS, 2mM L-glutamine, 100U/ml penicillin,

[1] Sarstedt Ltd., Leicester, UK
[2] Sigma-Aldrich Ltd., Gillingham, UK
[3] Life Technologies Ltd., Paisley, UK

100µg/ml streptomycin, and 1× 8-azaguanine (QED Bioscience, USA)[1] in 75cm^2 tissue culture flasks at 37°C with 5% CO_2. Cells were collected by agitation and centrifugation at 1,000×g for 10 minutes and split 1 in 4 every 3-4 days in order to maintain log-phase growth.

2.1.4. Polyclonal hybridomas

Polyclonal hybridoma cells were maintained in DMEM supplemented with 10% FBS, 100U/ml penicillin, 100µg/ml streptomycin, 2mM L-glutamine, and 5% Briclone[2] in 175cm^2 Nunc triple layer tissue culture flasks (Nalge Nunc, USA)[3] at 37°C with 5% CO_2 overlay. Cells were collected by agitation and centrifugation at 1,000×g for 5 minutes.

2.2. Antigen preparation

2.2.1. *A. castellanii* lysate

10^8 *A. castellanii* trophozoites were collected from flasks by incubation on ice for 30 minutes followed by centrifugation at 1,000×g for 5 minutes. PYG growth medium was aspirated and the cell pellet was washed in sterile phosphate-buffered saline (PBS)[4] by resuspension and centrifugation, with the process repeated three times. Cells were again resuspended in 15ml of

[1] QED Bioscience Inc. San Diego, CA, USA
[2] QED Bioscience Inc. San Diego, CA, USA
[3] Nalge Nunc International, Rochester, NY, USA
[4] Life Technologies Ltd., Paisley, UK

PBS and subjected to three freeze-thaw cycles (-80°C to 37°C). The suspension was sonicated on ice for 5 minutes as 20s bursts with 20s intervening rest periods. Remaining whole cells and large debris were removed by centrifugation at 2000×g and the supernatant was inspected microscopically to confirm the absence of surviving whole cells. The protein content of the lysate was estimated by measuring the ratio of 280nm versus 260nm absorbance measurements (Warburg-Christian method) using a Nanodrop 8000 instrument[1] (see also section 2.5.1). Samples were stored at -80°C as 1ml aliquots.

2.2.2. *A. castellanii*-conditioned medium (ACM)

Flasks of trophozoites were prepared as described in section 2.1.1 so that at least 90% of cells were adherent. PYG was then removed from flasks which were then washed with RPMI twice to remove trace media and non-adherent cells. 50ml of RPMI was then added to the flasks, and they were returned to the incubator for three days to accumulate excretory-secretory (ES) products. Supernatant from several flasks was then collected and cysts/non-adherent trophozoites removed by passage through 0.22µm sterile vacuum filters[2]. Samples were stored at -20°C (short term) or -80°C (long term) as 50ml aliquots.

---

[1] Thermo Fisher Scientific Ltd., Basingstoke, UK
[2] Sarstedt Ltd., Leicester, UK

2.3. *In vivo* antibody generation

All animal experiments were carried out at the UoN Medical School animal facility with ethical approval from University of Nottingham (project number RP10/07). Animal handling was carried out by Professor Richard J. Pleass, personal license number PPL 40/3287.

2.3.1. *A. castellanii* preparation for *in vivo* experiments

2×10^7 *A. castellanii* trophozoites were collected as described in section 2.2.1 and washed in 10ml of sterile Dulbecco's phosphate-buffered saline (DPBS)[1] three times to remove trace PYG. The pellet was suspended in 200µl of DPBS and 200µl Imject Alum (Pierce™, Thermo Fisher Scientific, UK)[2] was added, with immunogen subsequently left on a roller to mix thoroughly.

2.3.2. Immunisation protocol

Six BALB/c mice (4♀, 2♂) all aged between 6-8 weeks were immunised with four receiving antigen preparation (3♀, 1♂) and two controls with DPBS + Alum alone (1♀, 1♂). An immunisation schedule of three bi-weekly injections was set, with each animal receiving 200µl of DPBS + 10^7

[1] Life Technologies Ltd., Paisley, UK
[2] Thermo Fisher Scientific Ltd., Basingstoke, UK

amoebae + Alum or DPBS + Alum intraperitoneally. Mice were sacrificed three days after the final injection by CO_2 asphyxiation and exsanguination.

2.3.3. Serum testing

Terminal blood was collected from mice and deposited in lithium heparin-coated vaccutainers (BD Bioscience, UK)[1] to limit clotting. Blood samples were then centrifuged at 10,000×g for 10 minutes to separate plasma which was then collected and stored at -20°C. Serum samples were tested for the presence of *A. castellanii*-specific antibody by enzyme-linked immunosorbant assay (ELISA) and Western blot assay (see sections 2.8.1-2.8.3 & 2.8.5).

2.3.4. Splenocyte extraction

Spleens from experimental mice were dissected out aseptically within the animal facility and deposited in DMEM supplemented with 4mM L-glutamine, 100U/ml penicillin, and 100µg/ml streptomycin for transport back to the lab (Complete Medium No Serum, CMNS). Splenocytes were extracted by crushing two spleens in 10ml of warmed CMNS with the plunger from a sterile 5ml syringe (Terumo Medical, USA)[2]. Spleen extracts were collected into sterile 50ml tubes and any large debris was allowed to

[1] BD Bioscience Ltd., Oxford, UK
[2] Terumo Medical Corporation, Somerset, NJ, USA

settle out by gravity. Supernatant containing extracted splenocytes was then carefully collected by pipette into a fresh 50ml tube. Splenocytes were pelleted by centrifugation at 1,000×g for 10 minutes and subjected to four further wash steps under identical conditions.

2.3.5. Fusion

Fusion was carried out using a Fuse-It® hybridoma development kit[1] which incorporates a short-duration polyethylene glycol (PEG) based fusion technique with a dedicated post-fusion cloning factor (Briclone) obviating the need for feeder layers. Sp2/0 myelomas were collected as described in section 2.1.3 and adjusted to a concentration of 1×10^6 cells/ml. Two splenocyte extracts were counted on a haemocytometer (Weber Scientific, USA)[2], yielding $5x10^6$ and $7x10^6$ cells respectively, which were likewise suspended in CMNS. Splenocytes and myelomas were then combined in a 5:1 splenocyte to myeloma ratio (Table 2.1). The cell suspension was thoroughly mixed and then centrifuged at 1,000×g for 10 minutes. Supernatant was then aspirated with a 10ml pipette to leave the pellet as dry as possible.

[1] QED Bioscience Inc. San Diego, CA, USA
[2] Weber Scientific Corporation, Hamilton, NJ, USA

Splenocytes	Myelomas	Total Cells
100×10^6 (5×10^6/ml in 20ml)	20×10^6 (1×10^6/ml in 20ml)	120×10^6 (3×10^6/ml in 40 ml)
140×10^6 (7×10^6/ml in 20ml)	28×10^6 (1×10^6/ml in 28ml)	168×10^6 (3.5×10^6/ml in 48ml)

Table 2.1 Combination ratios for splenocytes and myelomas during fusion.

The PEG fusion reagent was prepared by melting 2g of PEG[1] in a water bath at 56°C and adding 2ml of CMNS to create a 50% solution as prescribed by the kit instructions. 1ml of this solution was then added to the cell pellet dropwise over a 30-second period with gentle agitation to disrupt the pellet. Over a further 30 seconds, 1ml of CMNS was added dropwise to gradually dilute out the PEG and then over the course of three minutes an additional 10ml of CMNS was added in small increments. Gentle agitation by hand was continued throughout the fusion process.

The fusion mixture was then centrifuged at 1,000×g for 10 minutes to completely remove PEG traces. Cells were resuspended to 3×10^6/ml in DMEM plus 10% FBS, 100U/ml penicillin, 100µg/ml streptomycin, 4mM L-glutamine, 10% BriClone[1] and 1× hypoxanthine-aminopterin-thymidine (HAT)[1] (Hybridoma Cloning Medium, HCM) and aliquoted into 96-well plates with 3×10^5 cells/well in a final volume of 100µl. Plates were then placed in a 37°C incubator at 5% CO_2 and left to grow for 7 days prior to

[1] QED Bioscience Inc. San Diego, CA, USA

microscopic inspection to check for colony formation. At this inspection stage 50µl of fresh HCM was added regardless of whether growth was detected and cultures were then returned to the incubator for a further three days.

2.3.6. Post-fusion screening

After 10 days of culture 50µl of supernatant was removed from wells and used neat as the primary antibody stage in ELISA assays as described in sections 2.8.1 to 2.8.3. Culture supernatants were screened for production of IgG, IgM and IgA antibodies.

2.4. *In vitro* infections

2.4.1. 24 and 48-well plates

HBMEC were collected by trypsin treatment as outlined in section 2.1.2 and a 2.5×10^5/ml cell suspension was made by addition of fresh complete media. One millilitre of this suspension was seeded into tissue culture grade 24-well plates[1] (300µl in 48-well plates[1]) and cell monolayers were then allowed to grow to confluence over 18-24 hours. Once monolayers had fully formed culture media was removed and cell layers were gently washed by three rounds of addition and removal of 1ml RPMI 1640. Monolayers were

[1] Sarstedt Ltd., Leicester, UK

then treated with either a suspension of *A. castellanii* trophozoites in RPMI or ACM according to the demands of specific assays.

2.4.2. Flow chambers

HBMEC were collected by trypsin treatment as outlined in section 2.1.2 and a 5×10^6/ml cell suspension was made by addition of fresh complete media. Fifty microliters of this suspension was pipetted into the anterior chamber of 0.2µm chamber microslides (Ibidi, Germany)[1] that had been allowed to equilibrate for gas and temperature for 10 minutes prior to use. The cell suspension was then allowed to draw through by capillary action. Both anterior and posterior chambers were then filled with 60µl of fresh HBMEC growth medium and the slide was returned to incubation at 37°C, 5% CO_2. Media in microslide chambers was replaced daily by allowing slides to flush by capillary action and under these conditions cells reached confluence after 18-24 hours. 60 minutes before commencement of experiments slides were inspected for monolayer quality and if necessary were flushed with fresh medium once again to maintain monolayer integrity.

Immediately prior to experiments anterior and posterior chambers were brim-filled with fresh media to prevent the entry of air bubbles and attached via elbow Luer connectors[2] to 0.8mm silicone piping[3] which had also been

[1] Ibidi GmbH, Martinsried, Germany
[2] Ibidi GmbH, Martinsried, Germany
[3] Thermo Fisher Scientific Ltd., Basingstoke, UK

pre-filled with media. Tubing was passed through a Thermo FH10 peristaltic pump[2] to provide constant circulating flow. Connectors and piping were sterilised before each experiment. Prior to initiation of the experiment microslides were flushed with RPMI 1640 for 5 minutes to remove waste growth media. For the experimental runs the system was first primed with a suspension of trophozoites or ACM and once flow was initiated experimental solutions were re-circulated through the initial stock to avoid it running dry and exposing the cells to air bubbles. The system was maintained at 37°C by use of a heat block.

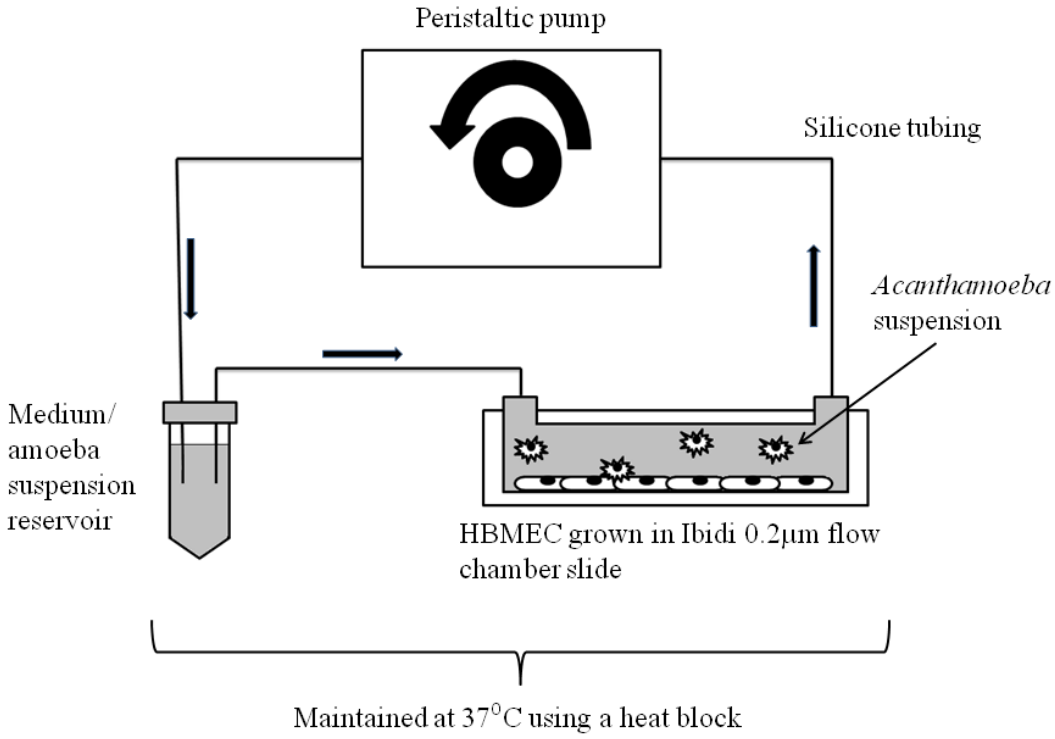

Figure 2.1 Schematic diagram of *in vitro* flow system.

Including illustration of use to circulate a suspension of *A. castellanii* cells.

2.5. Cell binding assay

2.5.1. Static

A 2×10^5/ml suspension of *A. castellanii* trophozoites was prepared as described in section 2.2.1 with the exception that all washes and the final suspension stage were carried out in warm RPMI 1640. One millilitre, or 300µl of cell suspension was then added to prepared HBMEC plates (see section 2.4.1) and returned to the cell culture incubator. After a period of three hours the plate was gently agitated to suspend non-adherent trophozoites and the number of unbound cells was counted using a haemocytometer. During counting *A. castellanii* cells were distinguished from non-adherent HBMEC based on morphological criteria: irregular cell shape, presence of acanthopodia and presence of vacuoles. Cells of ambiguous identity were excluded from counts.

2.5.2. Flow

2×10^5/ml trophozoites in RPMI 1640 were prepared as before (section 2.2.1) with the exception of an increased final volume of 20ml. The cell suspension was held in a stock tube so that constant circulation could be maintained as described in section 2.4.2, whilst the temperature of the system during the experimental period was maintained by a heat block set to 37°C. After priming the system with cell suspension a constant flow rate was set and maintained for a period of three hours. At the end of this period

the number of unbound amoeba was counted by sampling from the stock suspension as described in section 2.5.1.

2.6. Monolayer disruption assay

2.6.1. Microscopy

At the conclusion of the experimental period tissue culture plates or flow chamber slides were examined under the 10× objective lens of a Leica DMIL instrument with DFC490 camera (Leica Microsystems, UK)[1]. Three representative fields of view from each sample were selected and standardised by applying in-built auto-exposure and white balancing, and were then photographed under phase contrast. These settings provided optimal contrast between cell and background during downstream semi-quantification of monolayer disruption.

2.6.2. Quantifying monolayer disruption

TIFF image files were processed using open-source ImageJ analysis software (available from http://rsbweb.nih.gov/ij/) (Schneider et al., 2012) with monolayer disruption measured using a semi-quantitative method based on grid scoring. A grid of 1600 pixels per square to give a total of 5000 squares was superimposed over the image and five representative

[1] Leica Microsystems Ltd., Milton Keynes, UK

blocks of 196 squares per block (14×14) were then selected. Each individual square in a block was scored as disrupted if cell coverage was ≤50%. Total scores for the five representative blocks were then expressed as a percentage of the total 980 squares counted.

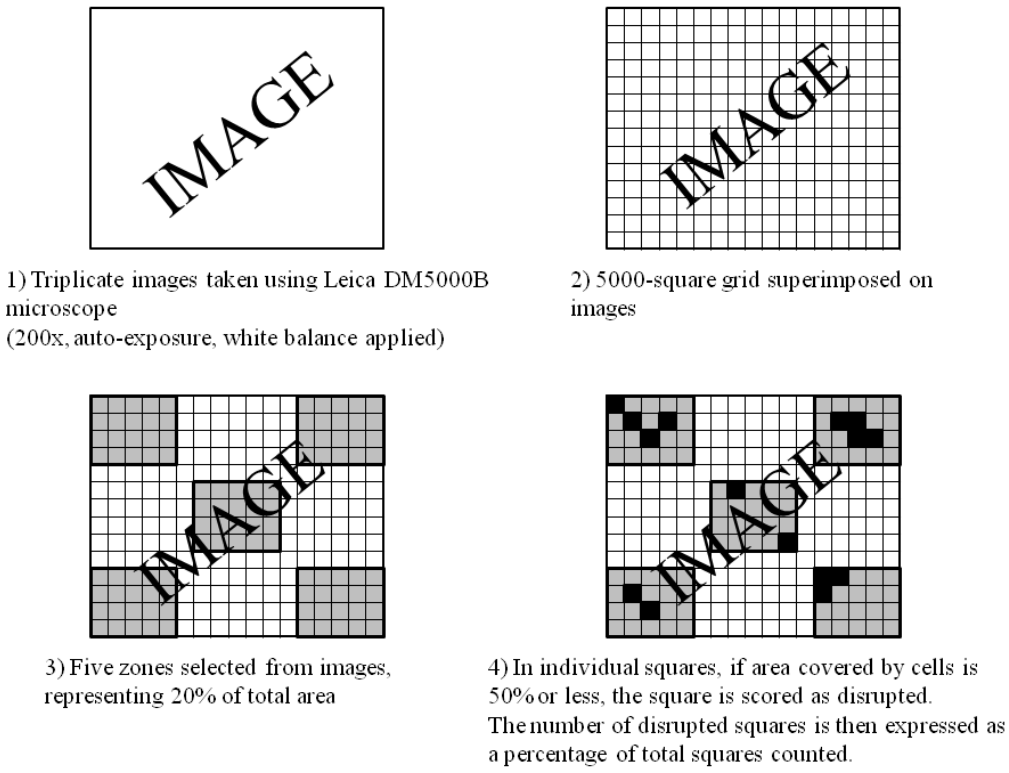

Figure 2.2 Schematic illustration of semi-quantitation method for micrographs.

Semi-quantitative measurements of monolayer disruption are obtained by expressing the number of squares scored as disrupted as a percentage of the total number examined.

2.6.3. Haematoxylin staining

Supernatant was carefully removed from plates that had been treated with either a suspension of trophozoites or ACM and the cell layer with/without adherent trophozoites was fixed in 1ml or 300µl (24 or 48-well plates) of an

ice-cold mix of equal parts glacial acetone to ethanol for 15 minutes. The supernatant was carefully removed and discarded and 1ml/300µl of Harris haematoxylin (VWR International, UK)[1] was added to cell layers which were then left to stain for 15 minutes. Haematoxylin was then carefully removed and wells were washed three times by pipetting with 1ml/300µl PBS to remove unincorporated stain and non-adherent cells. Stained monolayers were then photographed using an ImageQuant 300 instrument (GE Healthcare, UK)[2] and qualitatively scored based on the gross level of disruption.

2.6.4. Lactate dehydrogenase (LDH) release assay

Supernatants from either ACM or trophozoite-treated cultures were collected after 3 and/or 24 hours and centrifuged at 1000×g for 5 minutes to pellet cells and cell debris. Positive control supernatants were obtained by adding an equal volume of lysis buffer (Roche, UK)[2] to untreated HBMEC and incubating for 15 minutes. Thereafter supernatants from lysed cells were treated identically to those from inoculated wells. Fifty microliters of supernatant was removed and placed in a 96-well microtitre plate to be analysed for LDH release using a cytotoxicity detection kit[3]. Briefly the catalyst and enzyme components of the kit were thawed on ice and a detection mix was prepared with 125µl of reconstituted lyophilized catalyst

[1] VWR International Ltd., Lutterworth, Leicestershire, UK
[2] GE Healthcare Ltd., Buckinghamshire, UK
[3] Roche Ltd., Burgess Hill, UK

and 5.625ml of dye solution. This was then kept on ice until use. Equal volumes (50µl) of sample and detection mix were pipetted into a 96-well microtitre plate and incubated for 10 minutes protected from light. Absorbance was then measured at 490nm using a LT-4000 plate reader (Labtech, UK)[1] and the percentage cell death calculated using the equation below.

$$\%\ \text{cell death} = \frac{\text{sample} - \text{negative control}}{100\%\ \text{cell death control} - \text{negative control}} \times 100$$

A background reading of supernatant alone was made prior to addition of the reaction mix and this was subtracted from the final readings before cell death was calculated to correct for optical interference by RPMI.

2.6.5. Antibody treatment

A full list of antibodies used in all experiments with supplier and specificity is given in Table 2.2.

In experiments to determine the effect of specific and nonspecific antibody and antibody fragments, HBMEC static plates were set up as described in section 2.4.1. Cell suspensions of 2×10^5/ml trophozoites were then prepared in RPMI with antibody variants added to a final concentration of 200µg/ml. Where necessary antibody solutions were concentrated and dialysed to remove sodium azide prior to use (see sections 2.7.2 and 2.7.4). With the

[1] Labtech Ltd., Uckfield, UK

exception of polyclonal antibody generated as part of the project antibodies were purchased from external suppliers as follows: mouse IgM isotype control MCA692 (AbD Serotec, UK)[1], mouse IgG isotype control I8765 (Sigma-Aldrich, UK)[2], human purified IgG Fc fragment (Alpha Diagnostic, UK)[3]. Prior to infection, antibody was added to the *A. castellanii* cell suspension and treated samples were then moved to an APT Line rotary incubator (Biometra, Germany)[4] set at 37°C for 3 hours to maximise binding and/or aggregation effects.

[1] AbD Serotec, Ltd., Kidlington, UK
[2] Sigma-Aldrich Ltd., Gillingham, UK
[3] Alpha Diagnostic International Inc., San Antonio, TX, USA
[4] Biometra GmbH, Goettingen, Germany

Text reference number	Antibody	Supplier	Catalogue number	Specificity
1	Mouse IgM negative control	AbD Serotec	MCA692	Negative control
2	Mouse IgG (from serum)	Sigma-Aldrich	I8765	Negative control (from serum)
3	Mouse IgA isotype control	Alpha Diagnostic Intl.	20102-100	Negative control
4	Mouse IgE isotype control	Alpha Diagnostic Intl.	20102-106	Negative control (anti-dimethylaminonaphtalene-1-sulfonyl)
5	Human IgG Fc fragment	Alpha Diagnostic Intl.	20007-1-Fc	Negative control (from serum)
6	Goat anti-mouse IgM – HRP	AbD Serotec	STAR86P	IgM mu heavy chain specific
7	Goat anti-mouse IgG – AP	Sigma-Aldrich	A3673	Gamma chain specific
8	Goat anti-mouse IgG - HRP	Sigma-Aldrich	A9917	IgG Fab
9	Goat anti-mouse IgA – AP	Sigma-Aldrich	A4937	Alpha chain specific
10	Mouse anti-human IgG Fc - FITC	Sigma-Aldrich	F5016	Monoclonal (clone HP-6017), Fc-specific
11	Goat anti-mouse IgM - FITC	AbD Serotec	OBT1713F	IgM (Heavy and Light chain)
12	Goat anti-mouse IgG - Texas Red	AbD Serotec	103007	IgG1, 2a, 2b, 3 Heavy chain

Table 2.2 List of antibodies used in all experiments.

Detailing supplier, catalogue number, and specificity. When referenced in chapter texts antibodies are referred to by list number (first column)

2.6.6. Aggregation assay

Samples that had been incubated with specific and nonspecific antibody as described in section 2.6.5 were removed from the rotary incubator and 1ml of suspension was deposited in 24-well tissue culture plates. Wells were then photographed immediately using a Leica DMIL microscope and DFC490 camera[1] instrument and after a further 24 hour incubation at 37°C, 5% CO_2. The degree of trophozoite aggregation visible in each image was the scored qualitatively using the following criteria:

+++ = ≥20 trophozoites per aggregate and/or high aggregate number.

++: 10-20 trophozoites per aggregate and/or medium aggregate number.

+: 5-10 trophozoites per aggregate and/or low aggregate number.

+/-: <5 trophozoites per aggregate and/or very low aggregate number.

-: No visible aggregation.

2.6.7. Protease Activated Receptor (PAR) antagonist treatment

HBMEC cultures were set up as described in section 2.4.1 and grown to confluence overnight. HBMEC monolayers were washed three times in 1ml RPMI to remove trace growth media and were then treated with either:

[1] Leica Microsystems Ltd., Milton Keynes, UK

100nM N3-Cyclopropyl-7-[[4-(1-methylethyl)phenyl]methyl]-7H-pyrrolo[3,2-f]quinazoline-1,3-diamine dihydrochloride (SCH 79797) - a PAR1 antagonist (Tocris Bioscience, UK)[1];

Or,

100nM Trans-Cinnamoyl-Tyr-Pro-Gly-Lys-Phe-NH2 (tcY-NH_2)[1] - a PAR4 antagonist.

Both PAR antagonists were dissolved in RPMI. Concentrations were based on previous reports and datasheet values. Where IC50 values were stated a higher concentration was used to achieve maximal inhibition (Ahn et al., 2000, Hollenberg et al., 2004, Lidington et al., 2005).

PAR antagonists were diluted to working concentration from 10mM and 1mM stock solutions respectively and so an equal volume of stock solution solvent was included in matched controls for each antagonist (DMSO or ddH_2O). After 30 minutes of stimulation, PAR solutions were removed and replaced with 1ml ACM or 1ml of a suspension of 2×10^5/ml trophozoites, containing either PAR1 antagonist, PAR4 antagonist, matched controls (antagonist solvent), no PAR antagonist (positive control) or 1ml of RPMI only (negative control). Plates were then returned to incubation at 37°C, 5% CO_2 and cell layers were photographed at 3 and 24 hour time points using a Leica DMIL microscope and DFC490 camera[2] (see section 2.6). Micrographs from these time points

[1] Tocris Bioscience Ltd., Bristol, UK
[2] Leica Microsystems Ltd., Milton Keynes, UK

were analysed for monolayer disruption using the methods outlined in sections 2.6.2 and 2.6.3.

2.6.8. TdT-mediated dUTP Nick-End Labelling (TUNEL) assay

HBMEC cultures were set up as described in section 2.4.1 and infected with trophozoites/ACM plus PAR inhibitors as described in section 2.6.7. Since the assay was to be used to detect apoptotic cells, positive control wells were included on the plates and were treated with 50µM cisplatin[1] in RPMI at the time of infection. Post-treatment, culture plates were returned to incubation at 37°C, 5% CO_2 for 18 hours. Monolayers were photographed at 3 and 18 hours using a Leica DMIL microscope and DFC490 camera[2] and disruption quantified as described in section 2.6.2. After 18 hours had elapsed, cells were collected by vigorous pipetting in the case of infected wells, or trypsin treatment (as per section 2.1.2) followed by pipetting in the case of negative and positive control wells, where HBMEC remained adherent. Cells were pelleted at 2000rpm for 5 minutes and then fixed in 4% formaldehyde for 15 minutes. Cells were then washed twice in PBS by centrifugation and resuspended to a final concentration of 1×10^6/ml. 200µl of cell suspension was affixed to microscope slides using a Shaydon cytospin, set to 500rpm for 5 minutes.

---

[1] Sigma-Aldrich Ltd., Gillingham, UK
[2] Leica Microsystems Ltd., Milton Keynes, UK

After cytospinning, cells were stained for nuclear fragmentation using DeadEnd™ fluorometric TUNEL system (Promega, USA)[1] and following the accompanying protocol. Briefly, cells were permeabilised with 0.2% w/v Triton X-100 in PBS for 5 minutes, and then rinsed by immersion in PBS for 2× 5 minutes. Excess PBS was tapped onto tissue paper and then cells were covered with 100µl of equilibration buffer for 10 minutes. A reaction mix was then made up with 45µl equilibration buffer, 5µl nucleotide mix, and 1µl of rTdT enzyme per reaction. The mix was kept on ice until use and protected from light. Slides were again tapped on tissue paper to remove equilibration buffer before adding 50µl of reaction mix per slide and covering with film coverslips. Slides were then placed in a humidified chamber protected from light and incubated at 37°C for 60 minutes. Samples were continually protected from light during all subsequent steps.

After the incubation period reactions were terminated by immersion of slides for 15 minutes in 2× Saline Sodium Citrate (SSC) diluted from 20× stock with ultrapure water. Slides were then washed 3× in PBS to remove unincorporated fluorescein-12-dUTP and finally mounted with Vectashield mounting medium containing 4',6-diamidino-2-phenylindole (DAPI) (Vector Labs, UK)[2] to counterstain nuclei. Cells were examined and photographed under a Leica DM5000B fluorescent microscope with a DFC350FX camera (Leica Microsystems, UK)[xi]. Fluorescent filters applied for visualisation of DAPI and fluorescein isothiocyanate (FITC) used excitation wavelengths of 360nm and

[1] Promega Corp., Madison, WI, USA
[2] Vector Labs Ltd., Peterborough, UK

480nm respectively. In addition to representative images, counts of TUNEL-positive cells were also made per field-of-view under a magnification of 40×.

2.7. Antibody preparation

2.7.1. Protein quantification

Concentrations of proteins in solution were measured using a Nanodrop 8000 instrument[1]. The instrument was first blanked against 2µl of solvent without protein, cleaned and then 2µl of protein solution was pipetted onto pedestals and concentration measured by absorbance at 280nm.

2.7.2. Protein concentration

Protein solutions which were too dilute to be usefully used were concentrated using Amicon regenerated cellulose 10kDa or 50kDa molecular weight cut-off concentrator columns (Millipore, USA)[2]. 10kDa columns were used for ACM to ensure that low Mw components were not lost whilst 50kDa columns were used to concentrate large, polymeric, high Mw IgM. Sample was introduced into the upper chamber of the column, which was then centrifuged at 4,000×g for 20 minutes at a temperature of 5°C. Concentrate was retrieved from the upper chamber and quantified by absorbance at 280nm by Nanodrop (see

[1] Thermo-Fisher Scientific Ltd., Basingstoke, UK
[2] Merck-Millipore, Billerica, MA, USA

section 2.7.1). Approximately ten to twentyfold levels of concentration were achieved by this method. Protein solutions were then stored at 4°C for short-term use or frozen at 20°C as small aliquots to minimise damage from multiple freeze-thaw cycles.

2.7.3. Immunoaffinity purification

Polyclonal IgM was purified from raw bulk culture supernatant by affinity purification on a CaptureSelect® anti-mouse-IgM agarose matrix (BAC, The Netherlands)[1]. 10ml of matrix slurry was placed in disposable plastic columns[2] on top of a semi-permeable membrane disk and allowed to settle to yield a final capillary bed volume of 5ml. The column was carefully filled with sterile PBS so as not to disturb the settled slurry bed and a second disk was gently pushed down to a distance of 1-2mm from the top of the slurry. The column was then equilibrated with five washes of 5ml sterile PBS.

250ml of bulk culture supernatant (see section 2.1.4) was concentrated tenfold using protein concentration columns (section 2.7.2) and was passed dropwise through the equilibrated column five times. A small volume of pre-column supernatant and the column run-off was collected at this stage to assess the efficiency of protein recovery. The column was re-equilibrated with five washes of 5ml sterile PBS and then protein was eluted in 5ml of 0.1M glycine pH3 and washed through with a further 5ml of sterile PBS. Elute was collected

[1] BAC B.V., Naarden, The Netherlands
[2] Thermo-Fisher Scientific Ltd., Basingstoke, UK

as fifteen 1ml fractions and 250µl of 1M Tris Base pH8.8 added to raise the pH and neutralise the glycine elution buffer. Each fraction was then individually quantified in duplicate by Nanodrop (section 2.7.1). Positive fractions were pooled and dialysed against sterile PBS to remove glycine and return samples to neutral pH. The column was then washed with 25ml of sterile PBS and finally stored in 20% ethanol for future use. Throughout the procedure care was taken to avoid air bubbles entering the column and lowering binding efficiency and rate of flow.

2.7.4. Antibody dialysis

IgM elutes from affinity purification (section 2.7.3) in glycine buffer and commercially purchased antibody, with sodium azide preservative not suitable for direct use *in vitro*, were dialysed into PBS. Solutions were injected into pre-wetted 3kDa Mw dialysis cassettes[1] using a 5ml syringe and a 21 gauge needle[2]. The cassette was clipped into a foam float and then placed in a large beaker containing 3L of sterile PBS. A stirring bar was added and the beaker was covered and left on a magnetic stirrer set to 50rpm. The apparatus was left at room temperature for 1 hour and then transferred to a 5°C coldroom for 18 hours. After this period, solutions were recovered from the dialysis cassette again using a 5ml syringe and 21ga needle, and kept at 4°C for frequent use or -20°C as small aliquots for longer-term storage.

---

[1] Thermo-Fisher Scientific Ltd., Basingstoke, UK
[2] Terumo Medical Corporation, Somerset, NJ, USA

2.8. Immunoassays

2.8.1. Enzyme-Linked Immunosorbent Assay (ELISA)

General ELISA protocols followed the method detailed below. Additional details and assay-specific modifications are given in relevant chapters.

For ELISA, capture antibody or *A. castellanii* antigen coated plates were prepared by overnight incubation in carbonate/bicarbonate buffer at 4°C. 96-well microtitre plates were coated with 100µl/well of 10µg/ml *A. castellanii* lysate (see section 2.2.1) or isotype control antibody. Plates were washed three times in PBS plus 0.05% Tween-20 (PBST) to remove coating buffer and then blocked for one hour at room temperature or overnight at 4°C, using 5% Bovine Serum Albumin (BSA) in PBST. Blocking solution was removed and wells were washed three times in PBST before 50µl of sample was added at a series of dilutions. Plates were then incubated for 90 minutes at room temperature and washed five times in PBST prior to addition of secondary antibody.

2.8.2. Alkaline Phosphatase (AP) chemistry

Alkaline Phosphatase conjugated antibody was used during the screening stage of hybridoma production. Thereafter all ELISAs were performed using horseradish peroxidase detection chemistry. 100µl of a 1:1000 dilution of AP

conjugated anti-mouse IgG (γ-chain specific)[1] detecting antibody was added and plates were once again incubated at room temperature for 90 minutes. Subsequently wells were washed five times in PBST and 200µl of SigmaFAST AP substrate[1] was added and allowed to develop for 20 minutes at room temperature and protected from light. Absorbance values at 405nm were read using an LT-4000 plate reader[2].

2.8.3. Horseradish peroxidase (HRP) chemistry

IgM and IgA ELISAs were conducted using Horseradish peroxidise-conjugated secondary antibodies and HRP detection chemistry. 100µl of a 1:1000 dilution of HRP-conjugated goat anti-mouse IgM STAR86P[3], or anti-mouse IgA (α-chain specific) A4937[4] detecting antibody was added and plates were incubated at room temperature for 90 minutes. Wells were washed five times in PBST and then developed with 100µl of 3,3',5,5'-tetramethylbenzidine (TMB)[2] substrate for 15 minutes at room temperature and protected from light. Reactions were stopped by addition of 50µl 2M sulphuric acid and absorbance values at 450nm were read using an LT-4000 plate reader.

---

[1] Sigma-Aldrich Ltd., Gillingham, UK
[2] Labtech Ltd., Uckfield, UK
[3] AbD Serotec, LTD., Kidlington, UK
[4] Sigma-Aldrich Ltd., Gillingham, UK

2.8.4. Dot Blot

Whatman® Protran nitrocellulose membrane (GE Healthcare, UK)[1] was cut into 10×10cm squares, subdivided into a grid and blotted with 20µl of test antigen (either raw hybridoma culture supernatant, 50µg/ml isotype control mouse IgG[2], 50µg/ml negative control mouse IgM[1], 50µg/ml *Acanthamoeba* PBS lysate or blank culture medium). The membrane was allowed to dry out completely before transfer into blocking buffer (PBST plus 5% BSA) for 90 minutes at room temperature. Blots were washed in PBST for 3× 3 minutes and then probed with 20µl of test antibody (either raw hybridoma culture supernatant, 50µg/ml negative control mouse IgG, 50µg/ml negative control mouse IgM, 1:1000 dilution of mouse hyperimmune serum or blank culture medium). Blots were incubated for 90 minutes at room temperature and then washed for 3× 3 minutes in PBST. Detecting antibody was either goat anti-mouse IgG-HRP (Fab specific)[2] or goat anti-mouse IgM-HRP[3], diluted 1:1000 in PBST. 20µl of detecting antibody solution was pipetted onto target spots and the blot was incubated for an hour at room temperature. After incubation, blots were washed for 3× 3 minutes in PBST, and developed by adding 20µl of TMB solution to each spot and photographing after 5 minutes.

---

[1] GE Healthcare Ltd., Buckinghamshire, UK
[2] Sigma-Aldrich Ltd., Gillingham, UK
[3] AbD Serotec, LTD., Kidlington, UK

2.8.5. Western Blotting

Prior to beginning the blotting procedure an SDS-PAGE gel was run with 90µg per well of *A. castellanii* PBS lysate (see section 2.2.1), alongside 1µg of negative control IgM and molecular weight ladder at 120V for 90 minutes (see section 2.9.1 for full methodology). After the run, the gel was equilibrated in cold 1× TGS blotting buffer (Expedeon, UK)[1] for 15 minutes alongside blotting paper and sponges. A sheet of polyvinylidine fluoride (PVDF)[2] was activated by washing in 100% methanol for one minute, then ultrapure water for 2× 1 minute washes before equilibration in cold transfer buffer for 10 minutes. All components were assembled into a transfer sandwich and run at 110V for 90 minutes using an Owl VEP-2[4] blotting module.

After transfer, PVDF membrane was washed for 3× 5 minutes in ultrapure water then blocked overnight with 5% BSA. The next day membrane was washed for 3× 5 minutes in PBST, then cut into strips each of which was incubated with either 25ml of 50ng/ml purified anti-*A. castellanii* polyclonal antibody or negative control mouse IgM[3], or 1:50 polyclonal bulk culture supernatant or control culture medium. Strips and antibody/control solutions were placed in 50ml centrifuge tubes on a roller and incubated at room temperature for 60 minutes. Solutions were carefully discarded and strips

[1] Expedeon Ltd., Harston, Cambridgeshire, UK
[2] Thermo-Fisher Scientific Ltd., Basingstoke, UK
[3] AbD Serotec Ltd., Kidlington, UK

washed for 3× 5 minutes in 30ml PBST on a roller, before addition of 25ml 1:10,000 goat anti-mouse IgM-HRP[1] in PBST. Samples were returned to the roller for a further 60 minutes then washed again for 3× 5 minutes in 30ml PBST.

Development of samples was carried out using Amersham ECL$^+$ chemiluminescent substrate[1] as per kit instructions. Briefly 3ml of room temperature solutions A and B were mixed in a centrifuge tube and pipetted so that the entire surface of the PVDF membranes was covered. Membrane strips were incubated at room temperature for five minutes, excess ECL$^+$ was drained and then blots were sealed inside plastic film. CL-XPosure x-ray film[2] was then exposed to blots for 10 seconds in a darkroom exposure box and developed with an SRX101A x-ray instrument (Konika Minolta, UK)[3].

2.8.6. Immunofluorescence

Cell populations of HBMEC, *Acanthamoeba* and K562 (a chronic myeloid leukaemia cell line) were prepared in PBS to a final concentration of 10^6/ml following procedures outlined in sections 2.1.2 and 2.2.1. K562 were obtained from the Health Protection Agency Culture Collection[4] (catalogue number 89121407) from a line first isolated in 1979 (Lozzio and Lozzio, 1979, Lozzio et al., 1981). Cells were first retrieved from liquid nitrogen storage and

[1] GE Healthcare Ltd., Buckinghamshire, UK
[2] Thermo-Fisher Scientific Ltd., Basingstoke, UK
[3] Konika Minolta Ltd., Basildon, UK
[4] Health Protection Agency Culture Collections, Salisbury, UK

resuspended in 1ml RPMI + 10% FBS + 1× penicillin/streptomycin by centrifugation at 1000×g to remove cryopreservative (DMSO).

200µl of the cell suspension (200,000 cells) was then affixed to microscope slides using a Shaydon Cytospin 4[1] set to 450rpm for 5 minutes. Slides were then fixed by immersion in 4% formaldehyde, and washed twice in PBS prior to continuing with experiments.

Slides were firstly blocked with 600µl of 5% BSA in PBS for an hour at 37°C, and then washed by immersion five times in PBST. Slides were dabbed dry to remove excess liquid and then 300µl of primary antibody, antibody Fc fragment, dilutions of mouse serum, or dilutions of culture supernatant were added before returning to incubate at 37°C for 60 minutes. Slides were again washed five times in PBST, dabbed dry and then incubated with appropriate fluorochrome-conjugated secondary antibody again at 37°C for 60 minutes. Finally slides were washed three times in PBST and twice in PBS without Tween-20 before allowing to air-dry protected from light. Once slides were almost dry they were mounted in Vectashield with DAPI mountant[2] and coverslips were sealed with nail polish. A Leica DM5000B fluorescent microscope with DFC 350FX camera[3] was then used to observe and photograph fluorescing cells at excitation wavelengths of 360, 480 and/or 640nm respectively. Antibodies, dilutions and microscope settings for individual assays are given in relevant experimental chapters.

---

[1] Thermo-Fisher Scientific Ltd., Basingstoke, UK
[2] Vector Labs Ltd., Peterborough, UK
[3] Leica Microsystems Ltd., Milton Keynes, UK

2.8.7. Fluorescence-Activated Cell Sorting (FACS)

5×10^6 HBMEC and *A. castellanii* cells were collected as outlined in sections 2.1.2 and 2.2.1 and washed 3× in RPMI by centrifugation at 1,000×g. Cells were then fixed in 4% formaldehyde for 10 minutes and washed twice in PBS by centrifugation at 2,000×g before blocking in 5% BSA for 30 minutes at 37°C. Cells were washed twice in PBS, then incubated with either 1:300 human IgG Fc fragment (Alpha Diagnostic International)[1] in PBST+1% BSA, or PBST/BSA alone at 37°C for 60 minutes. Cells were then washed again in PBS + 1% BSA before incubation with 1:300 anti-human IgG (Fc-specific)-FITC secondary antibody[2] in PBST/BSA, or PBST/BSA alone at 37°C for 60 minutes. Finally, cells were washed 3× in PBS and stored at 4°C, protected from light until use. A FACSCantoII instrument was used to analyse cells, recording 50,000 events. FACS data was analysed using WEASEL version 3.0 software (The Walter and Eliza Hall Institute, Australia)[3] as follows. Unlabelled control cells were used to define populations for all samples based on forward scatter (FSC) versus side scatter (SSC) dotplots. Dotplots of FITC signal versus FSC were then drawn, gated against unlabelled cells. The percentage of each cell population positive for FITC signal was automatically calculated by the software based on this gating.

---

[1] Alpha Diagnostic International Inc., San Antonio, TX, USA
[2] Sigma-Aldrich Ltd., Gillingham, UK
[3] The Walter and Eliza Hall Institute of Medical Research, Victoria, Australia

2.9. Polyacrylamide Gel Electrophoresis (PAGE)

2.9.1. Sodium Dodecyl Sulphate PAGE (SDS-PAGE)

Precast polyacrylamide 12% and gradient 4-20% gels (Expedeon, UK)[1] were prepared by rinsing in distilled water prior to use so that wells were filled and free of bubbles. The gel was locked into a Verti-gel Mini electrophoresis tank[2] and 1L of 1× SDS running buffer[2] was poured in to the fill line.

Per lane, 15µl of the sample to be run was mixed with 4µl of LDS loading buffer[2] and either 1µl of dithiothreitol (DTT)[2] if reducing conditions were required or ultrapure water for non-reducing conditions. Samples were denatured by heating to 75°C for 5 minutes and then loaded onto the gel alongside 10µl of ColorPlus prestained protein marker (New England BioLabs, USA)[3]. A voltage of 120V was applied to the tank for 90 minutes, after which the gel was retrieved from its cartridge and washed in ultrapure water for five minutes.

2.9.2. Coomassie Blue staining

Samples to be visualised by coomassie blue staining were prepared using an acetic acid/ethanol–based stain (see Appendix 1). Gels were immersed in stain,

---

[1] Expedeon Ltd., Harston, Cambridgeshire, UK
[2] Thermo-Fisher Scientific Ltd., Basingstoke, UK
[3] New England BioLabs Inc., Ipswich, MA, USA

gently heated for 1 minute in a microwave oven and placed on a rocker for 60 minutes at room temperature. Gels were then washed for 3× 5 minutes in ultrapure water to remove unincorporated stain. To resolve protein bands gels were then placed in destaining buffer, again gently heated, and then placed on a rocker for 30 minutes. Finally gels were washed for 3× 5 minutes in ultrapure water prior to photography of visible bands.

2.9.3. Silver Nitrate staining

Where Coomassie staining was insufficiently sensitive to visualise low-abundance bands, silver staining was used as an alternative. This was carried out using a GE healthcare PlusOne kit[1] following the instructions provided (see Appendix 1 for solutions used). Briefly, gels were soaked for 30 minutes in acetic acid/ethanol fixing solution then placed in sensitising solution for 30 minutes under shaking. Gels were washed for 3× 5 minutes in ultrapure water before transfer to 0.1% w/v silver nitrate solution for 20 minutes under shaking. The gels were then washed again for 2× 1 minute in ultrapure water and developed for three minutes with developing solution. Once bands of appropriate intensity were visible the reaction was terminated by immersing gels in stopping solution for 10 minutes under shaking. Finally, gels were washed for 3× 5 minutes in ultrapure water prior to photography of visible bands.

---

[1] GE Healthcare Ltd., Buckinghamshire, UK

2.9.4. Zymography

ACM collected from confluent *Acanthamoeba* cultures was concentrated using a 10kDa column as described in section 2.7.2 yielding a final protein content of 2.5mg/ml. Dilutions of ACM were made in ddH_2O and 15µl of sample mixed with 5µl of non-reducing sample buffer and heated to 75°C, alongside 0.1× Trypsin to act as a control. Samples were then run alongside ColorPlus prestained protein marker[1] using Bio-Rad precast 10% gelatin gels (Bio-Rad, UK)[2] at 110V for 60 minutes. After completion of the run gels were washed in 50mM Tris buffer pH7.5 with 2.5% w/v TritonX-100 for one hour to remove SDS, then 18mΩ distilled water 3× 5 minute washes to remove remaining detergent. Proteins were refolded and the zymogram developed by incubation in 50mM Tris buffer pH7.5 with 0.5M $CaCl_2$ for 3 hours at 37°C after which the gel was again washed for 3× 5 minutes in ultrapure water. Gels were then stained in Coomassie Blue staining buffer for one hour, washed three times in ultrapure water, and then destained for one hour. Finally, gels were washed three times in ultrapure water and photographed using an ImageQuant 300 instrument[3].

[1] New England BioLabs Inc., Ipswich, MA, USA
[2] Bio-Rad Laboratories Ltd., Hemel Hempstead, UK
[3] GE Healthcare Ltd., Buckinghamshire, UK

2.9.5. Antibody cleavage

Fifty millilitres of ACM was collected as described in section 2.2.2 and concentrated using 10kDa Mw columns as per section 2.7.2 yielding a final concentration of 1mg/ml as assessed by Nanodrop. Cleavage reactions were then prepared with 1µg of either mouse IgA[1], IgM[2], IgG[3] or IgE[2] isotype controls, or specific polyclonal IgM generated as described in sections 2.3 and 2.1.4. 3.6µg of concentrated ACM was then added to each reaction. For each antibody class, serine (phenylmethylsulfonyl fluoride (PMSF))[4], cysteine (iodoacetamide)[4] or metalloprotease ((2R,3S)-N4-Hydroxy-N1-[(1S)-2-(methylamino)-2-oxo-1-(phenylmethyl)ethyl]-2-(2-methylpropyul)-3-[(2-thienylthio)methyl] butanediamide (Batimastat))[4] inhibitors were added, to a final concentration of 100µM. Ultrapure water was used to bring the total volume of each reaction to 30µl. Reaction mixes were incubated at 37°C for 2 hours and then subjected to SDS-PAGE under reducing conditions, using 4-20% gradient precast polyacrylamide gels (see section 2.9.1). Gels were subsequently washed for 3× 5 minutes in ultrapure water and silver stained as described in section 2.9.3.

Analysis of cleavage products was performed using ImageJ software (Schneider et al., 2012) using an adapted method of Western blot band density quantification. Briefly, lanes on gel images were delineated using the 'Outline

[1] Alpha Diagnostic International Inc., San Antonio, TX, USA
[2] AbD Serotec Ltd., Kidlington, UK
[3] Sigma-Aldrich Ltd., Gillingham, UK
[4] Tocris Bioscience Ltd., Bristol, UK

Lane' tool and then expressed as density peaks using the Analyze>Gels>Plot Lanes command sequence. Peaks of interest were then identified based on molecular weight and closed off at either side using the 'Straight Line' tool. The 'Wand' tool was then used to collect area measurements. Contributions to peak area by ACM were corrected for by subtracting the area of any ACM peaks at equivalent Mw and the remaining peak areas were expressed as a proportion of the uncleaved control sample.

2.10. Peptide sequence identification by tandem mass spectrometry

Due to the sensitivity of mass spectrometry analysis gel equipment and tanks were washed thoroughly with ultrapure water prior to use. Running and washing buffers were made fresh and used only once and trays used for washing/staining had not previously been used for protein or immunological procedures. Extra caution was used throughout the procedure to avoid keratin contamination. Fresh *A. castellanii* PBS lysate was prepared as described in section 2.2.1, with the addition of 1× P2714 protease inhibitor cocktail[1] to limit sample degradation. Thirteen microliters of 5mg/ml sample was then mixed with 5µl of LDS loading buffer[2] and 2µl of DTT[2], denatured, and run on a precast polyacrylamide gel (see section 2.9.1). After completion of the run the gel was washed for 3× 5minutes in 18mΩ ultrapure water and then stained

[1] Sigma-Aldrich Ltd., Gillingham, UK
[2] Expedeon Ltd., Harston, Cambridgeshire, UK

overnight at 4°C with SafeStain colloidal coomassie blue[1]. Bands were then resolved by 3× 60 minute washes in ultrapure water to remove background staining.

Tandem MS sequencing was performed by Dr S. Liddell at the Sutton Bonington Proteomics Facility, University of Nottingham using standard in-house procedures. Briefly, gel bands were excised with a clean scalpel and diced into cubes (~1mm^3), then placed into individual wells of a microtitre plate. Gel cubes were then processed (destained, reduced, and alkylated) and trypsin digested using standard procedures on the MassPREP station. Digestion buffer was 25mM ammonium bicarbonate; trypsin gold was diluted in this buffer at 10ng/µl and 30µl of the enzyme/buffer mixture was added to each well. Trypsin was allowed to absorb into gel pieces at 4°C for 15 minutes, then digestion proceeded at 40°C for 5 hours. The resulting peptides were delivered via nanoLC to a Q-ToF2 instrument for tandem MS analysis.

An automated experiment (DDA = data dependent acquisition) was run where selected peptides automatically enter MS/MS for fragmentation. The obtained sequence data was then searched against the public databases using MS/MSIONS search on the MASCOT web site using standard default settings. Searches were made against the NCBInr and ESTs databases with the standard variable modifications of 1) carbamidomethylation of Cysteine and 2) oxidation of Methionine. Output was interpreted on the basis of E-values

[1] Sigma-Aldrich Ltd., Gillingham, UK

reported from MASCOT. The level for significance was set as E ≤0.05, representing a less than 5% chance of false-positive identification.

2.11. Bioinformatics

Bionformatics analysis was carried out using a combination of the NCBI and UNIPROT databases and NCBI's Basic Local Alignment Search Tool (BLAST). Sequences were obtained from the UNIPROT and NCBI protein databases and compared with the *A. castellanii* genome assembly using individual queries via the tBLASTn algorithm. Sequences from predicted or observed extracellular domains were used where identified by annotation. Where significant similarity was shown, matching *A. castellanii* transcriptomic sequence was retrieved and translated into protein sequence using the most appropriate reading frame (fewest interrupting STOP codons), identified with SeaView version 4.4.1 software (Gouy et al., 2010). Reciprocal tBLASTn queries were then run, comparing each peptide sequence to all others. Results from reciprocal BLAST were then filtered for stringency. Sequences were accepted as significantly similar if the length of the aligned region was ≥50aa and the E-score for the alignment was ≤0.00001.

2.12. Statistical analyses

Statistical analyses were performed using Prism version 5.04 software (GraphPad Software Inc.)[1]. Types of analysis varied according to the nature of each experiment and are detailed in individual chapters. These included 1-way or 2-way Analysis of Variance (ANOVA), Regression and Mann-Witney tests. Significance levels for individual groups were determined using Bonferroni or Tukey post-tests for each treatment versus a control, or individual comparisons of all treatments. The alpha level for significance was set at $p \leq 0.05$ for all tests.

[1] GraphPad Software Inc., La Jolla, CA, USA

3. Use of polyclonal antibody to investigate pathogenesis of AGE, with focus on *in vitro* functional assays and identifying antigenic targets

3.1. Abstract

In the bloodstream and at the site of blood-brain barrier penetration in the brain microvasculature *A. castellanii* is exposed to host humoral immunity. The host responses and the amoebic antigens that form the target for this response have yet to be fully identified and few studies have focussed on the effect specific antibody has on pathogenesis in AGE. We generated a polyclonal antibody (HE2) by hybridoma fusion and utilised it to investigate binding, monolayer disruption and host cell death in an *in vitro* model of the BBB. HE2 reacted strongly with trophozoite cell surface antigens by immunofluorescence, and caused parasites to aggregate *in vitro*. Binding to endothelial cells was also reduced, albeit to a similar extent as an isotype control; however this did not result in a reduction of host cell death. Disruption of the cell layer was reduced by high concentrations of antibody but this effect was seen in only one of the two *in vitro* assay types employed. Identification of immunodominant antigens using Western blotting and tandem MS sequencing techniques revealed metabolic and protein synthesis enzymes as well as actin as targets of HE2. These data provide insights into *A. castellanii* pathogenesis and the identity of amoeba antigens that serve as targets for immunity.

3.2. Introduction

Acanthamoeba granulomatous encephalitis (AGE) is a disease characterised by the formation of large lesions in neural tissue, and the formation of granulomas comprising of living and dead parasites and host material preceded by loss of integrity in the blood-brain barrier (Martínez et al., 1980). In clinical disease presentation the host response is insufficient to control infection, which as a result is often fatal even with medical intervention (Sarica et al., 2009, Bloch and Schuster, 2005, Carter et al., 1981). Granuloma formation and accompanying neural inflammation depends to a large extent on macrophage and neutrophil recruitment (Guarner et al., 2007, Hurt et al., 2003c, Stewart et al., 1994) however beyond this relatively little is known about the immune response to *Acanthamoeba*. In particular the haematogenous stage of infection, during which trophozoites are exposed to many arms of the host immune system is especially poorly understood. This includes the immune microenvironment at the sites of BBB penetration in the brain microvasculature, and as loss of BBB integrity is a key event in the establishment of AGE it is important to increase our understanding of host and parasite processes occurring in this zone.

One of the ways in which large extracellular pathogens are controlled by the immune system is the secretion of specific antibodies. The role of antibody within the host immune response includes: initiation of the complement cascade resulting in pathogen lysis, recruitment and activation of other immune cells at sites of infection, and limiting pathogen motility by aggregation. Their high specificity for target antigens is the basis for recognition of a wide variety of infectious agents. This results from

hypervariability in the F*ab* (variable) region of the molecule, variants of which are generated during somatic recombination in B-cells. Serum antibody is of particular importance in haematogenous parasitic infections as the pathogen in question may be too large to be ingested by phagocytes and must therefore be targeted by the complement lysis cascade. Parasite material and fragments are then phagocytised in order to promote antigen presentation to effector and helper cells. Additionally antibody is of importance in inactivating pathogen excretory/secretory (E/S) proteins, for example neutralisation of parasite proteases and bacterial toxins (Smith et al., 1994, Adekar et al., 2008). *Acanthamoeba* is known to express several classes of secreted protease (Ferreira et al., 2009, Kim et al., 2003, Na et al., 2001) and so neutralisation by antibody is likely to be of importance in AGE.

Due to their specificity antibodies are also very useful tools for molecular dissection of parasite antigens. For example, antibody generated from *in vivo* infections can assist in the identification of antigens important for immune recognition of a pathogen. Additionally, specific immunoglobulin is a valuable diagnostic marker for infection and can also be used for therapeutic purposes. In the particular case of *Acanthamoeba* there have been attempts by several groups to develop specific monoclonal antibodies using differing methodological approaches. Khan *et al.* used phage display technology, panning against amoeba antigens to identify molecules with novel specificities (Khan et al., 2000a). By contrast Kennett *et al.* and Turner *et al.* adopted a more classical approach based on polyethylene glycol (PEG) fusion (Turner et al., 2005, Kennett et al., 1999). Both approaches yielded specific antibody however they have yet to enter routine use due to low specificity and the

difficulty of identifying clones that react well with both trophozoites and cysts (Turner et al., 2005). Additionally, where reactivity to both life stages of the parasite was shown, specific antigen targets were not determined and as such relevance to known mechanisms of pathogenesis remains to be demonstrated.

In this study our aim was to understand the role played by the humoral immune response in the interactions between trophozoites and the microvascular endothelium and to examine relevance to pathogenesis. To accomplish this polyclonal antibody was generated by classical hybridoma fusion from immunised BALB/c mice. One strongly reacting clone was tested against a range of parameters in an *in vitro* model of the blood-brain barrier. We then used immunological methods to identify immunodominant antigens and assigned sequence identities based on peptide fragments retrieved by tandem MS sequencing. This study contributes to the understanding of important antigens expressed by *A. castellanii* during infection, and also the role played by specific antibody in controlling AGE at the endothelium.

3.3. Materials and Methods

3.3.1. Antibody generation

Polyclonal hybridomas were generated from splenocytes of BALB/c mice immunised with 2×10^7 trophozoites in Alum using a protocol of three bi-weekly injections as described in sections 2.3.1 and 2.3.2. Terminal blood serum was collected (section 2.3.3) and used to assess IgG levels in immunised mice by ELISA (section 2.6.1 and 2.6.1.1). Splenocytes were collected

aseptically from mouse spleens and fused with Sp2/0 mouse myelomas using PEG (sections 2.3.4 and 2.3.5) to produce hybridomas for downstream use.

3.3.2. Screening – ELISA

Microtitre plates were coated with *A. castellanii* PBS lysate then blocked and incubated with either dilutions of mouse serum, cell culture supernatant or purified polyclonal antibody as described in section 2.6.1. For initial IgG screening of mouse hyperimmune serum, secondary reagents and detection chemistry was based on alkaline phosphatase as described in section 2.6.1.1. Thereafter ELISAs used were based on HRP detection chemistry (see section 2.6.1.2).

3.3.3. Screening – Dot Blot

50µg/ml *Acanthamoeba* PBS lysate (prepared as described in section 2.2.1) was blotted onto subdivided nitrocellulose membrane, which was then dried and blocked. Test samples (either culture supernatant, dilutions of positive/negative serum or isotype control antibody) were then added to blots, and binding detected by addition of anti-IgG and anti-IgM secondary antibodies (Table 2.2 #6 and 8) as described in section 2.6.2.

3.3.4. Screening – Immunofluorescence

A. castellanii trophozoites were affixed to microscope slides by cytospin, blocked and treated with neat culture supernatant, 1:500 serum dilutions,

2µg/ml purified polyclonal antibody or 2µg/ml isotype control antibody as described in section 2.6.4. Primary antibody was detected using 1:500 goat anti-mouse IgG – Texas Red conjugate (Table 2.2 #12) or 1:500 goat anti-mouse IgM – FITC conjugate (Table 2.2 #11) and cells were counterstained with DAPI. Photomicrographs were taken using exposures of 300ms (360nm filter), and 500ms (480nm and 640nm filters). Gamma and gain settings were both 1×.

3.3.5. Purification

Unpurified bulk culture supernatant was collected from polyclonal hybridoma cultures (section 2.1.4) and concentrated using regenerated cellulose columns as described in section 2.5.2. Concentrated antibody solutions were then purified by elution from immunoaffinity column as described in section 2.5.3. Purified antibody was then dialysed into PBS for use *in vitro* (see section 2.5.4), quantified (section 2.5.1) and if necessary re-concentrated to obtain solutions of the required strength.

3.3.6. Functional assays

HBMEC were cultured as described in section 2.1.2 and grown in 24 or 48-well plates (section 2.4.1). 2×10^5 *A. castellanii* trophozoites were incubated with 200µg/ml of purified polyclonal antibody or isotype control in RPMI at 37°C under constant motion prior to use *in vitro* as described below.

3.3.7. Binding inhibition

Binding of treated trophozoites was assessed by haemocytometer counts of unbound amoeba from 24 or 48-well plates, as described in section 2.4.3.1.

3.3.8. Monolayer protection

Protection of HBMEC monolayers was assessed using both haematoxylin staining of fixed monolayers and photomicrographs taken during the experimental period (see section 2.4.4). Monolayer disruption visible in photomicrographs was quantified using a grid counting method as described in section 2.4.4.2.

3.3.9. Aggregation

Trophozoites were treated with specific and nonspecific antibody for 3 hours as described above (section 3.3.6). Cell suspensions were then deposited in 24-well plates, photographed and the degree of aggregation scored qualitatively using the method outlined in section 2.4.7.

3.3.10. Cytotoxicity

Cytotoxicity in treated HBMEC was examined by detection of LDH release into culture supernatants. Samples were collected after 24 hours and assessed as described in section 2.4.5.

3.3.11. Western Blotting

Following SDS-PAGE of amoeba lysate (see section 2.7.1), samples were electrotransferred to PVDF membrane and probed with specific (HE2), or nonspecific IgM antibody. Bands were then detected with anti-IgM secondary reagent and ECL^{+} chemiluminescent substrate, and exposed to X-ray film. Full details are given in section 2.6.3.

3.3.12. Tandem mass spectrometry (MS/MS) sequencing

A. castellanii lysate (see section 2.2.1) was resolved by SDS-PAGE under ultra-clean conditions and bands of interest corresponding to those recognised by specific polyclonal antibody on Western blot were excised and peptide fragments sequenced using MS/MS methodology (see section 2.8). Sequence data was searched against the NCBInr and ESTs public databases using MS/MSIONS search on the MASCOT web site. Output was interpreted on the basis of E-values reported from MASCOT. The level for significance was set as $E \leq 0.05$, representing a less than 5% chance of false-positive identification.

3.3.13. Statistical analysis

Analyses were performed using GraphPad Prism software version 5.04. Data was analysed using 1-way ANOVA for multiple group comparisons. Analysis of seroconversion data was conducted using the nonparametric Mann-Witney test due to the presence of unequal sample numbers per group. The alpha level for significance was set at $p \leq 0.05$ for all tests (see section 2.10).

3.4. Results

3.4.1. Mice seroconvert in response to immunisation with *Acanthamoeba*

Immunisation of mice with *A. castellanii* produced a strong response as demonstrated by ELISA (Figure 3.1). Conversely, unimmunised mice showed a weakly positive response at low dilutions, however this is consistent with background serum reactivity seen in other studies (Cerva, 1989, Chappell et al., 2001, Schuster et al., 2006, Kiderlen et al., 2009). Immunised mice demonstrated significantly higher serum antibody titres compared with unimmunised animals (Mann-Whitney test, $p<0.05$). It was possible to clearly distinguish between positive and negative reactions at dilutions up to 1 in 500 using pooled sera from immunised versus unimmunised animals.

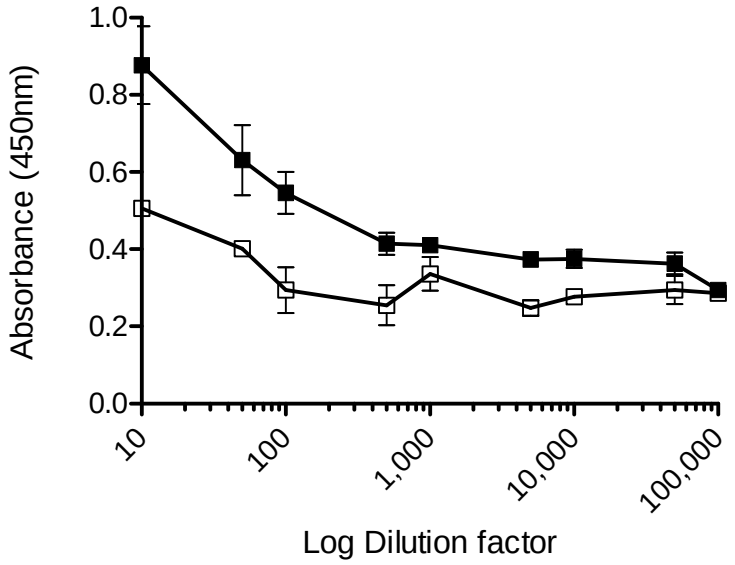

Figure 3.1 Mice produced a positive immune response against *Acanthamoeba* by ELISA. Serum was collected from mice immunised with 10^7 trophozoites in PBS + Alum and a control group immunised with PBS + Alum alone. Plates were coated with 10µg/ml amoeba lysate, blocked overnight and then incubated with a range of serum dilutions for 90 minutes. Plates were washed several times and bound antibody detected with goat anti-mouse IgG conjugated to alkaline phosphatase. Immunised mice showed higher antibody titres than unimmunised mice (Mann-Whitney, $p<0.05$). Values are mean ± S.E.M. from four immunised mice (filled points) and two negative control mice (open points).

3.4.2. Fused hybridoma colonies produced specific IgG and IgM

Given the positive immune response seen in experimental mice, splenocytes were extracted and fused with Sp2/0 myelomas as detailed in section 2.3.4 and 2.3.5. Fused cultures were tested for IgG, IgM and IgA using class-specific secondary antibodies. Wells were considered positive if they showed absorbance equal to or higher than a 1:500 dilution of negative serum (abs = 0.1). Under these criteria IgG and IgM positive wells were identified from four

plates tested. Six plates were tested for IgA but showed no response above background levels. Wells demonstrating the highest absorbance readings were picked from each plate and cell populations expanded by subculture in 25cm^3 tissue culture flasks. After a week of growth cultures were examined visually to determine which had survived transfer.

Non-proliferating clones were discarded and flasks with visible colonies were screened by ELISA for the continued presence of antibody using IgG and IgM-specific detecting reagents. 32 hybridoma pools tested positive for a combination of one or both isotypes at this stage (Figure 3.2). All 32 clones were subcultured to select for ability to sustain *in vitro* growth and hybridoma populations which died at this stage were discarded.

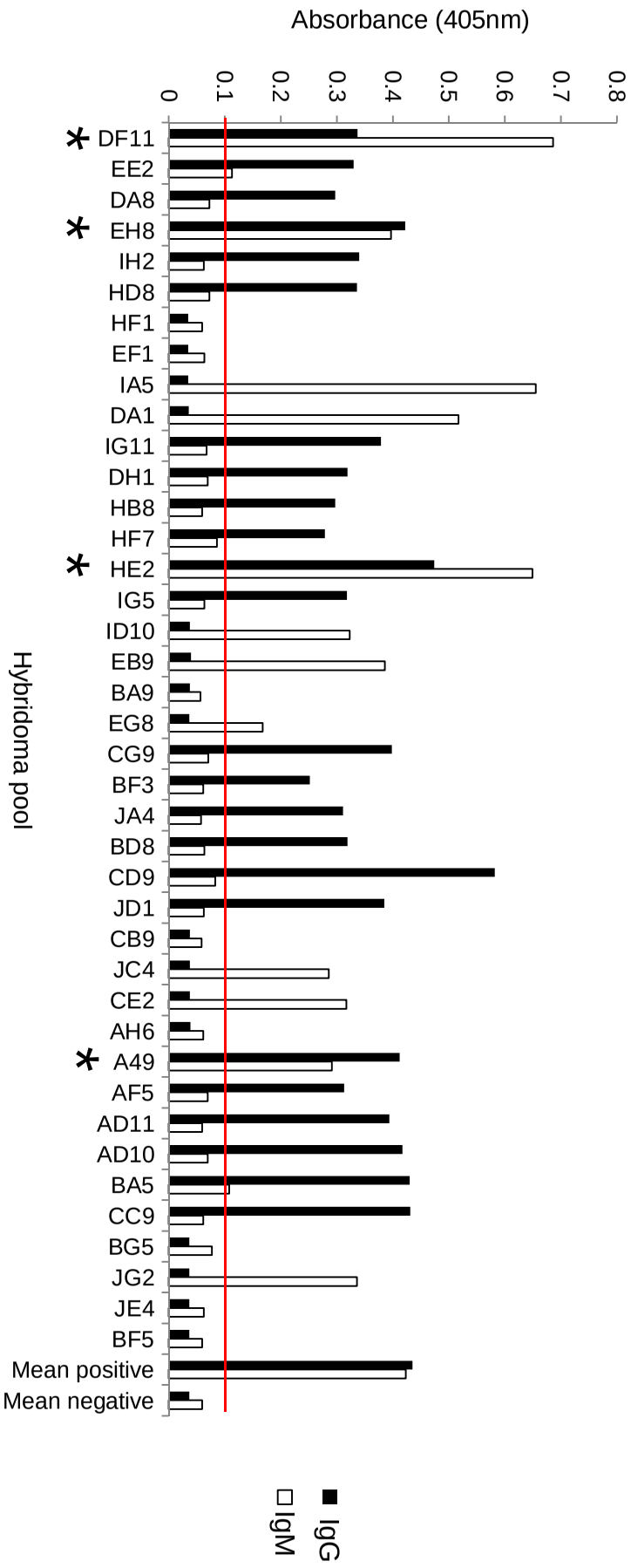
Absorbance (405nm)
0
0.1
0.2
0.3
0.4
0.5
0.6
0.7
0.8
Hybridoma pool
DF11
EE2
DA8
EH8
IH2
HD8
HF1
EF1
IA5
DA1
IG11
DH1
HB8
HF7
HE2
IG5
ID10
EB9
BA9
EG8
CG9
BF3
JA4
BD8
CD9
JD1
CB9
JC4
CE2
AH6
A49
AF5
AD11
AD10
BA5
CC9
BG5
JG2
JE4
BF5
Mean positive
Mean negative
IgG
IgM

Figure 3.2 Hybridoma anti-*Acanthamoeba* antibody secretion.

32 of 40 hybridoma pools test positive for secretion of A. castellanii-specific IgG, IgM or both. ELISA plates were coated with 1µg/ml of sonicated PBS extract of amoeba. Plates were washed and blocked with PBST + 5% milk protein and 50µl of supernatant from hybridomas cultures added and incubated for 90 minutes at room temperature. Antibody was detected with goat anti-mouse IgG (γ-chain specific) and goat anti-mouse IgM conjugated to horseradish peroxidase, diluted 1:1000 in PBST (see section 2.2.3). Wells displaying absorbance of >0.1 (red line) were considered positive. *denotes hybridomas testing positive for both IgG and IgM.

3.4.3. Immunofluorescence analysis of positive clones

Hybridoma pools displaying the strongest ELISA signal and most robust growth characteristics were examined using immunofluorescence assays in order to assess binding specificity and antibody target site. Binding of both IgG and IgM isotypes was tested for each clone. In the IgG assay, hybridomas DA1, DF11 and HE2 demonstrated higher levels of fluorescence than negative control samples, however in all cases signal was weak relative to the positive control. Staining was largely localised in the cytoplasm, although reactivity with the membrane was seen with DF11 (Figure 3.3 D).

In the IgM assay, only hybridomas IA5 and HE2 produced fluorescence above background levels. Signal for both clones was strong relative to the positive control and showed specific localised staining. Fluorescence was observed in both the cytoplasm and on the cell membrane for HE2 supernatants (Figure 3.4 F), but was tightly confined to the nucleus in IA5 (Figure 3.4 E). Acanthopodia were also visibly stained by HE2 antibodies raising the possibility that antigens for this hybridoma might be concentrated in these membrane structures.

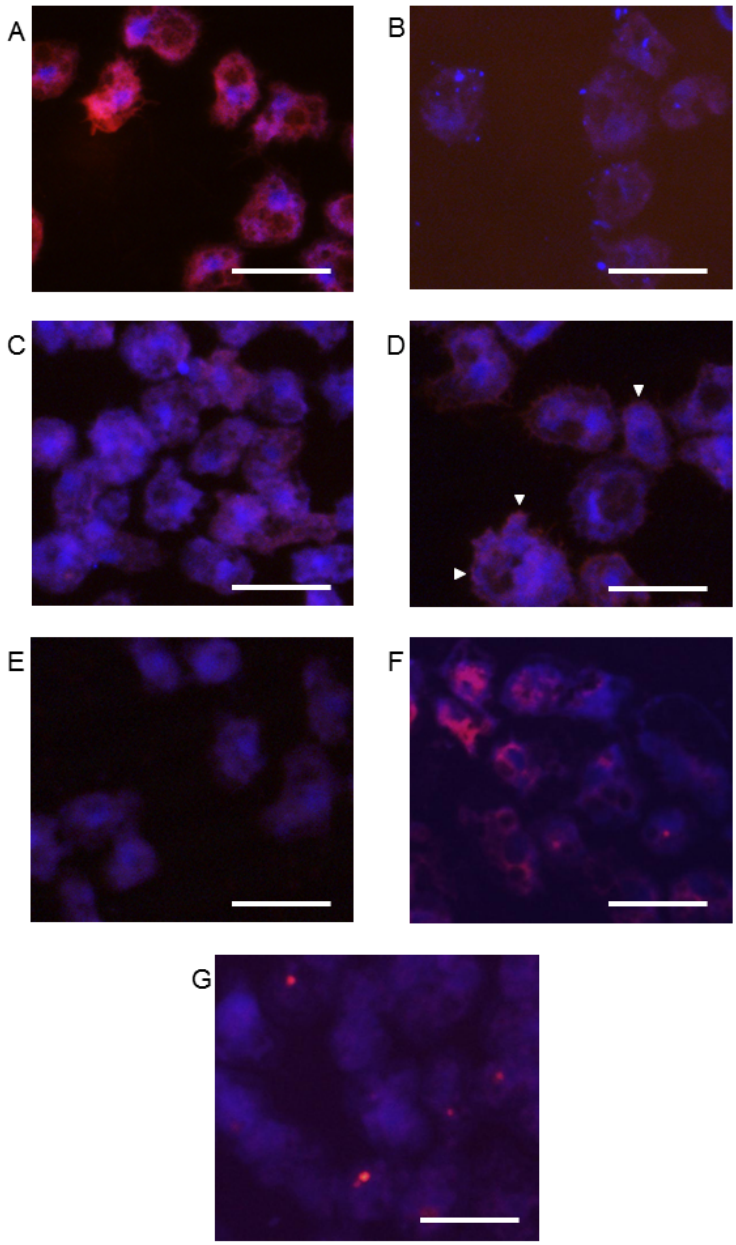

Figure 3.3 Supernatants from hybridomas contain *Acanthamoeba*-specific IgG.

Fixed *A. castellanii* trophozoites were blocked and incubated with 1:500 hyperimmune mouse positive/negative control serum, or neat supernatants from hybridoma cultures. Texas Red-conjugated anti-mouse IgG secondary antibody was then used to detect binding and nuclei were counterstained with DAPI. (A) Positive serum, (B) negative serum, (C) DA1 hybridoma, (D) DF11 hybridoma, (E) IA5 hybridoma, (F) HE2 hybridoma, (G) CD9 hybridoma. Arrows indicate sites of membrane staining. Bar = 50µm.

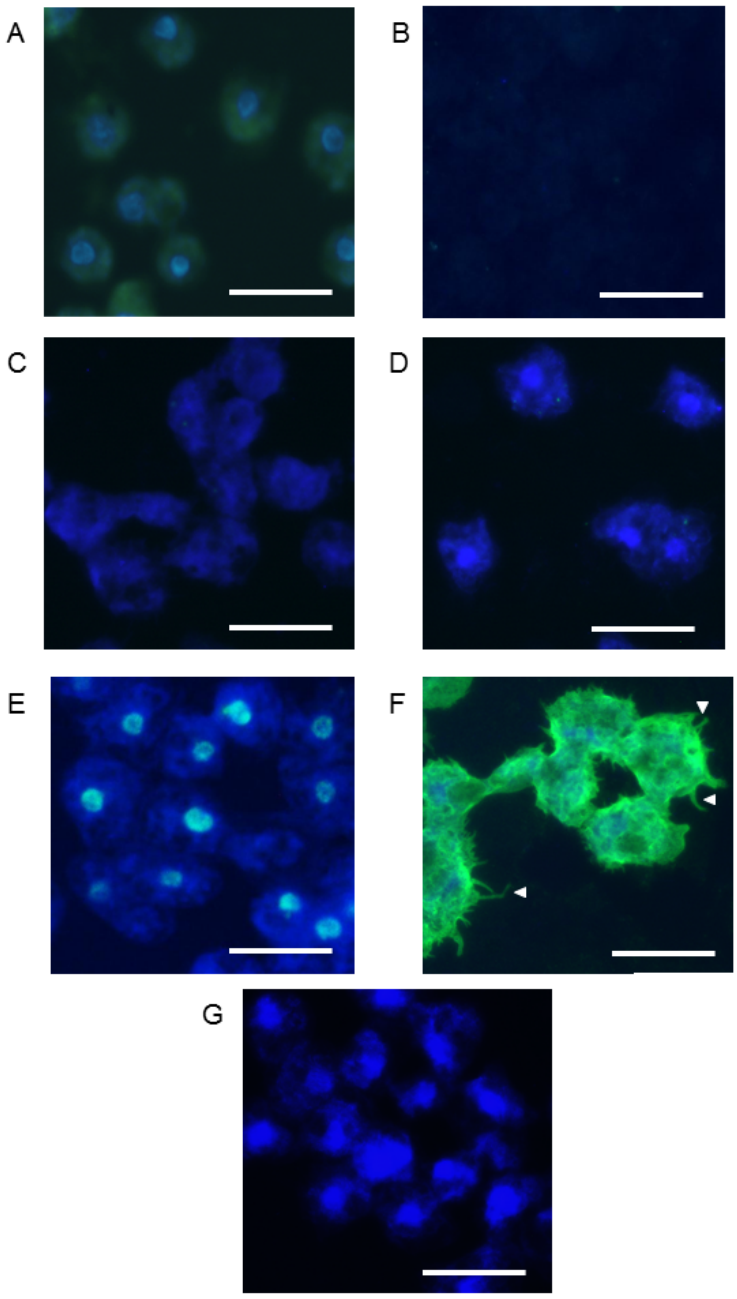

Figure 3.4 Supernatants from hybridomas contain *Acanthamoeba*-specific IgM.

Fixed *A. castellanii* trophozoites were blocked and incubated with 1:500 hyperimmune mouse positive/negative control serum, or neat supernatants from hybridoma cultures. FITC-conjugated anti-mouse IgM secondary antibody was then used to detect binding and nuclei were counterstained with DAPI. (A) Positive serum, (B) negative serum, (C) DA1 hybridoma, (D) DF11 hybridoma, (E) IA5 hybridoma, (F) HE2 hybridoma, (G) CD9 hybridoma. Arrows indicate staining of acanthopodia. Bar = 50µm.

3.4.4. Clone HE2 reacts with a PBS lysate of *Acanthamoeba* by dot blot

The hybridoma pool with the strongest responses from ELISA and IF assays were screened by dot blot against a trophozoite lysate. IA5 supernatant showed no reaction when screened for IgG (Figure 3.5 A) but was positive for the presence of IgM, although at lower levels than was observed in positive controls (Figure 3.5 B). By contrast HE2 supernatant reacted with a response against amoeba lysate of equal magnitude to positive serum, using both anti-IgG and anti-IgM secondary antibody (Figure 3.5 A and B). Levels of IgM in particular were high in comparison to controls, and in accordance with the strong absorbance and fluorescence readings seen in previous assays.

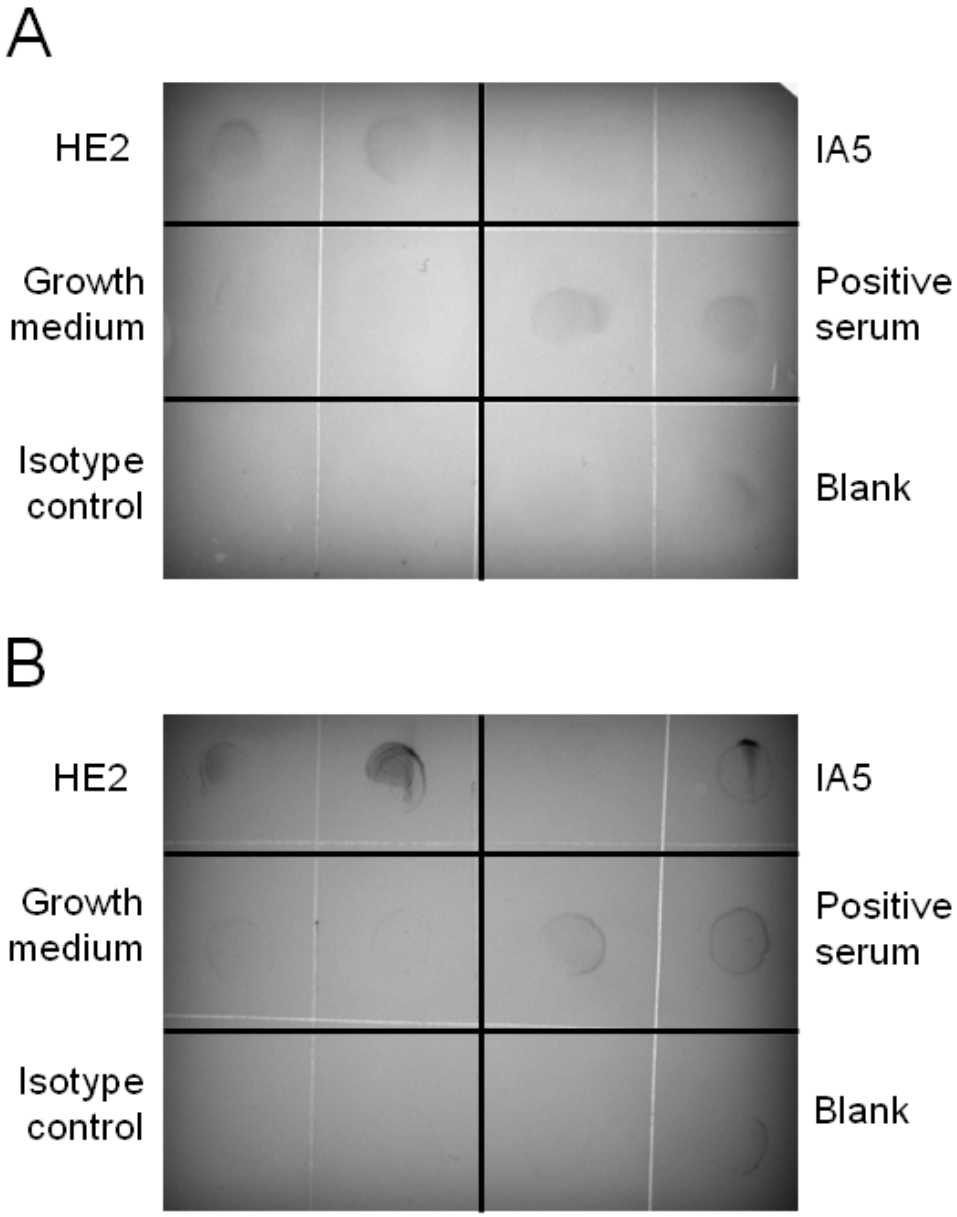

Figure 3.5 IA5 and HE2 supernatants react with *A. castellanii* lysate by dot blot.

Amoeba lysate was spotted onto nitrocellulose membrane, blocked, and probed with unpurified culture supernatants from cultures of IA5 and HE2 hybridomas. Binding was detected with HRP-conjugated anti-IgG or anti-IgM secondary antibody and developed with TMB substrate. (A) Anti-IgG secondary, (B) anti-IgM secondary. Samples were loaded and probed in duplicate.

3.4.5. Unpurified hybridoma culture supernatants do not reduce amoeba binding to HBMECs

Having established reactivity of hybridoma culture supernatants with both *A. castellanii* lysate (ELISA, dot blot) and whole trophozoites (IF), we sought to observe whether hybridoma supernatants produced any functional effects in the context of parasite binding or host cell pathology. Trophozoite suspensions were prepared in hybridoma supernatant as described in section 3.3.6. Suspensions were then used to infect cultures of HBMEC in 24-well tissue culture plates (see section 3.3.6.1 and 2.4.3.1) with binding assessed by haemocytometer count (section 2.4.3.1). Data analysis showed no significant difference between any treatment groups ($p>0.05$, 1-way ANOVA, Figure 3.6) however binding did appear reduced in the HE2 treatment group.

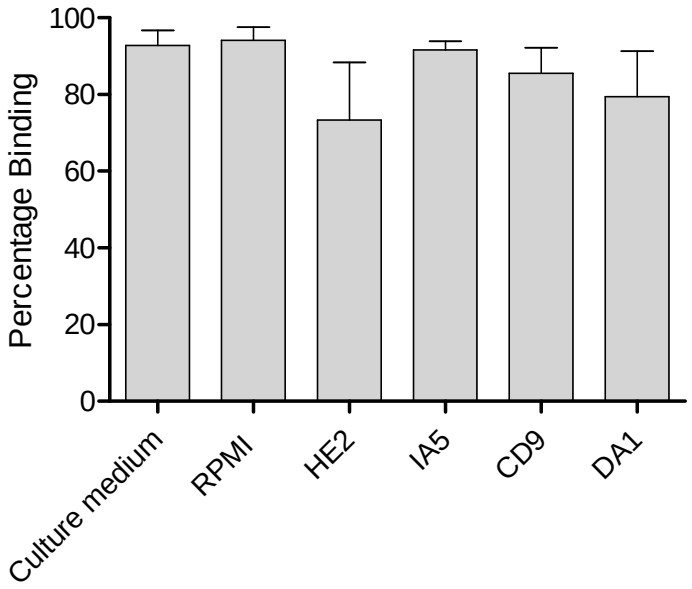

Figure 3.6 Hybridoma supernatants do not decrease binding of trophozoites to HBMEC monolayers.

Trophozoites were treated with hybridoma supernatants and used to infect HBMEC monolayers in 24-well plates. Numbers of unbound amoeba were counted in triplicate by haemocytometer after 3 hours, and used to calculate percentage binding. No significant differences were seen between treatment groups ($p>0.05$, 1-way ANOVA). Each treatment was performed in triplicate and results are mean + S.E.M. from three independent experiments.

Additionally there was a slight effect in terms of monolayer protection as assessed by post-infection staining of infected monolayers. Monolayers fixed and stained with haematoxylin (see sections 2.4.4.3) showed marginally reduced disruption of the cell layer in wells containing HE2-treated trophozoites (Figure 3.7), compared with other hybridomas and controls. Taken together with data from Figure 3.6 this implied that greater functional effects on pathogenesis by HE2 might be detected using purified antibody at higher concentrations. We therefore used purification procedures described in

section 2.5 to obtain purified HE2 IgM and then repeated and extended the presented range of immune- and functional assays.

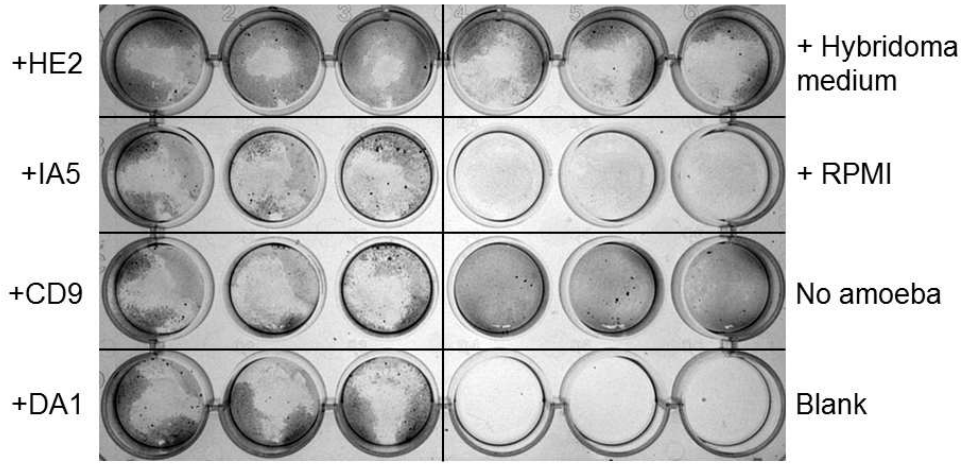

Figure 3.7 Hybridoma supernatants provide partial protection from monolayer destruction by trophozoites.

Trophozoites were treated with hybridoma supernatants and used to infect triplicate HBMEC monolayers in 24-well plates. Monolayers were fixed and stained with haematoxylin after 24 hours. All hybridomas and hybridoma growth medium provided partial protection from monolayer disruption, with HE2 supernatants having the greatest protective effect. Results are representative of three independent experiments.

3.4.6. Purified HE2 polyclonal antibody maintains reactivity with *Acanthamoeba* trophozoites

On the basis of strong responses and membrane reactivity (see sections 3.4.2 to 3.4.4) the hybridoma HE2 was selected as a source of antibody for use in subsequent assays. In order to obtain purified antibody solution with which to work, HE2 supernatants were collected and then purified as described in section 2.5. Purified solutions were then used in immunofluorescence assays

(section 3.3.4) to ensure that the purification process had no adverse effects on the strength or specificity of antibody binding.

Compared with positive control serum and a negative IgM isotype control purified HE2 maintained a high level of binding to *A. castellanii* trophozoites. Levels of fluorescence were consistent with those seen in assays conducted with unpurified culture supernatant (see Figure 3.4) and as before, were in excess of that seen in the positive control sample. Purified HE2 also retained membrane binding specificity including localisation to acanthopodia (Figure 3.8 C, white arrows).

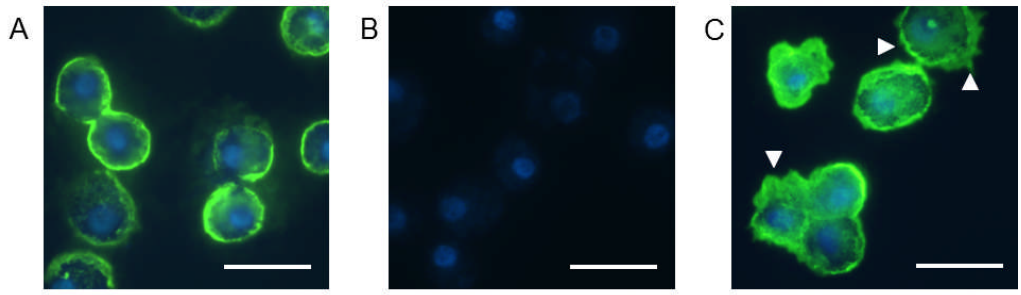

Figure 3.8 Purified HE2 supernatant retains membrane binding activity.

Fixed *Acanthamoeba* trophozoites were blocked and incubated with 1:500 hyperimmune mouse positive control serum, IgM isotype control, or purified HE2 antibody. 1:500 FITC-conjugated anti-mouse IgM secondary antibody was then used to detect binding and nuclei were counterstained with DAPI. (A) Positive serum, (B) isotype control, (C) HE2. Arrows indicate membrane staining and acanthopodia. Bar = 50µm.

3.4.7. Unpurified and purified HE2 culture supernatants cause aggregation of *Acanthamoeba* trophozoites

The antibody produced by the HE2 hybridoma displayed characteristics of membrane reactivity and belonged to the IgM class. This class of antibody has a pentameric structure constructed around a central conserved J-chain which promotes agglutination of its target, immobilising recognised pathogens and enhancing detection and destruction by the immune system. Because of these characteristics we hypothesised that HE2 might have agglutination activity against *A. castellanii* trophozoites, and that this might provide protection in terms of parasite binding, or host cell death/monolayer disruption. Figure 3.9 and Table 3.1 show that aggregates of amoeba cells do indeed form *in vitro* and that this effect is specific, as an isotype control IgM did not produce an equivalent effect. However the ability of both unpurified and purified HE2 to agglutinate trophozoites diminishes after 24 hours, potentially due to degradation by the amoeba. This possibility is discussed further in Chapter 4.

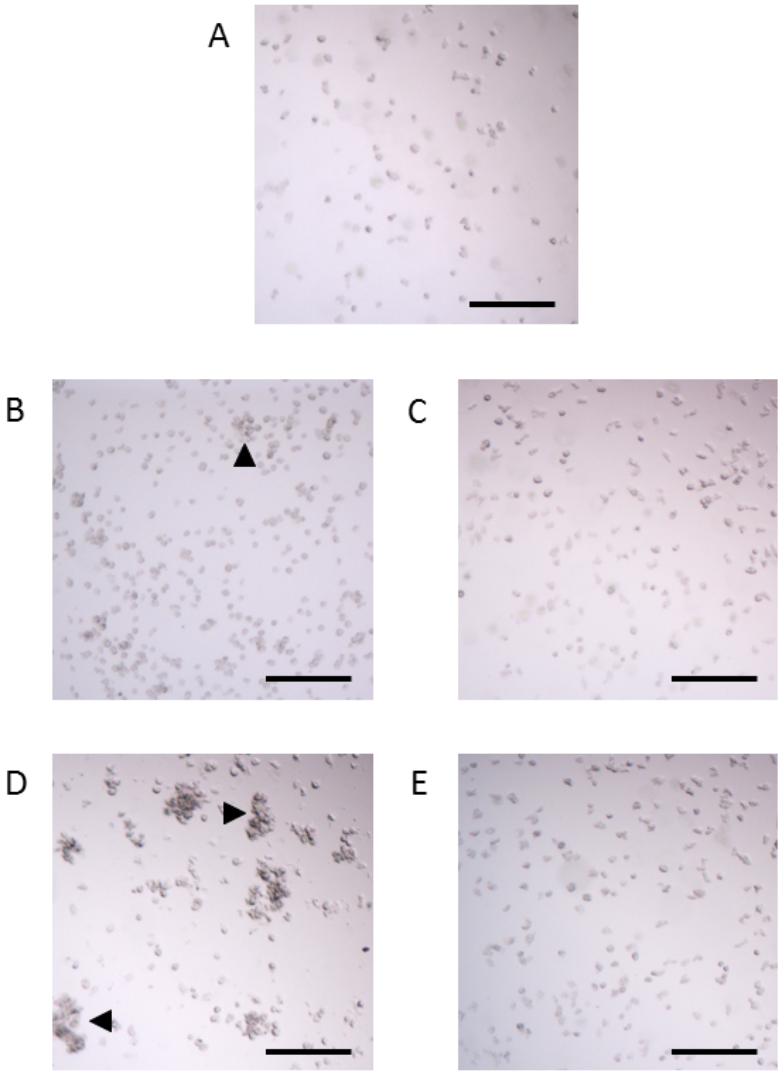

Figure 3.9 Unpurified and purified HE2 supernatant causes trophozoites to aggregate in vitro.

Suspensions of trophozoites were made in unpurified HE2 culture supernatant, control hybridoma medium; 200µg/ml purified HE2, 200µg/ml isotype control IgM or RPMI alone and incubated under constant mixing for 3 hours. (A) RPMI negative control, (B) HE2 unpurified culture supernatant, (C) hybridoma growth medium, (D) purified HE2, (E) isotype control IgM. Images are representative of results from three independent experiments. Arrows indicate trophozoite aggregation. Bar = 200µm.

	Unpurified HE2			Hybridoma medium	Purified HE2			Isotype control	RPMI (-ve control)
	A	B	C		A	B	C		
3h	+	+	++	+/-	+	+++	+++	+/-	-
	+	+/-	+	-	++	+++	+++	+/-	-
	++	+/-	+	-	+	+++	+++	-	-
24h	+	-	+	+	+	+	+	+	+/-
	+	+/-	++	+/-	+/-	++	+	+/-	+/-
	+	+/-	+	+	+/-	++	+/-	+/-	+/-

Table 3.1 Trophozoite aggregation in unpurified and purified HE2 supernatant.

After incubation for 3 and 24 hours. (A, B, C) represent three different antibody batches. Results are from three independent experiments.

3.4.8. Purified HE2 antibody reduces trophozoite binding, but to no greater extent than an isotype control IgM

HE2 antibody had demonstrated an ability to bind to membrane antigens of *A. castellanii* trophozoites and cause them to aggregate (sections 3.4.6 and 3.4.7). We hypothesised that this may affect trophozoites' ability to bind to HBMEC *in vitro* and investigated this possibility by infecting monolayers with pre-adsorbed amoeba and measuring percentage binding as described in sections 3.3.6.1 and 2.4.3.1. HE2-treated trophozoites behaved as predicted, showing a significant decrease of approximately 20% ($p<0.001$ 1-way ANOVA) in comparison with an untreated positive control. However this was matched by an equivalent inhibition of binding in samples treated with a nonspecific isotype negative control IgM.

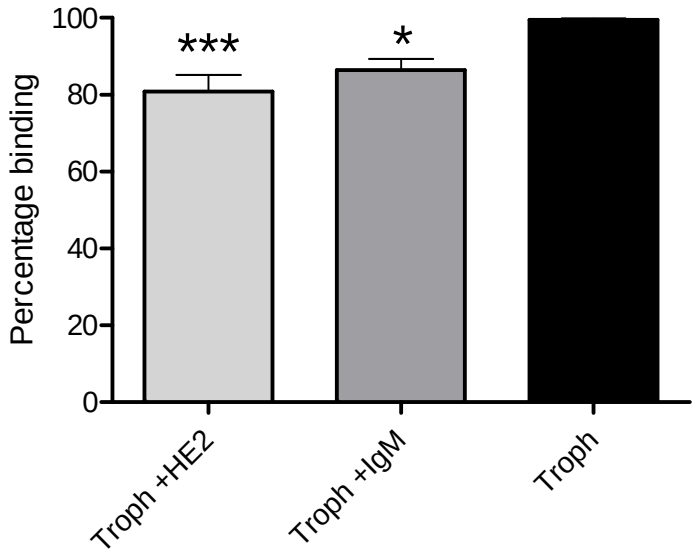

Figure 3.10 Binding to HBMEC of trophozoites pre-adsorbed with specific/nonspecific antibody.

Suspensions of 2×10^5/ml trophozoites treated with 200µg/ml HE2, isotype control IgM, or left untreated were used to infect HBMEC monolayers. Binding was assessed by triplicate haemocytometer counts after 3h. Each treatment was performed in triplicate and results are mean + S.E.M. from three independent experiments. *** $p< 0.001$, * $p< 0.05$, 1-way ANOVA.

3.4.9. HE2 does not protect HBMEC monolayers from damage

Binding assays suggested that IgM antibody (both specific and nonspecific) acted to reduce the percentage of amoeba binding to HBMEC monolayers *in vitro* (section 3.4.8, Figure 3.10). We sought to determine whether this effect was matched by a reduction in measures of pathology and cell death using methods outlined in sections 3.3.6.2 and 3.3.6.4.

3.4.10. Haematoxylin staining

Monolayers fixed and stained with haematoxylin as described in section 2.4.4.3 showed no substantial reduction in disruption of the cell layer in any treated well (Figure 3.11), although very small patches of the monolayer were preserved by the highest concentration (200µg/ml) of HE2 and to a lesser extent by isotype IgM.

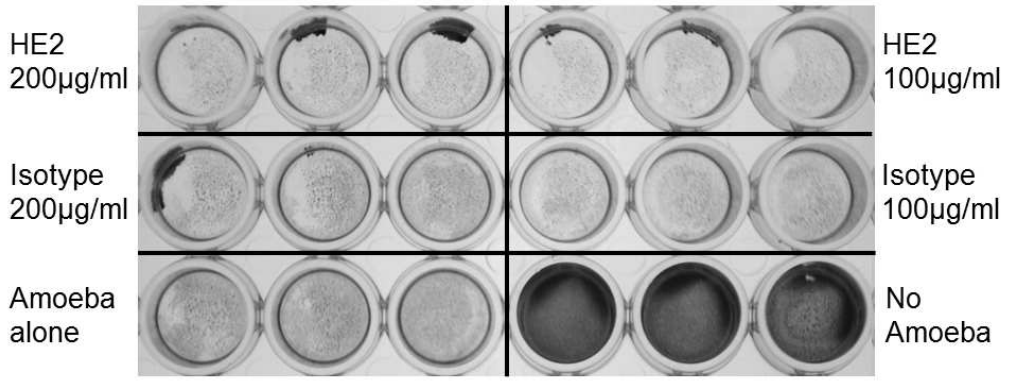

Figure 3.11 HE2 and isotype control IgM do not protect HBMEC monolayers from destruction by trophozoites.

Trophozoites were treated with HE2 and isotype IgM at two concentrations and used to infect HBMEC monolayers in 24-well plates. Monolayers were fixed and stained with haematoxylin after 24 hours. No treatment provided substantial protection against monolayer protection. Results are representative of three independent experiments.

3.4.11. Monolayer counting

Prior to the fixation step for haematoxylin staining (see section 3.4.9.1), wells were photographed and analysed for monolayer disruption using a grid counting method as described in section 2.4.4.2. Results were similar to those seen with haematoxylin staining, although the higher concentration of HE2 did

produce a small but significant protective effect when compared with a positive control of untreated amoeba ($p<0.05$, 1-way ANOVA, Figure 3.12.). The magnitude of this effect was small however (approximately 10%), in accordance with data obtained from other assays (see Figures 3.7 and 3.10).

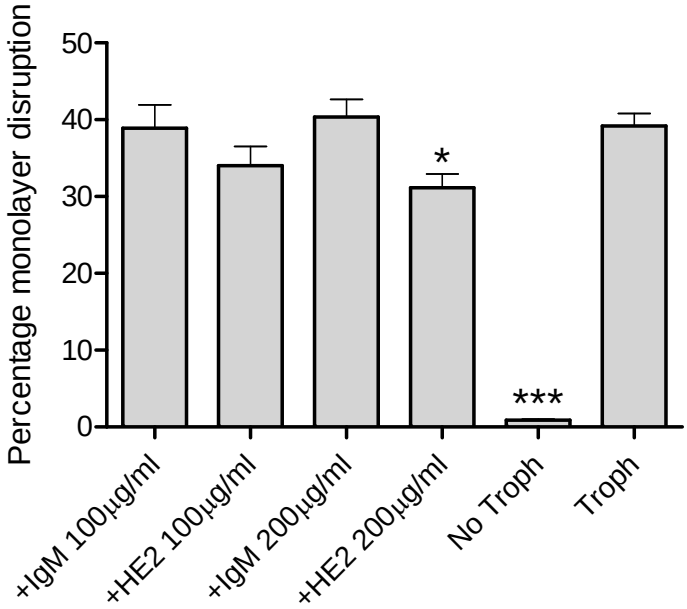

Figure 3.12 Treatment with antibody reduces percentage monolayer disruption only with high concentrations of HE2.

Trophozoites were treated with HE2 and isotype IgM at two concentrations and used to infect HBMEC monolayers in 24-well plates. Percentage monolayer disruption was estimated from photomicrographs by a grid counting method. Significant reductions were seen in 200µg/ml HE2 treatment (* $p<0.05$) and in controls without trophozoites (*** $p<0.001$, 1-way ANOVA). Each treatment was performed in triplicate and results shown are mean + S.E.M from three independent experiments.

3.4.12. Cytotoxicity

Assays of monolayer disruption in sections 3.4.9.1 revealed that HE2 or isotype IgM did not prevent monolayer disruption at the gross level, although at the microscopic level there was some suggestion that high concentrations of HE2 could increase monolayer protection (section 3.4.9.2, Figure 3.12). These parameters do not necessarily correlate with cell death however, and so in order to measure the necrotic response directly, supernatants from treated wells were examined for release of LDH as a measure of cell death (see sections 3.3.6.4 and 2.4.5). Results showed that although a small reduction is apparent by eye, in accordance with data from other assays there was no significant difference between the percentage cell death in any of the treatment groups ($p>0.05$, 1-way ANOVA, Figure 3.13), or relative to a positive control of untreated amoeba.

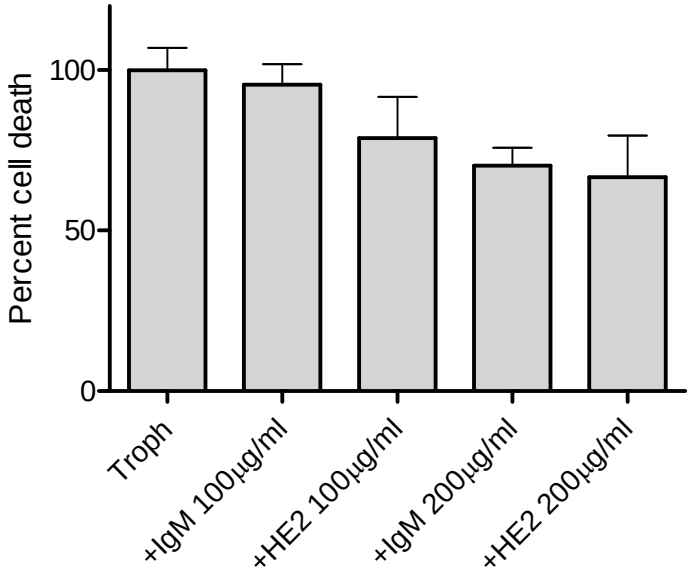

Figure 3.13 HE2 and isotype control IgM do not affect LDH release from HBMEC.
Trophozoites were treated with HE2 and isotype IgM at two concentrations and used to infect HBMEC monolayers in 24-well plates. Culture supernatants were collected after 24 hours and analysed for LDH release, relative to a 100% cell lysis control. Each treatment was performed in triplicate. No treatment caused significant differences in percentage cell death ($p>0.05$ 1-way ANOVA). Results are mean + S.E.M from three independent experiments.

3.4.13. Western Blot

Assays investigating the properties of HE2 in respect of *A. castellanii* binding and pathological responses of HBMEC had proved inconclusive using a range of *in vitro* assays. Therefore in order to gain an insight into antigenic targets, Western blots were prepared and probed with purified HE2 and isotype control as described in sections 3.3.7 and 2.6.3. The polyclonal nature of the antibody, and the fact that it was raised against a mixed antigen target meant a range of

bands of different sizes was recognised in a range of 30 to >175kDa (Figure 3.14).

Blots that corresponded to high abundance bands seen on an SDS-PAGE gel of the same amoeba lysate used for the blot were predicted to be of importance in the immune response. Bands of particular interest were seen at just over 50kDa, 80kDa, and three between 120kDa and 140kDa (Figure 3.14, marked as 5, 4, 2/3, and 1 respectively.) Bands identified at these molecular weights were excised from the gel (Figure 3.14, panel C) and analysed by tandem MS sequencing, in order to ascertain antigen identity.

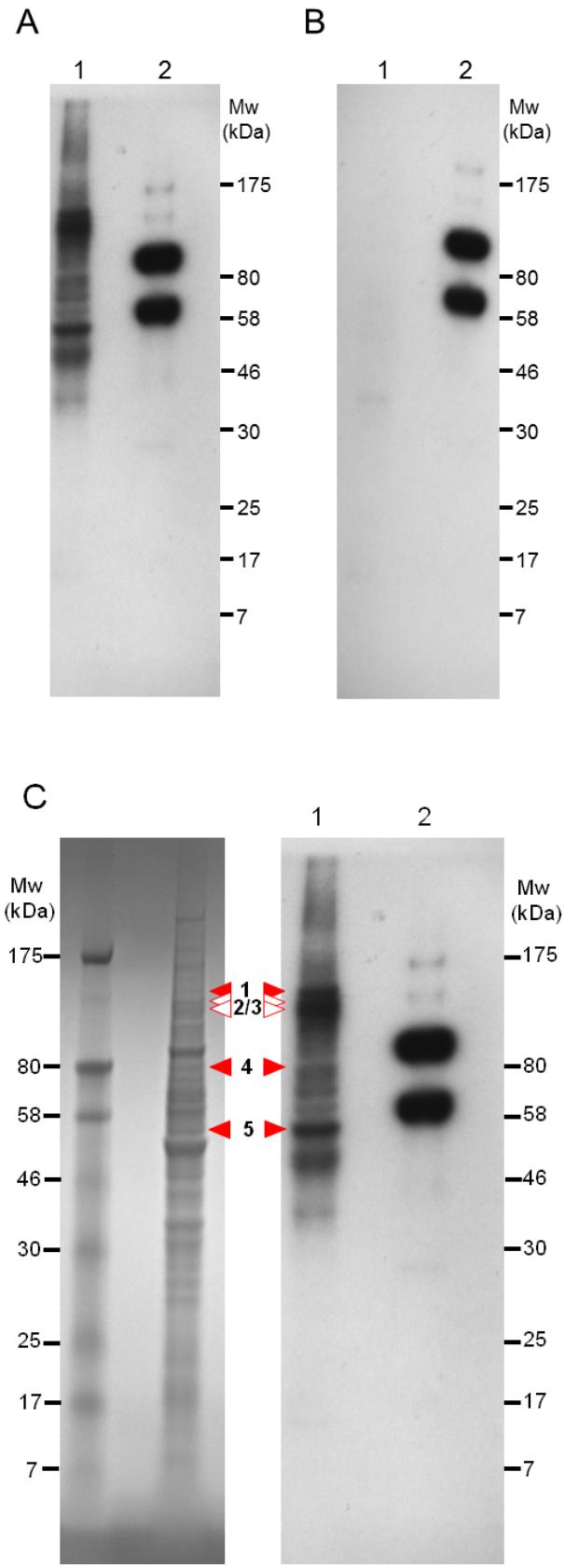
A
1
2
Mw
(kDa)
175
80
58
46
30
25
17
7
B
1
2
Mw
(kDa)
175
80
58
46
30
25
17
7
C
1
2
Mw
(kDa)
175
80
58
46
30
25
17
7
1
2/3
4
5
Mw
(kDa)
175
80
58
46
30
25
17
7

Figure 3.14 Western blot of *A. castellanii* lysate detected with purified HE2.

90µg of lysate (1) and 1µg of control IgM (2) were run on 12% polyacrylamide gels, blotted to PVDF and then probed with 50ng/ml of (A) HE2 polyclonal antibody, or (B) isotype control IgM. Binding was detected with goat anti-mouse IgM-HRP and 5s exposure to X-ray film. (C) Bands with high intensity on both SDS-PAGE (left panel) and Western blot (right panel) were identified and excised for peptide sequencing (C 1-5). Where multiple PAGE bands were potentially responsible for a strong Western blot signal, all within the appropriate range of molecular weights were excised and sequenced (C 1-3). Images are representative of two (C) or three (A&B) experiments.

3.4.14. MS/MS sequencing

Mass spectrometry data was obtained using a Q-ToF2 instrument and analysed according to standard parameters. Searches were performed against the NCBInr database in the first instance and peptide matches to likely protein identities were retrieved using MASCOT software version 2.4.01 (sections 2.9 and 3.3.8).

All peptides used to interrogate NCBInr sequence data returned matches from *A. castellanii* and in the main peptides corresponded to sequences of enzymes involved in metabolic pathways, such as malate dehydrogenase and oxoglutarate dehydrogenase (Table 2.2). Additional hits to enzymes involved in the translation machinery and protein synthesis were also seen (eukaryotic translation elongation factor 2 and elongation factor 1γ) and there was a significant match to the cytoskeletal component actin.

Further searches against “ESTs others” produced a limited number of additional hits within the amoebazoa and in other organisms (Appendix 2). Where sequence matched to known (i.e. non-hypothetical) proteins, the best matches were found for the mitochondrial F1 complex ATP synthase in *Polysphondylium pallidum* and *Dictyostelium fasciculatum.*

Band	Identity (Best Match)	Peptides	Match Score	Expectation Value
1	oxoglutarate dehydrogenase (succinyltransferring)	K.AAINDVAIVR.V R.ETGETYQPLR.H **R.VEQLAPFPFDR.V**	48 22 72	2 8.1E+02 0.007
2/3†	eukaryotic translation elongation factor 2	K.YGWDVTEAR.K K.DLQDEFTGVELK.T K.SGTITTSETAHNLR.V	42 31 53	9.4 1E+02 0.74
2/3†	cobalamin independent methionine synthase	K.HLTLGAGVVDAR.N K.ANLLAQVDAGIER.I R.YIVGGAQQAAPETK.A	41 31 39	14 1.1E+02 21
2/3†	No data returned‡	N/D	N/D	N/D
4	NAD-dependent malic enzyme	KHVDVIVVTDGSR.I R.TLPVTLDVGTNNEK.L R.AIVASGSPFDPVQYK.G **R.AIVASGSPFDPVQYK.G** R.AIVASGSPFDPVQYK.G K.NVWVVDADGLIAQGR.S	38 29 7 66 38 33	24 1.8E+02 3.3E+04 0.042 26 67
5	elongation factor 1γ family protein	R.VSLADIVVSMALYR.L **R.VSLADIVVSMALYR.L** R.VSLADIVVSMALYR.L **K.VPALETPEGPLFESNAIAR.Y** K.VPALETPEGPLFESNAIAR.Y	18 105 16 75 29	1.9E+03 3.2E-06 2.6E+03 0.003 1.2E+02

Table 3.2

Band	Identity (Best Match)	Peptides	Match Score	Expectation Value
5	actin	R.GYSFTTTAER.E K.IWHHTFYNELR.V **K.SYELPDGQVITIGNER.F**	37 36 99	25 25 1.1E-05
5	malate dehydrogenase	R.QTVPEIDR.A K.HQPVILQLLELEPAMK.A **K.YMAELEKPGAGPLSAVPPVR.V**	50 29 96	1.4 1.1E+02 2.1E-05
5	4-hydroxyphenylpyruvate dioxygenase	K.HGVAASAVGIEVEDAAEAYR.I R.IAVENGAVSIAEPATLVNEATGAK.T R.FISFSEGYDHPFLPGYETVTDQGPR.L	48 38 51	1.3 11 0.52
5	NADP-dependent isocitrate dehydrogenase	R.LIDDMVAFAMK.D	57	0.25

Table 3.2 MS/MS analysis of *A. castellanii* peptide matches.

Searches of peptide fragments generated by mass spectrometry against the NCBInr database were analysed using MASCOT v2.4.01 software. Where several peptide identifications were obtained from a single band excision from SDS-PAGE gel each is presented individually. Red text denotes samples with high match scores and low expectation values, i.e. match score > 50, E-value <0.05 representing a less than 5% chance of a false-positive identification. † Bands 2 and 3 could not be fully separated by dissection, so were analysed concurrently. ‡ No matches were returned for peptides obtained from this sample.

3.5. Discussion

The use of specific antibodies as tools for molecular and immunological dissection of host-parasite interactions is well established, originating with the hybridoma fusion technique developed and first used by Kohler and Milstein (1975). Additional techniques such as phage display technology and improvements to *in vitro* methods mean that specific monoclonal antibody can now be viably generated on a commercial basis. Nevertheless in many cases the original *in vitro* technique remains in common use. This is especially true where basic understanding of a particular pathogen and the host response to it is still developing, such as in the particular case of *A. castellanii*. The opportunity to make progress in this area has been recognised by previous authors who generated specific antibody for numerous purposes including diagnostics, therapeutics and as research tools (Turner et al., 2005, Khan et al., 2000a, Kennett et al., 1999, Leher et al., 1999). Our goal was aligned with this latter purpose, in order to discern molecular targets recognised by the immune system and the immunological basis for control of the disease.

We based our protocol on the classical PEG fusion method modified with specific experimental parameters published by Lane and Berry *et al*. (Berry et al., 2003, Lane, 1985, Kohler and Milstein, 1975). Typical approaches of this kind often incorporate feeder cell cultures to enhance post-fusion growth (de StGroth and Scheidegger, 1980); however we favoured the use of a dedicated cloning factor (BriClone) containing the cytokine Il-6, which has been shown

to promote the growth of B-cell hybridomas (Bazin and Lemieux, 1989). This dispensed with the need for any additional cell types.

The outcome of previous attempts to generate specific anti-*Acanthamoeba* antibody has been mixed and despite successes in obtaining antibody specific to some targets (Kennett et al., 1999) few, if any immunoglobulin reagents have entered routine use. Khan *et al.* used a phage display library to generate fragments which recognised a range of epitopes, and selected these for high specificity and affinity via rounds of specific and nonspecific panning (Khan et al., 2000a). The resulting antibodies were well suited for use in diagnostic assays but having been generated and selected for entirely *in vitro*, did not necessarily correspond to antigens and epitopes of *in vivo* relevance in either immunity or pathogenesis. Similar drawbacks also affect the usefulness of antibody produced by Flores *et al*. whose work focused on detection of the organism in fixed brain sections (Flores et al., 1990).

Alternative approaches by Turner *et al.* and Kennett *et al.* generated hybridomas using *in vivo* immunisations similar to those employed in our study, and as such their work is more applicable in terms of which antigens or epitopes are recognised by the immune system. In common with our data (Figure 3.2), Turner *et al.* were able to generate a large number of hybridoma clones in response to a similar immunisation protocol, many of which produced antibody belonging to the IgM isotype (Turner et al., 2005). The clone which produced the strongest reactivity against *Acanthamoeba* in a range of our assays (HE2, see Figures 3.4 and 3.5) was also an IgM, and this could point to a significant role for this antibody in controlling systemic *A.*

castellanii. The multivalent structure of IgM allows it to play a role in aggregation and immobilisation of pathogens, and specific HE2 IgM showed an ability to aggregate trophozoites *in vitro* (Figure 3.9, Table 3.1). IgM may also act to initiate lysis of pathogens by binding to complement proteins and this may be relevant to immunological control of trophozoites. However the precise role played by the complement cascade and whether amoebae are resistant or susceptible by either the classical or alternative pathways is subject to conflicting evidence (Pumidonming et al., 2011, Toney and Marciano-Cabral, 1998, Ferrante and Rowan-Kelly, 1983). We did not examine whether our HE2 antibody could enhance the efficacy of the complement cascade, however this should prove an interesting topic for further investigation.

Another point of note is that IgM is typically produced early in the immune response, as a precursor to the induction of other antibody classes. Its preponderance in serum (Kiderlen et al., 2010, Walochnik et al., 2001, Cursons et al., 1980) and in experimental infections (Turner et al., 2005, Flores et al., 1990) could therefore be an indicator of repeated or recent infections. This is in keeping with the wide environmental distribution of the parasite across the globe for example in heated, fresh, and natural water systems (Gianinazzi et al., 2009, Magliano et al., 2009, Rivera and Adao, 2008, De Jonckheere, 2007, Lorenzo-Morales et al., 2006).

Our focus in this study was to understand the role played by antibody in adhesion to and penetration of the blood-brain barrier. Kennett *et al.* and Leher *et al.* demonstrated that specific antibody (monoclonal IgG and IgA respectively) can act to prevent adhesion of trophozoites to layers of Chinese

Hamster Corneal Epithelial Cells (CHCECs) both *in vitro* and *in vivo* (Kennett et al., 1999, Leher et al., 1999). Building on these findings we used cell types from within the brain microvasculature (HBMECs) as a model system to investigate the effects of specific polyclonal HE2. Given the ability of HE2 to aggregate trophozoites we hypothesised that this might have an effect on the ability of treated trophozoites to adhere to or disrupt the cell layer.

Initial experiments with unpurified culture supernatants suggested that HE2 may reduce binding and monolayer disruption (Figures 3.6 and 3.7) but were ultimately inconclusive, however experiments with quantified and purified antibody proved easier to interpret. In terms of binding inhibition significant reductions were seen in wells treated with HE2 (Figure 3.10), however the magnitude of this effect was small (-20%) in comparison with the reduction in binding seen by Leher (-60%) and Kennett (-80%). Notably, a similar significant reduction was also seen with a nonspecific isotype control antibody. This suggested the possibility that the antibody was acting to inhibit binding in a nonspecific manner, perhaps by steric hindrance or due to capture by surface factors on the parasite (discussed at greater length in Chapter 4).

As well as the effect of HE2 on binding we also examined the outcomes of *in vitro* infections in terms of disruption of cell monolayers and host cell death. Little protection was seen in terms of monolayer integrity at a gross level (Figure 3.11) however a small reduction in monolayer disruption was seen when using semi-quantified photomicrographs, which was statistically significant at high antibody concentrations (Figure 3.12). This did not align with measurements of cell death however, which demonstrated a small

reduction in LDH release at higher antibody concentrations not reaching statistical significance (Figure 3.13). Our use of LDH release assays is beneficial in providing quantitative cell death data that could not be obtained by analysis of monolayer disruption alone. One factor that should be considered in interpreting this data however is the difficulty of separating LDH release by dying HBMEC from LDH contributions made by trophozoites. No substantial levels of *A. castellanii* death were observed in our assays. However it is not certain that trophozoites did not release LDH in our experimental system as a result of stress induced by the growth medium (RPMI) or antibody treatment. We therefore suggest that future experiments take this into account by including a trophozoite-only control to monitor LDH release by isolated *A. castellanii*. Experiments to optimise conditions and designate appropriate controls will also be of use for this widely utilised assay. There may also be scope for a dedicated investigation into the use of *A. castellanii* LDH as a stress marker for trophozoites.

The absence of a strong protective effect taken in the context of high levels of reactivity to trophozoites shown in Figures 3.8 suggests that the antigens recognised by HE2 are not of primary importance in host cell death and may only be secondary factors in host cell binding. To investigate this further we used tandem MS sequencing to elucidate the identity of *A. castellanii* proteins recognised by HE2 polyclonal antibody.

As expected, due to the use of a complex whole parasite antigen and the polyclonal nature of the antibody HE2 recognised a wide range of parasite proteins (Figure 3.14). Those bands which gave the strongest signal and which

corresponded to bands on a coomassie-stained SDS-PAGE gel were excised and analysed by MS/MS. Interpretation of peptide identities was complicated by the presence of multiple proteins within single SDS-PAGE bands, representing several different proteins of equivalent molecular weight. For example data from band 5 in Figure 3.14 C returned identities for five proteins in the range of 45 to 46.5 kDa (Table 3.2). Three of these matched significantly to annotated proteins in the *A. castellanii* genome. Similarly, difficulty was encountered where Western blot bands had been insufficiently separated for them to be individually resolved and matched to distinct SDS-PAGE bands (Figure 3.14 C, bands 2/3). In this case bands were excised together and analysed concurrently however not all peptides matched to database sequences. It is not clear in this case whether non-matching peptides represent an inability to obtain reliable data from this sample, or whether they instead correspond to a unique *A. castellanii* sequence not previously reported. In the absence of additional supporting data or further characterisation however it is difficult to support this latter hypothesis.

Protein matches were nevertheless obtained for other bands recognised by HE2 supernatant. The majority of these corresponded either to metabolic enzymes or key mediators of protein synthesis, and appeared highly immunogenic. Uninhibited functioning of these molecules is likely to be critical to trophozoite survival, and it is therefore straightforward to see why the host mounts a strong immune response to them. It is pertinent however to sound a note of caution that due to immunisation with a mixed antigen a strong immunoassay response does not necessarily indicate that the most abundant protein in any given sample is the most immunogenic. It is possible that the

relative abundance of metabolic enzymes in our analysis masks detection of less abundant, but more immunogenic proteins at the same molecular weight. Finer separation of proteins or isolation of nuclear, mitochondrial, cytosolic, and membrane fractions would assist in confirming our antigen identifications.

Nevertheless the protein identities that we were able to obtain from tandem MS analysis open up interesting lines of inquiry regarding AGE pathogenesis and the immune response to *A. castellanii*. Several of the proteins for which hits were obtained have homologues in other pathogenic protozoa that have been implicated in disease generation or control. Probst *et al.* generated and characterised T-cell-stimulating antigens from *Leishmania major* and identified malate dehydrogenase and elongation factor 2 amongst the resulting targets (Probst et al., 2001). Another translation elongation factor (EF-1γ) has also been shown to be of importance in *Trypanosoma cruzi* infections where it may play a role in resistance to clomipramine treatment, although this finding was based on deliberate overexpression of the associated gene (Billaut-Mulot et al., 1997). In addition, cobalamin-independent methionine synthase has been suggested to be of use as an antifungal target (Suliman et al., 2007).

Perhaps most interestingly one enzyme in particular that emerged from our analysis has been shown to have a direct role in virulence. The AP65 protein of *Trichomonas vaginalis* is one of five which enable binding of the parasite to its target cells (Alderete and Garza, 1988). Intriguingly AP65 also shares considerable sequence homology with malic enzyme from a variety of organisms (Engbring et al., 1996). There is evidence to suggest that it not only associates with the cell surface (O'Brien et al., 1996) but may also be released

into the extracellular environment, having a role in *T. vaginalis* perforin-mediated pathogenesis (Addis et al., 1997). A peptide match to *A. castellanii* malic enzyme was seen in our analysis (Table 2.2, band 4). This does not necessarily imply a similar pathogenic role for this enzyme in *A. castellanii* as its usual function of catalysing oxidative decarboxylation of malate to pyruvate is highly conserved. Nevertheless further examination of the localisation and function of *A. castellanii* malic enzyme may be warranted in future studies.

Another target that may be of relevance is actin (Table 3.2, band 5). This key component of the cytoskeleton has been well-studied in *Acanthamoeba* and has been acknowledged to be of pathogenic importance (da Rocha-Azevedo and Costa e Silva-Filho, 2007). For example, Alsam *et al.* demonstrated that inhibition of actin polymerisation abolishes phagocytosis of bacteria. Furthermore a protective effect on host cell death using the same treatment was observed in a study by Taylor and colleagues, demonstrating the importance of phagocytosis to disease (Taylor et al., 1995, Alsam et al., 2005a). Additionally the cellular distribution of the actin cytoskeleton was investigated by Gonzales-Robles *et al.* with actin bundles observed at the cell periphery. Actin bundles also associate with membrane structures such as acanthopodia which may mediate attachment to host cells (Gonzalez-Robles et al., 2008). Furthermore actin also has a critical role to play in endo- and exocytosis, processes of importance in disease due to the high levels of pathogenic protease secretion (Alfieri et al., 2000).

One pertinent question arising from the results of tandem MS analysis is the apparent localisation of fluorescent staining to the trophozoite cell membrane

(Figures 3.4 and 3.8). The majority of peptide identities returned from tandem MS analysis matched to either mitochondrial or cytosolic proteins so it is not clear why such staining should be observed.

One possibility is that recognised antigens in the cytosol are associated with the cell membrane or a membrane-bound organelle, either via a transmembrane or other membrane-associated domain. This has been previously observed for the *T. vaginalis* AP65 protein which possesses homology with malic enzyme (O'Brien et al., 1996). Similarly EF-1γ is also known to associate with membrane structures (Janssen and Moller, 1988) and actin too also associates closely with the cell membrane (Gonzalez-Robles et al., 2008).

Secondly it might be the case that the antigens selected for MS/MS analysis are not those which are recognised on the trophozoite cell surface at all. HE2 showed broad recognition of several antigen bands (Figure 3.14 C) from which those giving the strongest signal were selected for further analysis. However this does not exclude the possibility that antigens giving a lower signal might localise on the cell membrane. This may be particularly true of antigens involved in recognition of, or binding to host cells. For example *A. castellanii* are known to possess a mannose-binding protein (MBP) which is involved in adhesion and recognition of host cells (Cao et al., 1998, Hurt et al., 2003b, Garate et al., 2006b). Characterisation of this molecule by Garate and colleagues revealed the molecule to have a molecular weight of 400 kDa (composed of 130kDa subunits), which if present in our trophozoite lysate would give a band in the range considerably above the highest molecular weight marker (Garate et al., 2004).

A diffuse area of staining can be observed in the range corresponding to MBP subunits, and also at a molecular weight corresponding to another >207kDa adhesion molecule described by Kennett *et al.* (1999). Reliable isolation of specific bands from these areas could not be made in our study due to uncertainty over the precise molecular weights represented, and unreliable correspondence with SDS-PAGE bands. It may prove enlightening to isolate the protein recognised by this area of staining in the future. However if specific antibody to MBP is desired in order to conduct blocking experiments an approach based on immunisation with MBP alone, or an equivalent *in vitro* method is more likely to yield success.

Since our analysis of the proteins recognised by HE2 did not reveal any unambiguous membrane proteins a reduction in trophozoite binding such as was seen in our assays (Figure 3.10) could be viewed as an unexpected result. As discussed above such proteins may well be recognised. If this was the case however a greater reduction in binding than the 20% observed in our assays would be expected. In addition the role which *A. castellanii* adhesins have already been shown to play in host cell death means a reduction in this parameter might reasonably be predicted. However the lack of a protective effect as demonstrated in our assays (Figure 3.13) implies that whatever antigens are the target of HE2 they are not directly involved in host cell death mechanisms. Instead the targeted antigens may represent proteins which are sufficiently specific to the parasite to prompt rapid recognition, followed by phagocytic clearance and/or complement fixation and lysis. We did not perform experiments examining the interaction between HE2-treated

trophozoites and either of these factors, so this would be a valuable next step to determine the contribution of each pathway to elimination of trophozoites.

Alternatively it is possible that HE2 in particular and immunoglobulin in general is effective at blocking certain aspects of pathogenesis, but that amoebae are able to remove or degrade bound antibody. This point is raised by Cursons *et al.* in their survey of humoral immunity to pathogenic free-living amoebae, and indeed mechanisms for inactivation of antibody have been shown in pathogenic amoebae (Garcia-Nieto et al., 2008, Na et al., 2002a, Cursons et al., 1980). The potential for *A. castellanii* to evade the humoral immune response is evaluated and discussed in Chapter 4.

4. *In vitro* effects of specific polyclonal antibody and evasion of host immunity mediated by parasite Fc-receptor and antibody cleavage

4.1. Abstract

During haematogenous spread, circulating *A. castellanii* trophozoites are open to attack by the humoral immune system which is in most cases sufficient to prevent development of the disease. However purified antibody has only a limited protective effect *in vitro*, equivalent to that of a nonspecific control antibody. It is therefore unclear what role circulating immunoglobulin plays in preventing penetration of the blood-brain barrier, and whether trophozoites can alter the efficacy of the immune response. Previously published data demonstrated that amoeba proteases can degrade antibody. Here we extend these findings to include all Ig classes including physiologically-derived antibody. Degradation was found to be mediated by secreted serine- and metallo-proteases. We also attributed nonspecific binding of polyclonal antibody to Fc-binding activity by trophozoites as shown by immunofluorescence and FACS analysis. Evidence from bioinformatics analysis also demonstrated similarity between Fc-binding proteins in other parasites and regions of the *A. castellanii* genome.

4.2. Introduction

Characterisation of the mechanism by which *Acanthamoeba* trophozoites circumvent or abolish the integrity of the BBB is further advanced than other areas of understanding with respect to the pathogenesis of AGE. However the immune response to systemic *Acanthamoeba* infections and in particular the evasion of humoral immunity by the parasite has only been partially defined.

Experimental immunisations in rabbits, pigs, and hamsters produce strong antibody titres with high specificity which confers protection in these most commonly-used keratitis models (Leher et al., 1998b, Said et al., 2004, Garate et al., 2006a). *In vitro* assays have also demonstrated that as a part of serum, antibody can act effectively to limit trophozoite adhesion to host cells (Sissons et al., 2006b).

Surveys of both vulnerable and healthy populations demonstrate widespread positive titres indicating common exposure but also effective control as clinical disease manifests in only rare cases (Alizadeh et al., 2001, Schuster et al., 2006, Brindley et al., 2009, Kiderlen et al., 2010). Nevertheless purified antibody was seen only to contribute non-specifically to a reduction in binding to endothelial cells, and to have no effect on cytotoxicity or barrier integrity in our experiments (see Chapter 3). Additionally, systemic immunisation does not always produce favourable outcomes or translate to mucosal immunity that is capable of combating the parasite (Van Klink et al., 1997). There is evidence from some studies however that *Acanthamoeba* keratitis is responsive to antibody-based intervention (Alizadeh et al., 1995, Leher et al., 1999). These

confounding results would suggest that effective host antibody-mediated responses and parasite evasion mechanisms both influence the outcome of antibody-dependent immunity. In light of this we considered how *A. castellanii* might evade host antibody.

Mechanisms for degradation of antibody are known to occur in a number of parasites of medical importance including *Schistosoma mansoni*, *Faciola hepatica* and *Trypanosoma cruzi* (Pleass et al., 2000, Berasain et al., 2003, Smith et al., 1993). Antibody cleavage has additionally been observed in less distantly related species such as *Entamoeba histolytica* which possesses both IgG and IgA-degradation activity (Tran et al., 1998, Garcia-Nieto et al., 2008). There is also evidence to suggest that secreted proteases of *A. castellanii* can degrade immune components including antibody and inflammatory mediators such as cytokines (Na et al., 2001, Na et al., 2002a). However substrate specificity of the three main groups of *Acanthamoeba* proteases (serine, cysteine, and metalloproteases) has not been fully determined. Uncertainties also remain as regards action against immunoglobulin classes, and specific antibody raised generated *in vivo*. In this study we sought to address these questions with the application of electrophoretic techniques and image analysis, examining the cleavage products of antibody-protease mixtures under the action of various protease inhibitors.

A second mechanism by which parasites can avoid the action of antibodies, and in turn inhibit forward stimulation of the cell-mediated response and other effector mechanisms is by antibody capture. By either coating themselves with ineffective Ig or recruiting it in incorrect orientation, parasites can inhibit the usual activity of the molecule and interfere with downstream immune

activation (Garcia et al., 1997, Holder et al., 1999). This is because the conserved (Fc) portion of antibody is the basis for initiation of immune effector functions.

Proteins with binding affinity for the Fc region (Fc receptors) are expressed on phagocytes such as macrophages and neutrophils, and Fc/FcR recognition prompts pathogens to be ingested and destroyed by phagocytes. IgG is the most important antibody class in this response due to its high antigen affinity and may be especially important in AGE due to its high expression level in the bloodstream.

Additionally the Fc region plays an important role in activating the complement cascade by binding to C1q, the first of the subunits which eventually form the lytic Membrane Attack Complex (Sledge and Bing, 1973). Whilst both IgG and IgM can fix complement IgM is the more efficient of the two as a result of its pentameric structure. This means that only one IgM molecule is required to bind to the C1 complement subunit and initiate the cascade, whereas at least two IgG molecules in close proximity are required to do the same.

Pathogens that are able to bind to the Fc region can thus dampen the stimulatory signal to either phagocyte or complement effector mechanisms may thereby protect themselves from the inflammatory response. In our experiments (detailed in Chapter 3) the ability of both specific and nonspecific IgM to inhibit trophozoite adhesion to endothelial monolayers raised the possibility that *A. castellanii* might possess an immunoglobulin binding mechanism, which could include a dedicated Fc binding protein. We sought to

interrogate this possibility via the use of Fc-only Ig fragments, as well as the possible structural effects (and steric binding inhibition) occurring as a result of capturing different antibody classes. This was combined with a bioinformatics approach, examining Fc binding residues characterised in mammalian and parasitic organisms for sequences with similarity to the recently-published *A. castellanii* genome (Clarke et al., 2013).

4.3. Materials and Methods

4.3.1. Polyclonal antibody generation

Polyclonal antibody was generated by hybridoma fusion from splenocytes of BALB/c mice immunised with 2×10^7 trophozoites in Alum, as described in Chapter 2 (section 2.3) and Chapter 3 (section 3.3.1).

4.3.2. Zymography

Dilutions of ACM were made in ddH_2O and 15µl of sample was mixed with 5µl of non-reducing sample buffer and heated to 75°C (see section 2.7.2). Samples were run on 10% gelatin gels at 110V for 60 minutes. After completion of the run gels were washed in 50mM Tris buffer pH7.5 + 2.5% w/v TritonX-100 for one hour, and then ddH_2O for 3× 5 minutes. Proteins were refolded by incubation in 50mM Tris buffer pH7.5 + 0.5M $CaCl_2$ for 3 hours at 37°C. Gels were then stained with Coomassie Blue, destained and photographed.

4.3.3. Cleavage reaction

Fifty millilitres of ACM was collected and concentrated as described in section 2.2.2 and 2.5.2, yielding a final concentration of 1mg/ml. Cleavage mixes were then set up with 1µg of either mouse IgA, IgM, IgG, IgE negative controls (Table 2.2 #1-4), or specific polyclonal IgM generated as described in sections 2.3, 2.1.4 and 2.5. 3.6µg of concentrated ACM was added and for each antibody class, protease inhibitors were added to a final concentration of 100µM (see section 2.7.3). Reaction mixes were then incubated at 37°C for 2 hours.

4.3.4. SDS-PAGE

15µl of cleavage mixture was mixed with 4µl of LDS loading buffer and reduced by adding 1µl of DTT and heating to 75°C for 5 minutes. Samples were loaded onto 4-20% polyacrylamide gels alongside 10µl of ColorPlus prestained protein marker and run at 120V for 90 minutes (see section 2.7). Gels were retrieved from their cartridges and washed in ultrapure water for five minutes prior to visualisation of peptide bands by silver staining (see section 2.7.1.2 for additional details).

4.3.5. Silver Nitrate staining

Silver staining was carried out using a GE healthcare PlusOne kit (see Reagents and Buffers, Chapter 2, for solutions used). Gels were soaked for 30 minutes in acetic acid/ethanol fixing solution, then placed in sensitising

solution for 30 minutes under shaking. Gels were washed for 3× 5 minutes in ultrapure water before transfer to 0.1% w/v silver nitrate solution for 20 minutes under shaking. The gels were then washed again and developed for three minutes. Reactions were terminated by immersing gels in stopping solution for 10 minutes under shaking.

4.3.6. Gel analysis

Analysis of cleavage products was performed using ImageJ software (Schneider et al., 2012) using an adapted method of Western blot band density quantification. Lanes were plotted onto gel images and expressed as density peaks as described in section 2.7.3. Peaks corresponding to heavy and light chain were closed off at either side and the 'wand' tool was then used to collect area measurements. Any contribution to peak areas from bands present in ACM was discounted by subtracting peak areas of these bands from samples containing ACM. Areas were then expressed as a proportion of measurements from uncleaved control samples.

4.3.7. Functional assays

HBMEC were cultured as described in section 2.1.2 and grown in 24 or 48-well plates (section 2.4.1). 2×10^5 *A. castellanii* trophozoites were incubated with 200µg/ml of purified polyclonal antibody, negative isotype control IgM, negative control IgG, or IgG Fc fragment (Table 2.2 #1, 2 and 5) in RPMI. Treated trophozoites were incubated at 37°C under shaking prior to use *in vitro* as described below.

4.3.8. Functional assays: Binding Inhibition

Binding of treated trophozoites to HBMEC monolayers was assessed by haemocytometer counts of unbound amoeba from 24 or 48-well plates, as described in section 2.4.3.1.

4.3.9. Functional assays: Monolayer protection

Protection of HBMEC monolayers was assessed using both haematoxylin staining of fixed monolayers and photomicrographs taken during the experimental period (see section 2.4.4). Monolayer disruption visible in photomicrographs was quantified using a grid counting method as described in section 2.4.4.2.

4.3.10. Functional assays: Cytotoxicity

Cytotoxicity in treated HBMEC was examined by detection of LDH release into culture supernatants. Samples were collected after 24 hours and assessed as described in section 2.4.5.

4.3.11. Bioinformatics

Bionformatics analysis was carried out using a combination of the NCBI and UNIPROT databases and NCBI's Basic Local Alignment Search Tool (BLAST) (see section 2.9). Sequences were obtained from the UNIPROT and

NCBI protein databases and compared with the *A. castellanii* genome assembly using individual queries via the tBLASTn algorithm. Sequences from predicted or observed extracellular domains were used where identified by annotation. Where significant similarity was shown, matching *A. castellanii* transcriptomic sequence was retrieved and translated into protein sequence using the "Props > view as proteins" menu sequence in SeaView version 4.4.1. The most appropriate reading frame was selected based on fewest stop codons. Reciprocal tBLASTn queries were then run, comparing each peptide sequence to all others and filtered for stringency. Sequences were accepted as significantly similar if the length of the aligned region was ≥50aa and the E-score for the alignment was ≤0.00001 (Wallner et al., 2004).

4.3.12. Immunofluorescence (IF)

A. castellanii trophozoites and K562 cells were affixed to microscope slides by cytospin, fixed, blocked and treated with 1:300 human IgG Fc fragment (Table 2.2, #5) as described in section 2.6.4. Primary antibody was detected using 1:1000 anti-human-Fc-fragment FITC conjugate (Table 2.2, #10) and cells were counterstained with DAPI. Photomicrographs were taken using exposures of 1s (360nm filter), and 3s (640nm filters). Gamma and gain settings were both 1×.

4.3.13. Fluorescence-Activated Cell Sorting (FACS)

A. castellanii trophozoites and HBMECs were fixed in 4% paraformaldehyde for 10 minutes, and then blocked in PBS + 5% BSA. Cells were then treated

with 1:300 human IgG Fc fragment (Table 2.2, #5) as described in section 2.6.4. Primary antibody was detected using 1:1000 anti-human-Fc-fragment FITC conjugate (Table 2.2, #10) and after 3 washes in PBS + 1% BSA cells were run using a BD FACSCantoII instrument. Voltages were adjusted to bring cell populations within range and 50,000 events were recorded and analysed using Weasel software (see section 2.6.5).

4.3.14. Statistical analysis

Analyses were performed using GraphPad Prism software version 5.04. Data was analysed using 1-way analysis of variance (ANOVA) and significance levels for individual group comparisons were obtained using Bonferroni post-tests (see section 2.10). The alpha level for significance was set at $p \leq 0.05$ for all tests except bioinformatics analysis for which a higher stringency threshold was set (see section 4.3.11).

4.4. Results

4.4.1. Protease secretion

Previous studies have demonstrated the secretion of a variety of proteases by *A. castellanii.* In order to confirm protease secretions for the strain and growth conditions used in this study, cell-free supernatant (*Acanthamoeba* conditioned medium, ACM) from *A. castellanii* cultures was collected and run on 10% gelatin zymograms at a range of concentrations (see section 4.3.2). Concentration-dependent cleavage of gelatin substrate by ACM was observed,

with bands visible in the range 30 to >175kDa. Cleavage bands were visible between 80 and 175 kDa, and at >175kDa, with an additional diffuse band visible between 30 and 58kDa at high concentrations (Figure 4.1). Bands approximately corresponded to previously identified proteases of 33, 85 and 130-150kDa as elucidated by Kim *et al.*, Hurt *et al*., and Sissons *et al.* although accurate size determination was not possibly due to the impaired mobility of molecular weight markers through substrate gels (Hurt et al., 2003a, Kim et al., 2006, Sissons et al., 2006a).

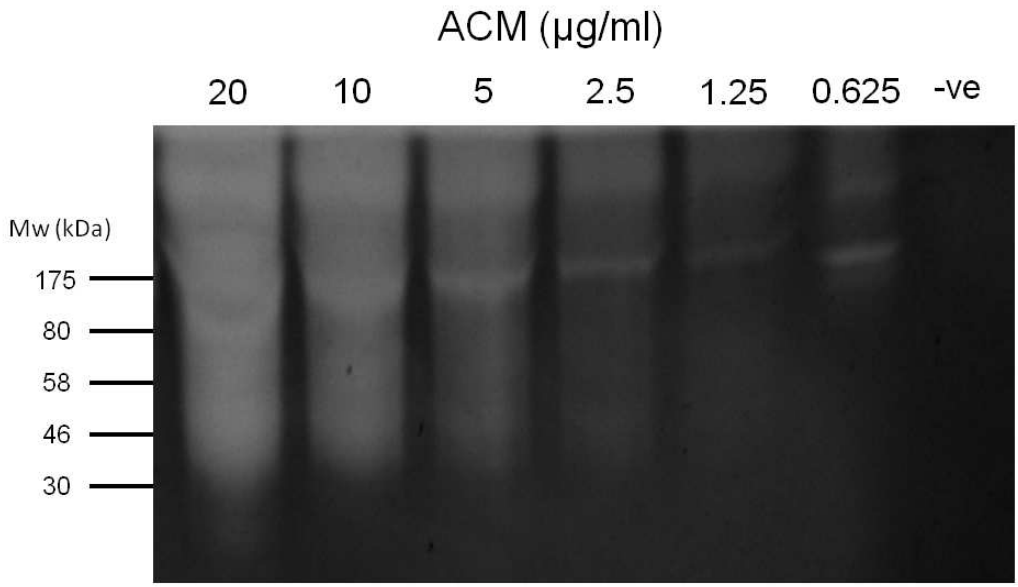

Figure 4.1 *A. castellanii* trophozoites secrete proteases *in vitro*.

ACM was serially diluted 1 in 2 with RPMI alone as a negative control. Dilutions were run on 10% gelatin gels at 110V for 60 minutes. Gels were washed to deplete SDS, and proteins were then refolded in calcium chloride buffer and allowed to digest gelatine. Gels were then stained with Coomassie Blue, destained and imaged. Light bands indicate where digestion of gelatin substrate has occurred due to protease activity. Image is representative of three independent experiments.

4.4.2. Antibody cleavage

Secreted proteases of *Acanthamoeba* have activity against a number of components of the immune system including cytokines and immunoglobulin (Na et al., 2002a). We were able to confirm and expand upon this data, demonstrating proteolytic activity across all subclasses of antibody, as well as against polyclonal antibody that had been raised against trophozoites *in vivo* (antibody HE2, as described in Chapter 3). Use of PMSF (a serine protease inhibitor) and Batimastat (a metalloprotease inhibitor) resulted in limited protection of Ig fragments from cleavage in the majority of cases (Figures 4.2 to 4.6, lanes 3 and 5). Banding patterns and peak traces corresponded closely with Ig alone after subtracting bands present in ACM and clear peaks were observed corresponding to antibody heavy and light chain fragments (Figures 4.2 to 4.6, panels B1 to B3). This effect was not observed with Iodoacetamide (a cysteine protease inhibitor), which produced banding patterns and peak traces indistinguishable from untreated controls.

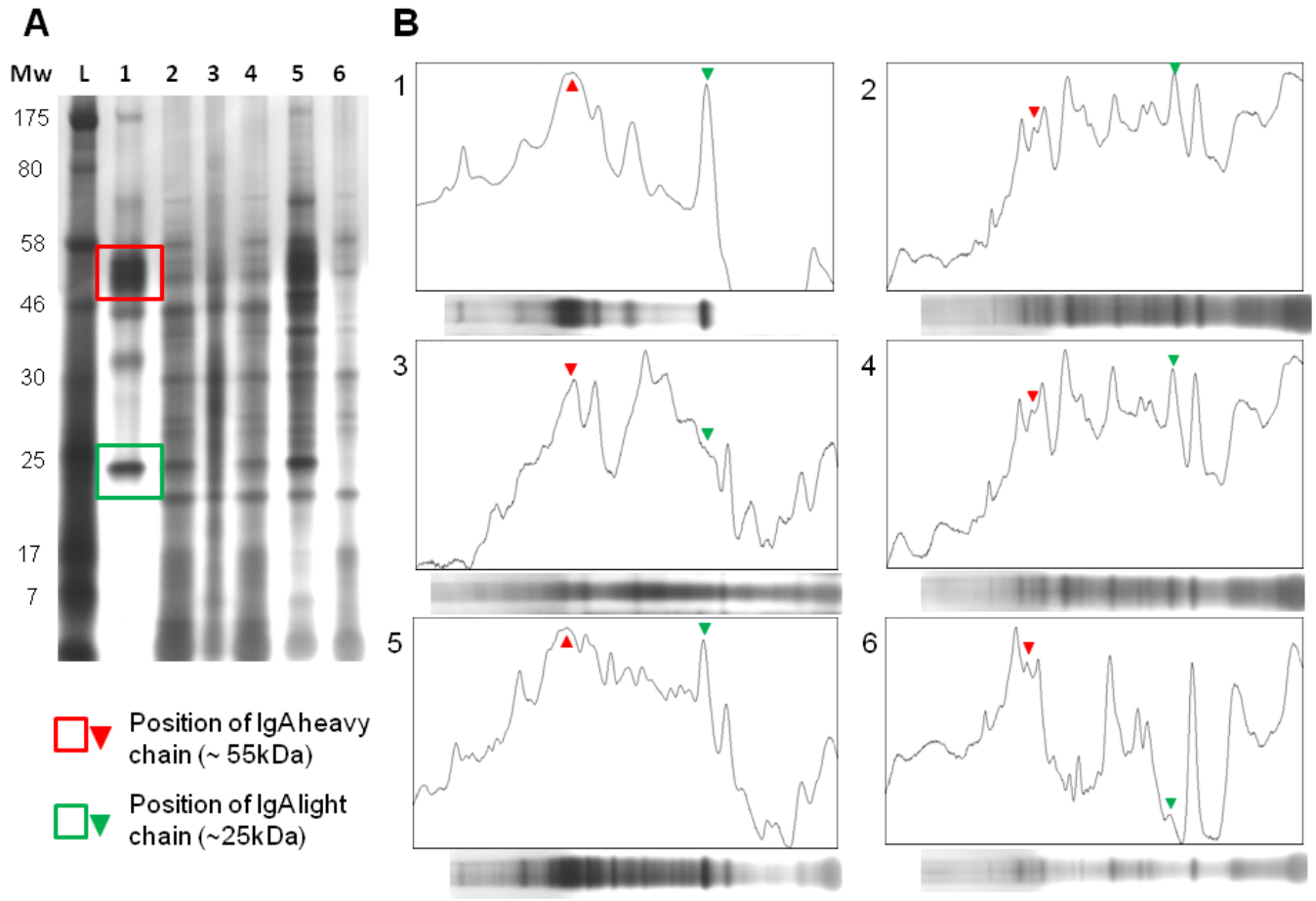
A
Mw
L
1
2
3
4
5
6
175
80
58
46
30
25
17
7
Position of IgA heavy chain (~ 55kDa)
Position of IgA light chain (~25kDa)
B
1
2
3
4
5
6

Figure 4.2 Murine IgG cleavage by ACM is reduced by addition of class-specific protease inhibitors.

Cleavage mixtures of ACM and antibody were prepared with or without protease inhibitor, incubated for 2 hours at 37°C and separated by SDS-PAGE (Panel A). Gels were silver stained, photographed and peak density analysed using ImageJ software (Panel B). (L) Ladder, (1) Ig alone, (2) Ig + ACM, (3) Ig + ACM + Batimastat, (4) Ig + ACM + Iodoacetamide, (5) Ig + ACM + PMSF, (6) ACM alone. Trace peaks correspond to protein bands on SDS-PAGE gel. Boxes denote Ig heavy (red) or light (green) chain. Bands corresponding to IgG heavy and light chains showed greatest preservation in samples treated with serine and metalloprotease inhibitors indicating these classes of protease to be primarily responsible for IgG degradation. Results are representative of two independent experiments.

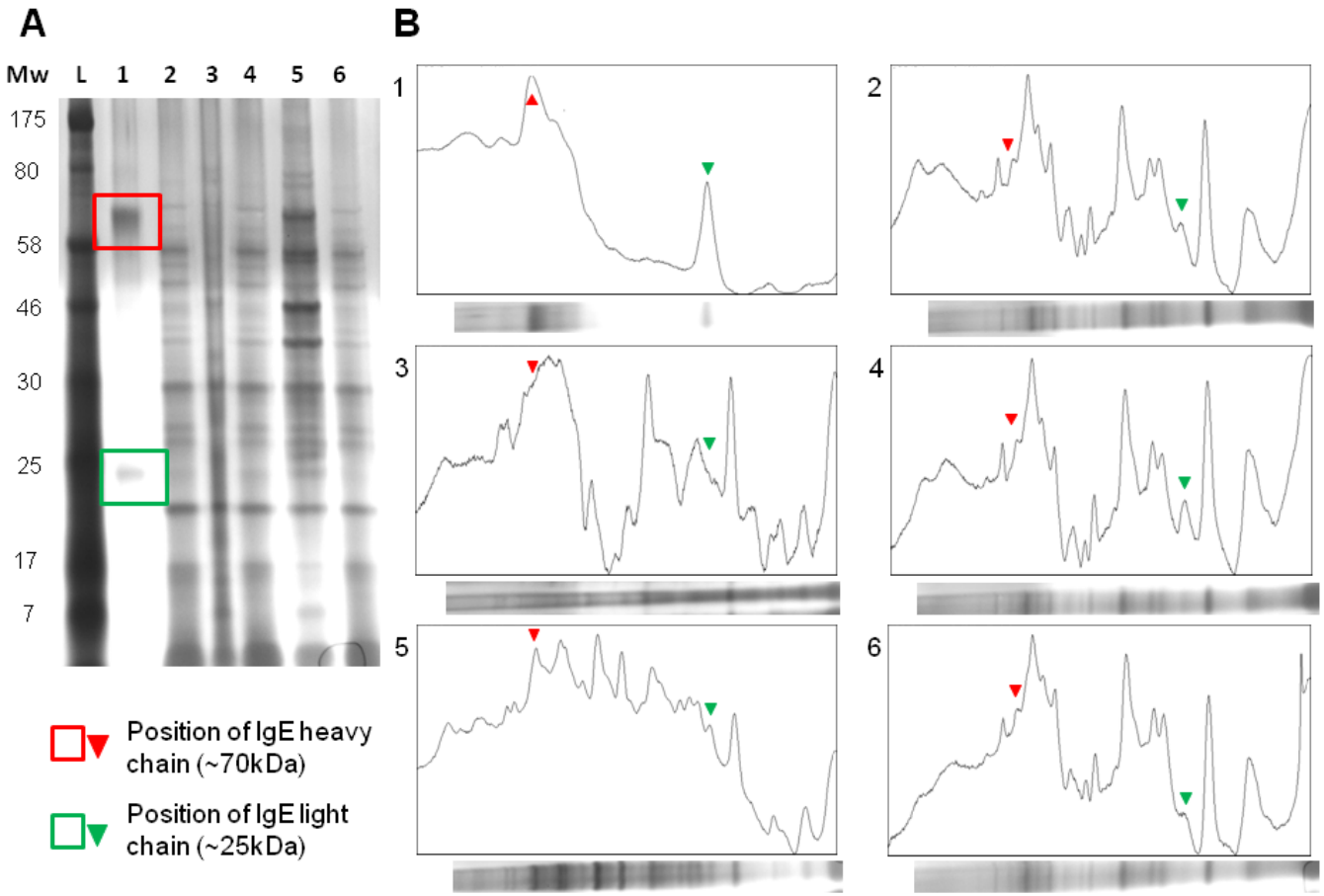
A
Mw
L
1
2
3
4
5
6
175
80
58
46
30
25
17
7
Position of IgE heavy chain (~70kDa)
Position of IgE light chain (~25kDa)
B
1
2
3
4
5
6

Figure 4.3 Murine IgE cleavage by ACM is reduced by addition of class-specific protease inhibitors.

Cleavage mixtures of ACM and antibody were prepared with or without protease inhibitor, incubated for 2 hours at 37°C and separated by SDS-PAGE (Panel A). Gels were silver stained, photographed and peak density analysed using ImageJ software (Panel B). (L) Ladder, (1) Ig alone, (2) Ig + ACM, (3) Ig + ACM + Batimastat, (4) Ig + ACM + Iodoacetamide, (5) Ig + ACM + PMSF, (6) ACM alone. Trace peaks correspond to protein bands on SDS-PAGE gel. Boxes denote Ig heavy (red) or light (green) chain. Bands corresponding to IgE heavy and light chains showed greatest preservation in samples treated with serine protease inhibitors indicating this class of protease to be primarily responsible for IgE degradation.Results are representative of two independent experiments.

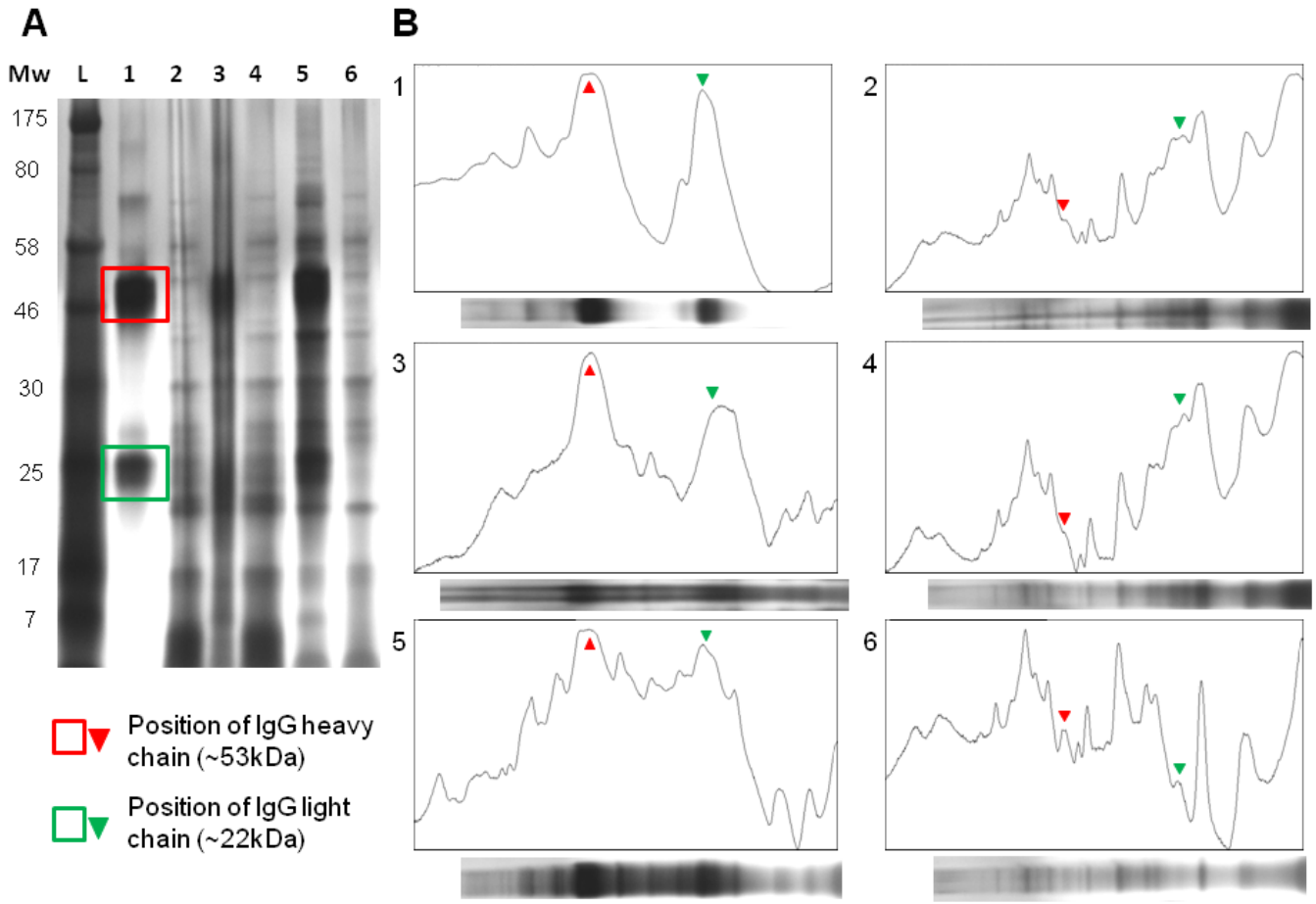
A
Mw
L
1
2
3
4
5
6
175
80
58
46
30
25
17
7
Position of IgG heavy chain (~53kDa)
Position of IgG light chain (~22kDa)
B
1
2
3
4
5
6

Figure 4.4 Murine IgA cleavage by ACM is reduced by addition of class-specific protease inhibitors.

Cleavage mixtures of ACM and antibody were prepared with or without protease inhibitor, incubated for 2 hours at 37°C and separated by SDS-PAGE (Panel A). Gels were silver stained, photographed and peak density analysed using ImageJ software (Panel B). (L) Ladder, (1) Ig alone, (2) Ig + ACM, (3) Ig + ACM + Batimastat, (4) Ig + ACM + Iodoacetamide, (5) Ig + ACM + PMSF, (6) ACM alone. Trace peaks correspond to protein bands on SDS-PAGE gel. Boxes denote Ig heavy (red) or light (green) chain. Bands corresponding to IgA heavy and light chains showed greatest preservation in samples treated with serine and metalloprotease inhibitors indicating these classes of protease to be primarily responsible for IgA degradation. Results are representative of two independent experiments.

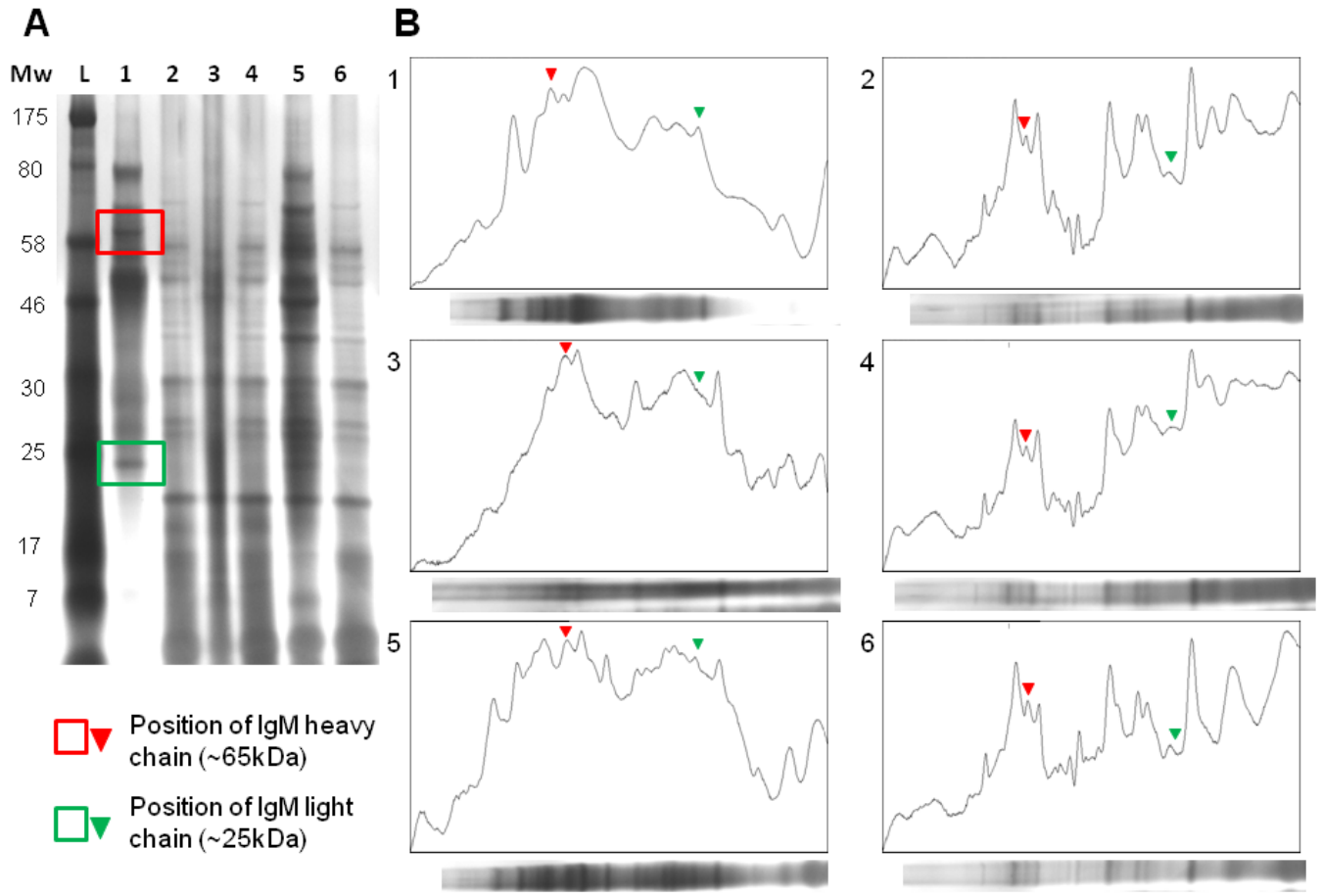
A
Mw
L
1
2
3
4
5
6
175
80
58
46
30
25
17
7
Position of IgM heavy chain (~65kDa)
Position of IgM light chain (~25kDa)
B
1
2
3
4
5
6

Figure 4.5 Murine IgM cleavage by ACM is reduced by addition of class-specific protease inhibitors.

Cleavage mixtures of ACM and antibody were prepared with or without protease inhibitor, incubated for 2 hours at 37°C and separated by SDS-PAGE (Panel A). Gels were silver stained, photographed and peak density analysed using ImageJ software (Panel B). (L) Ladder, (1) Ig alone, (2) Ig + ACM, (3) Ig + ACM + Batimastat, (4) Ig + ACM + Iodoacetamide, (5) Ig + ACM + PMSF, (6) ACM alone. Trace peaks correspond to protein bands on SDS-PAGE gel. Boxes denote Ig heavy (red) or light (green) chain. Bands corresponding to IgM heavy and light chains showed greatest preservation in samples treated with serine and metalloprotease inhibitors indicating these classes of protease to be primarily responsible for IgM degradation. Results are representative of two independent experiments.

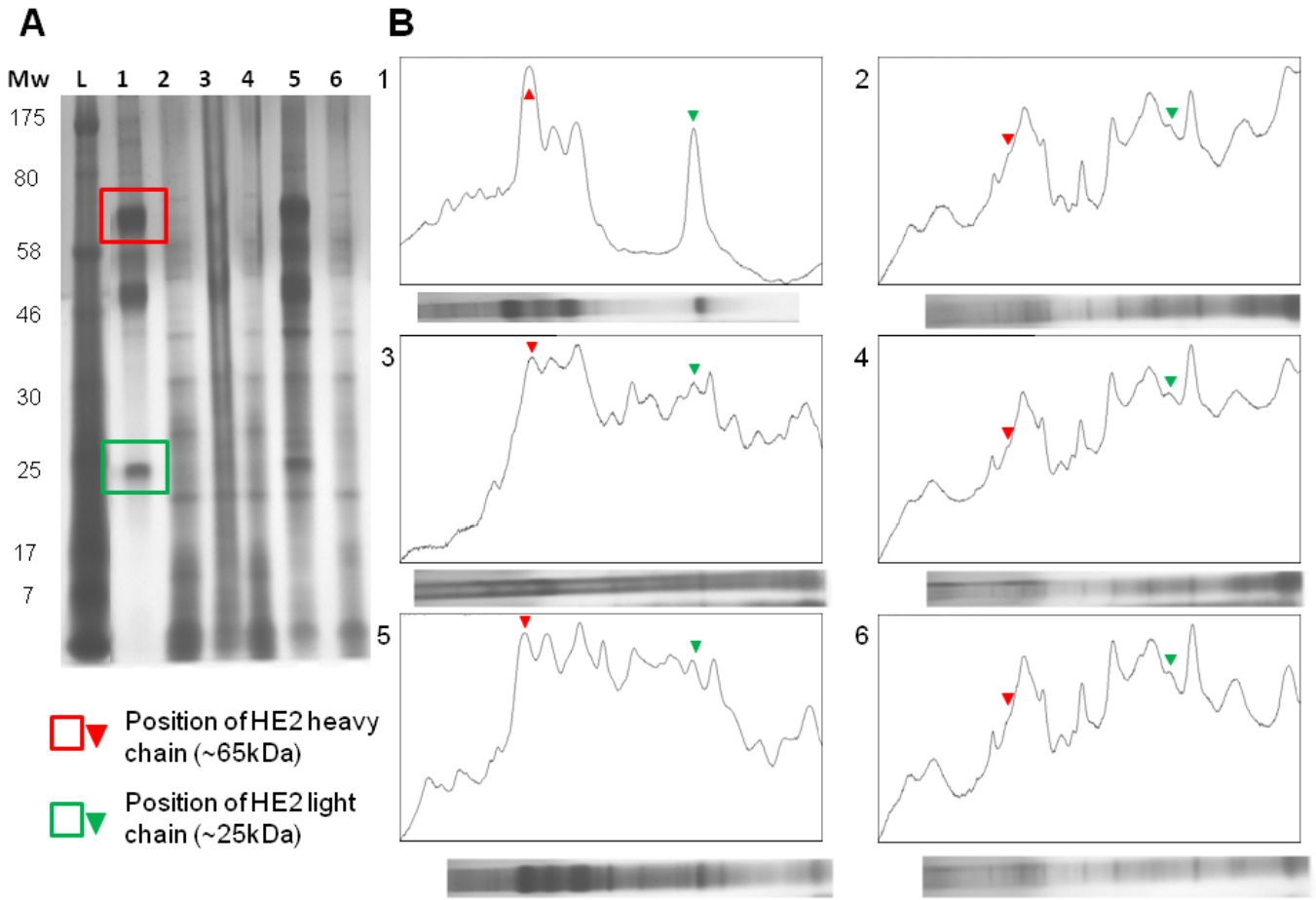
A
B
Mw
L
1
2
3
4
5
6
175
80
58
46
30
25
17
7
Position of HE2 heavy chain (~65kDa)
Position of HE2 light chain (~25kDa)

Figure 4.6 HE2 cleavage by ACM is reduced by addition of class-specific protease inhibitors.

Cleavage mixtures of ACM and antibody were prepared with or without protease inhibitor, incubated for 2 hours at 37°C and separated by SDS-PAGE (Panel A). Gels were silver stained, photographed and peak density analysed using ImageJ software (Panel B). (L) Ladder, (1) Ig alone, (2) Ig + ACM, (3) Ig + ACM + Batimastat, (4) Ig + ACM + Iodoacetamide, (5) Ig + ACM + PMSF, (6) ACM alone. Trace peaks correspond to protein bands on SDS-PAGE gel. Boxes denote Ig heavy (red) or light (green) chain. Bands corresponding to HE2 heavy and light chains showed greatest preservation in samples treated with serine and metalloprotease inhibitors indicating these classes of protease to be primarily responsible for HE2 degradation. Results are representative of two independent experiments.

Peak traces were also semi-quantified using the measurement protocol described in sections 4.3.6. Bands corresponding to heavy and light chains from each antibody subclass were identified based on molecular weight and peak area measured using digital tools included in the ImageJ analysis software package. Peak area measurements were corrected for contributions from ACM proteins and then expressed relative to control Ig. Analyses confirmed findings from SDS-PAGE, with PMSF and Batimastat providing the most consistent protection from cleavage (Figure 4.7). PMSF-mediated protection was observed across all subclasses (Figure 4.7 panels A to E) and also with HE2, an anti-*A. castellanii* polyclonal IgM antibody generated *de novo* (Figure 4.7, panel E). Inhibition of cleavage by Batimastat was more restricted, with the clearest levels of protection seen for IgG and IgA subclasses (panels A and C), and either ambiguous or no protection for IgE, and IgM (panels B, D, and E).

Additionally, variation in susceptibility to cleavage was observed between heavy and light chains. The majority of classes, and treatments within classes exhibited lower relative peak areas for light than for heavy chain. This was the case even where protease inhibitor treatment prevented a substantial proportion of degradation, for example in PMSF treatments (panels C and E).

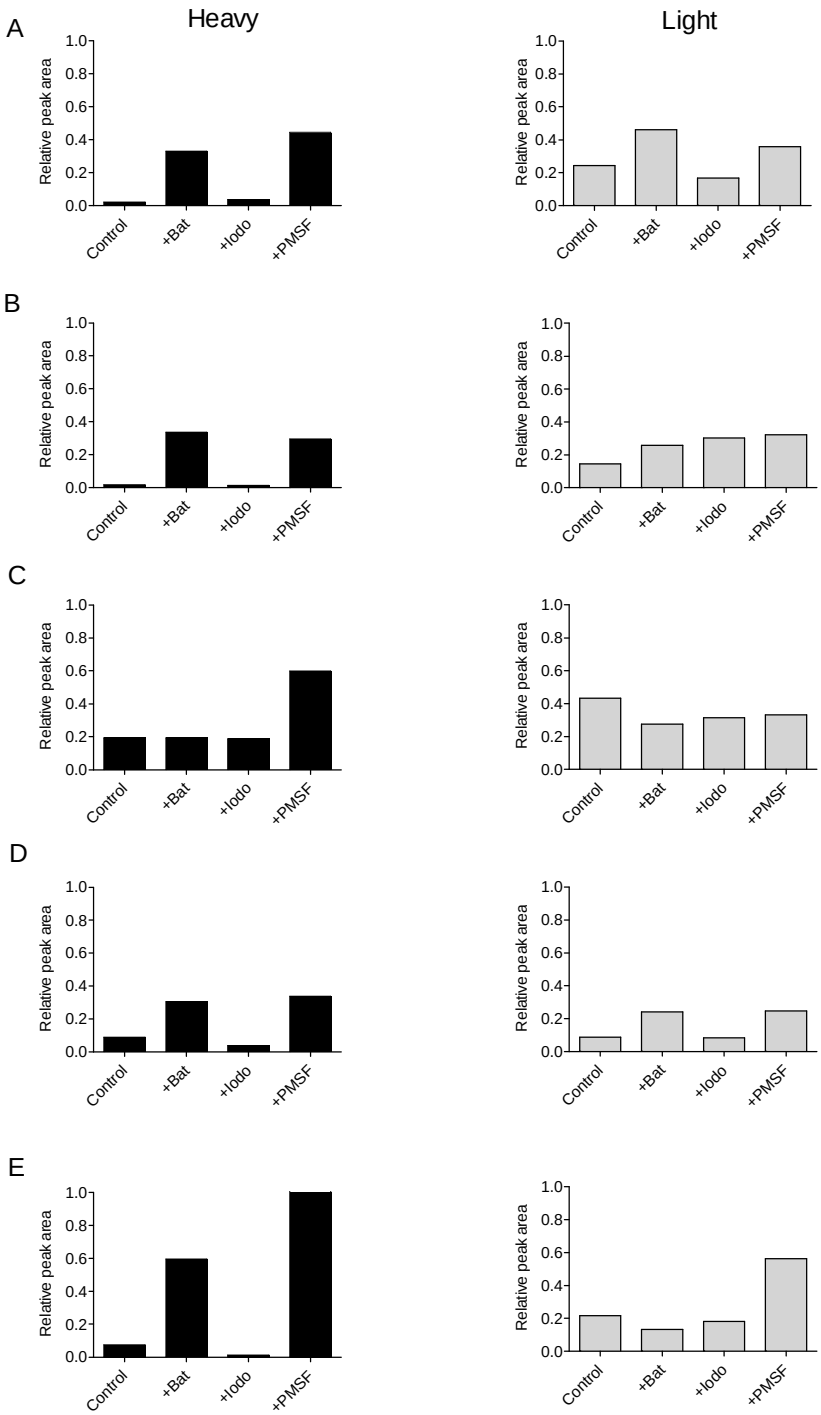

Figure 4.7 Peak area of Ig heavy and light chains in antibody plus ACM cleavage mixes. Peak areas are higher in PMSF and Batimastat treatments relative to control Ig (value set to 1). Peak density traces of silver-stained gels were analysed using ImageJ software. (A) IgG, (B) IgE, (C) IgA, (D) IgM, (E) HE2. Bat = Batimastat, Iodo = Iodoacetamide, PMSF= phenlymethylsulfonyl fluoride. Results are representative of two independent experiments.

4.4.3. Structural effects: Binding

Previous experiments had shown that polyclonal antibody generated by immunisation and *in vitro* hybridoma fusion did not protect HBMEC monolayers from cell death or loss of monolayer integrity (Chapter 3, section 3.4.9). However a decrease in binding was observed, both with polyclonal and negative control IgM (Chapter 3, section 3.4.8). To investigate whether this effect was confined to IgM or also extended to antibodies of other subclasses, binding experiments were set up as described in section 4.3.8. Examples of multimeric (IgM), monomeric (IgG), and fragmented (Fc fragment) antibody were included to determine which levels of structure produced a measurable effect. In accordance with the response in previous assays, both polyclonal HE2 and isotype control treatments produced a reduction in binding of approximately 20% relative to untreated controls (Figure 4.8, $p<0.001$, 1-way ANOVA). No effect on binding was observed in any other treatment group, implying that the ability to reduce trophozoite binding in a nonspecific manner is confined to multimeric Ig.

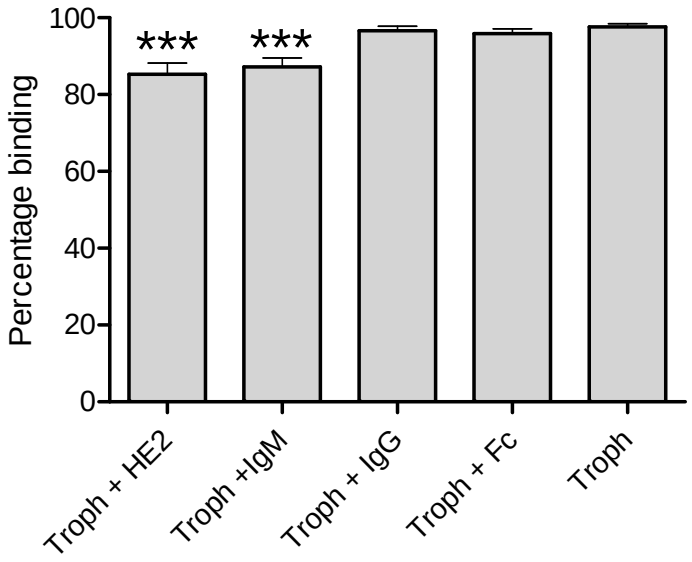

Figure 4.8 Adherence of trophozoites to HBMEC is reduced by multimeric, but not monomeric or fragmented immunoglobulin.

10^5 trophozoites were treated with 200µg/ml antibody/fragment for three hours and then used to infect HBMEC monolayers. Binding was assessed by triplicate haemocytometer counts of unbound trophozoites after three hours. Results are mean + S.E.M. from three independent experiments (*** $p<0.001$, 1-way ANOVA).

4.4.4. Structural effects: Monolayer protection

Given the observed reduction in binding confined to multimeric Ig, we sought to determine whether the same antibodies/fragments afforded protection to HBMEC monolayers. Experiments detailed as part of Chapter 3 (section 3.4.9) had not demonstrated a protective effect as assessed by a variety of measures, and these were extended to include negative control IgG and Fc fragment.

4.4.5. Haematoxylin staining

HBMEC monolayers were infected with antibody or Fc fragment-treated trophozoites and incubated overnight as described in section 4.3.7. Wells were then fixed and stained with haematoxylin to assess cell coverage, as described in section 4.3.9. No protection of the monolayer was observed in any treatment wells with levels of disruption being equivalent to those produced by untreated trophozoites, representing almost total loss of the cell layer (Figure 4.9).

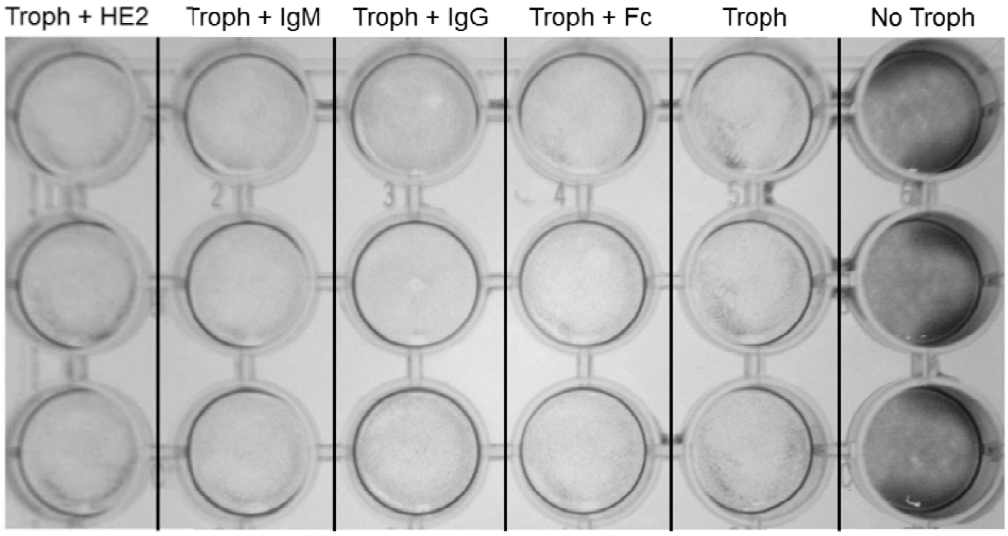

Figure 4.9 Disruption of HBMEC monolayers by trophozoites is not reduced by multimeric, monomeric or fragmented immunoglobulin.

10^5 trophozoites were treated with 200µg/ml antibody/ Fc fragment for three hours and then used to infect HBMEC monolayers. Monolayer disruption was assessed in triplicate by haematoxylin staining after 18-24 hours incubation. Image is representative of three independent experiments.

4.4.6. Monolayer disruption

Wells infected as described in sections 4.3.7 were photographed after 18-24 hours and percentage monolayer disruption estimated from photomicrographs using the method outlined in section 4.3.9. No protection was observed for any of the treatment groups versus the positive control (Figure 4.10) and a significant difference in percentage monolayer disruption was only observed in negative control samples ($p<0.0001$, 1-way ANOVA).

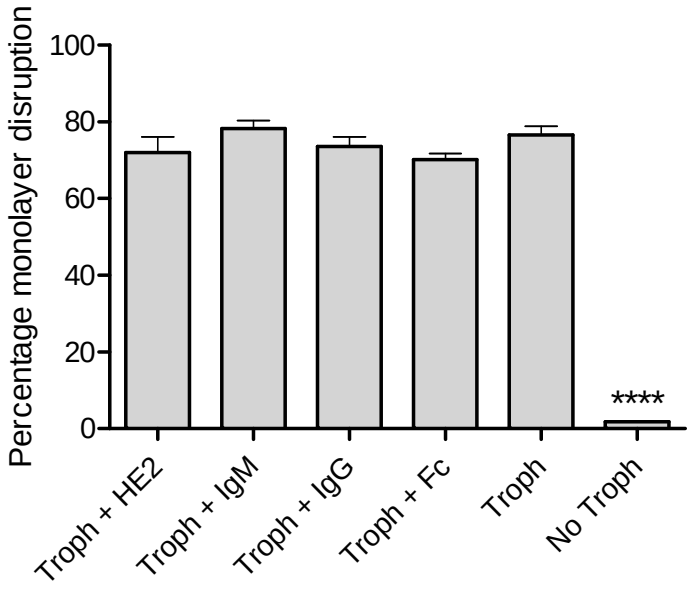

Figure 4.10 Percentage monolayer disruption of HBMEC monolayers by trophozoites is not reduced by multimeric, monomeric or fragmented immunoglobulin.

10^5 trophozoites were treated with 200µg/ml antibody/ Fc fragment for three hours and then used to infect HBMEC monolayers. Monolayer disruption was assessed in triplicate from photomicrographs by a grid counting method. No significant differences were observed between columns other than the negative control (**** $p<0.0001$ 1-way ANOVA). Results are mean + S.E.M. from three independent experiments.

4.4.7. Structural effects: Cytotoxicity

HBMEC monolayers were infected as described in sections 4.3.7, and cell free supernatants collected after 18-24 hours. The supernatants were then tested for LDH release as a necrotic marker, and percentage cell death calculated for each treatment (see section 4.3.10). Significant differences were seen between treatment groups ($p<0.0001$ 1-way ANOVA) however this did not correlate with protection as all groups produced cell death measurements in excess of untreated controls (Figure 4.11). Enhancement of cell death was statistically significant for both IgM treatments, and Fc fragment alone (Figure 4.11).

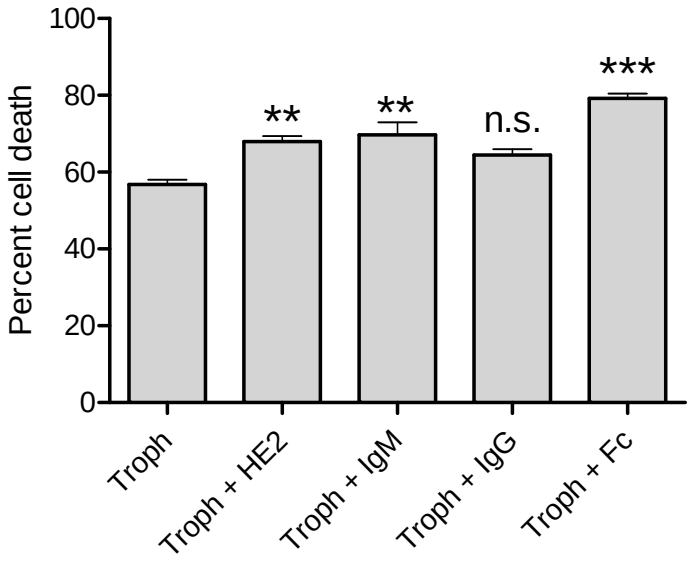

Figure 4.11 Percentage cell death in trophozoite-infected HBMEC monolayers is not reduced by multimeric, monomeric or fragmented immunoglobulin.

10^5 trophozoites were treated with 200µg/ml antibody/fragment for three hours and then used to infect HBMEC monolayers for up to 24 hours. Supernatants from each treatment were then assessed for LDH release in triplicate. Treatment values differed significantly from untreated controls ($p<0.0001$ 1-way ANOVA) and cell death was significantly enhanced by IgM and Fc fragment treatments (** $p<0.05$, *** $p<0.01$). Results are mean + S.E.M. from three independent experiments.

4.4.8. Fc receptor in *A. castellanii*

The reduction in binding by both polyclonal and negative control IgM that had been observed in sections 4.4.3 and in Chapter 3 was potentially explicable as capture of antibody by trophozoite surface factors. One such factor previously demonstrated in other parasitic protozoa is the presence of an Fc-binding protein. To investigate whether *A. castellanii* trophozoites demonstrated dedicated Fc-binding-like activity a bioinformatics approach, immunofluorescence assays and FACS analysis were performed.

4.4.9. Fc receptor in *A. castellanii:* Bioinformatics

No Fc-binding activity has previously been reported in *A. castellanii* and an interrogation of *A. castellanii* information deposited in the NCBI database (www.ncbi.nlm.nih.gov/) using the terms “Fc”, “Fc binding protein”, and “Fc receptor” produced no hits. An alternative approach was therefore used whereby sequences of proteins with known Fc-binding activity were retrieved from NCBI and UNIPROT databases and individually compared with the *A. castellanii* transcriptomic sequence using the tBLASTn algorithm (see section 4.3.11). The best five matches from queries producing significant hits were recorded, with sequences from *Schistosoma mansoni*, *Leishmania major*, *Trypanosoma cruzi*, *Trypanosoma brucei*, and *Toxoplasma gondii* demonstrating significant E-values (Table 4.1, Figures 4.12 - 4.14).

Protein	Accession	Query length	Match Length	Coverage	E-value
Homo sapiens IgG Fc receptor	CAA35642	323aa	40aa 48aa	12% 14%	2.5 5.5
Homo sapiens IgM Fc receptor	ACX94155.1	390aa	86aa	22%	6
Homo sapiens IgA Fc receptor	P24071.1	287aa	78aa 70aa 52aa	23% 22% 18%	0.41 0.91 2
Homo sapiens IgE Fc receptor	AAA52434.1	321aa	27aa 27aa	8% 8%	7.6 7.6
Mus musculus IgG Fc receptor	AAA16904.1	365aa	82aa 82aa 80aa 31aa 45aa	21% 21% 19% 8% 12%	1.2 1.2 3.3 4.7 6.6
Mus musculus IgA/IgM Fc receptor	EDL39730.1	310aa	91aa 91aa 38aa 63aa 63aa	28% 28% 12% 17% 17%	1.5 1.5 3.2 6.7 6.8

Table 4.1

Protein	Accession	Query length	Match Length	Coverage	E-value
Mus musculus IgE Fc receptor (II)	CAA45532	330aa	76aa 76aa 147aa 70aa 147aa	21% 21% 35% 17% 35%	3.5 3.5 3.6 8.2 8.9
Schistosoma mansoni paramyosin	AAA29915.1	866aa	446aa 446aa	50% 50%	3e-04 4e-04
Leishmania major Lmsp1	Not deposited†	152aa	96aa, 36aa, 28aa 96aa, 36aa, 28aa 57aa 57aa 57aa	125% 125% 40.4% 40.4% 32.3%	2e-44 9e-44 5e-04 5e-04 0.27
Trypanosoma cruzi Lmsp1	Not deposited†	154aa	91aa, 36aa 97aa, 25aa 42aa 58aa 48aa	79% 63% 27% 37% 29%	5e-40 1e-05 0.016 3.4 6.0
Trypanosoma brucei Lmsp1	Not deposited†	150aa	94aa, 36aa 43aa 65aa 46aa	85% 28% 43% 30%	1e-04 0.001 0.57 1.8
Toxoplasma gondii Beta antigen	EEA98208.1	303aa	214aa, 201aa, 205aa, 175aa 203aa, 195aa, 214aa, 180aa 203aa, 195aa, 214aa, 180aa 282aa, 157aa 282aa, 157aa	76% 73% 73% 92% 92%	4e-18 8e-17 9e-17 9e-16 1e-15

Table 4.1

Protein	Accession	Query length	Match Length	Coverage	E-value
Plasmodium falciparum PfEMP1‡	AAB87407.1	178aa	41aa, 65aa 31aa, 65aa 32aa, 34aa 19aa	20% 35% 16% 16%	0.19 3.2 6.5 7.1
Streptococcus sp. Protein G	CAA27638.1	480aa	45aa 45aa	9% 9%	5.2 5.3
Staphylococcus aureus Protein A	AGE10364.1	367aa	N/S	N/S	N/S
Finegoldia magna Protein L	AAA67503.1	992aa	N/S	N/S	N/S

Table 4.1 Results of BLAST searches of the *A. castellanii* genome using Fc-binding proteins derived from various organisms.

Peptide sequences were retrieved from the NCBI protein database and searched against the *A. castellanii* genome using the tBLASTn algorithm. Accession numbers, length of aligned regions, coverage and E-values for matches are shown for each search. The top five matches are shown for each BLAST query. N/S = no significant alignment. † Peptide sequence was not deposited in NCBI database, but retrieved in FASTA format from the original publication. ‡ PfEMP1 is encoded by a highly variable subset of genes (*var* genes). To correct for this, 10 variants were selected from data in GenBank and also searched against *A. castellanii* (Appendix 3). No reliable matches were returned for any PfEMP1 variants.

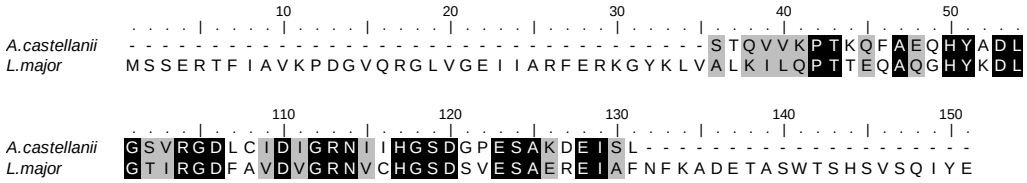

Figure 4.12 Alignment of *L. major* Lmsp1 with matching sequence from the *A. castellanii* transcriptome.

Sequences were retrieved from published data and NCBI databases and aligned using BioEdit software (available from http://www.mbio.ncsu.edu/bioedit/bioedit.html). Black highlighting indicates conserved residues, grey highlighting indicates similar residues. A high degree of similarity was observed in the central region of the alignment, corresponding to the significant E-value obtained by BLAST.

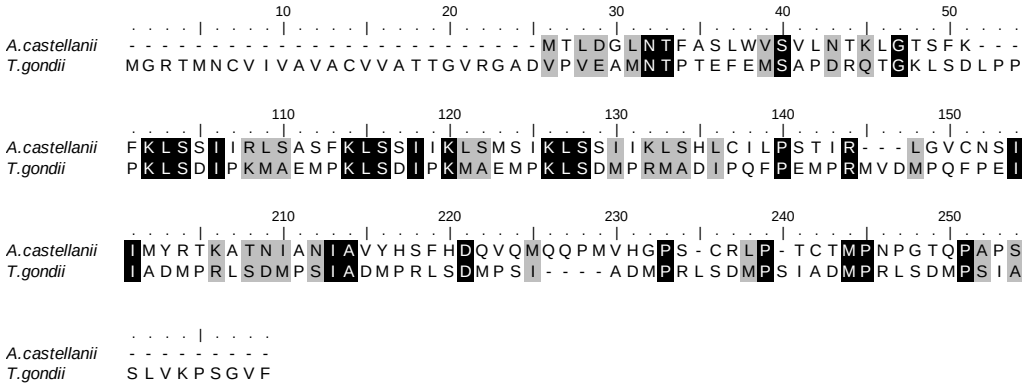

Figure 4.13 Alignment of *T. gondii* beta antigen with matching sequence from the *A. castellanii* transcriptome.

Sequences were retrieved from published data and NCBI databases and aligned using BioEdit software (available from http://www.mbio.ncsu.edu/bioedit/bioedit.html). Black highlighting indicates conserved residues, grey highlighting indicates similar residues. A high degree of similarity was observed in the central region of the alignment, corresponding to the significant E-value obtained by BLAST.

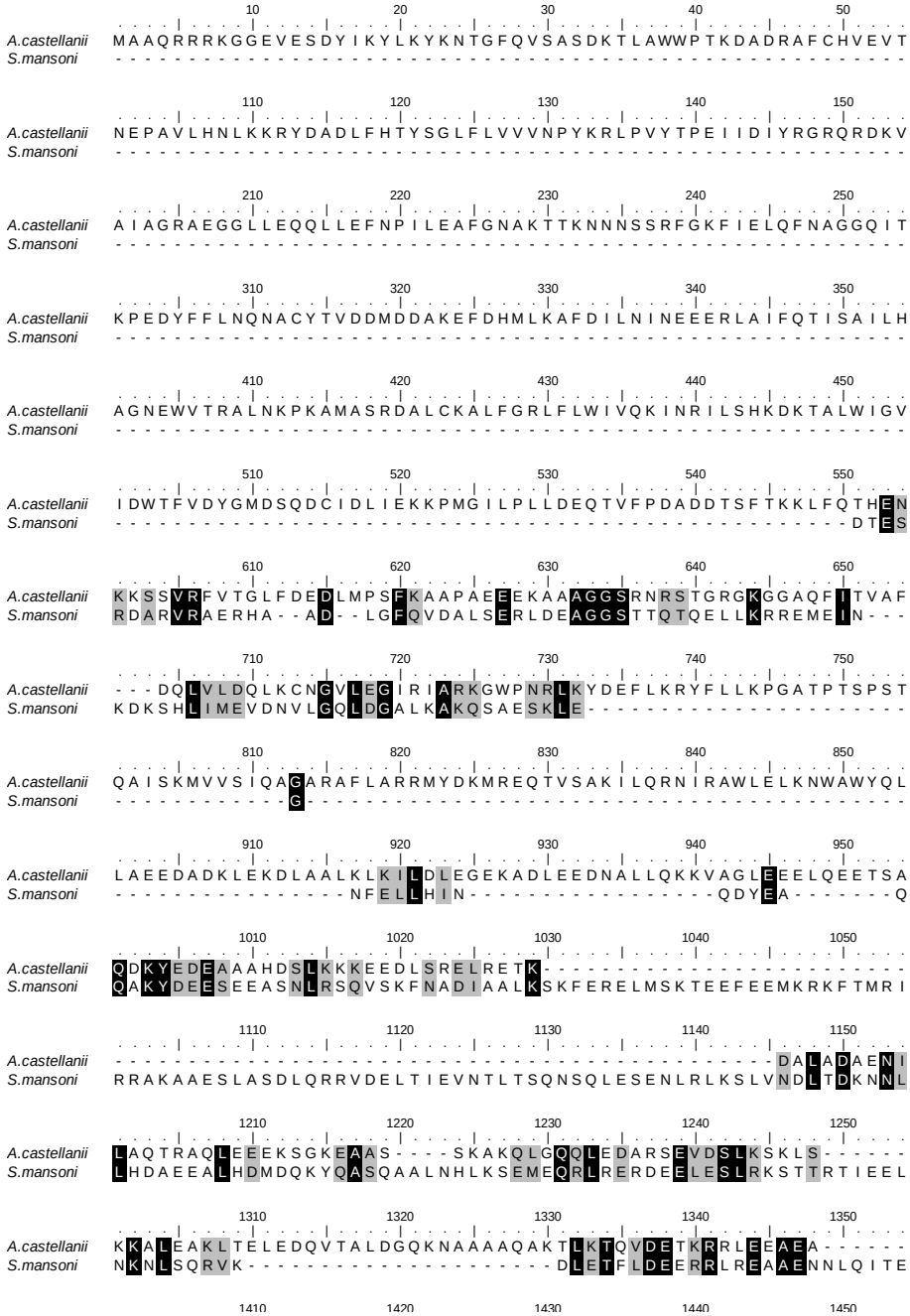

Figure 4.14 Alignment of *S. mansoni* paramyosin with matching sequence from the *A. castellanii* transcriptome.

Sequences were retrieved from published data and NCBI databases and aligned using BioEdit software (available from http://www.mbio.ncsu.edu/bioedit/bioedit.html). Black highlighting indicates conserved residues, grey highlighting indicates similar residues. Similarity was observed in the C-terminal half of the alignment, interrupted by large gaps. This explains the significant but relatively large E-value obtained by BLAST.

Sequences obtained from protein databases exhibited considerable dissimilarity, and it was not possible to obtain reliable phylogenetic trees. An alternative reciprocal BLAST approach was therefore taken to make pairwise comparisons between all sequences. As before, protein sequences were retrieved from UNIPROT and NCBI databases based on association with Fc-binding BLAST outputs (Appendix 4). These were restricted based on length and then interpreted according to E-scores. Filtering parameters for sequence length and alignment significance are given in section 4.3.11. Where individual BLAST results from searches performed against the *A. castellanii* genome produced sequences of sufficient length and significance (Table 4.2), sequence data from the appropriate transcriptomic contig was translated in an appropriate frame and included in the reciprocal BLAST.

Query I.D.	Subject I.D.	% Identity	alignment length (aa)	e-value
Acanthamoeba_Leishmania_Lmsp1_contig	Acanthamoeba_T.brucei_Lmsp1_contig	100	94	2.00E-54
Acanthamoeba_Leishmania_Lmsp1_contig	Acanthamoeba_T.cruzi_Lmsp1_contig	100	91	9.00E-53
Acanthamoeba_T.brucei_Lmsp1_contig	Acanthamoeba_T.cruzi_Lmsp1_contig	100	89	1.00E-51
Leishmania_major_Lmsp1	Acanthamoeba_Leishmania_Lmsp1_contig	55.91	93	7.00E-34
Leishmania_major_Lmsp1	Acanthamoeba_T.brucei_Lmsp1_contig	55.91	93	7.00E-34
Leishmania_major_Lmsp1	Acanthamoeba_T.cruzi_Lmsp1_contig	56.18	89	6.00E-33
Leishmania_major_Lmsp1	Trypanosoma_brucei_Lmsp1	82	150	5.00E-68
Leishmania_major_Lmsp1	Trypanosoma_cruzi_Lmsp1	84.25	127	4.00E-61
Mouse_FceR2	Streptococcus_pyogenes_FcgR	23.13	134	1.00E-05
Mouse_FceR2	Streptococcus_pyogenes_FcgR	19.64	112	1.00E-05
Streptococcus_agalactiae_FcaR	Schistosoma_mansoni_paramyosin	22.19	311	8.00E-10
Streptococcus_agalactiae_FcaR	Schistosoma_mansoni_paramyosin	19.81	631	2.00E-08
Streptococcus_agalactiae_FcaR	Schistosoma_mansoni_paramyosin	17.75	355	2.00E-07
Streptococcus_agalactiae_FcaR	Schistosoma_mansoni_paramyosin	19.13	345	1.00E-06
Streptococcus_agalactiae_FcaR	Schistosoma_mansoni_paramyosin	19.5	241	4.00E-06
Streptococcus_agalactiae_FcaR	Streptococcus_pyogenes_FcgR	19.14	324	9.00E-07
Streptococcus_agalactiae_FcaR	Streptococcus_pyogenes_FcgR	21.68	309	7.00E-06
Streptococcus_agalactiae_FcaR	Streptococcus_pyogenes_FcgR	18.36	207	7.00E-06
Streptococcus_agalactiae_FcaR	Taenia_solium_paramyosin	20.72	613	2.00E-08
Streptococcus_agalactiae_FcaR	Taenia_solium_paramyosin	16.22	333	6.00E-06
Streptococcus_agalactiae_FcaR	Taenia_solium_paramyosin	17.56	450	7.00E-06
Streptococcus_agalactiae_FcaR	Toxoplasma_gondii_Beta	36.07	122	5.00E-28
Streptococcus_agalactiae_FcaR	Toxoplasma_gondii_Beta	35.25	122	5.00E-28

Table 4.2

Query I.D.	Subject I.D.	% Identity	alignment length (aa)	e-value
Streptococcus_agalactiae_FcaR	Toxoplasma_gondii_Beta	36.13	119	9.00E-28
Streptococcus_agalactiae_FcaR	Toxoplasma_gondii_Beta	33.61	122	2.00E-27
Streptococcus_agalactiae_FcaR	Toxoplasma_gondii_Beta	31.41	156	2.00E-27
Streptococcus_agalactiae_FcaR	Toxoplasma_gondii_Beta	36.13	119	3.00E-27
Streptococcus_agalactiae_FcaR	Toxoplasma_gondii_Beta	33.61	122	3.00E-27
Streptococcus_agalactiae_FcaR	Toxoplasma_gondii_Beta	33.61	122	3.00E-27
Streptococcus_agalactiae_FcaR	Toxoplasma_gondii_Beta	30.14	146	2.00E-26
Streptococcus_agalactiae_FcaR	Toxoplasma_gondii_Beta	28.76	153	2.00E-25
Streptococcus_agalactiae_FcaR	Toxoplasma_gondii_Beta	31.5	127	3.00E-25
Streptococcus_agalactiae_FcaR	Toxoplasma_gondii_Beta	24.39	246	3.00E-20
Streptococcus_pyogenes_FcgR	Schistosoma_mansoni_paramyosin	25.43	173	4.00E-11
Streptococcus_pyogenes_FcgR	Schistosoma_mansoni_paramyosin	26.09	184	2.00E-10
Streptococcus_pyogenes_FcgR	Schistosoma_mansoni_paramyosin	26.84	231	5.00E-10
Streptococcus_pyogenes_FcgR	Schistosoma_mansoni_paramyosin	25.62	203	3.00E-09
Streptococcus_pyogenes_FcgR	Schistosoma_mansoni_paramyosin	26.92	182	5.00E-08
Streptococcus_pyogenes_FcgR	Schistosoma_mansoni_paramyosin	22.09	172	2.00E-06
Streptococcus_pyogenes_FcgR	Schistosoma_mansoni_paramyosin	24.83	149	3.00E-06
Streptococcus_pyogenes_FcgR	Taenia_solium_paramyosin	25.15	167	1.00E-12
Streptococcus_pyogenes_FcgR	Taenia_solium_paramyosin	24.47	237	1.00E-10
Streptococcus_pyogenes_FcgR	Taenia_solium_paramyosin	23.14	242	3.00E-09
Streptococcus_pyogenes_FcgR	Taenia_solium_paramyosin	26.28	156	6.00E-09
Streptococcus_pyogenes_FcgR	Taenia_solium_paramyosin	25.15	167	2.00E-08
Streptococcus_pyogenes_FcgR	Taenia_solium_paramyosin	22.18	275	4.00E-08

Table 4.2

Query I.D.	Subject I.D.	% Identity	alignment length (aa)	e-value
Streptococcus_pyogenes_FcgR	Taenia_solium_paramyosin	25.71	175	1.00E-07
Streptococcus_pyogenes_FcgR	Taenia_solium_paramyosin	23.43	175	7.00E-07
Streptococcus_pyogenes_FcgR	Taenia_solium_paramyosin	25.58	172	3.00E-06
Streptococcus_pyogenes_FcgR	Taenia_solium_paramyosin	21.98	182	5.00E-06
Taenia_solium_paramyosin	Schistosoma_mansoni_paramyosin	72.19	791	0
Taenia_solium_paramyosin	Schistosoma_mansoni_paramyosin	22.04	608	3.00E-30
Taenia_solium_paramyosin	Schistosoma_mansoni_paramyosin	22.4	308	1.00E-13
Toxoplasma_gondii_Beta	Acanthamoeba_Toxoplasma_beta_contig	18.95	190	1.00E-06
Toxoplasma_gondii_Beta	Acanthamoeba_Toxoplasma_beta_contig	21.89	169	2.00E-06
Toxoplasma_gondii_Beta	Acanthamoeba_Toxoplasma_beta_contig	27.06	85	6.00E-06
Toxoplasma_gondii_Beta	Acanthamoeba_Toxoplasma_beta_contig	29.41	68	8.00E-06
Toxoplasma_gondii_Beta	Acanthamoeba_Toxoplasma_beta_contig	27.66	94	8.00E-06
Trypanosoma_brucei_Lmsp1	Acanthamoeba_Leishmania_Lmsp1_contig	54.84	93	4.00E-28
Trypanosoma_brucei_Lmsp1	Acanthamoeba_T.brucei_Lmsp1_contig	54.84	93	4.00E-28
Trypanosoma_brucei_Lmsp1	Acanthamoeba_T.cruzi_Lmsp1_contig	55.06	89	3.00E-27
Trypanosoma_cruzi_Lmsp1	Acanthamoeba_Leishmania_Lmsp1_contig	52.81	89	6.00E-23
Trypanosoma_cruzi_Lmsp1	Acanthamoeba_T.brucei_Lmsp1_contig	52.81	89	5.00E-23
Trypanosoma_cruzi_Lmsp1	Acanthamoeba_T.cruzi_Lmsp1_contig	52.81	89	5.00E-23
Trypanosoma_cruzi_Lmsp1	Trypanosoma_brucei_Lmsp1	88.98	127	1.00E-52
Acanthamoeba_Leishmania_Lmsp1_contig	Acanthamoeba_T.brucei_Lmsp1_contig	100	94	2.00E-54
Acanthamoeba_Leishmania_Lmsp1_contig	Acanthamoeba_T.cruzi_Lmsp1_contig	100	91	9.00E-53
Acanthamoeba_T.brucei_Lmsp1_contig	Acanthamoeba_T.cruzi_Lmsp1_contig	100	89	1.00E-51
Leishmania_major_Lmsp1	Acanthamoeba_Leishmania_Lmsp1_contig	55.91	93	7.00E-34

Table 4.2

Query I.D.	Subject I.D.	% Identity	alignment length (aa)	e-value
Leishmania_major_Lmsp1	Acanthamoeba_T.brucei_Lmsp1_contig	55.91	93	7.00E-34
Leishmania_major_Lmsp1	Acanthamoeba_T.cruzi_Lmsp1_contig	56.18	89	6.00E-33
Leishmania_major_Lmsp1	Trypanosoma_brucei_Lmsp1	82	150	5.00E-68
Leishmania_major_Lmsp1	Trypanosoma_cruzi_Lmsp1	84.25	127	4.00E-61
Mouse_FceR2	Streptococcus_pyogenes_FcgR	23.13	134	1.00E-05
Mouse_FceR2	Streptococcus_pyogenes_FcgR	19.64	112	1.00E-05
Streptococcus_agalactiae_FcaR	Schistosoma_mansoni_paramyosin	22.19	311	8.00E-10
Streptococcus_agalactiae_FcaR	Schistosoma_mansoni_paramyosin	19.81	631	2.00E-08
Streptococcus_agalactiae_FcaR	Schistosoma_mansoni_paramyosin	17.75	355	2.00E-07
Streptococcus_agalactiae_FcaR	Schistosoma_mansoni_paramyosin	19.13	345	1.00E-06
Streptococcus_agalactiae_FcaR	Schistosoma_mansoni_paramyosin	19.5	241	4.00E-06
Streptococcus_agalactiae_FcaR	Streptococcus_pyogenes_FcgR	19.14	324	9.00E-07
Streptococcus_agalactiae_FcaR	Streptococcus_pyogenes_FcgR	21.68	309	7.00E-06
Streptococcus_agalactiae_FcaR	Streptococcus_pyogenes_FcgR	18.36	207	7.00E-06
Streptococcus_agalactiae_FcaR	Taenia_solium_paramyosin	20.72	613	2.00E-08
Streptococcus_agalactiae_FcaR	Taenia_solium_paramyosin	16.22	333	6.00E-06
Streptococcus_agalactiae_FcaR	Taenia_solium_paramyosin	17.56	450	7.00E-06
Streptococcus_agalactiae_FcaR	Toxoplasma_gondii_Beta	36.07	122	5.00E-28
Streptococcus_agalactiae_FcaR	Toxoplasma_gondii_Beta	35.25	122	5.00E-28
Streptococcus_agalactiae_FcaR	Toxoplasma_gondii_Beta	36.13	119	9.00E-28
Streptococcus_agalactiae_FcaR	Toxoplasma_gondii_Beta	33.61	122	2.00E-27
Streptococcus_agalactiae_FcaR	Toxoplasma_gondii_Beta	31.41	156	2.00E-27
Streptococcus_agalactiae_FcaR	Toxoplasma_gondii_Beta	36.13	119	3.00E-27

Table 4.2

Query I.D.	Subject I.D.	% Identity	alignment length (aa)	e-value
Streptococcus_agalactiae_FcaR	Toxoplasma_gondii_Beta	33.61	122	3.00E-27
Streptococcus_agalactiae_FcaR	Toxoplasma_gondii_Beta	33.61	122	3.00E-27
Streptococcus_agalactiae_FcaR	Toxoplasma_gondii_Beta	30.14	146	2.00E-26
Streptococcus_agalactiae_FcaR	Toxoplasma_gondii_Beta	28.76	153	2.00E-25
Streptococcus_agalactiae_FcaR	Toxoplasma_gondii_Beta	31.5	127	3.00E-25
Streptococcus_agalactiae_FcaR	Toxoplasma_gondii_Beta	24.39	246	3.00E-20
Streptococcus_pyogenes_FcgR	Schistosoma_mansoni_paramyosin	25.43	173	4.00E-11
Streptococcus_pyogenes_FcgR	Schistosoma_mansoni_paramyosin	26.09	184	2.00E-10
Streptococcus_pyogenes_FcgR	Schistosoma_mansoni_paramyosin	26.84	231	5.00E-10
Streptococcus_pyogenes_FcgR	Schistosoma_mansoni_paramyosin	25.62	203	3.00E-09
Streptococcus_pyogenes_FcgR	Schistosoma_mansoni_paramyosin	26.92	182	5.00E-08
Streptococcus_pyogenes_FcgR	Schistosoma_mansoni_paramyosin	22.09	172	2.00E-06
Streptococcus_pyogenes_FcgR	Schistosoma_mansoni_paramyosin	24.83	149	3.00E-06
Streptococcus_pyogenes_FcgR	Taenia_solium_paramyosin	25.15	167	1.00E-12
Streptococcus_pyogenes_FcgR	Taenia_solium_paramyosin	24.47	237	1.00E-10
Streptococcus_pyogenes_FcgR	Taenia_solium_paramyosin	23.14	242	3.00E-09
Streptococcus_pyogenes_FcgR	Taenia_solium_paramyosin	26.28	156	6.00E-09
Streptococcus_pyogenes_FcgR	Taenia_solium_paramyosin	25.15	167	2.00E-08
Streptococcus_pyogenes_FcgR	Taenia_solium_paramyosin	22.18	275	4.00E-08
Streptococcus_pyogenes_FcgR	Taenia_solium_paramyosin	25.71	175	1.00E-07
Streptococcus_pyogenes_FcgR	Taenia_solium_paramyosin	23.43	175	7.00E-07
Streptococcus_pyogenes_FcgR	Taenia_solium_paramyosin	25.58	172	3.00E-06
Streptococcus_pyogenes_FcgR	Taenia_solium_paramyosin	21.98	182	5.00E-06

Table 4.2

Query I.D.	Subject I.D.	% Identity	alignment length (aa)	e-value
Taenia_solium_paramyosin	Schistosoma_mansoni_paramyosin	72.19	791	0
Taenia_solium_paramyosin	Schistosoma_mansoni_paramyosin	22.04	608	3.00E-30
Taenia_solium_paramyosin	Schistosoma_mansoni_paramyosin	22.4	308	1.00E-13
Toxoplasma_gondii_Beta	Acanthamoeba_Toxoplasma_beta_contig	18.95	190	1.00E-06
Toxoplasma_gondii_Beta	Acanthamoeba_Toxoplasma_beta_contig	21.89	169	2.00E-06
Toxoplasma_gondii_Beta	Acanthamoeba_Toxoplasma_beta_contig	27.06	85	6.00E-06
Toxoplasma_gondii_Beta	Acanthamoeba_Toxoplasma_beta_contig	29.41	68	8.00E-06
Toxoplasma_gondii_Beta	Acanthamoeba_Toxoplasma_beta_contig	27.66	94	8.00E-06
Trypanosoma_brucei_Lmsp1	Acanthamoeba_Leishmania_Lmsp1_contig	54.84	93	4.00E-28
Trypanosoma_brucei_Lmsp1	Acanthamoeba_T.brucei_Lmsp1_contig	54.84	93	4.00E-28
Trypanosoma_brucei_Lmsp1	Acanthamoeba_T.cruzi_Lmsp1_contig	55.06	89	3.00E-27
Trypanosoma_cruzi_Lmsp1	Acanthamoeba_Leishmania_Lmsp1_contig	52.81	89	6.00E-23
Trypanosoma_cruzi_Lmsp1	Acanthamoeba_T.brucei_Lmsp1_contig	52.81	89	5.00E-23
Trypanosoma_cruzi_Lmsp1	Acanthamoeba_T.cruzi_Lmsp1_contig	52.81	89	5.00E-23
Trypanosoma_cruzi_Lmsp1	Trypanosoma_brucei_Lmsp1	88.98	127	1.00E-52

Table 4.2 Reciprocal BLAST of known and predicted Fc-binding sequences.

Amino acid sequences retrieved from UNIPROT and NCBI databases were compared using automated tBLASTn queries (817 individual comparisons). Results were filtered to exclude short alignments of less than 50aa. Alignments with E-values >0.00001 were considered non-significant and were also excluded.

Output of reciprocal BLAST data demonstrated high levels of similarity between mammalian Fc-receptors and FcR in less closely related species *Gallus gallus* and *Crassostrea gigas* (see Appendix 4). The reciprocal BLAST approach was also able to detect well conserved sequences between *Schistosoma mansoni* and *Taenia solius*, closely related species in which detection of conserved sequence was an expected outcome of the approach. However significant similarity was also observed between sequences from phylogenetically distant organisms. In particular a protein with Fc-binding properties from *Streptococcus pyogenes* (Protein G) had sequence similarity to *S. mansoni* and *T. solius* paramyosin, as well as human and mouse IgE2 receptor. Similarity between *Staphylococcus aureus* Protein A and mouse and human FcR was also observed. Taken together, this indicates that our experimental approach was sound and appropriate.

Using the initial genome BLAST significant matches to regions of the *A. castellanii* genome were observed with sequences from *L. major*, a homologue of the same Lmsp1 gene in *T. cruzi*, and sequence from *T. gondii* (Table 4.1, Figures 4.12 and 4.13). These regions corresponded to hypothesised Fc binding proteins from these organisms. Using a lower-stringency cut-off of 0.001, significant matches were also seen to a further Lmsp1 homologue in *T. brucei* and also to *S. mansoni* paramyosin (Figure 4.14) were also observed in this case. Similarly reciprocal BLAST confirmed matches between *L. major* Lmsp1 and its *Trypanosoma* homologues and sequence from the aligned *A. castellanii* sequence data (Table 4.2). Strong matches between *A. castellanii* sequence and *T. gondii* Beta antigen were again also observed. Reciprocal BLAST did not however detect significant similarity between *A. castellanii*

and *S. mansoni* or *T. solium* paramyosin; although as with the primary BLAST searches matches could be found by using a lower-stringency E-value cut-off.

4.4.10. Fc receptor in *A. castellanii*: Immunofluorescence

Cytospin preparations of K562, HBMEC, and *A. castellanii* trophozoites were made as described in section 4.3.12. Samples were then blocked and incubated with human IgG Fc fragment (Table 2.2, #5) followed by anti-human IgG FITC conjugate (Table 2.2, #10), as described in sections 4.3.12. Mounted slides were then observed and photographed under illumination at 360 and 540nm. Strong fluorescence was detected in K562, a cell type which are known to express Fc receptors whilst no fluorescence was observed in HBMECs (Figure 4.15). *A. castellanii* trophozoites demonstrated weak fluorescence (Figure 4.15, denoted by white arrows). In contrast to K562 cells however, this was observed in the Fc + anti-Fc-FITC treatment only.

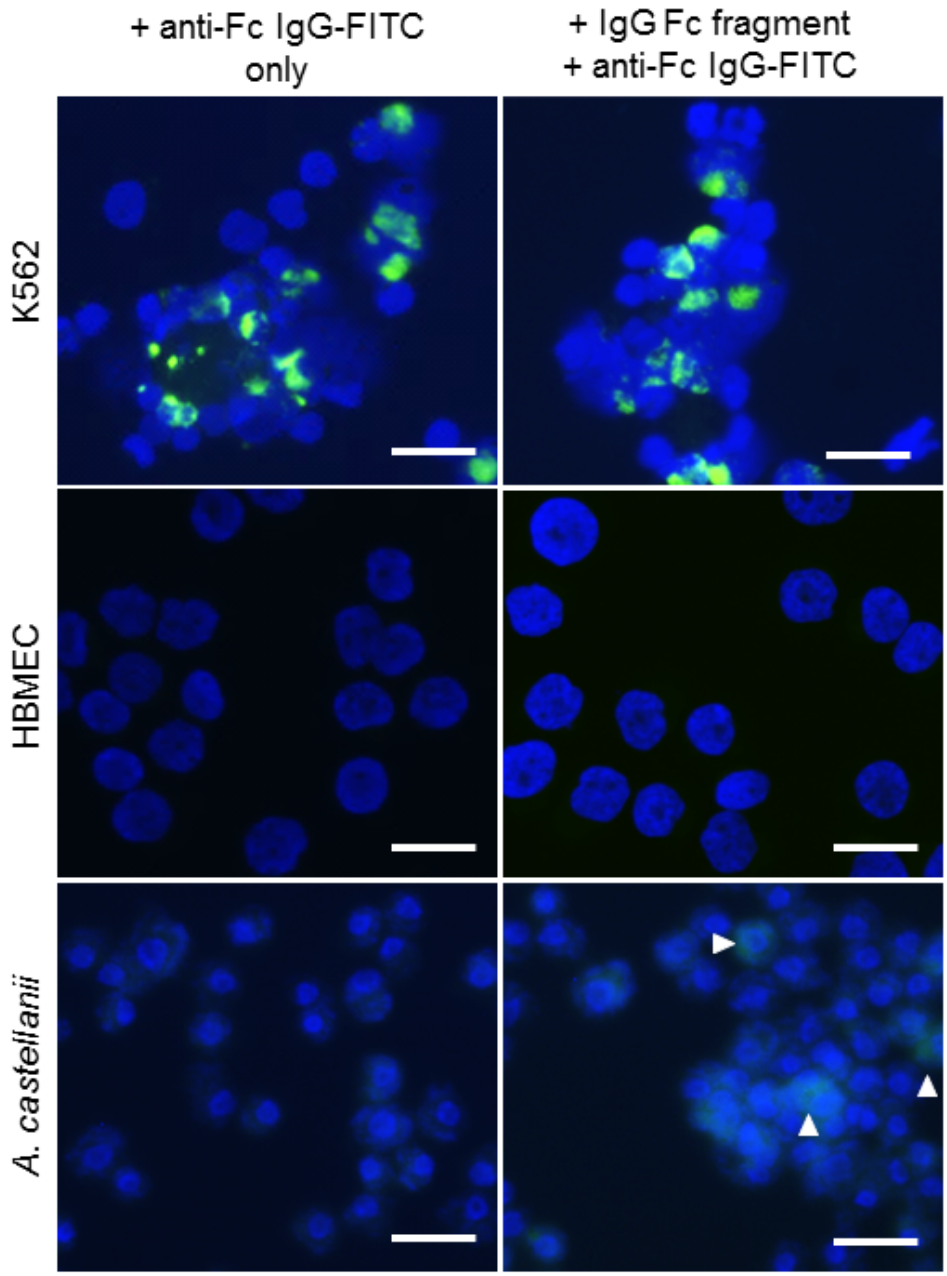

Figure 4.15 A. castellanii trophozoites treated with human Fc fragment plus FITC-conjugated anti-human Fc demonstrate weak fluorescence.

Fixed trophozoites were blocked and incubated with 1:300 human Fc fragment. FITC-conjugated anti-human Fc secondary antibody was then used to detect binding and nuclei were counterstained with DAPI. Left hand panels: secondary binding controls (no Fc fragment), right hand panels: Fc fragment + anti-Fc secondary. Arrows denote positive staining in *A. castellanii*. Images are representative of two independent experiments. Bar = 50µm.

4.4.11. Fc receptor in *A. castellanii*: FACS

To further explore findings indicating that *A. castellanii* was weakly positive for Fc-binding activity, populations of stained trophozoites were examined using FACS analysis. Cells were harvested, blocked, and stained as described in section 4.3.13 and then sorted using a FACSCantoII instrument as described in section 4.3.13. Single cell populations (R0) were identified for both HBMEC and *A. castellanii* (Figures 4.16 and 4.17, panel A), and cells from within these populations were then gated according to unlabelled controls (panel B). The percentage of stained cells was indicated by the proportion appearing outside the gate in appropriate treatments (panels C and D). Some degree of secondary antibody binding was observed for both HBMEC (36.5%) and *A. castellanii* (11.5%) Treatment with both Fc fragment and detecting antibody failed to produce a significant increase in fluorescence in either case (-0.2% for HBMEC, +1.4% for *A. castellanii*).

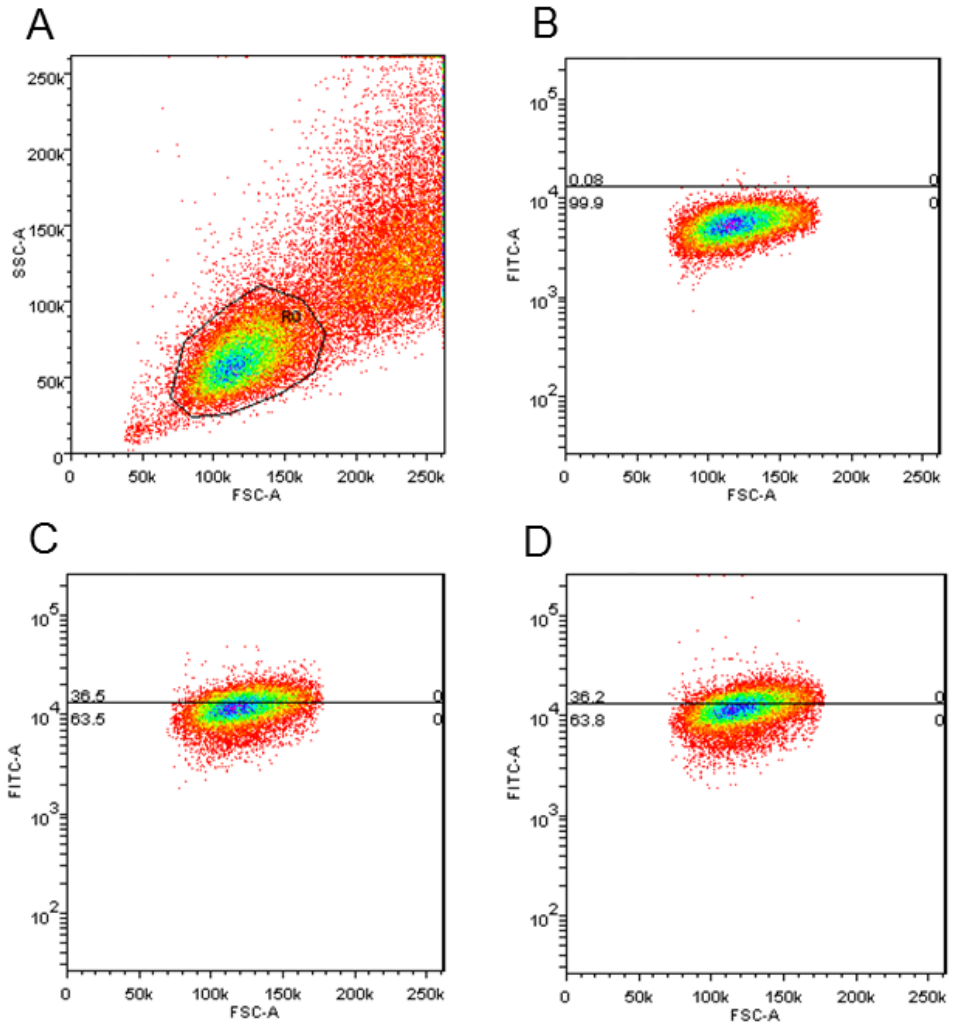

Figure 4.16 HBMEC display low levels of fluorescence attributable to secondary binding of detecting antibody, but no significant increase in fluorescence following incubation with human Fc fragment.

Cells were blocked and incubated with 1:300 Fc fragment plus anti-Fc-FITC secondary, secondary alone, or were left unlabelled. (A) Forward scatter versus side scatter, R0 defines a population of single cells. (B) Forward scatter versus FITC, unlabelled HBMEC were gated to calculate percentage shifts. (C) Secondary antibody only, line denotes gate of unlabelled cells. (D) Fc plus anti-Fc-FITC, line denotes gate of unlabelled cells. Data was analysed using Weasel software v3.0. Results are representative of two independent experiments.

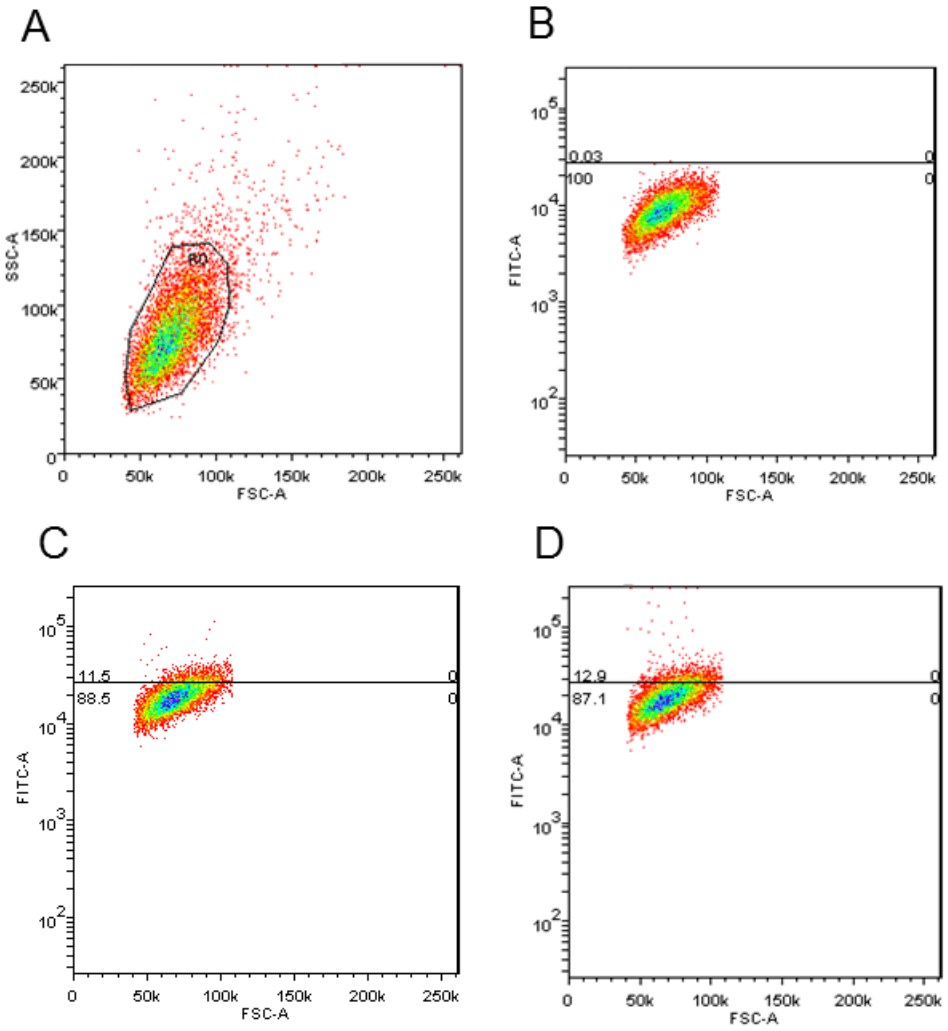

Figure 4.17 *A. castellanii* display low levels of fluorescence attributable to secondary binding of detecting antibody, but no significant increase in fluorescence following incubation with human Fc fragment.

Cells were blocked and incubated with 1:300 Fc fragment plus anti-Fc-FITC secondary, secondary alone, or were left unlabelled. (A) Forward scatter versus side scatter, R0 defines a population of single cells. (B) Forward scatter versus FITC, unlabelled *A. castellanii* were gated to calculate percentage shifts. (C) Secondary antibody only, line denotes gate of unlabelled cells. (D) Fc plus anti-Fc-FITC, line denotes gate of unlabelled cells. Data was analysed using Weasel software v3.0. Results are representative of two independent experiments.

4.5. Discussion

A fully competent immune system is generally recognised as sufficient to control *A. castellanii* infections and development of AGE. In disease states immune control fails, however it is not clear which arms and effectors of the immune response are primarily responsible for infection control in healthy individuals. As a result the specific immune impairments which result in the development of AGE also remain cryptic. As part of work presented in the previous chapter a polyclonal antibody was used to obtain information about *A. castellanii* proteins recognised by the immune system. This antibody impaired the amoeba's ability to bind to human endothelial cells but had no effect on host cell survival and was unable to preserve the integrity of a host cell monolayer. Given that the targeting of the antibody to a number of surface epitopes was apparently ineffective in terms of cell survival outcomes, we sought to examine whether this was due to any active process on the part of the parasite.

Work by previous authors has demonstrated that secreted proteases are an important contributor to the pathogenesis of AGE (Khan et al., 2000b, Alsam et al., 2005b, Sissons et al., 2006a). Aside from any role as virulence determinants during interactions with host cells, proteases may also play a part in immune evasion by degrading key components of the immune response. Mechanisms to degrade antibody have been demonstrated in the amoeba species *Entamoeba histolytica* and also in *A. castellanii* itself (Na et al., 2001, Na et al., 2002a, Garcia-Nieto et al., 2008). The *Acanthamoeba* studies in particular made use of either purified single enzymes, or an unpurified

excretory/secretory enzyme cocktail (ACM). Under the conditions detailed in this study ACM profiles similar to those reported and characterised by previous authors were obtained (Figure 4.1), with bands at molecular weights of 33, 85 and 130-150kDa (Kim et al., 2003, Hurt et al., 2003a, Sissons et al., 2006a)

Using ACM we were able to confirm and extend results from previous studies which demonstrated cleavage activity against immunoglobulin. Na *et al.* showed that both IgA and IgG were vulnerable to degradation by ACM and later extended these findings to include IgM and secretory IgA (Na et al., 2001, Na et al., 2002a). Our data support these results (Figures 4.2, 4.4 and 4.5) and also demonstrate that IgE is similarly vulnerable to ACM-mediated degradation (Figure 4.3). Notably cleavage was observed not just with nonspecific control antibodies but also with polyclonal antibody raised against *A. castellanii* antigens (Figure 4.6). This demonstrates that ACM proteases can act within an environment of mixed specificities and epitopes and against Ig derived from a physiological source. This increases the likelihood that the antibody cleavage process occurs *in vivo* as well as *in vitro*, which although beyond the scope of the current analysis may prove an interesting area in which to direct future investigation.

Three major protease classes have been demonstrated in *A. castellanii* secretions however evidence for roles in infection are most frequently ascribed to serine and metallo-proteases (Hadas and Mazur, 1993, Cho et al., 2000, Kim et al., 2006, Blaschitz et al., 2006). In this regard previous experiments have focused mostly on cytotoxicity and blood-brain barrier breakdown (Alsam et

al., 2005a, Sissons et al., 2006a) however our results suggest that serine proteases in particular should also be considered as having potential immune evasion functions.

The SDS-PAGE profiles obtained from ACM during the course of the above experiment were observed to be highly complex, with multiple bands and correspondingly complicated peak traces (Figures 4.2 to 4.6, lane 6). *Acanthamoeba* secretions have been shown to contain multiple proteases falling within several broad classes; serine, cysteine and metallo-proteases (Alfieri et al., 2000, Alsam et al., 2005b). Using inhibitors specific to each class we sought to attribute cleavage activity to one or more of these classes. Protection from cleavage mediated by PMSF (a serine protease inhibitor) was observed for all antibody classes including polyclonal HE2 antibody (Figures 4.2 to 4.6, lane 5). Batimastat (a metalloprotease inhibitor) also provided partial protection although this effect was substantially less pronounced (Figures 4.2 to 4.6, lane 3). No protection was observed in Iodoacetamide-treated samples (cysteine protease inhibitor).

Similar results were obtained when relative peak areas of heavy and light chain peptides were analysed (Figure 4.7). PMSF again protected both heavy and light chain fragments most effectively whilst Batimastat also contributed to preservation of antibody peaks for each class except IgA. Results for heavy and light chain were broadly similar however the relative peak areas for control and Iodoacetamide-treated samples were higher in most cases, potentially indicating that antibody light chains were overall less sensitive to degradation. Nevertheless although PMSF and Batimastat treatments exhibited

elevated relative peak area compared with control samples, preservation was on the whole lower than observed in heavy chain samples. This contradiction is not easily interpreted but could be due to inaccuracies in measurement induced by variable background staining of gels or strong bands of equivalent molecular weight present in ACM.

Apparent differences between preservation of heavy or light chain under the same inhibitor might also be attributable to the site at which antibody is cleaved. Cleavage in the Fc region of the molecule would necessarily exclude any effects on the light chain and would be correspondingly unaffected by addition of protease inhibitors, as in IgE cleavage by *Schistosoma mansoni* (Aslam et al., 2008). However this is not the pattern observed in our data, which better fits a profile of multiple protease types from more than one class, possibly also acting at a variety of sites on the molecule. *Acanthamoeba* serine proteases have been shown to belong to more than one category of activity: trypsin-like (Sissons et al., 2006a), chymotrypsin-like (Na et al., 2001), and elastase-like (Ferreira et al., 2009). Each of these broad types demonstrate cleavage specificities for different amino acid residues. Chymotrypsin-like proteases for example have a deep and highly hydrophobic active site, creating a preference for large hydrophobic amino acids such as tryptophan and phenylalanine. By contrast elastase-like enzymes have shallower, less hydrophobic active sites and exhibit specificity for smaller or less hydrophobic amine acids such as valine and alanine (Hedstrom, 2002). This means there are many possible sites for cleavage along an antibody molecule depending on which class of protease is responsible for cleavage (an example for human IgG is shown in Appendix 5). Careful testing with purified single-protein fractions

will be required in order to resolve the role of individual enzyme classes and amino acid cleavage specificity.

A second mechanism by which parasites can evade the effects of the immune system is by sequestering antibody on the surface of the parasite. From the point of view of the infectious organism this has a twofold advantage: 1) sequestration of antibody prevents activation of downstream effector responses and 2) acquiring a coat of antibody can inhibit access to the parasite's surface thereby preventing recognition of surface antigens by phagocytes, and protecting against complement attack and lysis. Neither mechanism has previously been demonstrated in *A. castellanii* however such processes are known to occur in a variety of parasitic infections.

In *Plasmodium falciparum* for example the parasite merozoite surface protein MSP1 induces nonspecific blocking antibody which can prevent the binding of more active inhibitory antibodies (Holder et al., 1999). Also in malaria the erythrocyte membrane protein PfEMP1 has been shown to bind host IgM in an inverted orientation that prevents the Fc region from being exposed to additional immune mediators (Ghumra et al., 2008, Czajkowsky et al., 2010). This also has an additional benefit to the parasite of masking epitopes which would be protective if targeted by an IgG response. This process was demonstrated for a strain causing placental malaria where nonspecific IgM was shown to bind competitively with monoclonal IgG specific for immunogenic Duffy-binding-like (DBL) domains of PfEMP1. In the presence of IgM, IgG binding was reduced to less than 20% of control levels and this interference was shown to inhibit phagocytosis of opsonised parasites (Barfod et al., 2011).

Examples of parasites recruiting ineffective immunoglobulin in order to evade immunity have also been seen in *Trypanosoma cruzi* and *Schistosoma mansoni* (Garcia et al., 1997, McIntosh et al., 2006). In the latter case immunoglobulin binding has been ascribed to IgG Fc receptors expressed on the parasite tegument (Torpier et al., 1979, Tarleton and Kemp, 1981) and tentatively linked to the protein paramyosin, specific antiserum against which prevented subsequent binding of Fc-FITC to the parasite surface (Loukas et al., 2001) Other parasites such as *Toxoplasma gondii* possess immunoglobulin binding activity that is yet to be definitively linked to a specific evasion mechanism but is likely to play a role in host-parasite interaction (Vincendeau and Daeron, 1989, Rodriguez de Cuna et al., 1991, Villavedra et al., 2001).

Nonspecific binding of IgM had been observed in experiments forming a part of Chapter 3, alongside a lack of protection in terms of host cell death and monolayer disruption. These experiments were extended to investigate whether there is a structural component to binding inhibition and how this relates to pathogenic outcome. Initially we were able to replicate these earlier findings which continued to indicate that both anti-*Acanthamoeba* and isotype control IgM reduced binding by approximately 20% (Figure 4.8). However this effect did not extend to monomeric isotype control IgG or purified Fc fragment. Significantly, reduction in binding did not translate into protection of host cell monolayers in terms of macro- or microscopic monolayer disruption (Figures 4.9 and 4.10). Neither was a protective effect observed when cytotoxicity of host cells was measured, in fact the opposite was true with treatment groups showing elevated levels of cell death (Figure 4.11).

These data indicate several possible explanations. Binding is only reduced and not ameliorated by addition of antibody so it may be hypothesised that the usual course of infection can proceed for trophozoites that are not prevented from binding by antibody activity. The observed lack of protection might then be explained by the 20% reduction in amoeba binding being too small to produce any observable reduction in monolayer pathology.

Another possibility relates to the protease activity of the organism which has been demonstrated to degrade the Ig classes used by other groups and also those used in this study, including HE2 (see above). Rapid activity of these proteases could quickly counteract the effect of any binding inhibition, especially if intact protein structure of IgM is necessary to prevent binding, as indicated by the inability of IgG to affect adherence (Figure 4.8). Contact-mediated pathogenesis by trophozoites has been elucidated in some depth (Yang et al., 1997, Cao et al., 1998, Garate et al., 2005, Garate et al., 2006b) and links between trophozoite binding and protease expression have been made previously. For example the interaction of *A. castellanii* mannose-binding protein (MBP) with exogenous mannose or host cell mannose glycoproteins has been demonstrated to upregulate protease expression (Hurt et al., 2003a, Leher et al., 1998c).

Alternatively binding may not be necessary for the initiation of monolayer disruption and cell death processes at all. Pathways to endothelial pathology have been described for several *A. castellanii* protease secretions (Alsam et al., 2005b, Sissons et al., 2006a, Khan and Siddiqui, 2009, Harrison et al., 2010), and if these are unaffected by the presence of surface-bound antibody then

their molecular targets and processes are likely to be similarly unaffected. Given that proteases can be upregulated in response to external cues (see above) it is also tempting to speculate that trophozoites might mount a similar response to antibody. This could provide an explanation for the increased cytotoxicity observed in some treatment groups as seen in Figure 4.11 but will require careful additional experimentation to verify.

Considering the pentameric structure and high molecular weight of IgM (Chesebro et al., 1968) and the lack of binding inhibition exhibited by monomeric antibody and fragments (Figure 4.8) it is possible that IgM inhibits binding by structural interference with factors present on the amoeba cell membrane. This is one of the major functions of immunoglobulin within the immune response however the fact that this process occurs with both specific and non-specific antibody in our experiments is interesting. As described above parasites such as *T. cruzi* and *S. mansoni* have been observed to sequester antibody and this antibody coating is linked to immune evasion. One way in which this process is mediated is by expression of membrane proteins which bind to the conserved (Fc) region of Ig, and hence capture antibody in sub-optimal orientation. The ability of nonspecific IgM to impair trophozoite binding to HBMEC monolayers suggests that this process may be occurring in *A. castellanii* either specifically to IgM, or generically across all Ig classes with only IgM capable of inhibiting binding due to its large size.

In order to test this hypothesis a bioinformatics based approach was used alongside evidence from immunofluorescence and FACS experiments. BLAST searches against the *A. castellanii* genome with proteins possessing known or

predicted Fc-binding activity revealed little similarity to dedicated receptor classes from human, mouse, chicken or oyster sequences (Table 4.1), and this was confirmed by reciprocal BLAST (Table 4.2). Considering the large evolutionary distance between the amoebazoa and these multicellular organisms, there is only a low probability of a recognisable and intact FcR, or equivalent sequence being present in *A. castellanii.* Similarities in terms of invasion and pathogenesis strategies with other pathogens however provide a more likely scenario in which *A. castellanii* might share similar Fc binding protein activity and sequence. Searches were performed in a non-targeted manner using only organisms with previously reported or predicted Fc-binding activity, and where sequence of the putative binding factor was available. For some parasites annotation was available but too limited to reliably include in BLAST analyses. Fc-binding annotation is present in *Taenia crassiceps* for example, however this refers only to a very short (~30aa) sequence which could not be reliably incorporated into our experiments. Our approach therefore excludes some parasites with similar infection routes or mechanisms of pathogenesis to *A. castellanii*. Whilst this is a limitation at the present time continued future improvement in genome and transcriptome annotation will allow more far-reaching comparisons to be made between distantly related organisms which share similarities in lifestyle and pathogenesis. We consider this to be an important consideration for subsequent work in this field.

Our data indicates that the best matches to *A. castellanii* sequences were found in other pathogenic protozoa. In particular a short ~90 aa region of sequence matching to an Fc-binding protein (Lmsp1) in *Leishmania major* was discovered in initial BLAST searches (Table 4.1). Homologues of Lmsp1 have

been found in *Trypanosoma cruzi* and *Trypanosoma brucei* (Campos-Neto et al., 2003) and when retrieved and compared in our dataset (Table 4.2) these sequences were as expected highly similar to each other (>80% identity, E-values $<10^{-50}$). Matches of Lmsp1 sequences to the *A. castellanii* genome showed lower levels of similarity (>50% identity, E-values $<10^{-20}$), however this still represents a significant level of matching between the sequences and can be explained by the relatively large evolutionary distance between amoeba and the kinetoplastids. Notably, a conserved domain search of *A. castellanii* transcriptomic sequence that had aligned significantly with *L. major* Lmsp1 revealed conservation with group 1 from the nucleoside diphosphate kinase protein superfamily (Appendix 6). This is also the family to which Lmsp1 belongs and as such is likely to represent genuine homology between the two organisms.

Interestingly the binding targets for Lmsp1 as shown by Campos-Neto *et al.* were IgG and IgM antibody. Both of these classes are distributed mainly in the bloodstream and trophozoites are therefore exposed to both during systemic infection. Capture of both or either class could facilitate evasion of subsequent immune responses, although only IgM and not IgG binding activity was detected *in vitro* in our experiments. Whilst both antibodies are present in the blood IgM responses typically occur in the early stages of infection and as a result an ability to evade this class might allow *A. castellanii* to establish itself systemically and at the BBB before subsequent immune responses can clear trophozoites.

Another significant match obtained by reciprocal BLAST was between *A. castellanii* and *Toxoplasma gondii.* Several previous studies have identified *T. gondii* as possessing Fc binding activity (Budzko et al., 1989, Vercammen et al., 1998) and the *T. gondii* beta antigen is located in a region predicted by genome annotation to exhibit IgA-binding activity. It is this region which produced significant matches to *A. castellanii* in our study. Interestingly the beta antigen was also significantly similar to a protein from *Streptococcus agalactiae* which possesses IgA-binding activity (Coleman et al., 1990, Heden et al., 1991) indicating that any similar protein in *A. castellanii* might also exhibit binding to this antibody class. This targeted binding to IgA is of additional interest due to the tissue distribution of the antibody class. IgA and especially secretory IgA play an important role in protection from infection at mucosal surfaces. One such area of relevance to *A. castellanii* infections is the eye, and IgA has been hypothesised to be the main source of immune control in *Acanthamoeba* keratitis (Leher et al., 1999, Alizadeh et al., 2001, Campos-Rodríguez et al., 2004). Ocular infections occur in patients with fully functioning immune systems and *Acanthamoeba*-specific IgA is readily isolated from AK patients (Alizadeh et al., 2001). IgA binding activity by the parasite might therefore provide an explanation for the apparently ineffective immune response.

Other well-characterised bacterial Fc binding proteins originating from streptococci and staphylococci aligned with *S. mansoni* paramyosin sequence in our experiments (King and Wilkinson, 1981, Bjorck and Kronvall, 1984). *S. mansoni* also showed some degree of similarity to *A. castellanii* transcriptomic sequence with the same protein, which has previously been reported to exhibit

Fc-binding properties (Kalinna and McManus, 1993). This match is however less reliable than others detected by our approach as alignments only reach significance if a lower stringency cut-off is used. Nevertheless the fact that some level of similarity is seen to what is one of the better characterised parasite Fc binding proteins makes this an interesting candidate for further inquiry.

Where the presence of Fc-binding activity in protozoa has been demonstrated, the factor responsible for Ig binding has only been fully characterised in a minority of cases. As such, transcriptomic and proteomic databases may not contain the full extent of known Fc binding proteins. No entry was found for *Babesia caballi* antibody binding protein for example despite previous identification work (Ikadai et al., 2005), and trypanosome peptide sequences could only be identified by homology to the sequence obtained from *L. major* (Campos-Neto et al., 2003). Thus it is possible that sequence similarities between *Acanthamoeba* and Ig-binding proteins from other taxa exist but could not be identified using the methods outlined here.

Evidence from *in vitro* assays and *in silico* analysis suggested the presence of Fc binding protein homologues in *A. castellanii.* We sought confirmatory *in vitro* evidence by probing trophozoites with human Fc fragment and detecting signal with fluorescent microscopy and FACS analysis. Fluorescent signal was observed in labelled trophozoites and although faint by comparison to positive controls (FcR-expressing K562 cells), levels of staining were nevertheless higher than observed in HBMEC and unlabelled trophozoites (Figure 4.12). FACS analysis also showed this trend (Figure 4.14) although notably binding

of secondary antibody was observed for both HBMEC and trophozoites (Figures 4.13 and 4.14). This in itself is indicative of Fc-binding activity and accordingly there is evidence to suggest that other endothelial cell types express FcR (Sedmak et al., 1991, Lyden et al., 2001, Schlachetzki et al., 2002, Nishimura et al., 2006, Ganesan et al., 2012). With regard to *A. castellanii* trophozoites addition of purified Fc fragment did not substantially increase the observed levels of fluorescence (12.9% as opposed to 11.5%), however the number and distribution of Fc binding residues on the amoeba cell membrane are unknown and as such could already be saturated at the antibody concentrations used in this experiment.

Given the outcome of our *in silico* analysis it seems unlikely that Fc-binding activity demonstrated by *A. castellanii* is the result of proteins with significant similarity to mammalian Fc receptors. However, homology to Fc binding proteins from other pathogens was demonstrated by our analysis and low levels of binding activity could be detected with *in vitro* assays. Sequence matches to Fc binding proteins from other protozoa reveal several interesting candidates for proteins with similar activity in *A. castellanii* which interact with antibody classes known to be important in infection. We have also shown that antibodies including polyclonal antibody derived from immunised mice are cleaved by amoeba secreted proteases. Near complete loss of heavy and light chain bands was most apparent in IgA, IgG and IgM (Figures 4.2, 4.4 and 4.6) further underlining the influence of these classes in protection. The contextual importance of mechanisms for both degradation and capture of antibody in *A. castellanii* infections remains to be fully determined. However

the ability of trophozoites to evade antibody-mediated immunity should be considered in future studies.

5. Use of a novel *in vitro* flow system to elucidate aspects of host cell death and monolayer disruption

Material from this chapter has previously been published as:

Acanthamoeba interactions with the blood-brain barrier under dynamic fluid flow. Edwards-Smallbone J, Pleass RJ, Khan NA, Flynn RJ. Experimental Parasitology 2012 Nov, 132(3).

5.1. Abstract

The complete mechanism of pathogenesis for blood-brain barrier (BBB) breach in *Acanthamoeba* granulomatous encephalitis (AGE) remains unclear. Here we have developed a novel *in vitro* BBB infection model under flow conditions which demonstrates that increases in flow rates lead to decreased binding of *A. castellanii* to host cells. This is a distinct departure from previous findings under static conditions, however similiarly to static conditions binding of *A. castellanii* to host cells is host mannose dependent. Disruption of the host cell monolayer was independent of amoeba binding, but dependent on secreted serine proteases. Inhibition of host Protease Activated Receptors produced no significant effect on either host necrotic or apoptotic cell death. We report the binding dynamics of *A. castellanii* under physiological conditions, showing that BBB disruption is not directly linked to binding, instead it is reliant on secreted proteases. This disruption appears to be independent of PAR-mediated cell death as observed in other parasitic protozoa. Our results offer a platform on which modulation of physiological parameters will improve the accuracy of *in vitro* models of *A. castellanii* infection.

5.2. Introduction

Penetration of the blood-brain barrier is a key event in the establishment of AGE and frameworks for understanding how this occurs have been elaborated by previous authors, revealing contributions from direct binding proteins and protease secretions (Sissons et al., 2004, Sissons et al., 2006a, Khan and Siddiqui, 2009). However the scope of these studies is restricted by the use of static models of *Acanthamoeba* interaction with the BBB. The brain microcirculation is a dynamic system and varies significantly in response to metabolic demands (Ito et al., 2004, Paulson et al., 2010) so without this context it is likely that current methods do not provide an accurate representation of infection *in vivo*.

In light of this an *in vitro* system with improved physiological relevance was developed using human brain microvascular endothelial cells (HBMEC) grown in flow chamber slides and exposed to *A. castellanii* trophozoites or to *Acanthamoeba* conditioned medium (ACM) under flow conditions. Using data from measurements of cerebral blood flow rate made by Ito and Dörfler (Lassen, 1985, Dorfler et al., 2000, Ito et al., 2004) flow rates *in vitro* were matched to physiological parameters. Pathogenic response was then measured using published parasite binding and host cell death assays in addition to a new approach to quantify monolayer disruption as detailed in Chapter 2. These results were then compared with parallel experiments conducted using standard static techniques to examine whether the alterations made to *in vitro* techniques had produced substantial differences in terms of parasite binding, disruption of host cell monolayer integrity or host cell death.

The contribution made by protease secretions to pathogenesis in the flow model was of particular interest given the findings of previous chapters in respect of immune targets and evasion through antibody degradation. Previous experimentation has mainly focused on the degradation of tight-junction proteins by amoeba proteases however there is evidence from studies in other pathogenic protozoa that parasite proteases may also play a role in activating necrotic or apoptotic cell death (Sommer et al., 2005, Nikolskaia et al., 2006a, Lucas et al., 2008). Protease Activated Receptors (PARs) are one receptor class which parasites can exploit to induce host cell death, and are known to be of importance for neural infection in *T. brucei* (Grab et al., 2009). Although members of this class of receptor have not been examined as mediators of cell death in *Acanthamoeba* infections, the synergy of PARs with intracellular PI3K signalling in *T. b. gambiense* infection (Nikolskaia et al., 2006a) could suggest the involvement of equivalent cell death mechanisms in AGE, given the upregulation of PI3K in response to *A. castellanii* infection (Sissons et al., 2005). The importance of secreted proteases for other mechanisms of BBB disruption thus made PARs an interesting candidate for examination.

5.3. Materials and Methods

5.3.1. Parasite and Tissue Culture

A. castellanii were grown in PYG media as described in section 2.1.1, with cultures fed with fresh media 18 hours prior to experiments to maintain >95% trophozoites. Amoeba were then harvested by chilling on ice and collected in

RPMI (see section 2.3.1). *Acanthamoeba* conditioned medium (ACM) was produced as described in section 2.2.2.

HBMEC were cultured and harvested under conditions as described in sections 2.1.2 and 2.4.1 and used between passages 11-20. 2.5×10^5 cells from fully confluent flasks were seeded into 0.2µm chamber slides in standard growth medium. Media was changed daily to maintain steady growth and HBMEC reached confluence after 2-4 days.

5.3.2. Flow system

Flow chambers were set up as described in section 2.4.2, alongside 24-well plates used for comparison with standard techniques (see section 2.4.1). Both systems were treated with ACM or infected with a suspension of trophozoites (sections 2.4.3 and 2.4.4) for time points up to 3 hours and monitored for parasite binding and disruption of the host monolayer as outlined below.

5.3.3. Binding and disruption measurements

Binding was assessed by triplicate counts taken from the stock solution or tissue culture plate supernatant at time points during, or at the termination of, the experiment (see section 2.4.3). Counts of the number of unbound amoeba were converted to the number of adherent amoeba by subtraction from the initial cell concentration, and expressed as a percentage.

At time points during, or at the conclusion of the experiment, triplicate images of monolayers were taken using a Leica DMB5000B microscope, using inbuilt

auto-exposure and white balance settings. Open-source Image J software (available from http://rsbweb.nih.gov/ij/) was then used to quantify disruption using the method outlined in section 2.4.4.2.

5.3.4. Exogenous sugar treatment

To test the involvement of sugar residues in binding, amoeba suspensions were treated with either 50mM D-mannose, 50mM D-glucose, or were left untreated. Trophozoite suspensions were incubated for 30 minutes at 37°C prior to initiation of the experiment and then introduced into either the flow or static test systems.

5.3.5. Protease treatment

ACM was diluted 1 in 2 in RPMI and either treated with 5mM phenylmethylsulphonyl fluoride (PMSF), a broad-spectrum serine protease inhibitor or left untreated. A concentration of 5mM was selected as a midpoint between concentrations used by Khan *et al.* (2000b) and Ferreira *et al.* (2009) . Prior to the experiment, media was left to incubate for 90 minutes at 37°C to minimise the effect of active PMSF on cells. ACM was then circulated through the flow system or added to static plates in place of amoeba suspension. PMSF-treated RPMI was used as a control.

5.3.6. PAR inhibitor treatment

The role of PARs in *Acanthamoeba*-mediated host cell death was investigated by application of specific PAR1 and PAR4 inhibitors as described in section 2.4.8.

5.3.7. Cell death assays

HBMEC were monitored for both necrotic and apoptotic cell death, by lactate dehydrogenase (LDH) release and TdT-mediated dUTP Nick-End Labelling (TUNEL) assays respectively. Methodology for both assays is described in detail in sections 2.4.5 and 2.4.9.

5.3.8. Statistical analysis

Analyses were performed using GraphPad Prism software version 5.04. Data was analysed using 1-way ANOVA for comparisons of individual treatment groups and 2-way ANOVA where treatment groups were subdivided, for example where there were measures from multiple time points. Significance levels for individual groups were determined using Bonferroni post-tests for each treatment versus a control, or individual comparisons of all treatments. Where data appeared to follow a line or curve this was analysed using Regression models and the R^2 goodness-of-fit value given. The alpha level for significance was set at $p \leq 0.05$ for all tests (see section 2.10).

5.4. Results

5.4.1. Seeding density optimisation

HBMEC were seeded into 0.2µm Luer microslides and allowed to grow to confluence over a period of several days. Confluence estimates and approximate counts per field of view were made daily up to 7 days. An optimal seeding density of 5×10^6 cells/ml (2.5×10^5 individual cells per slide) produced confluence after three days. Higher seeding densities proved inhibitory to monolayer formation as cells stacked on top of one another and failed to adhere to the slide (Figure 5.1).

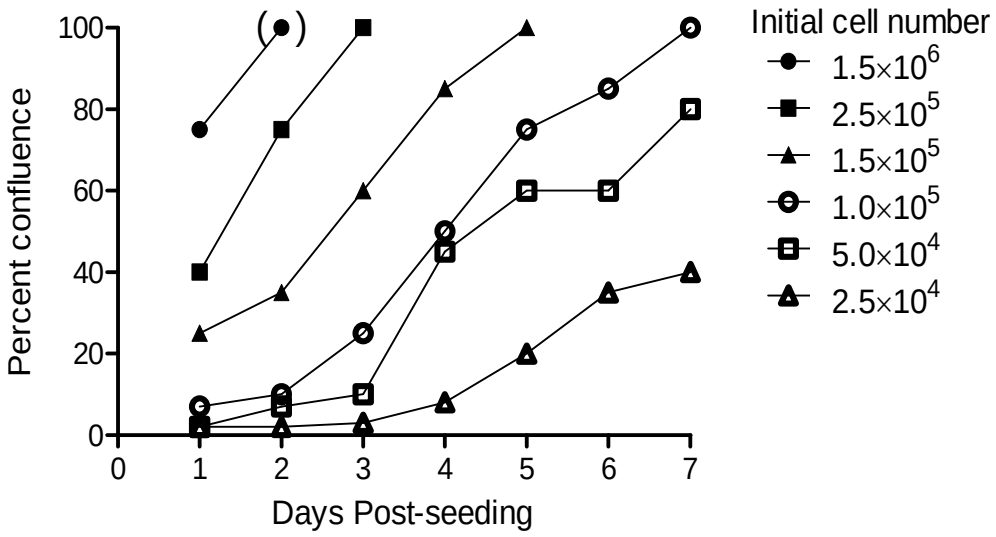

Figure 5.1 Optimisation of HBMEC seeding density with respect to confluence

2.5×10^5 cells produce a confluent monolayer after an optimal growth period of three days. Excessive seeding density inhibits monolayer formation (bracketed value on graph).

5.4.2. Calibration of pump flow rate settings

The flow system was set up without the inclusion of a chamber slide, to monitor flow rates achieved by each pump speed setting. RPMI was allowed to pass through the pump at various speed settings and the volume of outflow recorded. Prior measurements of cerebral blood flow rate per gram of tissue (Lassen, 1985, Dorfler et al., 2000, Ito et al., 2004) fell within the dynamic range of the pump and we calculated our flow rate based on these findings (Figure 5.2). This yielded a rate of approximately 25µl per minute for 0.05g of tissue and permitted replication of flow rates for up to 2g of neural tissue (box-out).

$$\text{CBF} \approx 50\text{ml/min for 100g of tissue}$$

(Lassen 1985, Dorfler *et al.* 2000, Ito *et al.* 2004)

$$\text{Mass of tissue in chamber} = 0.05\text{g}$$

$$\frac{50ml/min}{(100 \div 0.05)} = 0.025ml/min = 25\mu l/min$$

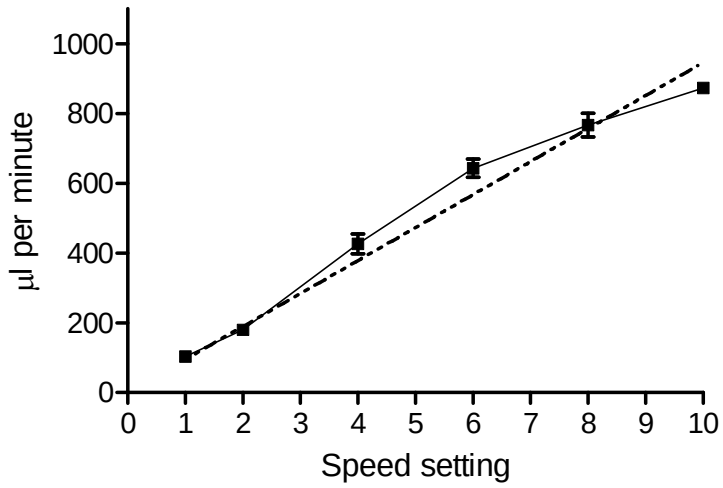

Figure 5.2 Calibration of pump flow rate settings.

The equation of the line of best fit (dashed line) was used to obtain flow rates (µl/min) for each setting (y = 95x). Results are mean ± S.E.M. of three independent experiments.

5.4.3. HBMEC retain monolayer characteristics under flow conditions

Flow slides seeded at optimal density and grown to confluence were attached to a peristaltic pump and incubated with warmed RPMI 1640 at a flow rate of 950µl/minute. Cells were examined microscopically every 15 minutes for 2 hours. HBMEC showed no visible alteration in morphology or monolayer integrity over this time (Figure 5.3).

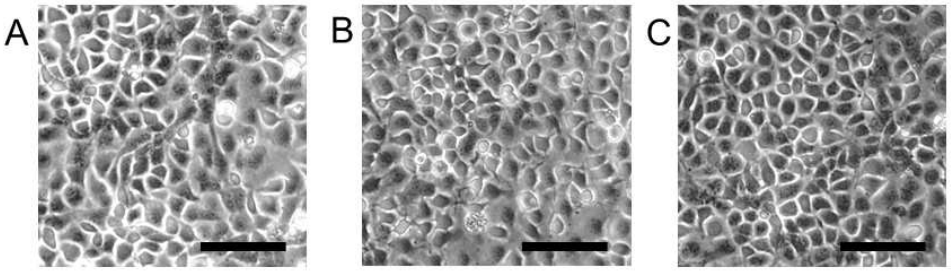

Figure 5.3 HBMEC monolayer morphology remains unaltered under flow.

Images taken after (**A**) 0 minutes, (**B**) 60 minutes, (**C**) 120 minutes. No alteration was seen in morphology or monolayer integrity. Images were taken under ×100 magnification, scale bar = 100µm.

5.4.4. Substantial reductions in amoeba binding are seen under flow conditions compared with static conditions

Measurements of binding were taken every 30 minutes for three hours using a minimal flow rate of 30µl/min, and compared with similar measurements taken from static plates (Figure 5.4 panel A). Significant differences were seen between static and flow conditions at each time point measured ($p<0.001$, 2-way ANOVA). Binding in static plates approached a plateau at the three hour time point and so this was set as the experimental period for subsequent experiments. The effect of flow rate on binding by amoeba was then investigated within a range of 30 to 950µl/min. Highly significant differences in percentage binding were seen between static and flow conditions ($p<0.001$, 1-way ANOVA). Significant differences were also seen between the highest and lowest flow rates (30 vs. 950µl/min) suggesting that amoeba binding is inversely correlated with flow rate. Furthermore the data conformed strongly to

a fitted exponential decay model (R^2 = 0.9105, one-phase decay), (Figure 5.4 panel B). Using these results and those from the flow rate calibration in section 5.4.2, a single flow rate of 95µl/min was set for use in further experiments.

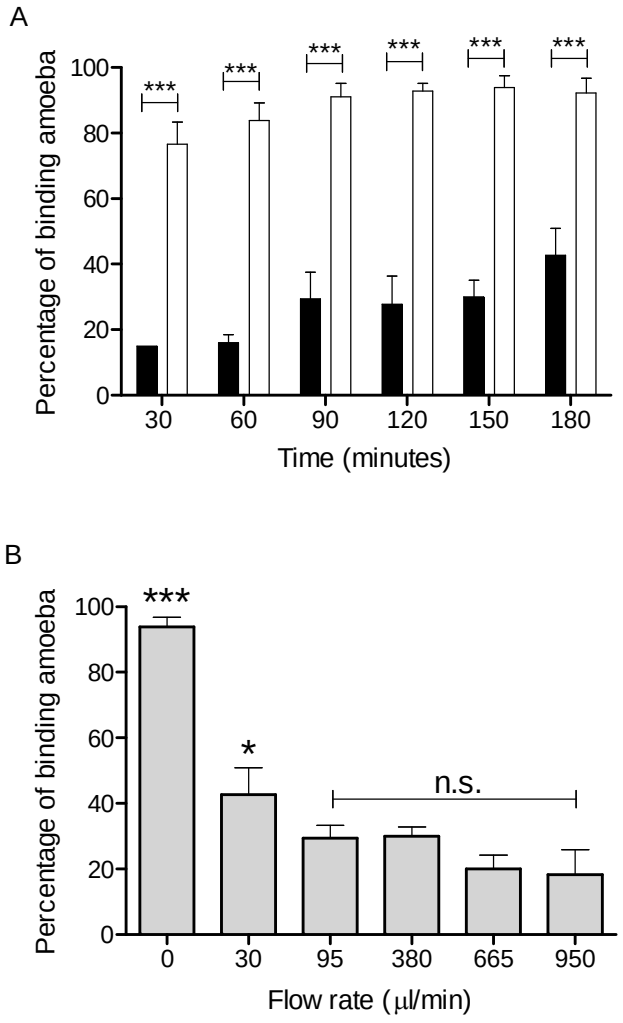

Figure 5.4 Binding of trophozoites to HBMEC is affected by flow rate.

(**A**) 2×10^5/ml *Acanthamoeba* trophozoites were added to HBMEC monolayers in either static plates (white bars) or flow chamber slides (black bars) and measurements of binding taken every thirty minutes for up to three hours. A flow rate of 95μl/min was used for flow treatments. Significant differences between static and flow were seen at each time point (*** $p<0.001$, 2-way ANOVA). Results are mean + S.E.M. of triplicate counts from two independent experiments. (**B**) 2×10^5/ml *A. castellanii* trophozoites were flowed over confluent HBMEC monolayers in microslides at a range of flow rates, including a zero rate obtained from static plates. Measurements of binding were taken after three hours. Significant differences were observed at the two lowest flow rates (*** $p<0.001$, * $p<0.05$, 1-way ANOVA). Data conformed closely to an exponential decay regression model ($R^2 = 0.91$). Results are mean + S.E.M. of triplicate counts from three independent experiments.

5.4.5. Exogenous mannose ameliorates binding under both static and flow conditions

A major surface mannose-binding protein (MBP) has been previously identified in *Acanthamoeba* and strongly implicated in endothelial cell attachment and BBB pathology (Garate et al., 2006b). We therefore tested the involvement of MBP in our modified *in vitro* model. Amoeba suspensions were treated with either 50mM mannose, 50mM glucose, or left untreated and their capacity for binding measured as before (Figure 5.5). The data confirmed that exogenous mannose significantly inhibits attachment to HBMEC in static conditions, whilst under a low flow rate significant decreases in binding were also observed ($p<0.0001$, 1-way ANOVA). However, the proportion of binding that was inhibited by mannose was greater under flow; a reduction of 62.5% (S.D. ±13.1) as opposed to 29.4% (S.D. ±8.6) in static treatments. Glucose treatment produced no alteration in binding capacity under either static or flow conditions ($p>0.05$ by Bonferroni Multiple Comparison Test).

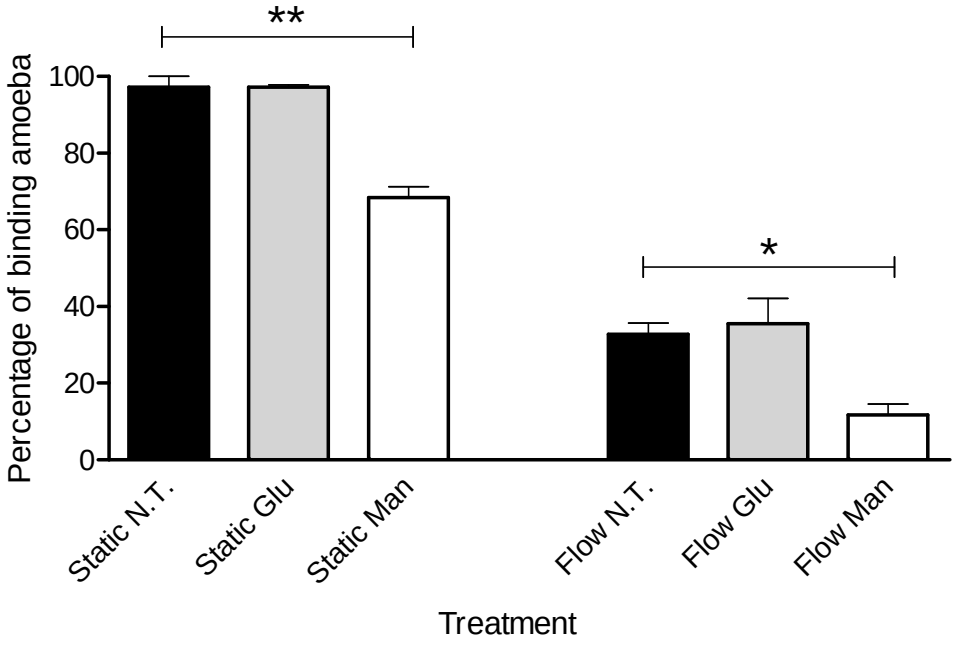

Figure 5.5 Binding of trophozoites to HBMEC is MBP-dependent.

2×10^5/ml *Acanthamoeba* trophozoites in RPMI containing 50mM mannose (Man), 50mM glucose (Glu), or left untreated (N.T.) were passed over confluent HBMEC monolayers in microslides at a flow rate of approximately 95ul/min, or added to static culture. Measurements of binding were taken after three hours. Overall, means differed significantly from each other (** $p<0.001$, 1-way ANOVA), and the effect of flow on all samples was also highly significant. A significant reduction in binding was observed in mannose treated samples under both static and flow conditions (** $p<0.01$, * $p<0.05$, 1-way ANOVA). The effect of glucose treatment was not significant. Results are mean + S.E.M of triplicate counts from three independent experiments.

5.4.6. Monolayer disruption by trophozoites remains constant over a range of flow rates

Given the interaction between flow rate and trophozoites' ability to bind to HBMEC, we were interested to investigate whether differences in monolayer

disruption by amoeba were related to flow rate. Images of HBMEC monolayers taken during binding experiments were analysed for monolayer disruption by a grid counting method. Analysis found no significant difference between percentage monolayer disruption over a range of flow rates including static conditions (p=0.128, 1-way ANOVA) (Figure 5.6) This is surprising given the model of binding established in earlier experiments which indicates maximal binding at the lower end of the range.

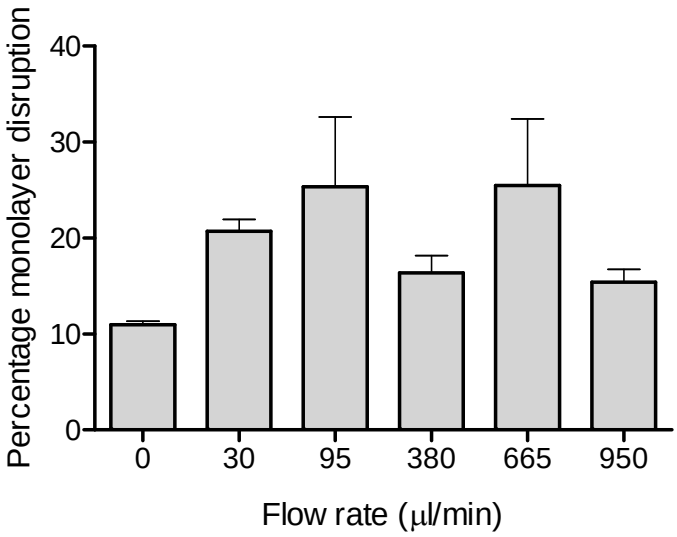

Figure 5.6 Monolayer disruption by trophozoites is unaffected by flow rate.

2×10^5/ml *Acanthamoeba* trophozoites were flowed over confluent HBMEC monolayers in flow chamber slides at a range of flow rates, including a zero rate obtained from static plates. Triplicate images were taken after three hours and percentage monolayer disruption estimated using a grid counting method (section 2.11). There was no significant difference between flow rates (p=0.13, 1-way ANOVA). Results are mean + S.E.M of triplicate measurements from three independent experiments.

5.4.7. *Acanthamoeba* conditioned medium causes equal disruption in both static and flow conditions

Acanthamoeba have been previously found to secrete a variety of proteases, which are implicated in blood-brain barrier disruption (Hadas and Mazur, 1993, Alsam et al., 2005b). Given findings which suggested there is no relationship between binding and monolayer disruption under flow conditions (section 5.4.6), we tested the effect of ACM alone in our model. 1 in 2 dilutions of ACM were made in RPMI and added to either static plates, or circulated through flow chamber slides. Triplicate images were taken every thirty minutes for three hours, and counted as before. Notably when images were analysed there was no significant difference between monolayer disruption under flow and static conditions, nor any significant differences between flow rates ($p=0.69$, linear regression) (Figure 5.7).

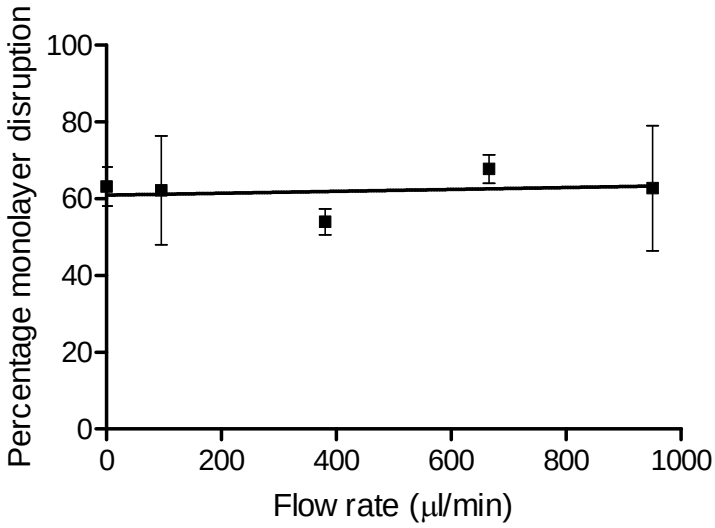

Figure 5.7 Monolayer disruption by ACM is constant over a range of flow rates.

1:2 dilutions of *Acanthamoeba* conditioned medium (ACM) were flowed over confluent HBMEC monolayers in flow chamber slides at a range of flow rates, including a zero rate obtained from static plates. Percentage monolayer disruption was estimated using a grid counting method (section 2.11). Again there was no significant difference between flow rates ($p= 0.69$, linear regression). Results are mean ± S.E.M. of triplicate measurements from three independent experiments. Regression line is displayed.

5.4.8. Protease inhibition alters the effects of ACM under static and flow conditions

Of the protease secretions made by *Acanthamoeba*, serine proteases are thought to be the major contributor to loss of BBB integrity. We investigated the contribution of serine protease to monolayer disruption in both static and flow conditions using PMSF, a broad-spectrum serine protease inhibitor (Figure 5.8). PMSF treatment produced highly significant reductions in monolayer disruption in both static and flow conditions ($p<0.0001$, 1-way ANOVA), reducing disruption to levels equivalent with control treatments,

however no significant differences between static or flow conditions were seen for untreated ACM. As with uninhibited ACM treatments there was no statistically significant difference between static or flow conditions for either PMSF-treated ACM or treatment controls ($p>0.05$, Bonferroni Multiple Comparison test).

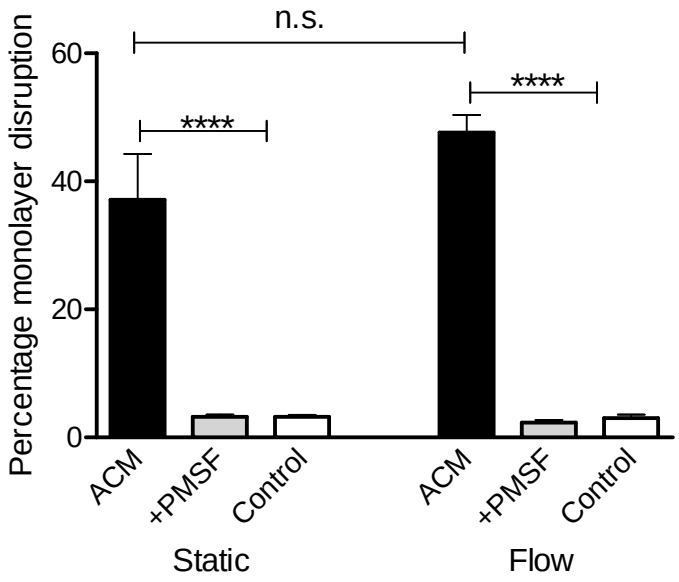

Figure 5.8 Protease inhibition alters the effects of ACM under static and flow conditions. 1:2 dilutions of ACM treated with 5mM PMSF, left untreated, or RPMI controls were passed over confluent HBMEC monolayers under flow conditions (95µl/min) or added to static plates. Monolayer disruption was estimated using a grid counting method as before. Highly significant differences were observed between PMSF-treated and untreated ACM (****$p<0.0001$, 1-way ANOVA), however there was no significant difference between ACM treatments under flow compared with static conditions. Results are mean + S.E.M. of triplicate measurements from three independent experiments.

5.4.9. Treatment with PAR inhibitors has no effect on the disruption of host cell monolayer

PARs have been implicated as a protease-mediated cell death mechanism in other parasitic infections. We selected PAR1 and PAR4 for study on the basis of previous reports which have identified these receptors in HBMEC (Kim et al., 2004). Selective inhibitors were used to investigate the role played by these molecules in *A. castellanii* infections. HBMEC cell monolayers were prepared in 24-well plates and treated with SCH 79797 dihydrochloride, a PAR1 inhibitor or tcY-NH_2, a PAR4 inhibitor. Plates were then infected with either ACM or trophozoites for up to 18 hours and processed for monolayer disruption analysis.

5.4.10. Monolayer protection - staining

24-well plates were fixed after 18 hours and stained with Harris' Haematoxylin to assess monolayer disruption visually. PAR inhibitor treated wells displayed qualitatively similar levels of monolayer staining to untreated ACM and trophozoites, and substantially lower levels of staining than were seen in negative control wells (RPMI-treated).

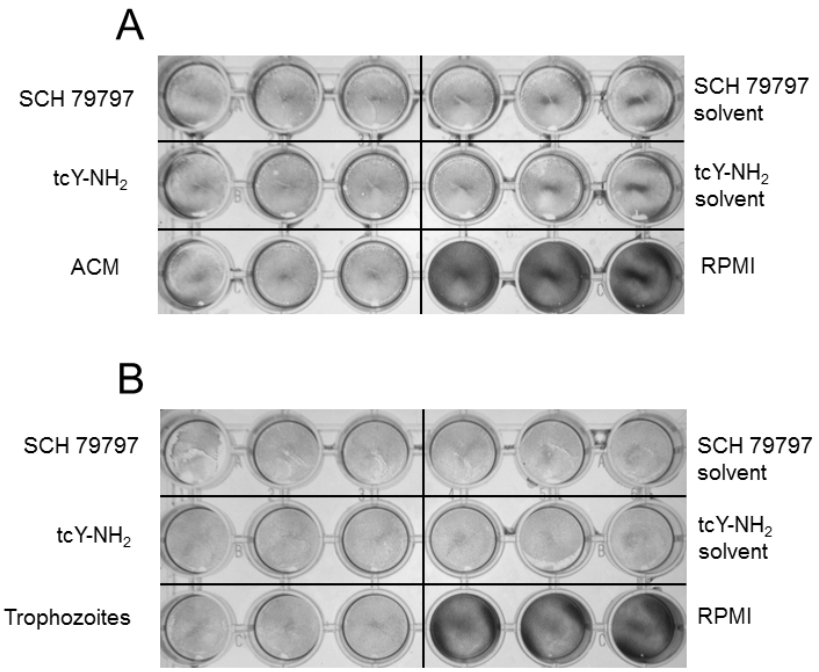

Figure 5.9 PAR inhibitor treatment does not protect HBMEC monolayers.

As assessed by haematoxylin staining. Cells were infected with ACM (**A**), or 2×10^5/ml trophozoites (**B**) and fixed/stained after 18 hours. Results are representative of two independent experiments.

5.4.11. Monolayer protection - photomicrographs

After 3 hours of the experimental period, micrographs of treated and infected monolayers were taken and analysed by grid counting. There was no significant reduction in monolayer disruption in any of the treatment groups when compared with positive controls of either untreated ACM or trophozoites. Negative controls treated only with RPMI exhibited no appreciable level of monolayer disruption.

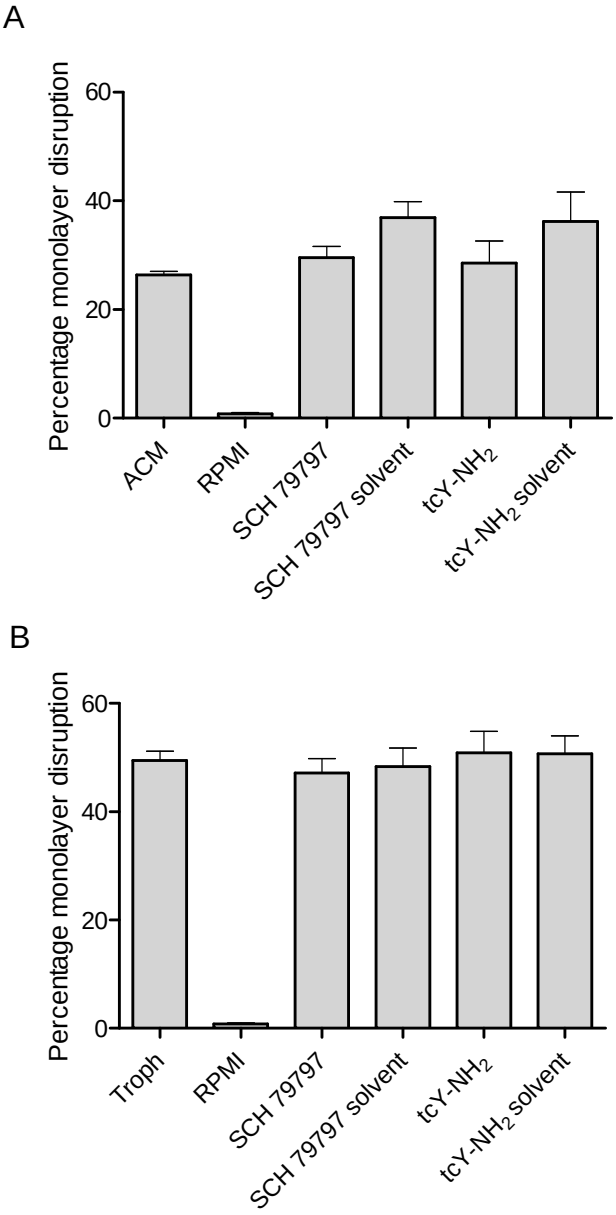

Figure 5.10 PAR inhibitor treatment does not significantly reduce host cell monolayer disruption.

Cells were infected with ACM (**A**), or 2×10^5/ml trophozoites (**B**), photographed after 3 hours and monolayer disruption estimated semi-quantitatively. Results are mean + S.E.M. of triplicate measurements from two independent experiments. Treatment groups did not differ significantly from positive controls (ACM or trophozoites) ($p>0.05$, 1-way ANOVA).

5.4.12. Treatment with PAR inhibitors has no effect on LDH release as a marker of necrotic cell death

HBMEC cultures were infected with ACM or trophozoites and treated with PAR inhibitors at concentrations from 0.001 to 1000nM. After 24 hours supernatants were collected and tested for release of lactate dehydrogenase and compared with levels obtained from controls. Results indicated only low levels of LDH release in ACM treated samples, whilst higher levels were detected in trophozoite treatments. However, addition of PAR inhibitors produced no significant differences in either case, with no treatment concentration differing from positive control samples.

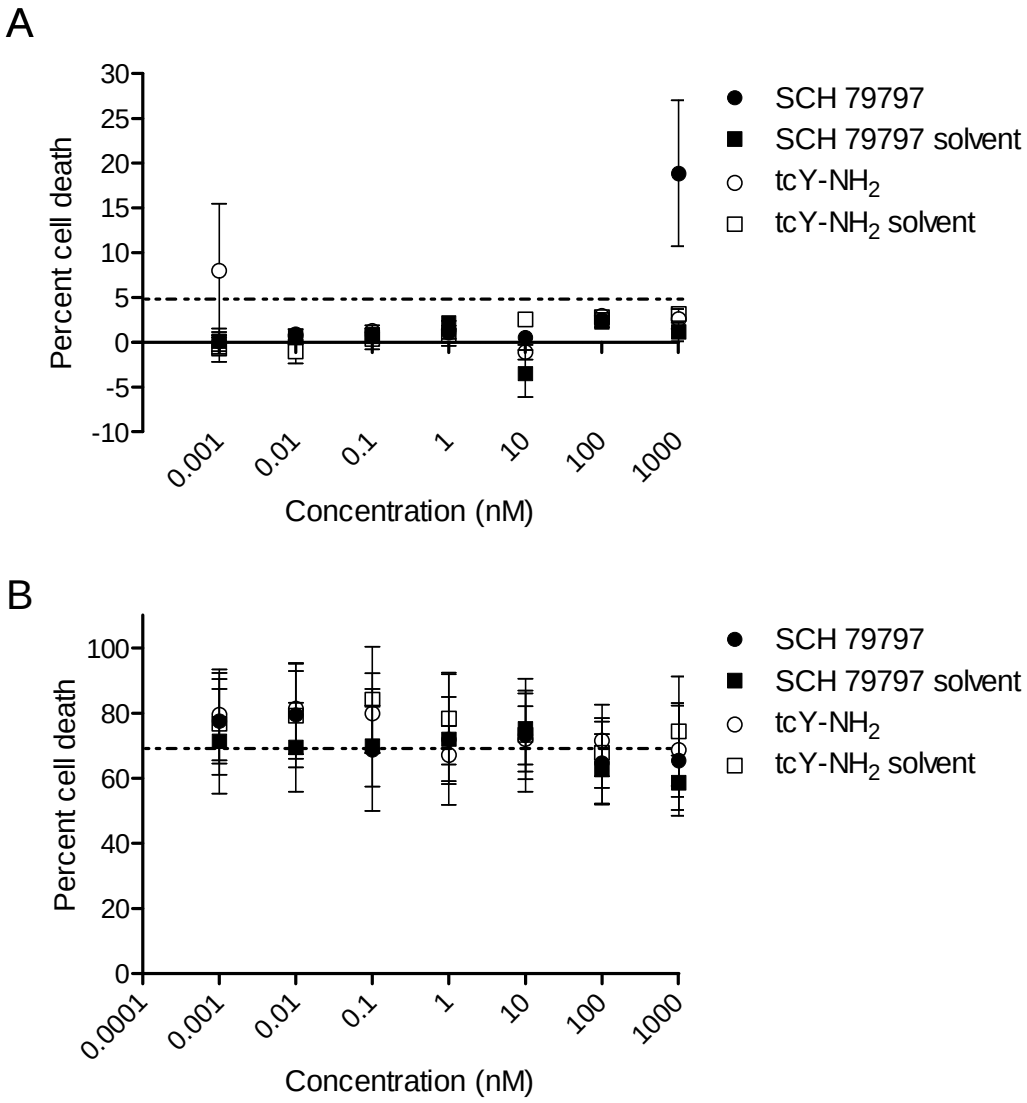

Figure 5.11 PAR inhibitor treatment has no significant effect on LDH release.

Cells were infected with ACM (**A**), or 2×10^5/ml trophozoites (**B**), treated with a range of PAR inhibitor concentrations for 24 hours and examined for release of LDH. Results are mean ± S.E.M. of triplicate measurements from two independent experiments. Treatment groups did not differ significantly from each other or positive control samples ($p > 0.05$, 1-way ANOVA). The dashed line denotes percentage cell death in positive control wells, treated with either ACM or trophozoites.

5.4.13. Treatment with PAR inhibitors has no effect on numbers of TUNEL +ve HBMEC, used as a marker of apoptotic cell death

Cultures of HBMEC were infected with either ACM or trophozoites and treated with PAR inhibitors. Samples were then transferred to microscope slides by cytospin and stained for nuclear fragmentation by TUNEL.

5.4.14. Imaging

Samples were photographed using a fluorescent microscope as described in section 2.4.9, with green fluorescence denoting cells positive for nuclear fragmentation, a marker for apoptotic cell death. TUNEL positive cells were observed in all samples except negative control HBMEC, however numbers of apoptotic cells were consistent across all inhibitors, solvent controls and untreated samples for both ACM exposure and trophozoite infections. An increase in apoptotic cell number was only observed in cultures treated with cisplatin, a known inducer of apoptosis.

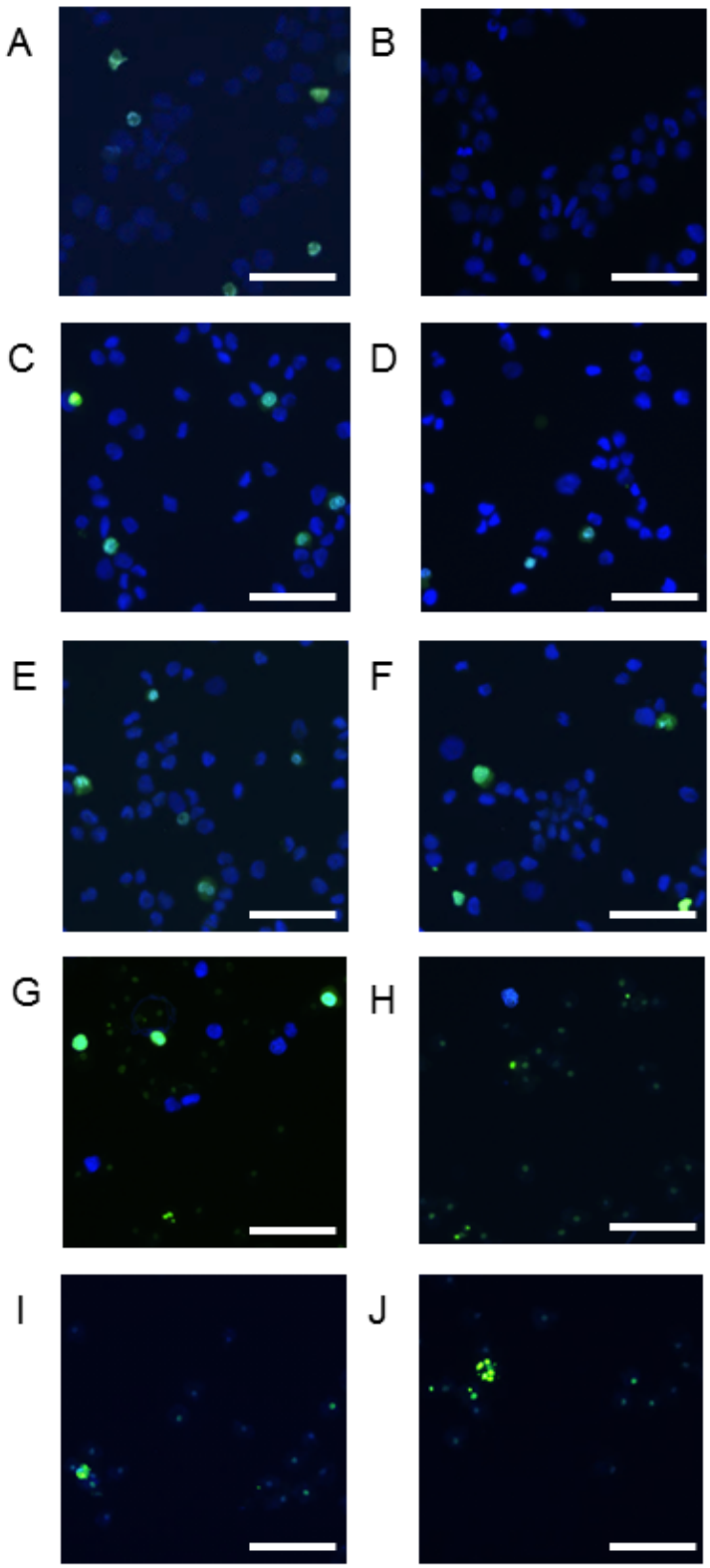
A
B
C
D
E
F
G
H
I
J

Figure 5.12 PAR inhibitor treatment has no effect on gross levels of host cell apoptosis.
HBMEC were treated with PAR inhibitors and infected with ACM or trophozoites, fixed, stained by TUNEL and counterstained with DAPI. Green fluorescence indicates TUNEL +ve nuclei, blue fluorescence indicates TUNEL –ve nuclei. (**A**) 50µM cisplatin, (**B**) untreated HBMEC, (**C**) SCH 79797/ACM, (**D**) SCH 79797 solvent control/ACM, (**E**) tcY-NH_2/ACM, (**F**) tcY-NH_2 solvent control/ACM, (**G**) SCH 79797/trophozoites, (**H**) SCH 79797 solvent control/trophozoites, (**I**) tcY-NH_2/trophozoites, (**J**) tcY-NH_2 solvent control/trophozoites. Images are representative of two independent experiments. Images are ×200 magnification, bar = 50µm.

5.4.15. Counts

Fluorescence microscopy images from ACM-treated samples were additionally analysed by counting the number of TUNEL positive HBMEC visible in five fields of view under ×200 magnification, using the green (FITC) fluorescence channel. PAR treatments produced no significant alteration in the number of TUNEL +ve cells observed, with only cisplatin treated positive controls showing a significant difference to any of the other treatment groups.

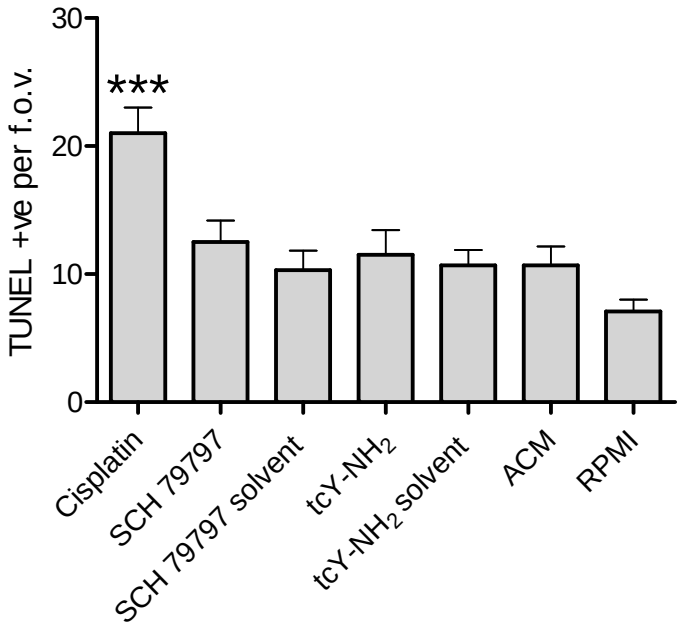

Figure 5.13 PAR inhibitor treatment does not alter the number of TUNEL +ve cells.

Counts of positive cells in five fields of view were made from individual slides stained by TUNEL. Cisplatin treatment demonstrated significantly higher levels of TUNEL +ve cells compared to other treatments (*** $p<0.001$) however all other comparisons were not statistically significant ($p>0.05$ 1-way ANOVA). Results are mean + S.E.M. of five replicates from two independent experiments.

5.5. Discussion

Static culture systems for determining the adherence of *Acanthamoeba* to HBMEC are well established in the literature and have been used with great success to elucidate many important aspects of AGE pathogenesis (Sissons et al., 2004, Sissons et al., 2006a, Khan and Siddiqui, 2009). However in many cases *in vitro* findings have proved confusing when placed into a wider context. Levels of trophozoite binding are typically high *in vitro* (Alsam et al., 2003, Khan and Siddiqui, 2009); however the confinement of the disease largely to individuals with underlying immune deficiencies suggests that *Acanthamoeba* is a comparatively inefficient/low virulence pathogen. The discrepancy between *in vitro* findings and the *in vivo* condition is in a sense unsurprising; the brain microcirculation is a dynamic system in which any pathogen must contend with physical forces in order both to adhere and remain bound (Chen and Springer, 2001, Mairey et al., 2006, Zhang et al., 2009). Therefore static culture systems are not truly representative of the dynamics of binding, and so provide an incomplete picture of *Acanthamoeba* pathogenesis.

The limitations of static cultures in general as an effective model of the brain microvasculature are increasingly recognised and as a result many groups have added increasing levels of sophistication to their *in vitro* models. Two major approaches have been taken aiming either to produce more accurate representations of the structure of the blood-brain barrier (BBB), or more accurate modelling of the physical forces and conditions experienced in brain microcapillaries. The former approach incorporates not only endothelial cells but other cell types in the BBB architecture: pericytes and astrocytes. Pericytes

have important regulatory functions within the BBB (Armulik et al., 2010) however *in vitro* methods have typically used Transwell co-cultures of endothelium and astrocytes to induce or enhance barrier function. Astrocytes in particular have been shown to enhance the barrier properties of the endothelium and produce measurements of trans-endothelial electrical resistance (TEER) which are closer to those seen *in vivo* when either cells or only a cell-conditioned medium are present (Janzer and Raff, 1987, Sobue et al., 1999, Hayashi et al., 1997). Transwell co-culture models of this sort are advantageous in having only simple technical requirements and being amenable for use in high-throughput screening, however for examining parameters such as parasite binding they possess the same discrepancies with the *in vivo* condition as simple static cultures.

In order to study these dynamic effects the addition of fluid flow is necessary. Typical methodologies apply flow to endothelial cells cultured in sterile chambers, and then monitor the properties of the cells themselves or adhesion/other parameters relating to a second cell type in suspension (Lawrence and Springer, 1991, Chen and Springer, 2001, Cucullo et al., 2002, Grab et al., 2004). As a representation of the physical microenvironment this approach has considerable advantages. There is evidence to suggest that the effect of local physical forces can act to enhance BBB integrity by upregulation of tight junction proteins (Santaguida et al., 2006, Siddharthan et al., 2007) and the inclusion of flow can help to eliminate passive and nonspecific effects caused by cells 'settling out' in static culture.

The distinct advantages of both approaches have driven the development of ever more sophisticated experimental methods incorporating co- and multi-cultures into flow environments (Booth and Kim, 2012, Griep et al., 2012), however expense and complex technical requirements mean these are for the moment impractical for use in every research setting. In light of this we sought to improve the accuracy of current *in vitro* models of binding and pathogenesis in AGE by using a flow system with rates comparable to physiological conditions. Cerebral blood flow rate (CBF) has been measured by numerous authors employing a variety of methodologies, and typically falls in a range of 40-50ml/100g/min (Lassen, 1985, Dorfler et al., 2000, Okazawa et al., 2001, Ito et al., 2004). We calculated our flow rate based on these findings for the mass of cells grown in flow chambers, yielding a rate of approximately 25µl per minute, for 0.05g of tissue or cell mass and permitting us to replicate flow rates for up to 2g of neural tissue.

The contention that our model differs substantially from previous static systems is supported by our findings that even low rates of flow significantly reduce the ability of amoeba to adhere to host cells (Figure 5.4 B). This effect increases with increasing flow rate, although seeming to approach a plateau at the upper end of the tested range, conforming strongly to an exponential decay curve (Figure 5.4). At low flow rates therefore relatively small alterations may have a proportionally greater effect upon binding than they do at higher flow rates. Capillary microvessels have long been thought to be the site of invasion in AGE, due to their narrow width and the presence of only a single endothelial cell layer. Blood flow rates are known to be heterogeneous across neural tissue and capillaries in particular may only be transiently perfused,

with flow rates intermittently trending towards zero (Hertz and Paulson, 1980, Hudetz, 1997, Zhang et al., 2009). Such low-flow conditions produced significantly increased binding in our model, implicating flow rate as a major contributory factor to invasion.

Notably, several studies have indicated that cerebral blood flow rates are lowered by up to 10ml/min in HIV^+ patients and that this is the case both early and later in the infection process (Ances et al., 2009, Ances et al., 2011). This is significant due to the association between AGE and AIDS and our results which indicate that low flow rates correlate with increased trophozoite binding to endothelial cells. The clinical implications of this are that as well as AIDS patients, pre-AIDS HIV^+ patients may also be at heightened risk of developing AGE due to increased trophozoite binding in the brain microvasculature. This is important for monitoring and treatment of vulnerable patients and also has relevance to other underlying conditions where lowered CBF might cause patients to be at increased risk. The physical properties of our flow system may also apply to other parasitic CNS infections in terms of the increased vulnerability of patients with lowered CBF. This may be an interesting avenue to be pursued in future studies.

Given the differences observed between static and flow conditions we were interested to assess whether the contributions of amoeba adhesins to binding also differed from previous reports, when under flow. The major adhesin to have been identified is a mannose-binding protein (MBP) that is thought to be responsible for the majority of binding (Cao et al., 1998, Hurt et al., 2003b, Garate et al., 2004, Imbert-Bouyer et al., 2004, Garate et al., 2005, Garate et

al., 2006b). Our findings provide further evidence for the importance of MBP, showing that exogenous mannose significantly reduces binding in both static and dynamic systems (Figure 5.5). Moreover mannose treatment seemingly causes a greater proportional decrease in binding under flow conditions, up to twofold (Figure 5.5, section 5.4.5). Once again this suggests that the *in vivo* condition has not been accurately represented by standard static culture systems and whilst the existence of a second mannose-independent adhesin has been proposed (Kennett et al., 1999), our study showed that any mannose-independent subset of binding may not be the primary means of active binding *in vivo*.

Whilst adhesion (particularly mannose-mediated) is an important step in initiating AGE it is not the sole factor that merits consideration. Many *Acanthamoeba* genotypes secrete proteolytic enzymes which may play important roles in pathogenesis (Khan et al., 2000b, Alsam et al., 2005b) however the response of endothelial cells to these protease secretions has not been studied under flow conditions. We used a method based on counting grid squares superimposed over photomicrographs to estimate the degree of monolayer disruption, as a marker for loss of blood-brain barrier integrity.

Using this method we initially analysed images of adherent trophozoites to assess the degree to which binding affects monolayer disruption. Interestingly, given the wide variation seen in binding over a range of flow rates there was no significant difference in the extent of monolayer disruption (Figure 5.6). This null relationship was particularly evident at low flow rates and under

static conditions, where high levels of adherence had been observed but levels of monolayer disruption did not show any significant differences.

This raises the possibility of a decoupling of binding and BBB pathology and to investigate this further we made use of a cell free conditioned supernatant (ACM). This contains a number of secreted proteases which have been shown to break down tight junctions *in vitro,* leading to a loss of integrity in the blood-brain barrier (Alsam et al., 2005b, Kim et al., 2006, Sissons et al., 2006a, Khan and Siddiqui, 2009). Testing ACM in our flow model revealed that monolayer integrity is affected by the presence of secreted proteases under both static and flow conditions (Figure 5.7) however we once more found that flow is not a significant contributory factor, as disruption occurs at a constant level irrespective of rate. The main driving forces behind BBB disruption are thought to be serine proteases, with other secreted molecules playing a complementary role (Alsam et al., 2005b, Sissons et al., 2006a, Alizadeh et al., 2008). Our experiments suggest that this holds true for flow as well as for static conditions, with PMSF treatment able to reduce the degree of disruption to levels indistinguishable from untreated controls (figure 5.8). Given these significant reductions and the apparently minimal contribution of trophozoite adherence it is tempting to infer that the greater part of the mechanism of BBB disruption occurring under flow conditions is serine protease dependent.

One mechanism by which proteases are known to have effects on the integrity of the BBB is through the action of a class of G-protein coupled receptors known as Protease Activated Receptors (PARs). These are expressed on endothelial cells where they act in consort with thrombin to promote

haemostasis and inflammation (Kataoka et al., 2003, Gudmundsdottir et al., 2008, Gudmundsdottir et al., 2006). PARs have also been implicated in parasitic disease (Yang et al., 2009, Park et al., 2011) and notably blood-brain barrier traversal (Grab et al., 2009). Nikolskaia *et al.* demonstrated that *Trypanosoma brucei* proteases were responsible for activation by cleavage of these molecules, leading to intracellular signalling and host cell death by apoptosis.

General induction of apoptotic cell death has been reported in a wide range of parasitic protozoa including *Plasmodium falciparum*, *Toxoplasma gondii*, *Cryptosporidium parvum*, *Trypanosoma cruzi* and *Trypanosoma brucei* (Lopes et al., 1995, Toure-Balde et al., 1996, McCole et al., 2000, Nishikawa et al., 2002, Wei et al., 2002, Stiles et al., 2004, Wilson et al., 2008). In a number of cases this process has been linked to protein secretions and more specifically to cysteine proteases, especially in groups of large extracellular protozoa such as trypanosomatids and trichomonads (Lucas et al., 2008, Sommer et al., 2005, Grab et al., 2009). Extensive cysteine protease secretions have also been observed in *Entamoeba histolytica* although they have not yet been definitively linked with host apoptotic cell death (Hirata et al., 2007, Becker et al., 2010). Indeed for the majority of protozoan pathogens the host mechanisms inducing cell death have not been fully determined although evidence from *E. histolytica* and *Giardia intestinalis* suggests that pro-apoptotic enzymes caspases 8, 9 and 3 play a substantial role (Huston et al., 2000, Kim et al., 2007, Panaro et al., 2007). As with *A. castellanii* however the relative importance of secreted versus nonsecreted virulence factors and the

necrotic/apoptotic balance is debated (Berninghausen and Leippe, 1997, Seydel and Stanley, 1998, Huston et al., 2000).

Given the widespread expression of proteases as virulence factors and the role played by PARs in linking secreted proteases to apoptotic cell death in *T. brucei* (Nikolskaia et al., 2006a, Grab et al., 2009), we sought to determine whether a similar mechanism might contribute to BBB penetration in AGE. PAR1 and PAR4 were selected for study from receptors previously identified in HBMEC (Kim et al., 2004). Our intention was to conduct a brief initial investigation of PARs in *A. castellanii* pathogenesis and to examine whether global PAR activation contributes to monolayer disruption and cell death. As such our experiments did not include other receptors which may also contribute to endothelial injury by similar mechanisms, such as PAR2.

We treated cells with specific PAR antagonists during *in vitro* infections with trophozoites or ACM. Outcomes of infection (i.e. cell death) were studied in terms of apoptotic (Figures 5.12 and 5.13) and necrotic (Figure 5.11) mechanisms, as well as measures of gross pathology such as monolayer disruption (Figure 5.9 and 5.10). However the presence of PAR inhibitors did not make any significant difference to the outcome of infection in either case. It is reasonable to conclude therefore that HBMEC cell death in AGE does not proceed by PAR1 and/or PAR4 activation. Nevertheless this is not sufficient evidence to rule out a possible contribution by other PAR classes, in particular PAR2 which is known to be expressed on endothelial cells and has been implicated in BBB traversal by *T. brucei* (Grab et al., 2009). Future examination of this, and other PAR classes will be required in order to rule out

or confirm direct PAR activation as a contributory factor to AGE. Our data suggests however that any such activation is not global and must either be specific to individual PAR classes or result from the action of endogenous host PAR activators.

Discounting a contribution from PARs, tight junction (TJ) proteins appear to be one candidate for the molecular target of secreted proteases as elucidated from experiments with the standard static model (Khan and Siddiqui, 2009). These proteins are of critical importance in maintaining the integrity of the BBB and interestingly there is evidence to suggest that loss of TJs may result in cells entering apoptosis (Beeman et al., 2012). *A. castellanii* proteases have also been demonstrated to degrade components of the extracellular matrix (ECM) (Sissons et al., 2006a, Rocha-Azevedo et al., 2009a, Rocha-Azevedo et al., 2009b). These, via integrins, are important in rescuing cells from otherwise entering apoptosis (Frisch and Francis, 1994, Bates et al., 1994). It is therefore possible that cell death processes caused by the degradation of TJs, ECM and potentially integrin may contribute to pathology in AGE. Kumar *et al.* have suggested a similar mechanism contributes to *E. histolytica* gut pathology where the process is mediated by secreted cysteine proteases (Kumar et al., 2012). Direct evidence to support this conjecture is not provided by our work however, and substantial additional experiments are required if this hypothesis is to be upheld.

In consideration of the contribution of blood flow rate to pathogenesis, if the paradigm of TJs and/or ECM/integrins as the major molecular target for proteases holds true under flow conditions then the process of tight junction

degradation may be ruled solely by enzyme-substrate kinetics, independently from trophozoite binding. In this scenario flow rate may not make a substantial contribution until cells are detached from each other or their substrate. It is at this point that cells are then swept away by the action of flow. This may explain why levels of disruption appear relatively constant in our model, especially if physical forces or timeframes in excess of those we have used are required to fully detach cells.

Taking our findings as they stand binding appears to have little connection to monolayer disruption, however there is ample evidence that trophozoites are able to induce BBB perturbations and that binding may induce *Acanthamoeba* to upregulate protease production (Cao et al., 1998, Alsam et al., 2003, Hurt et al., 2003a, Khan and Siddiqui, 2009). Adherence is also thought to induce apoptosis in HBMEC and this could prove to be an additional contributory factor to pathogenesis (Alizadeh et al., 1994, Mattana et al., 2001, Mattana et al., 2002, Zheng et al., 2004, Sissons et al., 2005). A further factor to consider is that over longer timeframes adherent trophozoites may begin to replicate, increasing the disruptive effect upon the BBB. If this is the case then a colonisation phase may precede invasion and thus pathology may correlate with amoeba population growth. Apoptotic processes are likely to occur at a slower rate than protease-dependent perturbations however and thus they may not be relevant during the initial stages of infection which our model represents. The significance of host cell death during the later stages of host-parasite interactions remains an important issue to be addressed in future studies.

6. General Discussion

Throughout this study we have examined the immunology and pathogenesis of the haematogenous stage of AGE. Our experiments focus in particular on events occurring in the brain microvasculature, within the context of host antibody and the local environment of endothelial cells. Data previously collected concerning this aspect of AGE pathogenesis is sparse and has not considered the role that humoral immunity may play in preventing initiation of disease in healthy individuals.

Our data shows the isolation and functional analysis of a polyclonal antibody (HE2) derived *in vivo*, including elucidation of the antigenic targets of this antibody. Analysis of HE2 function *in vitro* revealed an ability to limit trophozoite adhesion to HBMEC alongside a similar effect observed with an isotype control. Binding inhibition did not however translate into a protective phenotype by measures of cell death and monolayer disruption. This suggests two major findings: 1) that binding plays a less crucial role in pathogenesis than had previously been thought; and 2) that trophozoites may possess multiple means to interfere with normal antibody function. This first conclusion is supported by results from a novel *in vitro* flow model of disease, whilst our second conclusion is supported by our *in vitro* and *in silico* analysis and comparisons across other parasite models.

Both protozoa and helminths have been shown to evade the action of the humoral immune response by both sequestration and degradation of antibody. Our evaluation of these two mechanisms confirmed previous reports of antibody cleavage by *A. castellanii* and additionally suggested that amoebae, like some other protozoa, exhibit a low level of Fc-binding activity. We

investigated the dynamics of amoeba/host interaction in brain microcapillaries by adapting the standard *in vitro* model to incorporate the effect of blood flow, resulting in substantial reductions in the ability of trophozoites to bind to endothelial cells. Two important mediators of pathogenesis, mannose-binding protein and serine proteases behaved as previously described in this system. However results reveal a disconnection between the number of trophozoites binding to endothelial cells and the extent of both host cell death and the disruption observed in the cell monolayer. In light of these findings we have proposed several modifications to the current concept of AGE pathogenesis and suggest that adoption of more refined *in vitro* techniques may produce a more thorough understanding of this life-threatening infection.

In examining AGE it is important to consider the context in which the disease occurs, predominantly where the host immune system is compromised. The underlying cause of immune deficiency may be due to a number of factors. Deliberate suppression of the immune response, for example during organ transplant or as a result of chemotherapy can leave patients at increased risk of infection (Duarte et al., 2006, Mutreja et al., 2007). Underlying states affecting immunity such as alcoholism, malnutrition, primary immune deficiency, or infection also heighten risk. The severe immune deficiencies resulting from HIV infection in particular are thought to be a strong predisposing factor in the development of AGE (Rosenberg and Morgan, 2001, MacLean et al., 2007). HIV infection causes a progressive loss in lymphocyte function leading to severe immune deficiencies, with the individual typically succumbing to opportunistic infections. Loss of B-cell and $CD4^+$ T-cell function is debilitating to humoral immunity as these cell types have critical roles in antibody

production. Plasma cells differentiated from B-cells synthesise antibody specific to invading microbes and are the source for antibodies of a given class and with affinity-matured antigen specificity. $CD4^+$ T-cells play a crucial role in initiating and regulating this process by co-stimulation of B-cells in the context of APC and secretion of the stimulatory cytokines IL-2, IL-4, IL-5, IFNγ, and TGFβ. In AIDS the humoral response, its associated effector functions, and acquired immunological memory are seriously impaired and so even commonly encountered microbes can re-emerge as a threat to the individual.

The ubiquity of *A. castellanii* is demonstrated by the large proportion of healthy individuals who display seroconversion (Chappell et al., 2001); however the role antibody plays in controlling infection and the antigens that initiate immunity in healthy individuals are not known. We addressed these areas by generating antibody experimentally.

Our panel of antibodies yielded a number of colonies positive for IgG and IgM classes (Figure 3.2), in support of observations from previous studies (Kennett et al., 1999, Leher et al., 1999, Turner et al., 2005). Whilst a number of the antibodies produced during these earlier studies were reactive only against the amoeba's encysted form, antibody screened during our experiments reacted strongly with trophozoites (Figure 3.4). This is of greater benefit in assisting our understanding of factors expressed by the active, proliferating cell and therefore those which are likely to be of importance during BBB penetration. Nevertheless when translated into an *in vitro* model system the ultimate protective effect of antibody on host endothelial cells was minimal. This raises

interesting questions regarding the role being filled by antibody during infection and parasite evasion strategies specific to host antibody.

Studies of the intestinal amoeba *E. histolytica* have revealed that secretory IgA at the gut mucosa acts to inhibit trophozoite binding by targeting surface adhesion factors (Haque et al., 2001, Abd-Alla et al., 2006). One of these (Gal/GalNAc) is a lectin, a class of sugar-binding proteins of which a member has also been identified in *Acanthamoeba* - MBP (Garate et al., 2006b). A small reduction in binding of trophozoites to endothelial cells was prompted by antibody treatment in our experiments and this could indicate a role for antibody in limiting adhesion by targeting amoeba binding proteins (Figures 3.10 and 4.8). This hypothesis seems especially attractive given the localisation of HE2 immunofluorescent staining to the cell membrane (Figure 3.8). However the loss in binding capacity as a result of antibody treatment was low in our experiments when compared with similar studies and when compared with the reduction seen when trophozoites are treated solely with mannose. Furthermore, MBP was not identified as a target antigen of HE2, although polyclonal supernatant showed diffuse staining in the molecular weight range of single MBP subunits. HE2 represents only a single hybridoma from a range of those generated and so it is possible that protective anti-MBP activity may lie with other hybridoma clones. Nevertheless of the hybridoma lines generated and tested, HE2 demonstrated the greatest ability to inhibit trophozoite binding (Figure 3.6). Therefore if *in vivo* protective immunity to *A. castellanii* is mediated by an adhesin-specific antibody it is unlikely to be one which was detected in our study.

One point that is worthy of consideration is that fact that all previous attempts to classify the effect of antibody on adhesion of *A. castellanii* trophozoites have used static (standard tissue culture or Transwell) model systems (Leher et al., 1998a, Kennett et al., 1999). We have presented evidence which demonstrates that using an *in vitro* flow system substantially reduces the ability of trophozoites to adhere to microvascular endothelial cells (Figure 5.4). Separately we have also shown that binding is reduced in the presence of antibody in a static culture system (Figure 4.8). Due to time and resource constraints we did not explore these two effects in combination; however we predict that a synergistic interaction would reduce binding to minimal levels. Testing this hypothesis is suggested as a priority for subsequent research.

As a more accurate representation of *in vivo* conditions, flow systems have been used to great effect to investigate the dynamics of endothelial binding, for example in *P. falciparum* (Adams et al., 2000, Gray et al., 2003, Phiri et al., 2009). In the context of work by these groups, and other similar studies in different organisms the flow system we have presented has wider applications than solely in *Acanthamoeba* research. In particular the physical and fluidic properties of *in vitro* flow systems can be applied to many disease states, and provide a platform on which the interaction of microbes with the brain endothelium can be studied. As such, the improved knowledge of AGE resulting from incorporation of the effect of flow will also contribute to understanding of other cerebral infections.

Static systems for investigating pathogenesis of *Acanthamoeba* have yielded valuable discoveries however our preliminary data has shown that effects seen

in these *in vitro* systems are unrepresentative of what may occur *in vivo*. This is especially true of trophozoite binding which our data suggests is considerably overestimated in static culture. This has relevance to immune control of binding in that if levels of binding *in vivo* are lower than current static *in vitro* models suggest the small antibody-mediated reductions seen in our data could prove proportionally highly influential in determining whether trophozoites can invade the BBB.

These reductions need not necessarily result from specific recognition of binding proteins. MS/MS analysis of antigens recognised by HE2 produced matches to proteins involved in metabolism and protein synthesis (Tables 4.1 and 4.2). Some of these proteins have been ascribed roles in virulence in other organisms, for example the *Trichomonas vaginalis* AP65 adhesin exhibits sequence homology with malic enzyme (O'Brien et al., 1996). Furthermore even where antigens have no reported involvement in virulence, recognition may prompt reductions in adhesion due to localisation on the cell membrane. Especially in the case of IgM which has a polymeric structure and high molecular weight, binding to non-adhesive antigens proximal to binding factors could physically inhibit the interaction between binding receptors and their relevant ligands.

Impairment of pathogen motility is another means by which antibody protects the host. One target revealed by our experiments is the cytoskeletal component actin. Formation of amoebastomes and other rearrangements of the cytoskeleton are known virulence mechanisms both in *A. castellanii* (Khan, 2001, Mattana et al., 1997) and in other pathogenic amoebae (Bailey et al.,

1987, Sohn et al., 2010). Therefore targeting this pathway is one means by which host antibody could prevent invasion. This possibility is given further credence by our observation of the capacity of HE2 to aggregate trophozoites (Figure 3.9), providing an additional means by which trophozoite motility might be limited.

Despite the reductions in trophozoite binding observed in antibody and antibody fragment treated cultures no reduction was observed in monolayer disruption or cell death. The interpretation that immune targeting of trophozoite binding (whether mediated by membrane antigens, the cytoskeleton or both) is the primary means of humoral immunity against *A. castellanii* is therefore not a reliable one. In this case other possibilities must be considered.

One possibility specific to the IgM isotype antibody seen in our experiments relates to activation of the complement cascade. *A. culbertsoni* is known to fix complement by the alternative pathway (Ferrante and Rowan-Kelly, 1983, Pumidonming et al., 2011) although this process may not lead to trophozoite lysis (Toney and Marciano-Cabral, 1998). However the role played by classical activation has not been determined. IgM is a particularly effective complement activator because of its multiple valency which means that only a single molecule is required to initiate the cascade (Plaut et al., 1972). Cleavage or sequestration of IgM in particular as well as other classes may therefore represent an important mechanism for evasion of complement. We did not investigate the interaction between complement and IgM in AGE however this may be an important topic to be addressed by future studies.

Another possibility is that antibody might act to neutralise secreted proteases which have been shown to be an important factor in BBB disruption *Acanthamoeba* trophozoites (Alsam et al., 2005b). Soluble virulence factors such as proteases may be inactivated by specific antibody in a number of ways. The most straightforward is direct neutralisation where antibody binding is sufficient to interfere with the normal function of the target molecule. For proteases this may include binding at or near to the active site inhibiting the interaction between enzyme and substrate. The most thoroughly characterised examples of this are seen in responses to bacterial toxins for example the *Clostridium botulinum* neurotoxins (Babcock et al., 2006, Hussack et al., 2011). Antibody binding also acts as a signal for phagocytosis of the target antigen by phagocytes, where it is degraded internally. Additionally, complexes can form consisting of multiple antibody and antigen molecules. Activation of the complement cascade causes deposition of complement subunits onto the immune complex, prompting recognition and binding by cell types expressing complement receptor such as erythrocytes which facilitate transport of complexes to the liver and spleen. Macrophages resident in these organs then recognise and internalise the complex via their own Fc and complement receptors. Due to its multiple valency IgM is a particularly efficient complement activator and can also bind multiple antigens per single molecule. It may therefore play an especially important role in inactivating secreted amoeba proteases.

Serine proteases in particular play a major role in degrading tight junction proteins as demonstrated in work by Alsam *et al.* (2005) and Sissons *et al.* (2006). As tight junctions are responsible for the enhanced barrier properties of

the brain microvasculature compared with other endothelial types their targeting by *A. castellanii* is a major risk factor in the development of AGE. The importance of secreted proteases in tight junction disruption has been reported for infections caused by other protozoan parasites. For example, *E. histolytica* secretes proteases which act on epithelial tight junctions in a similar way to *A. castellanii* secretions (Leroy et al., 2000, Lauwaet et al., 2004, Kumar et al., 2012). In more general terms proteases are virulence factors for a wide variety of other parasites for example *T. brucei*, where they participate in signalling mechanisms which lead to host cell death (Nikolskaia et al., 2006a, Grab et al., 2009). As a result proteases have been explored as targets for therapeutic intervention across a range of species (Doyle et al., 2007, Mahmoudzadeh-Niknam and McKerrow, 2004, Vermeire et al., 2012).

Our experiments further underline the importance of proteases to pathogenesis. *In vitro* treatment with the serine protease inhibitor PMSF reduced the extent of monolayer disruption to a level equivalent to that seen in uninfected HBMEC, demonstrating that protease inhibition can be effective in limiting BBB perturbations (Figure 5.8). Monolayer disruption also occurred to the same extent regardless of the flow rate applied to cells, not just for cell-free ACM treatment but also with trophozoite infections (Figure 5.7). The implication of this finding is that the number of trophozoites binding (which we found to increase with decreasing flow rate) has less effect upon endothelial monolayers than the presence of trophozoite secretions. Therefore proteases may be more important to BBB invasion than has previously been considered. This effect is paralleled in the BBB perturbations caused by *T. brucei* which have also been found to depend on parasite proteases. In the

specific instance of sleeping sickness endothelial cells become apoptotic as the result of induction by the cysteine protease brucipain and this process has been elucidated by Grab and colleagues (2009) to occur via Protease Activated Receptors (PARs). We investigated whether PAR transduction might also have a role in *A. castellanii*-induced cell death but discovered no evidence to suggest that antagonists of PAR1 or PAR4 prevent BBB disruption by either trophozoites or ACM. It therefore seems more likely that induction of cell death occurs via alternative pathways such as tight junction loss-mediated apoptosis as seen in *E. histolytica* (Kumar et al., 2012).

Regardless of the mechanisms by which proteases induce cell death, as a result of their secretion into the extracellular environment or association with the cell surface it might be assumed that *A. castellanii* proteases would be likely target antigens for humoral immunity. This assertion is supported by studies in other parasites demonstrating targeting of proteases during infection. For example cruzipain, the major pathogenic protease of *T. cruzi* initiates B and $CD4^+$ T-cell responses (Schnapp et al., 2002), with specific antibody detectable in sera of human patients (Martinez et al., 1991). Studies of *S. mansoni* proteases have also shown the importance of protease targets to immunity. IgE responses are rapidly induced by parasite cysteine protease with a vital contribution from $CD4^+$ T-cells (de Oliveira Fraga et al., 2010). Acquired immunity to a different protease (calpain) has also been demonstrated to enhance macrophage activation and ultimately killing of the parasite (Jankovic et al., 1996).

However our MS/MS sequencing of a range of protein bands recognised by polyclonal antibody failed to demonstrate the presence of any proteases. This

was the case both for proteases integral to cell survival and the parasite lifecycle e.g. cysteine (Leitsch et al., 2010), and also those previously implicated as virulence factors e.g. serine (Cho et al., 2000). It is possible that these may reside in unsequenced or low abundance bands, however given the apparent inability of HE2 to prevent monolayer disruption by ACM it seems more likely that our isolation procedure did not produce antibody specific to proteases. One proviso to this assertion is that although proteases themselves may not be specifically targeted by antibody some of the antigens which were detected are potentially involved in protease synthesis and export. Strong matches were obtained for peptides from elongation factors (eukaryotic translation elongation factor 2 and elongation factor 1γ) which play a role in protease synthesis and also for actin, which as a component of the cytoskeleton is crucial for exocytosis. These are however intracellular antigens and so unless they are present in complexes associated with the plasma membrane or there is a process of active uptake by the parasite, the way in which antibody specific to these antigens reaches its target is not clear.

The interaction between antibody and secreted/non-secreted virulence factors in AGE is a complex one. Our data does not fully support an assertion that one aspect of pathogenesis is of superior importance. HE2 appears to target amoeba surface or surface-associated antigens and reduces host cell binding however this is not protective in terms of host cell death or monolayer protection. Conversely inhibition of proteases protects host monolayers from disruption but proteases appear not to be a major antibody target.

In order to reconcile this apparently conflicting evidence we considered whether the inability of antibody to protect host cells *in vitro* resulted from parasite immune evasion mechanisms. Amongst the most well characterised evasion mechanisms in other pathogenic protozoa are the antigenic variation type, where surface factors that might be recognised and targeted by the immune system are altered or exchanged for unrecognised ones. Prominent examples include the Variant Surface Glycoprotein (VSG) molecules of *T. brucei* which are responsible for the waves of parasitaemia characteristic in African sleeping sickness, and *P. falciparum var* genes, which create polymorphic versions of PfEMP-1, a protein of key importance in malarial pathogenesis. No evidence for antigenic variation in *A. castellanii* has ever been described although the large number of genotypes (sixteen known to date (Kong, 2009, Corsaro and Venditti, 2010)) of which only a few have been described as pathogenic suggests that strain-specific variations could be responsible for enhancing virulence. Protease expression has been suggested as a candidate for correlation with differential virulence (Hadaś and Mazur, 1993), however this connection has not yet been conclusively made, and it is unknown whether any *A. castellanii* virulence factors vary in response to the host immune environment.

The most likely role for proteases in immune evasion lies in their ability to cleave and/or degrade antibody. By degrading antibody parasites can protect themselves from immune effector mechanisms such as complement fixation (which is enhanced by antibody via the classical activation pathway) and phagocytosis (phagocytes recognise opsonised pathogens via the antibody Fc domain). The ability to cleave antibody has been observed in both other

protozoa and also in multicellular parasites. For example *E. histolytica* degrades host IgA via surface-associated cysteine protease activity (Garcia-Nieto et al., 2008) and serine proteases from two life stages of *S. mansoni* cleave IgE (Pleass et al., 2000). Evidence for similar cleavage by *Acanthamoeba* proteases has been detailed by Na *et al.* for IgA, IgG and IgM classes. Our data supports these conclusions and also extends findings to include cleavage of IgE and a physiologically derived IgM antibody (Figures 4.2 to 4.6). The protease classes responsible for this cleavage activity were primarily serine proteases with an additional contribution from metalloproteases. This is a similar finding to the trypsin-like proteases of importance in *S. mansoni* infections (Pleass et al., 2000, Aslam et al., 2008), however stands in contrast with findings from the parasites *T. cruzi* and *F. hepatica* where cleavage activity has been instead ascribed to cysteine protease activity (Berasain et al., 2000, Berasain et al., 2003).

It should be considered that the data presented both by our study and by the work of other researchers was obtained from *in vitro* experiments that may not reflect cleavage processes as they occur *in vivo*. Contributions from blood serum components such as endogenous protease inhibitors or antimicrobial peptides could stabilise antibody or inhibit protease activity and so it would be an interesting strategy to examine the status and structure of antibody from infected patients. However if cleavage activity is maintained *in vivo* this will have interesting implications for the outcome of immune recognition. The precise molecular mechanisms of evasion depend on the location of any cleavage site within the molecule. Trophozoites could inhibit activation of phagocytes by removing the Fc region as in *S. mansoni* for example (Aslam et

al., 2008). Alternatively degradation might occur at the hinge region as has been seen in *F. hepatica* (Berasain et al., 2000) or proteases could act at multiple sites in the protein depending on local conditions as with *T. cruzi* (Berasain et al., 2003). Semi-quantitation of band intensity in our experiments suggested that if any such preferential cleavage occurs it is most likely to be found in the heavy chain subunit (Figure 4.7). However cleavage is not necessarily so specific. Overall our data suggests that proteases of different classes may act in consort, possibly at a variety of sites along the antibody leading to a more generalised degradation of structure than the single specific cleavage events seen in, for example, *S. mansoni*. Further experiments will be required in order to address this point in detail.

Aside from the ability of trophozoites to render antibody ineffective via cleavage, other data from our experiments suggested the presence of an evasion mechanism mediated by antibody binding. Isotype control antibody proved equally as effective at reducing trophozoite adherence to HBMEC monolayers as polyclonal HE2; however this did not translate into a protective phenotype in either case. Sequestration of antibody by parasites is a general phenomenon that has been observed on a number of occasions in a variety of species with examples reported in *P. falciparum*, *T. cruzi*, *S. mansoni*, *T. gondii* and *L. major* (Budzko et al., 1989, Garcia et al., 1997, Loukas et al., 2001, Campos-Neto et al., 2003, Czajkowsky et al., 2010). Our analysis identified regions of similarity between proteins previously implicated in antibody-binding activity and homologous regions in the *A. castellanii* genome (Tables 4.1 and 4.2). In some cases these results conformed to protein families conserved across a number of species for example the nucleoside diphosphate

kinase superfamily, to which *L. major* Lmsp1 and its Trypanosome homologues belong. *A. castellanii* also showed similarity to regions from other genes involved in antibody binding from *T. gondii*, and *S. mansoni*. This *in silico* evidence is further supported by immunofluorescence and FACS assays which demonstrate nonspecific binding of secondary antibody, and also a small enhancement of the effect when Fc fragment was used as a probe (Figures 4.12 and 4.14).

Taken together this data suggests that - if not necessarily a dedicated Fc-binding protein - trophozoites do exhibit some level of antibody-binding activity and that this should be investigated in subsequent experimental work. To use an example from our studies, this effect could be responsible for overestimation of signal or false-positive membrane specificity for hybridoma or serum antibody. This point has been raised in papers describing antibody-binding properties of *T. gondii* for example (Budzko et al., 1989) and a similar awareness amongst researchers investigating immunoglobulin interactions with *A. castellanii* is advised. Nevertheless it should be considered that the concentrations of antibody required to observe an effect under our experimental conditions were high. Thus this may not represent a specific blocking effect but rather a passive outcome of high protein concentrations in experimental media. We did not perform a titration of antibody in order to determine whether this was the case, and as such this is suggested as an important next stage in the analysis of the Fc-binding activity exhibited by *A. castelanii*. An experiment of this kind would also have the additional benefit of determining the minimum concentration at which antibody produces a measurable effect on trophozoite binding. This will prove informative for

determining the specificity of binding inhibition and the likelihood of an equivalent process occurring *in vivo*.

Overall, the data we have presented increases our understanding of how *A. castellanii* interacts with antibody at the endothelial interface. That infected and exposed individuals produce antibody has been demonstrated in a number of studies (Alizadeh et al., 2001, Kiderlen et al., 2009) but the role of immunoglobulin in controlling infection has not been fully determined. The prominence of IgM in our experiments is especially interesting due to the prominence of this class in serum surveys and its role in complement fixation. This relationship also provides an insight into the potential purpose of antibody-binding activity on the parasite's surface. Recruitment of IgM in an inverted orientation (i.e. mediated through binding to the Fc region) could prevent interaction with complement subunits and phagocytes, thereby protecting trophozoites from phagocytosis and/or lysis. In addition protease activity may play a role in antibody inactivation via cleavage events. These processes may be of particular interest in *Acanthamoeba* keratitis which occurs in individuals with functional immune systems.

From our experiments it appears that both specific and nonspecific antibody reduce trophozoite binding, however antibody alone has little bearing on cell survival or monolayer preservation. Indeed the synergy between the cellular and humoral components of the immune system means that control solely by antibody is in any case an unlikely scenario. Future advances in the field may therefore depend on identifying important control mechanisms by systematic elimination of individual immune components. The most efficient

methodology for this approach may be to make use of knockout mouse strains. Mice with total immune deficiency (e.g. SCID) have already been used to simulate free-living amoeba infections (Janitschke et al., 1996). However use of strains with more specific deficiencies will allow protective immune control mechanisms to be traced more precisely. For example μMT mice are deficient in B-cells and thus useful for investigating immune function in the absence of antibody. Similarly $RAG^{-/-}$ T-cell deficient animals may be used to examine the effects of a loss of T-cell mediated immunity.

In AGE depletion of normal immune processes allows trophozoite growth to continue unchecked. Knowledge of the ways in which trophozoites interact with the immune system therefore has the potential to enhance therapeutic strategies aimed at restoring essential disease prevention processes. Whilst having minimal preservation ability on the BBB, antibody may still combat haematogenous spread by aggregation and immobilisation of trophozoites or limiting adhesion. This is especially the case if as indicated by results from our *in vitro* flow system the ability of trophozoites to bind to HBMEC is lower than that estimated using static models.

Our work also has applications in therapeutic strategies targeting essential processes of the parasite itself. We have identified a number of amoeba antigens that are targets for the immune system and which therefore may be exploited through vaccination or immunotherapy. These may prove to be valuable targets for drug development and widen the limited array of pharmaceutical compounds available to clinicians. We hope that this will improve the prognosis for patients suffering *Acanthamoeba* infections.

Bibliography

ABD-ALLA, M. D., JACKSON, T. F., ROGERS, T., REDDY, S. & RAVDIN, J. I. (2006) Mucosal immunity to asymptomatic *Entamoeba histolytica* and *Entamoeba dispar* infection is associated with a peak intestinal anti-lectin immunoglobulin A antibody response. *Infect Immun,* 74**,** 3897-903.

ABD, H., SAEED, A., JALAL, S., BEKASSY, A. & SANDSTRÖM, G. (2009) Ante mortem diagnosis of amoebic encephalitis in a haematopoietic stem cell transplanted patient. *Scand J Infect Dis,* 41**,** 619-22.

ADAMS, S., TURNER, G. D., NASH, G. B., MICKLEM, K., NEWBOLD, C. I. & CRAIG, A. G. (2000) Differential binding of clonal variants of *Plasmodium falciparum* to allelic forms of intracellular adhesion molecule 1 determined by flow adhesion assay. *Infect Immun,* 68**,** 264-9.

ADDIS, M. F., RAPPELLI, P., CAPPUCCINELLI, P. & FIORI, P. L. (1997) Extracellular release by *Trichomonas vaginalis* of a NADP+ dependent malic enzyme involved in pathogenicity. *Microb Pathog,* 23**,** 55-61.

ADEKAR, S. P., TAKAHASHI, T., JONES, R. M., AL-SALEEM, F. H., ANCHARSKI, D. M., ROOT, M. J., KAPADNIS, B. P., SIMPSON, L. L. & DESSAIN, S. K. (2008) Neutralization of botulinum neurotoxin by a human monoclonal antibody specific for the catalytic light chain. *PLoS One,* 3**,** e3023.

AHN, H. S., FOSTER, C., BOYKOW, G., STAMFORD, A., MANNA, M. & GRAZIANO, M. (2000) Inhibition of cellular action of thrombin by N3-cyclopropyl-7-[[4-(1-methylethyl)phenyl]methyl]-7H-pyrrolo[3, 2-f]quinazoline-1,3-diamine (SCH 79797), a nonpeptide thrombin receptor antagonist. *Biochem Pharmacol,* 60**,** 1425-34.

AICHELBURG, A., WALOCHNIK, J., ASSADIAN, O., PROSCH, H., STEUER, A., PERNECZKY, G., VISVESVARA, G., ASPÖCK, H. & VETTER, N. (2008) Successful treatment of disseminated *Acanthamoeba* sp. infection with miltefosine. *Emerg Infect Dis,* 14**,** 1743-6.

AKSOZEK, A., MCCLELLAN, K., HOWARD, K., NIEDERKORN, J. Y. & ALIZADEH, H. (2002) Resistance of *Acanthamoeba castellanii* cysts to physical, chemical, and radiological conditions. *J Parasitol,* 88**,** 621-3.

ALDERETE, J. F. & GARZA, G. E. (1988) Identification and properties of *Trichomonas vaginalis* proteins involved in cytadherence. *Infect Immun,* 56**,** 28-33.

ALFIERI, S., CORREIA, C., MOTEGI, S. & PRAL, E. (2000) Proteinase activities in total extracts and in medium conditioned by *Acanthamoeba polyphaga* trophozoites. *J Parasitol,* 86**,** 220-7.

ALIZADEH, H., APTE, S., EL-AGHA, M., LI, L., HURT, M., HOWARD, K., CAVANAGH, H., MCCULLEY, J. & NIEDERKORN, J. (2001) Tear IgA and serum IgG antibodies against *Acanthamoeba* in patients with *Acanthamoeba* keratitis. *Cornea,* 20**,** 622-7.

ALIZADEH, H., HE, Y., MCCULLEY, J., MA, D., STEWART, G., VIA, M., HAEHLING, E. & NIEDERKORN, J. (1995) Successful immunization against *Acanthamoeba* keratitis in a pig model. *Cornea,* 14**,** 180-6.

ALIZADEH, H., LI, H., NEELAM, S. & NIEDERKORN, J. (2008) Modulation of corneal and stromal matrix metalloproteinase by the mannose-induced *Acanthamoeba* cytolytic protein. *Exp Eye Res,* 87**,** 286-91.

ALIZADEH, H., NEELAM, S., HURT, M. & NIEDERKORN, J. (2005) Role of contact lens wear, bacterial flora, and mannose-induced pathogenic protease in the pathogenesis of amoebic keratitis. *Infect Immun,* 73**,** 1061-8.

ALIZADEH, H., PIDHERNEY, M., MCCULLEY, J. & NIEDERKORN, J. (1994) Apoptosis as a mechanism of cytolysis of tumor cells by a pathogenic free-living amoeba. *Infect Immun,* 62**,** 1298-303.

ALSAM, S., JEONG, S., DUDLEY, R. & KHAN, N. (2008) Role of human tear fluid in *Acanthamoeba* interactions with the human corneal epithelial cells. *Int J Med Microbiol,* 298**,** 329-36.

ALSAM, S., KIM, K., STINS, M., RIVAS, A., SISSONS, J. & KHAN, N. (2003) *Acanthamoeba* interactions with human brain microvascular endothelial cells. *Microb Pathog,* 35**,** 235-41.

ALSAM, S., SISSONS, J., DUDLEY, R. & KHAN, N. (2005a) Mechanisms associated with *Acanthamoeba castellanii* (T4) phagocytosis. *Parasitol Res,* 96**,** 402-9.

ALSAM, S., SISSONS, J., JAYASEKERA, S. & KHAN, N. (2005b) Extracellular proteases of *Acanthamoeba castellanii* (encephalitis isolate belonging to T1 genotype) contribute to increased permeability in an *in vitro* model of the human blood-brain barrier. *J Infect,* 51**,** 150-6.

ANCES, B. M., SISTI, D., VAIDA, F., LIANG, C. L., LEONTIEV, O., PERTHEN, J. E., BUXTON, R. B., BENSON, D., SMITH, D. M., LITTLE, S. J., RICHMAN, D. D., MOORE, D. J. & ELLIS, R. J. (2009) Resting cerebral blood flow: a potential biomarker of the effects of HIV in the brain. *Neurology,* 73**,** 702-8.

ANCES, B. M., VAIDA, F., CHERNER, M., YEH, M. J., LIANG, C. L., GARDNER, C., GRANT, I., ELLIS, R. J. & BUXTON, R. B. (2011) HIV and chronic methamphetamine dependence affect cerebral blood flow. *J Neuroimmune Pharmacol,* 6**,** 409-19.

ARMULIK, A., GENOVE, G., MAE, M., NISANCIOGLU, M. H., WALLGARD, E., NIAUDET, C., HE, L., NORLIN, J., LINDBLOM, P., STRITTMATTER, K., JOHANSSON, B. R. & BETSHOLTZ, C. (2010) Pericytes regulate the blood-brain barrier. *Nature,* 468**,** 557-61.

ASLAM, A., QUINN, P., MCINTOSH, R. S., SHI, J., GHUMRA, A., MCKERROW, J. H., BUNTING, K. A., DUNNE, D. W., DOENHOFF, M. J., MORRISON, S. L., ZHANG, K. & PLEASS, R. J. (2008) Proteases from *Schistosoma mansoni* cercariae cleave IgE at solvent exposed interdomain regions. *Mol Immunol,* 45**,** 567-74.

AWWAD, S., HEILMAN, M., HOGAN, R., PARMAR, D., PETROLL, W., MCCULLEY, J. & CAVANAGH, H. (2007) Severe reactive ischemic posterior segment inflammation in acanthamoeba keratitis: a new potentially blinding syndrome. *Ophthalmology,* 114**,** 313-20.

AYALA-SUMUANO, J. T., TELLEZ-LOPEZ, V. M., DOMINGUEZ-ROBLES MDEL, C., SHIBAYAMA-SALAS, M. & MEZA, I. (2013) Toll-like receptor signaling activation by *Entamoeba histolytica* induces beta defensin 2 in human colonic epithelial cells: its possible role as an element of the innate immune response. *PLoS Negl Trop Dis,* 7**,** e2083.

BABCOCK, G. J., BROERING, T. J., HERNANDEZ, H. J., MANDELL, R. B., DONAHUE, K., BOATRIGHT, N., STACK, A. M., LOWY, I., GRAZIANO, R., MOLRINE, D., AMBROSINO, D. M. & THOMAS, W. D., JR. (2006) Human monoclonal antibodies directed against toxins A and B prevent *Clostridium difficile*-induced mortality in hamsters. *Infect Immun,* 74**,** 6339-47.

BAILEY, G. B., DAY, D. B., NOKKAEW, C. & HARPER, C. C. (1987) Stimulation by target cell membrane lipid of actin polymerization and phagocytosis by *Entamoeba histolytica*. *Infect Immun,* 55**,** 1848-53.

BARBEAU, J. (2007) Lawsuit against a dentist related to serious ocular infection possibly linked to water from a dental handpiece. *J Can Dent Assoc,* 73**,** 618-22.

BARFOD, L., DALGAARD, M. B., PLEMAN, S. T., OFORI, M. F., PLEASS, R. J. & HVIID, L. (2011) Evasion of immunity to *Plasmodium falciparum* malaria by IgM masking of protective IgG epitopes in infected erythrocyte surface-exposed PfEMP1. *Proc Natl Acad Sci U S A,* 108**,** 12485-90.

BARRAGAN, A., BROSSIER, F. & SIBLEY, L. (2005) Transepithelial migration of *Toxoplasma gondii* involves an interaction of intercellular adhesion molecule 1 (ICAM-1) with the parasite adhesin MIC2. *Cell Microbiol,* 7**,** 561-8.

BARRAGAN, A. & SIBLEY, L. (2002) Transepithelial migration of *Toxoplasma gondii* is linked to parasite motility and virulence. *J Exp Med,* 195**,** 1625-33.

BATES, R. C., BURET, A., VAN HELDEN, D. F., HORTON, M. A. & BURNS, G. F. (1994) Apoptosis induced by inhibition of intercellular contact. *J Cell Biol,* 125**,** 403-15.

BAZIN, R. & LEMIEUX, R. (1989) Increased proportion of B cell hybridomas secreting monoclonal antibodies of desired specificity in cultures containing macrophage-derived hybridoma growth factor (IL-6). *J Immunol Methods,* 116**,** 245-9.

BECKER, S. M., CHO, K. N., GUO, X., FENDIG, K., OOSMAN, M. N., WHITEHEAD, R., COHN, S. M. & HOUPT, E. R. (2010) Epithelial cell apoptosis facilitates *Entamoeba histolytica* infection in the gut. *Am J Pathol,* 176**,** 1316-22.

BEEMAN, N., WEBB, P. G. & BAUMGARTNER, H. K. (2012) Occludin is required for apoptosis when claudin-claudin interactions are. *Cell Death Dis,* 3**,** e273.

BENEDETTO, N. & AURIAULT, C. (2002) Prolactin-cytokine network in the defence against *Acanthamoeba castellanii* in murine microglia [corrected]. *Eur Cytokine Netw,* 13**,** 447-55.

BENEDETTO, N., ROSSANO, F., GORGA, F., FOLGORE, A., RAO, M. & ROMANO CARRATELLI, C. (2003) Defense mechanisms of IFN-

gamma and LPS-primed murine microglia against *Acanthamoeba castellanii* infection. *Int Immunopharmacol,* 3**,** 825-34.

BERASAIN, P., CARMONA, C., FRANGIONE, B., CAZZULO, J. J. & GONI, F. (2003) Specific cleavage sites on human IgG subclasses by cruzipain, the major cysteine proteinase from *Trypanosoma cruzi*. *Mol Biochem Parasitol,* 130**,** 23-9.

BERASAIN, P., CARMONA, C., FRANGIONE, B., DALTON, J. P. & GONI, F. (2000) *Fasciola hepatica*: parasite-secreted proteinases degrade all human IgG subclasses: determination of the specific cleavage sites and identification of the immunoglobulin fragments produced. *Exp Parasitol,* 94**,** 99-110.

BERNINGHAUSEN, O. & LEIPPE, M. (1997) Necrosis versus apoptosis as the mechanism of target cell death induced by *Entamoeba histolytica*. *Infect Immun,* 65**,** 3615-21.

BERRY, J. D., LICEA, A., POPKOV, M., CORTEZ, X., FULLER, R., ELIA, M., KERWIN, L., KUBITZ, D. & BARBAS, C. F., 3RD (2003) Rapid monoclonal antibody generation via dendritic cell targeting in vivo. *Hybrid Hybridomics,* 22**,** 23-31.

BILLAUT-MULOT, O., FERNANDEZ-GOMEZ, R. & OUAISSI, A. (1997) Phenotype of recombinant *Trypanosoma cruzi* which overexpress elongation factor 1-gamma: possible involvement of EF-1gamma GST-like domain in the resistance to clomipramine. *Gene,* 198**,** 259-67.

BJORCK, L. & KRONVALL, G. (1984) Purification and some properties of streptococcal protein G, a novel IgG-binding reagent. *J Immunol,* 133**,** 969-74.

BLACKMAN, H., RAO, N., LEMP, M. & VISVESVARA, G. (1984) *Acanthamoeba* keratitis successfully treated with penetrating keratoplasty: suggested immunogenic mechanisms of action. *Cornea,* 3**,** 125-30.

BLASCHITZ, M., KÖHSLER, M., ASPÖCK, H. & WALOCHNIK, J. (2006) Detection of a serine proteinase gene in *Acanthamoeba* genotype T6 (Amoebozoa: Lobosea). *Exp Parasitol,* 114**,** 26-33.

BLOCH, K. & SCHUSTER, F. (2005) Inability to make a premortem diagnosis of *Acanthamoeba* species infection in a patient with fatal granulomatous amebic encephalitis. *J Clin Microbiol,* 43**,** 3003-6.

BOOTH, R. & KIM, H. (2012) Characterization of a microfluidic in vitro model of the blood-brain barrier. *Lab Chip,* 12**,** 1784-92.

BOWER, K., DONNELLY, S., STUTZMAN, R., WARD, T. & WEBER, E. (2006) *Acanthamoeba* keratitis in a U.S. Army soldier after unauthorized use of contact lenses in the combat theater. *Mil Med,* 171**,** 833-7.

BRINDLEY, N., MATIN, A. & KHAN, N. (2009) *Acanthamoeba castellanii*: high antibody prevalence in racially and ethnically diverse populations. *Exp Parasitol,* 121**,** 254-6.

BROWN, H., HIEN, T., DAY, N., MAI, N., CHUONG, L., CHAU, T., LOC, P., PHU, N., BETHELL, D., FARRAR, J., GATTER, K., WHITE, N. & TURNER, G. (1999a) Evidence of blood-brain barrier dysfunction in human cerebral malaria. *Neuropathol Appl Neurobiol,* 25**,** 331-40.

BROWN, H., TURNER, G., ROGERSON, S., TEMBO, M., MWENECHANYA, J., MOLYNEUX, M. & TAYLOR, T. (1999b)

Cytokine expression in the brain in human cerebral malaria. *J Infect Dis,* 180**,** 1742-6.

BROWN, R., BASS, H. & COOMBS, J. (1975) Carbohydrate binding proteins involved in phagocytosis by *Acanthamoeba*. *Nature,* 254**,** 434-5.

BUDZKO, D. B., TYLER, L. & ARMSTRONG, D. (1989) Fc receptors on the surface of *Toxoplasma gondii* trophozoites: a confounding factor in testing for anti-*Toxoplasma* antibodies by indirect immunofluorescence. *J Clin Microbiol,* 27**,** 959-61.

CAMPOS-NETO, A., SUFFIA, I., CAVASSANI, K. A., JEN, S., GREESON, K., OVENDALE, P., SILVA, J. S., REED, S. G. & SKEIKY, Y. A. (2003) Cloning and characterization of a gene encoding an immunoglobulin-binding receptor on the cell surface of some members of the family Trypanosomatidae. *Infect Immun,* 71**,** 5065-76.

CAMPOS-RODRÍGUEZ, R., OLIVER-AGUILLÓN, G., VEGA-PÉREZ, L., JARILLO-LUNA, A., HERNÁNDEZ-MARTÍNEZ, D., ROJAS-HERNÁNDEZ, S., RODRÍGUEZ-MONROY, M., RIVERA-AGUILAR, V. & GONZÁLEZ-ROBLES, A. (2004) Human IgA inhibits adherence of *Acanthamoeba polyphaga* to epithelial cells and contact lenses. *Can J Microbiol,* 50**,** 711-8.

CAMPOSAMPIERO, D., CARAMELLO, G., INDEMINI, P., GERTEN, G., FRANCH, A., BIRATTARI, F., DONISI, P., PAOLIN, A., FERRARI, S. & PONZIN, D. (2009) Two red eyes and one asymptomatic donor. *Lancet,* 374**,** 1792.

CANTRILL, C. A., SKINNER, R. A., ROTHWELL, N. J. & PENNY, J. I. (2012) An immortalised astrocyte cell line maintains the in vivo phenotype of a primary. *Brain Res,* 1479**,** 17-30.

CAO, Z., JEFFERSON, D. & PANJWANI, N. (1998) Role of carbohydrate-mediated adherence in cytopathogenic mechanisms of *Acanthamoeba*. *J Biol Chem,* 273**,** 15838-45.

CARTER, R., CULLITY, G., OJEDA, V., SILBERSTEIN, P. & WILLAERT, E. (1981) A fatal case of meningoencephalitis due to a free-living amoeba of uncertain identity--probably *Acanthamoeba* sp. *Pathology,* 13**,** 51-68.

CERVA, L. (1989) *Acanthamoeba culbertsoni* and *Naegleria fowleri*: occurrence of antibodies in man. *J Hyg Epidemiol Microbiol Immunol,* 33**,** 99-103.

CHAPPELL, C., WRIGHT, J., COLETTA, M. & NEWSOME, A. (2001) Standardized method of measuring *Acanthamoeba* antibodies in sera from healthy human subjects. *Clin Diagn Lab Immunol,* 8**,** 724-30.

CHEN, S. & SPRINGER, T. A. (2001) Selectin receptor-ligand bonds: Formation limited by shear rate and dissociation governed by the Bell model. *Proc Natl Acad Sci U S A,* 98**,** 950-5.

CHESEBRO, B., BLOTH, B. & SVEHAG, S. E. (1968) The ultrastructure of normal and pathological IgM immunoglobulins. *J Exp Med,* 127**,** 399-410.

CHO, J., NA, B., KIM, T. & SONG, C. (2000) Purification and characterization of an extracellular serine proteinase from *Acanthamoeba castellanii*. *IUBMB Life,* 50**,** 209-14.

CLAESSENS, A., ADAMS, Y., GHUMRA, A., LINDERGARD, G., BUCHAN, C. C., ANDISI, C., BULL, P. C., MOK, S., GUPTA, A. P.,

WANG, C. W., TURNER, L., ARMAN, M., RAZA, A., BOZDECH, Z. & ROWE, J. A. (2012) A subset of group A-like var genes encodes the malaria parasite ligands for binding to human brain endothelial cells. *Proc Natl Acad Sci U S A,* 109**,** E1772-81.

CLARKE, D. W., ALIZADEH, H. & NIEDERKORN, J. Y. (2006) Intracorneal instillation of latex beads induces macrophage-dependent protection against *Acanthamoeba* keratitis. *Invest Ophthalmol Vis Sci,* 47**,** 4917-25.

CLARKE, M., LOHAN, A. J., LIU, B., LAGKOUVARDOS, I., ROY, S., ZAFAR, N., BERTELLI, C., SCHILDE, C., KIANIANMOMENI, A., BURGLIN, T. R., FRECH, C., TURCOTTE, B., KOPEC, K. O., SYNNOTT, J. M., CHOO, C., PAPONOV, I., FINKLER, A., SOON HENG TAN, C., HUTCHINS, A. P., WEINMEIER, T., RATTEI, T., CHU, J. S., GIMENEZ, G., IRIMIA, M., RIGDEN, D. J., FITZPATRICK, D. A., LORENZO-MORALES, J., BATEMAN, A., CHIU, C. H., TANG, P., HEGEMANN, P., FROMM, H., RAOULT, D., GREUB, G., MIRANDA-SAAVEDRA, D., CHEN, N., NASH, P., GINGER, M. L., HORN, M., SCHAAP, P., CALER, L. & LOFTUS, B. (2013) Genome of *Acanthamoeba castellanii* highlights extensive lateral gene transfer and early evolution of tyrosine kinase signaling. *Genome Biol,* 14**,** R11.

COLEMAN, S. E., BRADY, L. J. & BOYLE, M. D. (1990) Colloidal gold immunolabeling of immunoglobulin-binding sites and beta antigen in group B streptococci. *Infect Immun,* 58**,** 332-40.

CORSARO, D. & VENDITTI, D. (2010) Phylogenetic evidence for a new genotype of *Acanthamoeba* (Amoebozoa, Acanthamoebida). *Parasitol Res*.

COULON, C., COLLIGNON, A., MCDONNELL, G. & THOMAS, V. (2010) Resistance of *Acanthamoeba* cysts to disinfection treatments used in health care settings. *J Clin Microbiol,* 48**,** 2689-97.

COURRET, N., DARCHE, S., SONIGO, P., MILON, G., BUZONI-GATEL, D. & TARDIEUX, I. (2006) CD11c- and CD11b-expressing mouse leukocytes transport single *Toxoplasma gondii* tachyzoites to the brain. *Blood,* 107**,** 309-16.

CUCULLO, L., MCALLISTER, M. S., KIGHT, K., KRIZANAC-BENGEZ, L., MARRONI, M., MAYBERG, M. R., STANNESS, K. A. & JANIGRO, D. (2002) A new dynamic in vitro model for the multidimensional study of. *Brain Res,* 951**,** 243-54.

CULBERTSON, C., ENSMINGER, P. & OVERTON, W. (1965a) The Isolation of Additional Strains of Pathogenic *Hartmanella* sp. (*Acanthamoeba*): Proposed Culture Method for Application to Biological Material. *Am J Clin Pathol,* 43**,** 383-7.

CULBERTSON, C., HOLMES, D. & OVERTON, W. (1965b) *Hartmanella castellani* (*Acanthamoeba* sp): Preliminary Report on Experimental Chemotherapy. *Am J Clin Pathol,* 43**,** 361-4.

CULBERTSON, C., SMITH, J., COHEN, H. & MINNER, J. (1959) Experimental infection of mice and monkeys by *Acanthamoeba*. *Am J Pathol,* 35**,** 185-97.

CULBERTSON, C., SMITH, J. & MINNER, J. (1958) *Acanthamoeba*: observations on animal pathogenicity. *Science,* 127**,** 1506.

CURSONS, R., BROWN, T., KEYS, E., MORIARTY, K. & TILL, D. (1980) Immunity to pathogenic free-living amoebae: role of humoral antibody. *Infect Immun,* 29**,** 401-7.

CZAJKOWSKY, D. M., SALANTI, A., DITLEV, S. B., SHAO, Z., GHUMRA, A., ROWE, J. A. & PLEASS, R. J. (2010) IgM, Fc mu Rs, and malarial immune evasion. *J Immunol,* 184**,** 4597-603.

DA ROCHA-AZEVEDO, B. & COSTA E SILVA-FILHO, F. (2007) Biological characterization of a clinical and an environmental isolate of *Acanthamoeba polyphaga*: analysis of relevant parameters to decode pathogenicity. *Arch Microbiol,* 188**,** 441-9.

DA ROCHA-AZEVEDO, B., TANOWITZ, H. & MARCIANO-CABRAL, F. (2009) Diagnosis of infections caused by pathogenic free-living amoebae. *Interdiscip Perspect Infect Dis,* 2009**,** 251406.

DAGGETT, P., LIPSCOMB, D., SAWYER, T. & NERAD, T. (1985) A molecular approach to the phylogeny of *Acanthamoeba*. *Biosystems,* 18**,** 399-405.

DE JONCKHEERE, J. (1991) Ecology of *Acanthamoeba*. *Rev Infect Dis,* 13 Suppl 5**,** S385-7.

DE JONCKHEERE, J. (2007) Molecular identification of free-living amoebae of the Vahlkampfiidae and Acanthamoebidae isolated in Arizona (USA). *Eur J Protistol,* 43**,** 9-15.

DE OLIVEIRA FRAGA, L. A., LAMB, E. W., MORENO, E. C., CHATTERJEE, M., DVORAK, J., DELCROIX, M., SAJID, M., CAFFREY, C. R. & DAVIES, S. J. (2010) Rapid induction of IgE responses to a worm cysteine protease during murine pre-patent schistosome infection. *BMC Immunol,* 11**,** 56.

DE STGROTH, S. F. & SCHEIDEGGER, D. (1980) Production of monoclonal antibodies: strategy and tactics. *J Immunol Methods,* 35**,** 1-21.

DI CAVE, D., MONNO, R., BOTTALICO, P., GUERRIERO, S., D'AMELIO, S., D'ORAZI, C. & BERRILLI, F. (2009) *Acanthamoeba* T4 and T15 genotypes associated with keratitis infections in Italy. *Eur J Clin Microbiol Infect Dis,* 28**,** 607-12.

DI GREGORIO, C., RIVASI, F., MONGIARDO, N., DE RIENZO, B., WALLACE, S. & VISVESVARA, G. (1992) *Acanthamoeba* meningoencephalitis in a patient with acquired immunodeficiency syndrome. *Arch Pathol Lab Med,* 116**,** 1363-5.

DORFLER, P., PULS, I., SCHLIESSER, M., MAURER, M. & BECKER, G. (2000) Measurement of cerebral blood flow volume by extracranial sonography. *J Cereb Blood Flow Metab,* 20**,** 269-71.

DOYLE, P. S., ZHOU, Y. M., ENGEL, J. C. & MCKERROW, J. H. (2007) A cysteine protease inhibitor cures Chagas' disease in an immunodeficient-mouse model of infection. *Antimicrob Agents Chemother,* 51**,** 3932-9.

DUARTE, A., SATTAR, F., GRANWEHR, B., ARONSON, J., WANG, Z. & LICK, S. (2006) Disseminated acanthamoebiasis after lung transplantation. *J Heart Lung Transplant,* 25**,** 237-40.

ENGBRING, J. A., O'BRIEN, J. L. & ALDERETE, J. F. (1996) *Trichomonas vaginalis* adhesin proteins display molecular mimicry to metabolic enzymes. *Adv Exp Med Biol,* 408**,** 207-23.

ERTABAKLAR, H., TÜRK, M., DAYANIR, V., ERTUĞ, S. & WALOCHNIK, J. (2007) *Acanthamoeba* keratitis due to *Acanthamoeba* genotype T4 in a non-contact-lens wearer in Turkey. *Parasitol Res,* 100**,** 241-6.

FEINGOLD, J., ABRAHAM, J., BILGRAMI, S., NGO, N., VISVESARA, G., EDWARDS, R. & TUTSCHKA, P. (1998) *Acanthamoeba* meningoencephalitis following autologous peripheral stem cell transplantation. *Bone Marrow Transplant,* 22**,** 297-300.

FERRANTE, A. & BATES, E. (1988) Elastase in the pathogenic free-living amoebae *Naegleria* and *Acanthamoeba* spp. *Infect Immun,* 56**,** 3320-1.

FERRANTE, A. & ROWAN-KELLY, B. (1983) Activation of the alternative pathway of complement by *Acanthamoeba culbertsoni*. *Clin Exp Immunol,* 54**,** 477-85.

FERREIRA, G., MAGLIANO, A., PRAL, E. & ALFIERI, S. (2009) Elastase secretion in *Acanthamoeba polyphaga*. *Acta Trop,* 112**,** 156-63.

FIORI, P., MATTANA, A., DESSÌ, D., CONTI, S., MAGLIANI, W. & POLONELLI, L. (2006) *In vitro* acanthamoebicidal activity of a killer monoclonal antibody and a synthetic peptide. *J Antimicrob Chemother,* 57**,** 891-8.

FLORES, B., GARCIA, C., STAMM, W. & TORIAN, B. (1990) Differentiation of *Naegleria fowleri* from *Acanthamoeba* species by using monoclonal antibodies and flow cytometry. *J Clin Microbiol,* 28**,** 1999-2005.

FREVERT, U., MOVILA, A., NIKOLSKAIA, O. V., RAPER, J., MACKEY, Z. B., ABDULLA, M., MCKERROW, J. & GRAB, D. J. (2012) Early invasion of brain parenchyma by African trypanosomes. *PLoS One,* 7**,** e43913.

FRIEDLAND, L., RAPHAEL, S., DEUTSCH, E., JOHAL, J., MARTYN, L., VISVESVARA, G. & LISCHNER, H. (1992) Disseminated *Acanthamoeba* infection in a child with symptomatic human immunodeficiency virus infection. *Pediatr Infect Dis J,* 11**,** 404-7.

FRISCH, S. M. & FRANCIS, H. (1994) Disruption of epithelial cell-matrix interactions induces apoptosis. *J Cell Biol,* 124**,** 619-26.

GAGNON, M. & WALTER, K. (2006) A case of acanthamoeba keratitis as a result of a cosmetic contact lens. *Eye Contact Lens,* 32**,** 37-8.

GANESAN, L. P., KIM, J., WU, Y., MOHANTY, S., PHILLIPS, G. S., BIRMINGHAM, D. J., ROBINSON, J. M. & ANDERSON, C. L. (2012) FcgammaRIIb on liver sinusoidal endothelium clears small immune complexes. *J Immunol,* 189**,** 4981-8.

GARATE, M., ALIZADEH, H., NEELAM, S., NIEDERKORN, J. & PANJWANI, N. (2006a) Oral immunization with *Acanthamoeba castellanii* mannose-binding protein ameliorates amoebic keratitis. *Infect Immun,* 74**,** 7032-4.

GARATE, M., CAO, Z., BATEMAN, E. & PANJWANI, N. (2004) Cloning and characterization of a novel mannose-binding protein of *Acanthamoeba*. *J Biol Chem,* 279**,** 29849-56.

GARATE, M., CUBILLOS, I., MARCHANT, J. & PANJWANI, N. (2005) Biochemical characterization and functional studies of *Acanthamoeba* mannose-binding protein. *Infect Immun,* 73**,** 5775-81.

GARATE, M., MARCHANT, J., CUBILLOS, I., CAO, Z., KHAN, N. & PANJWANI, N. (2006b) In vitro pathogenicity of *Acanthamoeba* is associated with the expression of the mannose-binding protein. *Invest Ophthalmol Vis Sci*, 47**,** 1056-62.

GARCIA-NIETO, R. M., RICO-MATA, R., ARIAS-NEGRETE, S. & AVILA, E. E. (2008) Degradation of human secretory IgA1 and IgA2 by *Entamoeba histolytica* surface-associated proteolytic activity. *Parasitol Int,* 57**,** 417-23.

GARCIA, I. E., LIMA, M. R., MARINHO, C. R., KIPNIS, T. L., FURTADO, G. C. & ALVAREZ, J. M. (1997) Role of membrane-bound IgM in *Trypanosoma cruzi* evasion from immune clearance. *J Parasitol,* 83**,** 230-3.

GARDNER, H., MARTINEZ, A., VISVESVARA, G. & SOTREL, A. (1991) Granulomatous amebic encephalitis in an AIDS patient. *Neurology,* 41**,** 1993-5.

GHUMRA, A., SEMBLAT, J. P., MCINTOSH, R. S., RAZA, A., RASMUSSEN, I. B., BRAATHEN, R., JOHANSEN, F. E., SANDLIE, I., MONGINI, P. K., ROWE, J. A. & PLEASS, R. J. (2008) Identification of residues in the Cmu4 domain of polymeric IgM essential for interaction with *Plasmodium falciparum* erythrocyte membrane protein 1 (PfEMP1). *J Immunol,* 181**,** 1988-2000.

GIANINAZZI, C., SCHILD, M., WÜTHRICH, F., MÜLLER, N., SCHÜRCH, N. & GOTTSTEIN, B. (2009) Potentially human pathogenic *Acanthamoeba* isolated from a heated indoor swimming pool in Switzerland. *Exp Parasitol,* 121**,** 180-6.

GIRARD, M., GIRAUD, S., COURTIOUX, B., JAUBERTEAU-MARCHAN, M. & BOUTEILLE, B. (2005) Endothelial cell activation in the presence of African trypanosomes. *Mol Biochem Parasitol,* 139**,** 41-9.

GOLDSCHMIDT, P., DEGORGE, S., BENALLAOUA, D., SAINT-JEAN, C., BATELLIER, L., ALOUCH, C., LAROCHE, L. & CHAUMEIL, C. (2009) New tool for the simultaneous detection of 10 different genotypes of *Acanthamoeba* available from the American Type Culture Collection. *Br J Ophthalmol,* 93**,** 1096-100.

GOMEZ-COUSO, H., PANIAGUA-CRESPO, E. & ARES-MAZAS, E. (2007) *Acanthamoeba* as a temporal vehicle of *Cryptosporidium*. *Parasitology Research,* 100**,** 1151-1154.

GONZALEZ-ROBLES, A., CASTANON, G., HERNANDEZ-RAMIREZ, V. I., SALAZAR-VILLATORO, L., GONZALEZ-LAZARO, M., OMANA-MOLINA, M., TALAMAS-ROHANA, P. & MARTINEZ-PALOMO, A. (2008) *Acanthamoeba castellanii*: identification and distribution of actin cytoskeleton. *Exp Parasitol,* 119**,** 411-7.

GOOI, P., LEE-WING, M., BROWNSTEIN, S., EL-DEFRAWY, S., JACKSON, W. & MINTSIOULIS, G. (2008) *Acanthamoeba* keratitis: persistent organisms without inflammation after 1 year of topical chlorhexidine. *Cornea,* 27**,** 246-8.

GORDON, V., ASEM, E., VODKIN, M. & MCLAUGHLIN, G. (1993) *Acanthamoeba* binds to extracellular matrix proteins *in vitro*. *Invest Ophthalmol Vis Sci,* 34**,** 658-62.

GOUY, M., GUINDON, S. & GASCUEL, O. (2010) SeaView version 4: A multiplatform graphical user interface for sequence alignment and phylogenetic tree building. *Mol Biol Evol,* 27**,** 221-4.

GRAB, D., GARCIA-GARCIA, J., NIKOLSKAIA, O., KIM, Y., BROWN, A., PARDO, C., ZHANG, Y., BECKER, K., WILSON, B., DE A LIMA, A., SCHARFSTEIN, J. & DUMLER, J. (2009) Protease activated receptor signaling is required for African trypanosome traversal of human brain microvascular endothelial cells. *PLoS Negl Trop Dis,* 3**,** e479.

GRAB, D., NIKOLSKAIA, O., KIM, Y., LONSDALE-ECCLES, J., ITO, S., HARA, T., FUKUMA, T., NYARKO, E., KIM, K., STINS, M., DELANNOY, M., RODGERS, J. & KIM, K. (2004) African trypanosome interactions with an in vitro model of the human blood-brain barrier. *J Parasitol,* 90**,** 970-9.

GRAY, C., MCCORMICK, C., TURNER, G. & CRAIG, A. (2003) ICAM-1 can play a major role in mediating *P. falciparum* adhesion to endothelium under flow. *Mol Biochem Parasitol,* 128**,** 187-93.

GRIEP, L. M., WOLBERS, F., DE WAGENAAR, B., TER BRAAK, P. M., WEKSLER, B. B., ROMERO, I. A., COURAUD, P. O., VERMES, I., VAN DER MEER, A. D. & VAN DEN BERG, A. (2012) BBB ON CHIP: microfluidic platform to mechanically and biochemically modulate. *Biomed Microdevices.*

GUARNER, J., BARTLETT, J., SHIEH, W., PADDOCK, C., VISVESVARA, G. & ZAKI, S. (2007) Histopathologic spectrum and immunohistochemical diagnosis of amebic meningoencephalitis. *Mod Pathol,* 20**,** 1230-7.

GUDMUNDSDOTTIR, I. J., LANG, N. N., BOON, N. A., LUDLAM, C. A., WEBB, D. J., FOX, K. A. & NEWBY, D. E. (2008) Role of the endothelium in the vascular effects of the thrombin receptor. *J Am Coll Cardiol,* 51**,** 1749-56.

GUDMUNDSDOTTIR, I. J., MEGSON, I. L., KELL, J. S., LUDLAM, C. A., FOX, K. A., WEBB, D. J. & NEWBY, D. E. (2006) Direct vascular effects of protease-activated receptor type 1 agonism in vivo in. *Circulation,* 114**,** 1625-32.

HADAS, E. & MAZUR, T. (1993) Proteolytic enzymes of pathogenic and non-pathogenic strains of *Acanthamoeba* spp. *Trop Med Parasitol,* 44**,** 197-200.

HADAŚ, E. & MAZUR, T. (1993) Biochemical markers of pathogenicity and virulence of *Acanthamoeba* sp. strains. *Parasitol Res,* 79**,** 696-8.

HAQUE, R., ALI, I. M., SACK, R. B., FARR, B. M., RAMAKRISHNAN, G. & PETRI, W. A., JR. (2001) Amebiasis and mucosal IgA antibody against the *Entamoeba histolytica* adherence lectin in Bangladeshi children. *J Infect Dis,* 183**,** 1787-93.

HARRISON, J. L., FERREIRA, G. A., RABORN, E. S., LAFRENAYE, A. D., MARCIANO-CABRAL, F. & CABRAL, G. A. (2010) *Acanthamoeba culbertsoni* elicits soluble factors that exert anti-microglial cell activity. *Infect Immun,* 78**,** 4001-11.

HAYASHI, Y., NOMURA, M., YAMAGISHI, S., HARADA, S., YAMASHITA, J. & YAMAMOTO, H. (1997) Induction of various

blood-brain barrier properties in non-neural endothelial cells by close apposition to co-cultured astrocytes. *Glia,* 19**,** 13-26.

HE, Y., NIEDERKORN, J., MCCULLEY, J., STEWART, G., MEYER, D., SILVANY, R. & DOUGHERTY, J. (1990) *In vivo* and *in vitro* collagenolytic activity of *Acanthamoeba castellanii*. *Invest Ophthalmol Vis Sci,* 31**,** 2235-40.

HE, Y. G., MCCULLEY, J. P., ALIZADEH, H., PIDHERNEY, M., MELLON, J., UBELAKER, J. E., STEWART, G. L., SILVANY, R. E. & NIEDERKORN, J. Y. (1992) A pig model of *Acanthamoeba* keratitis: transmission via contaminated contact lenses. *Invest Ophthalmol Vis Sci,* 33**,** 126-33.

HEDEN, L. O., FRITHZ, E. & LINDAHL, G. (1991) Molecular characterization of an IgA receptor from group B streptococci: sequence of the gene, identification of a proline-rich region with unique structure and isolation of N-terminal fragments with IgA-binding capacity. *Eur J Immunol,* 21**,** 1481-90.

HEDSTROM, L. (2002) Serine protease mechanism and specificity. *Chem Rev,* 102**,** 4501-24.

HELTON, J., LOVELESS, M. & WHITE, C. J. (1993) Cutaneous *Acanthamoeba* infection associated with leukocytoclastic vasculitis in an AIDS patient. *Am J Dermatopathol,* 15**,** 146-9.

HERTZ, M. M. & PAULSON, O. B. (1980) Heterogeneity of cerebral capillary flow in man and its consequences for estimation of blood-brain barrier permeability. *J Clin Invest,* 65**,** 1145-51.

HIRASE, T., STADDON, J. M., SAITOU, M., ANDO-AKATSUKA, Y., ITOH, M., FURUSE, M., FUJIMOTO, K., TSUKITA, S. & RUBIN, L. L. (1997) Occludin as a possible determinant of tight junction permeability in endothelial cells. *J Cell Sci,* 110 (Pt 14)**,** 1603-13.

HIRATA, K. K., QUE, X., MELENDEZ-LOPEZ, S. G., DEBNATH, A., MYERS, S., HERDMAN, D. S., OROZCO, E., BHATTACHARYA, A., MCKERROW, J. H. & REED, S. L. (2007) A phagocytosis mutant of *Entamoeba histolytica* is less virulent due to deficient proteinase expression and release. *Exp Parasitol,* 115**,** 192-9.

HOLDER, A. A., GUEVARA PATINO, J. A., UTHAIPIBULL, C., SYED, S. E., LING, I. T., SCOTT-FINNIGAN, T. & BLACKMAN, M. J. (1999) Merozoite surface protein 1, immune evasion, and vaccines against asexual blood stage malaria. *Parassitologia,* 41**,** 409-14.

HOLLENBERG, M. D., SAIFEDDINE, M., SANDHU, S., HOULE, S. & VERGNOLLE, N. (2004) Proteinase-activated receptor-4: evaluation of tethered ligand-derived peptides as probes for receptor function and as inflammatory agonists in vivo. *Br J Pharmacol,* 143**,** 443-54.

HUDETZ, A. (1997) Blood flow in the cerebral capillary network: a review emphasizing observations with intravital microscopy. *Microcirculation,* 4**,** 233-52.

HURT, M., APTE, S., LEHER, H., HOWARD, K., NIEDERKORN, J. & ALIZADEH, H. (2001) Exacerbation of *Acanthamoeba* keratitis in animals treated with anti-macrophage inflammatory protein 2 or antineutrophil antibodies. *Infect Immun,* 69**,** 2988-95.

HURT, M., NEELAM, S., NIEDERKORN, J. & ALIZADEH, H. (2003a) Pathogenic *Acanthamoeba* spp secrete a mannose-induced cytolytic

protein that correlates with the ability to cause disease. *Infect Immun,* 71**,** 6243-55.

HURT, M., NIEDERKORN, J. & ALIZADEH, H. (2003b) Effects of mannose on *Acanthamoeba castellanii* proliferation and cytolytic ability to corneal epithelial cells. *Invest Ophthalmol Vis Sci,* 44**,** 3424-31.

HURT, M., PROY, V., NIEDERKORN, J. Y. & ALIZADEH, H. (2003c) The interaction of *Acanthamoeba castellanii* cysts with macrophages and neutrophils. *J Parasitol,* 89**,** 565-72.

HUSSACK, G., ARBABI-GHAHROUDI, M., VAN FAASSEN, H., SONGER, J. G., NG, K. K., MACKENZIE, R. & TANHA, J. (2011) Neutralization of *Clostridium difficile* toxin A with single-domain antibodies targeting the cell receptor binding domain. *J Biol Chem,* 286**,** 8961-76.

HUSTON, C. D., HOUPT, E. R., MANN, B. J., HAHN, C. S. & PETRI, W. A., JR. (2000) Caspase 3-dependent killing of host cells by the parasite *Entamoeba histolytica*. *Cell Microbiol,* 2**,** 617-25.

IKADAI, H., TAKAMATSU, Y., TAKASHIRO, R., SEGAWA, A., KUDO, N., IGARASHI, I. & OYAMADA, T. (2005) Short report: molecular cloning and characterization of a putative binding protein of *Babesia caballi*. *Am J Trop Med Hyg,* 73**,** 1135-8.

IMBERT-BOUYER, S., MERLAUD, A., IMBERT, C., DANIAULT, G. & RODIER, M. (2004) A mannose binding protein is involved in the adherence of *Acanthamoeba* species to inert surfaces. *FEMS Microbiol Lett,* 238**,** 207-11.

ITO, H., KANNO, I., KATO, C., SASAKI, T., ISHII, K., OUCHI, Y., IIDA, A., OKAZAWA, H., HAYASHIDA, K., TSUYUGUCHI, N., KUWABARA, Y. & SENDA, M. (2004) Database of normal human cerebral blood flow, cerebral blood volume, cerebral oxygen extraction fraction and cerebral metabolic rate of oxygen measured by positron emission tomography with 15O-labelled carbon dioxide or water, carbon monoxide and oxygen: a multicentre study in Japan. *Eur J Nucl Med Mol Imaging,* 31**,** 635-43.

JANITSCHKE, K., MARTINEZ, A. J., VISVESVARA, G. S. & SCHUSTER, F. (1996) Animal model *Balamuthia mandrillaris* CNS infection: contrast and comparison in immunodeficient and immunocompetent mice: a murine model of "granulomatous" amebic encephalitis. *J Neuropathol Exp Neurol,* 55**,** 815-21.

JANKOVIC, D., ASLUND, L., OSWALD, I. P., CASPAR, P., CHAMPION, C., PEARCE, E., COLIGAN, J. E., STRAND, M., SHER, A. & JAMES, S. L. (1996) Calpain is the target antigen of a Th1 clone that transfers protective immunity against *Schistosoma mansoni*. *J Immunol,* 157**,** 806-14.

JANSSEN, G. M. & MOLLER, W. (1988) Elongation factor 1 beta gamma from *Artemia*. Purification and properties of its subunits. *Eur J Biochem,* 171**,** 119-29.

JANZER, R. C. & RAFF, M. C. (1987) Astrocytes induce blood-brain barrier properties in endothelial cells. *Nature,* 325**,** 253-7.

JONES, B., MCGILL, J. & STEELE, A. (1975) Recurrent suppurative kerato-uveitis with loss of eye due to infection by *Acanthamoeba castellani*. *Trans Ophthalmol Soc U K,* 95**,** 210-3.

KAJI, Y., HU, B., KAWANA, K. & OSHIKA, T. (2005) Swimming with soft contact lenses: danger of *Acanthamoeba* keratitis. *Lancet Infect Dis,* 5**,** 392.

KALINNA, B. & MCMANUS, D. P. (1993) An IgG (Fc gamma)-binding protein of *Taenia crassiceps* (Cestoda) exhibits sequence homology and antigenic similarity with schistosome paramyosin. *Parasitology,* 106 (Pt 3)**,** 289-96.

KATAOKA, H., HAMILTON, J. R., MCKEMY, D. D., CAMERER, E., ZHENG, Y. W., CHENG, A., GRIFFIN, C. & COUGHLIN, S. R. (2003) Protease-activated receptors 1 and 4 mediate thrombin signaling in endothelial. *Blood,* 102**,** 3224-31.

KENNETT, M., HOOK, R. J., FRANKLIN, C. & RILEY, L. (1999) *Acanthamoeba castellanii*: characterization of an adhesin molecule. *Exp Parasitol,* 92**,** 161-9.

KHAN, N. (2001) Pathogenicity, morphology, and differentiation of *Acanthamoeba*. *Curr Microbiol,* 43**,** 391-5.

KHAN, N. (2005) Granulomatous Amoebic Encephalitis: Clinical Dianosis and Management. *American Journal of Infectious Diseases,* 1**,** 79-83.

KHAN, N. (2007) *Acanthamoeba* invasion of the central nervous system. *Int J Parasitol,* 37**,** 131-8.

KHAN, N., GREENMAN, J., TOPPING, K., HOUGH, V., TEMPLE, G. & PAGET, T. (2000a) Isolation of *Acanthamoeba*-specific antibodies from a bacteriophage display library. *J Clin Microbiol,* 38**,** 2374-7.

KHAN, N., JARROLL, E. & PAGET, T. (2002) Molecular and physiological differentiation between pathogenic and nonpathogenic *Acanthamoeba*. *Curr Microbiol,* 45**,** 197-202.

KHAN, N., JARROLL, E., PANJWANI, N., CAO, Z. & PAGET, T. (2000b) Proteases as markers for differentiation of pathogenic and nonpathogenic species of *Acanthamoeba*. *J Clin Microbiol,* 38**,** 2858-61.

KHAN, N. & SIDDIQUI, R. (2009) *Acanthamoeba* affects the integrity of human brain microvascular endothelial cells and degrades the tight junction proteins. *Int J Parasitol,* 39**,** 1611-6.

KIDERLEN, A., RADAM, E., SCHUSTER, F., ADJOGOUA, E., AKOUA-KOFFI, C. & LEENDERTZ, F. (2009) *Balamuthia* and *Acanthamoeba*-binding antibodies in West African human sera. *Exp Parasitol*.

KIDERLEN, A. F., RADAM, E., SCHUSTER, F. L., ADJOGOUA, E. V., AKOUA-KOFFI, C. & LEENDERTZ, F. H. (2010) *Balamuthia* and *Acanthamoeba*-binding antibodies in West African human sera. *Exp Parasitol,* 126**,** 28-32.

KIDERLEN, A. F., TATA, P. S., OZEL, M., LAUBE, U., RADAM, E. & SCHAFER, H. (2006) Cytopathogenicity of *Balamuthia mandrillaris*, an opportunistic causative agent of granulomatous amebic encephalitis. *J Eukaryot Microbiol,* 53**,** 456-63.

KIDNEY, D. & KIM, S. (1998) CNS infections with free-living amebas: neuroimaging findings. *AJR Am J Roentgenol,* 171**,** 809-12.

KIM, H., HA, Y., YU, H., KONG, H. & CHUNG, D. (2003) Purification and characterization of a 33 kDa serine protease from *Acanthamoeba lugdunensis* KA/E2 isolated from a Korean keratitis patient. *Korean J Parasitol,* 41**,** 189-96.

KIM, K. A., LEE, Y. A. & SHIN, M. H. (2007) Calpain-dependent calpastatin cleavage regulates caspase-3 activation during apoptosis of Jurkat T cells induced by *Entamoeba histolytica*. *Int J Parasitol,* 37**,** 1209-19.

KIM, W., KONG, H., HA, Y., HONG, Y., JEONG, H., YU, H. & CHUNG, D. (2006) Comparison of specific activity and cytopathic effects of purified 33 kDa serine proteinase from *Acanthamoeba* strains with different degree of virulence. *Korean J Parasitol,* 44**,** 321-30.

KIM, Y. V., DI CELLO, F., HILLAIRE, C. S. & KIM, K. S. (2004) Differential Ca2+ signaling by thrombin and protease-activated. *Am J Physiol Cell Physiol,* 286**,** C31-42.

KING, B. F. & WILKINSON, B. J. (1981) Binding of human immunoglobulin G to protein A in encapsulated *Staphylococcus aureus*. *Infect Immun,* 33**,** 666-72.

KOHLER, G. & MILSTEIN, C. (1975) Continuous cultures of fused cells secreting antibody of predefined specificity. *Nature,* 256**,** 495-7.

KONG, H. (2009) Molecular phylogeny of *Acanthamoeba*. *Korean J Parasitol,* 47 Suppl**,** S21-8.

KONG, H., KIM, T. & CHUNG, D. (2000) Purification and characterization of a secretory serine proteinase of *Acanthamoeba healyi* isolated from GAE. *J Parasitol,* 86**,** 12-7.

KUMAR, S., BANERJEE, R., NANDI, N., SARDAR, A. H. & DAS, P. (2012) Anoikis potential of *Entameba histolytica* secretory cysteine proteases: evidence of contact independent host cell death. *Microb Pathog,* 52**,** 69-76.

LACHENMAIER, S. M., DELI, M. A., MEISSNER, M. & LIESENFELD, O. (2011) Intracellular transport of *Toxoplasma gondii* through the blood-brain barrier. *J Neuroimmunol,* 232**,** 119-30.

LACKNER, P., BEER, R., BROESSNER, G., HELBOK, R., PFAUSLER, B., BRENNEIS, C., AUER, H., WALOCHNIK, J. & SCHMUTZHARD, E. (2010) Acute granulomatous *Acanthamoeba* encephalitis in an immunocompetent patient. *Neurocrit Care,* 12**,** 91-4.

LAM, D. S., HOUANG, E., FAN, D. S., LYON, D., SEAL, D. & WONG, E. (2002) Incidence and risk factors for microbial keratitis in Hong Kong: comparison with Europe and North America. *Eye (Lond),* 16**,** 608-18.

LANE, R. D. (1985) A short-duration polyethylene glycol fusion technique for increasing production of monoclonal antibody-secreting hybridomas. *J Immunol Methods,* 81**,** 223-8.

LARKIN, D. F. & EASTY, D. L. (1991) Experimental *Acanthamoeba* keratitis: II. Immunohistochemical evaluation. *Br J Ophthalmol,* 75**,** 421-4.

LASSEN, N. A. (1985) Normal average value of cerebral blood flow in younger adults is 50 ml/100 g/min. *J Cereb Blood Flow Metab,* 5**,** 347-9.

LAUWAET, T., OLIVEIRA, M. J., CALLEWAERT, B., DE BRUYNE, G., MAREEL, M. & LEROY, A. (2004) Proteinase inhibitors TPCK and TLCK prevent *Entamoeba histolytica* induced disturbance of tight junctions and microvilli in enteric cell layers *in vitro*. *Int J Parasitol,* 34**,** 785-94.

LAWRENCE, M. B. & SPRINGER, T. A. (1991) Leukocytes roll on a selectin at physiologic flow rates: distinction from and prerequisite for adhesion through integrins. *Cell,* 65**,** 859-73.

LEE, J., HAHN, T., CHOI, S., YU, H. & LEE, J. (2007) *Acanthamoeba* keratitis related to cosmetic contact lenses. *Clin Experiment Ophthalmol,* 35**,** 775-7.

LEHER, H., ALIZADEH, H., TAYLOR, W., SHEA, A., SILVANY, R., VAN KLINK, F., JAGER, M. & NIEDERKORN, J. (1998a) Role of mucosal IgA in the resistance to *Acanthamoeba* keratitis. *Invest Ophthalmol Vis Sci,* 39**,** 2666-73.

LEHER, H., KINOSHITA, K., ALIZADEH, H., ZARAGOZA, F., HE, Y. & NIEDERKORN, J. (1998b) Impact of oral immunization with *Acanthamoeba* antigens on parasite adhesion and corneal infection. *Invest Ophthalmol Vis Sci,* 39**,** 2337-43.

LEHER, H., SILVANY, R., ALIZADEH, H., HUANG, J. & NIEDERKORN, J. Y. (1998c) Mannose induces the release of cytopathic factors from *Acanthamoeba castellanii*. *Infect Immun,* 66**,** 5-10.

LEHER, H., ZARAGOZA, F., TAHERZADEH, S., ALIZADEH, H. & NIEDERKORN, J. (1999) Monoclonal IgA antibodies protect against *Acanthamoeba* keratitis. *Exp Eye Res,* 69**,** 75-84.

LEITSCH, D., KÖHSLER, M., MARCHETTI-DESCHMANN, M., DEUTSCH, A., ALLMAIER, G., DUCHÊNE, M. & WALOCHNIK, J. (2010) Major role for cysteine proteases during the early phase of *Acanthamoeba castellanii* encystment. *Eukaryot Cell,* 9**,** 611-8.

LEROY, A., LAUWAET, T., DE BRUYNE, G., CORNELISSEN, M. & MAREEL, M. (2000) *Entamoeba histolytica* disturbs the tight junction complex in human enteric T84 cell layers. *FASEB J,* 14**,** 1139-46.

LIDINGTON, E. A., STEINBERG, R., KINDERLERER, A. R., LANDIS, R. C., OHBA, M., SAMAREL, A., HASKARD, D. O. & MASON, J. C. (2005) A role for proteinase-activated receptor 2 and PKC-epsilon in thrombin-mediated induction of decay-accelerating factor on human endothelial cells. *Am J Physiol Cell Physiol,* 289**,** C1437-47.

LOPES, M. F., DA VEIGA, V. F., SANTOS, A. R., FONSECA, M. E. & DOSREIS, G. A. (1995) Activation-induced CD4+ T cell death by apoptosis in experimental Chagas' disease. *J Immunol,* 154**,** 744-52.

LORENZO-MORALES, J., MARTÍNEZ-CARRETERO, E., BATISTA, N., ALVAREZ-MARÍN, J., BAHAYA, Y., WALOCHNIK, J. & VALLADARES, B. (2007) Early diagnosis of amoebic keratitis due to a mixed infection with *Acanthamoeba* and *Hartmannella*. *Parasitol Res,* 102**,** 167-9.

LORENZO-MORALES, J., ORTEGA-RIVAS, A., MARTÍNEZ, E., KHOUBBANE, M., ARTIGAS, P., PERIAGO, M., FORONDA, P., ABREU-ACOSTA, N., VALLADARES, B. & MAS-COMA, S. (2006) *Acanthamoeba* isolates belonging to T1, T2, T3, T4 and T7 genotypes from environmental freshwater samples in the Nile Delta region, Egypt. *Acta Trop,* 100**,** 63-9.

LOUKAS, A., JONES, M. K., KING, L. T., BRINDLEY, P. J. & MCMANUS, D. P. (2001) Receptor for Fc on the surfaces of schistosomes. *Infect Immun,* 69**,** 3646-51.

LOURENSSEN, S., HOUPT, E. R., CHADEE, K. & BLENNERHASSETT, M. G. (2010) *Entamoeba histolytica* infection and secreted proteins proteolytically damage enteric neurons. *Infect Immun,* 78**,** 5332-40.

LOZZIO, B. B. & LOZZIO, C. B. (1979) Properties and usefulness of the original K-562 human myelogenous leukemia cell line. *Leuk Res,* 3**,** 363-70.

LOZZIO, B. B., LOZZIO, C. B., BAMBERGER, E. G. & FELIU, A. S. (1981) A multipotential leukemia cell line (K-562) of human origin. *Proc Soc Exp Biol Med,* 166**,** 546-50.

LUCAS, J. J., HAYES, G. R., KALSI, H. K., GILBERT, R. O., CHOE, Y., CRAIK, C. S. & SINGH, B. N. (2008) Characterization of a cysteine protease from *Tritrichomonas foetus* that induces host-cell apoptosis. *Arch Biochem Biophys,* 477**,** 239-43.

LYDEN, T. W., ROBINSON, J. M., TRIDANDAPANI, S., TEILLAUD, J. L., GARBER, S. A., OSBORNE, J. M., FREY, J., BUDDE, P. & ANDERSON, C. L. (2001) The Fc receptor for IgG expressed in the villus endothelium of human placenta is Fc gamma RIIb2. *J Immunol,* 166**,** 3882-9.

MACLEAN, R., HAFEZ, N., TRIPATHI, S., CHILDRESS, C., GHATAK, N. & MARCIANO-CABRAL, F. (2007) Identification of *Acanthamoeba* sp. in paraffin-embedded CNS tissue from an HIV+ individual by PCR. *Diagn Microbiol Infect Dis,* 57**,** 289-94.

MAGLIANO, A., DA SILVA, F., TEIXEIRA, M. & ALFIERI, S. (2009) Genotyping, physiological features and proteolytic activities of a potentially pathogenic *Acanthamoeba* sp. isolated from tap water in Brazil. *Exp Parasitol,* 123**,** 231-5.

MAHMOUDZADEH-NIKNAM, H. & MCKERROW, J. H. (2004) *Leishmania tropica*: cysteine proteases are essential for growth and pathogenicity. *Exp Parasitol,* 106**,** 158-63.

MAIREY, E., GENOVESIO, A., DONNADIEU, E., BERNARD, C., JAUBERT, F., PINARD, E., SEYLAZ, J., OLIVO-MARIN, J. C., NASSIF, X. & DUMÉNIL, G. (2006) Cerebral microcirculation shear stress levels determine *Neisseria meningitidis* attachment sites along the blood-brain barrier. *J Exp Med,* 203**,** 1939-50.

MARCIANO-CABRAL, F. & TONEY, D. (1998) The interaction of *Acanthamoeba* spp. with activated macrophages and with macrophage cell lines. *J Eukaryot Microbiol,* 45**,** 452-8.

MARTÍNEZ, A., GARCÍA, C., HALKS-MILLER, M. & ARCE-VELA, R. (1980) Granulomatous amebic encephalitis presenting as a cerebral mass lesion. *Acta Neuropathol,* 51**,** 85-91.

MARTÍNEZ, A., SOTELO-AVILA, C., GARCIA-TAMAYO, J., MORÓN, J., WILLAERT, E. & STAMM, W. (1977) Meningoencephalitis due to *Acanthamoeba* SP. Pathogenesis and clinico-pathological study. *Acta Neuropathol,* 37**,** 183-91.

MARTINEZ, A. & VISVESVARA, G. (1997) Free-living, amphizoic and opportunistic amebas. *Brain Pathol,* 7**,** 583-98.

MARTINEZ, A. J., MARKOWITZ, S. M. & DUMA, R. J. (1975) Experimental Pneumonitis and Encephalitis Caused by *Acanthamoeba* in Mice: Pathogenesis and Ultrastructural Features. *Journal of Infectious Diseases,* 131**,** 692-699.

MARTINEZ, J., CAMPETELLA, O., FRASCH, A. C. & CAZZULO, J. J. (1991) The major cysteine proteinase (cruzipain) from *Trypanosoma cruzi* is antigenic in human infections. *Infect Immun,* 59**,** 4275-7.

MASSILAMANY, C., ASOJO, O. A., GANGAPLARA, A., STEFFEN, D. & REDDY, J. (2011) Identification of a second mimicry epitope from *Acanthamoeba castellanii* that induces CNS autoimmunity by generating cross-reactive T cells for MBP 89-101 in SJL mice. *Int Immunol,* 23**,** 729-39.

MASSILAMANY, C., STEFFEN, D. & REDDY, J. (2010) An epitope from *Acanthamoeba castellanii* that cross-react with proteolipid protein 139-151-reactive T cells induces autoimmune encephalomyelitis in SJL mice. *J Neuroimmunol,* 219**,** 17-24.

MATHERS, W., NELSON, S., LANE, J., WILSON, M., ALLEN, R. & FOLBERG, R. (2000) Confirmation of confocal microscopy diagnosis of *Acanthamoeba* keratitis using polymerase chain reaction analysis. *Arch Ophthalmol,* 118**,** 178-83.

MATTANA, A., BENNARDINI, F., USAI, S., FIORI, P., FRANCONI, F. & CAPPUCCINELLI, P. (1997) *Acanthamoeba castellanii* metabolites increase the intracellular calcium level and cause cytotoxicity in wish cells. *Microb Pathog,* 23**,** 85-93.

MATTANA, A., CAPPAI, V., ALBERTI, L., SERRA, C., FIORI, P. & CAPPUCCINELLI, P. (2002) ADP and other metabolites released from *Acanthamoeba castellanii* lead to human monocytic cell death through apoptosis and stimulate the secretion of proinflammatory cytokines. *Infect Immun,* 70**,** 4424-32.

MATTANA, A., TOZZI, M., COSTA, M., DELOGU, G., FIORI, P. & CAPPUCCINELLI, P. (2001) By releasing ADP, *Acanthamoeba castellanii* causes an increase in the cytosolic free calcium concentration and apoptosis in wish cells. *Infect Immun,* 69**,** 4134-40.

MAY, L., SIDHU, G. & BUCHNESS, M. (1992) Diagnosis of *Acanthamoeba* infection by cutaneous manifestations in a man seropositive to HIV. *J Am Acad Dermatol,* 26**,** 352-5.

MCCLELLAN, K., HOWARD, K., MAYHEW, E., NIEDERKORN, J. & ALIZADEH, H. (2002) Adaptive immune responses to *Acanthamoeba* cysts. *Exp Eye Res,* 75**,** 285-93.

MCCOLE, D. F., ECKMANN, L., LAURENT, F. & KAGNOFF, M. F. (2000) Intestinal epithelial cell apoptosis following *Cryptosporidium parvum* infection. *Infect Immun,* 68**,** 1710-3.

MCINTOSH, R. S., JONES, F. M., DUNNE, D. W., MCKERROW, J. H. & PLEASS, R. J. (2006) Characterization of immunoglobulin binding by schistosomes. *Parasite Immunol,* 28**,** 407-19.

MILTON, S. G. & KNUTSON, V. P. (1990) Comparison of the function of the tight junctions of endothelial cells and epithelial cells in regulating the movement of electrolytes and macromolecules across the cell monolayer. *J Cell Physiol,* 144**,** 498-504.

MITRO, K., BHAGAVATHIAMMAI, A., ZHOU, O., BOBBETT, G., MCKERROW, J., CHOKSHI, R., CHOKSHI, B. & JAMES, E. (1994) Partial characterization of the proteolytic secretions of *Acanthamoeba polyphaga*. *Exp Parasitol,* 78**,** 377-85.

MONCADA, D., KELLER, K. & CHADEE, K. (2003) *Entamoeba histolytica* cysteine proteinases disrupt the polymeric structure of colonic mucin and alter its protective function. *Infect Immun,* 71**,** 838-44.

MOORE, M., MCCULLEY, J., LUCKENBACH, M., GELENDER, H., NEWTON, C., MCDONALD, M. & VISVESVARA, G. (1985) *Acanthamoeba* keratitis associated with soft contact lenses. *Am J Ophthalmol,* 100**,** 396-403.

MOORE, M., MCCULLEY, J., NEWTON, C., COBO, L., FOULKS, G., O'DAY, D., JOHNS, K., DRIEBE, W., WILSON, L. & EPSTEIN, R. (1987) *Acanthamoeba* keratitis. A growing problem in soft and hard contact lens wearers. *Ophthalmology,* 94**,** 1654-61.

MORITA, K., SASAKI, H., FURUSE, M. & TSUKITA, S. (1999) Endothelial claudin: claudin-5/TMVCF constitutes tight junction strands in endothelial cells. *J Cell Biol,* 147**,** 185-94.

MORTON, L., MCLAUGHLIN, G. & WHITELEY, H. (1991) Effects of temperature, amebic strain, and carbohydrates on *Acanthamoeba* adherence to corneal epithelium in vitro. *Infect Immun,* 59**,** 3819-22.

MULENGA, C., MHLANGA, J., KRISTENSSON, K. & ROBERTSON, B. (2001) *Trypanosoma brucei brucei* crosses the blood-brain barrier while tight junction proteins are preserved in a rat chronic disease model. *Neuropathol Appl Neurobiol,* 27**,** 77-85.

MUTREJA, D., JALPOTA, Y., MADAN, R. & TEWARI, V. (2007) Disseminated *Acanthamoeba* infection in a renal transplant recipient: a case report. *Indian J Pathol Microbiol,* 50**,** 346-8.

NA, B., CHO, J., SONG, C. & KIM, T. (2002a) Degradation of immunoglobulins, protease inhibitors and interleukin-1 by a secretory proteinase of *Acanthamoeba castellanii*. *Korean J Parasitol,* 40**,** 93-9.

NA, B., KIM, J. & SONG, C. (2001) Characterization and pathogenetic role of proteinase from *Acanthamoeba castellanii*. *Microb Pathog,* 30**,** 39-48.

NA, B. K., CHO, J. H., SONG, C. Y. & KIM, T. S. (2002b) Degradation of immunoglobulins, protease inhibitors and interleukin-1 by a secretory proteinase of *Acanthamoeba castellanii*. *Korean J Parasitol,* 40**,** 93-9.

NACHEGA, J., ROMBAUX, P., WEYNAND, B., THOMAS, G. & ZECH, F. (2005) Successful treatment of *Acanthamoeba* rhinosinusitis in a patient with AIDS. *AIDS Patient Care STDS,* 19**,** 621-5.

NIEDERKORN, J. (2002) The role of the innate and adaptive immune responses in *Acanthamoeba* keratitis. *Arch Immunol Ther Exp (Warsz),* 50**,** 53-9.

NIKOLSKAIA, O., DE A LIMA, A., KIM, Y., LONSDALE-ECCLES, J., FUKUMA, T., SCHARFSTEIN, J. & GRAB, D. (2006a) Blood-brain barrier traversal by African trypanosomes requires calcium signaling induced by parasite cysteine protease. *J Clin Invest,* 116**,** 2739-47.

NIKOLSKAIA, O., KIM, Y., KOVBASNJUK, O., KIM, K. & GRAB, D. (2006b) Entry of *Trypanosoma brucei gambiense* into microvascular endothelial cells of the human blood-brain barrier. *Int J Parasitol,* 36**,** 513-9.

NISHIKAWA, Y., MAKALA, L., OTSUKA, H., MIKAMI, T. & NAGASAWA, H. (2002) Mechanisms of apoptosis in murine fibroblasts by two intracellular protozoan parasites, *Toxoplasma gondii* and *Neospora caninum*. *Parasite Immunol,* 24**,** 347-54.

NISHIMURA, M., TAKANASHI, M., OKAZAKI, H., SATAKE, M. & NAKAJIMA, K. (2006) Role of CD7 expressed in lung microvascular endothelial cells as Fc receptor for immunoglobulin M. *Endothelium,* 13**,** 287-92.

NIYADURUPOLA, N. & ILLINGWORTH, C. (2006) *Acanthamoeba* keratitis associated with misuse of daily disposable contact lenses. *Cont Lens Anterior Eye,* 29**,** 269-71.

O'BRIEN, J. L., LAURIANO, C. M. & ALDERETE, J. F. (1996) Molecular characterization of a third malic enzyme-like AP65 adhesin gene of *Trichomonas vaginalis*. *Microb Pathog,* 20**,** 335-49.

OFORI-KWAKYE, S., SIDEBOTTOM, D., HERBERT, J., FISCHER, E. & VISVESVARA, G. (1986) Granulomatous brain tumor caused by *Acanthamoeba*. Case report. *J Neurosurg,* 64**,** 505-9.

OKAZAWA, H., YAMAUCHI, H., SUGIMOTO, K., TOYODA, H., KISHIBE, Y. & TAKAHASHI, M. (2001) Effects of acetazolamide on cerebral blood flow, blood volume, and oxygen metabolism: a positron emission tomography study with healthy volunteers. *J Cereb Blood Flow Metab,* 21**,** 1472-9.

OTRI, A. M., MOHAMMED, I., ABEDIN, A., CAO, Z., HOPKINSON, A., PANJWANI, N. & DUA, H. S. (2010) Antimicrobial peptides expression by ocular surface cells in response to *Acanthamoeba castellanii*: an in vitro study. *Br J Ophthalmol,* 94**,** 1523-7.

PANARO, M. A., CIANCIULLI, A., MITOLO, V., MITOLO, C. I., ACQUAFREDDA, A., BRANDONISIO, O. & CAVALLO, P. (2007) Caspase-dependent apoptosis of the HCT-8 epithelial cell line induced by the parasite *Giardia intestinalis*. *FEMS Immunol Med Microbiol,* 51**,** 302-9.

PARK, M. K., CHO, M. K., KANG, S. A., PARK, H. K., KIM, Y. S., KIM, K. U., AHN, S. C., KIM, D. H. & YU, H. S. (2011) Protease-activated receptor 2 is involved in Th2 responses against *Trichinella*. *Korean J Parasitol,* 49**,** 235-43.

PAULSON, O., HASSELBALCH, S., ROSTRUP, E., KNUDSEN, G. & PELLIGRINO, D. (2010) Cerebral blood flow response to functional activation. *J Cereb Blood Flow Metab,* 30**,** 2-14.

PEMÁN, J., JARQUE, I., FRASQUET, J., ALBEROLA, C., SALAVERT, M., SANZ, J., GOMILA, B. & ESTEBAN, G. (2008) Unexpected postmortem diagnosis of *Acanthamoeba* meningoencephalitis following allogeneic peripheral blood stem cell transplantation. *Am J Transplant,* 8**,** 1562-6.

PETERSON, R., SMITH, M. & PEPOSE, J. (1990) Recurrent *Acanthamoeba* keratitis following penetrating keratoplasty. *Arch Ophthalmol,* 108**,** 1482-3.

PETRY, F., TORZEWSKI, M., BOHL, J., WILHELM-SCHWENKMEZGER, T., SCHEID, P., WALOCHNIK, J., MICHEL, R., ZÖLLER, L., WERHAHN, K., BHAKDI, S. & LACKNER, K. (2006) Early diagnosis of *Acanthamoeba* infection during routine cytological examination of cerebrospinal fluid. *J Clin Microbiol,* 44**,** 1903-4.

PHIRI, H., MONTGOMERY, J., MOLYNEUX, M. & CRAIG, A. (2009) Competitive endothelial adhesion between *Plasmodium falciparum* isolates under physiological flow conditions. *Malar J,* 8**,** 214.

PINO, P., TAOUFIQ, Z., NITCHEU, J., VOULDOUKIS, I. & MAZIER, D. (2005) Blood-brain barrier breakdown during cerebral malaria: suicide or murder? *Thromb Haemost,* 94**,** 336-40.

PINO, P., VOULDOUKIS, I., KOLB, J. P., MAHMOUDI, N., DESPORTES-LIVAGE, I., BRICAIRE, F., DANIS, M., DUGAS, B. & MAZIER, D. (2003) *Plasmodium falciparum*--infected erythrocyte adhesion induces caspase activation and apoptosis in human endothelial cells. *J Infect Dis,* 187**,** 1283-90.

PLAUT, A. G., COHEN, S. & TOMASI, T. B., JR. (1972) Immunoglobulin M: fixation of human complement by the Fc fragment. *Science,* 176**,** 55-6.

PLEASS, R. J., KUSEL, J. R. & WOOF, J. M. (2000) Cleavage of human IgE mediated by *Schistosoma mansoni*. *Int Arch Allergy Immunol,* 121**,** 194-204.

PRABHAKARPANDIAN, B., SHEN, M. C., NICHOLS, J. B., MILLS, I. R., SIDORYK-WEGRZYNOWICZ, M., ASCHNER, M. & PANT, K. (2013) SyM-BBB: a microfluidic Blood Brain Barrier model. *Lab Chip,* 13**,** 1093-101.

PROBST, P., STROMBERG, E., GHALIB, H. W., MOZEL, M., BADARO, R., REED, S. G. & WEBB, J. R. (2001) Identification and characterization of T cell-stimulating antigens from *Leishmania* by CD4 T cell expression cloning. *J Immunol,* 166**,** 498-505.

PUMIDONMING, W., WALOCHNIK, J., DAUBER, E. & PETRY, F. (2011) Binding to complement factors and activation of the alternative pathway by *Acanthamoeba*. *Immunobiology,* 216**,** 225-33.

PUSSARD, M. & PONS, R. (1977) Morphology of cystic wall and taxonomy of genus *Acanthamoeba* (Protozoa, Amoebida). *Protistologica,* 13**,** 557-598.

RADFORD, C. F., MINASSIAN, D. C. & DART, J. K. (2002) *Acanthamoeba* keratitis in England and Wales: incidence, outcome, and risk factors. *Br J Ophthalmol,* 86**,** 536-42.

RAMA, P., MATUSKA, S., VIGANÒ, M., SPINELLI, A., PAGANONI, G. & BRANCATO, R. (2003) Bilateral *Acanthamoeba* keratitis with late recurrence of the infection in a corneal graft: a case report. *Eur J Ophthalmol,* 13**,** 311-4.

REDDY, A., BALNE, P., GAJE, K. & GARG, P. (2009) Polymerase Chain Reaction for the Diagnosis and Species Identification of Microsporidia in Patients with Keratitis. *Clin Microbiol Infect*.

REN, M., GAO, L. & WU, X. (2010) TLR4: the receptor bridging *Acanthamoeba* challenge and intracellular inflammatory responses in human corneal cell lines. *Immunol Cell Biol*.

REN, M. Y. & WU, X. Y. (2011) Toll-like receptor 4 signalling pathway activation in a rat model of *Acanthamoeba* Keratitis. *Parasite Immunol,* 33**,** 25-33.

RIVERA, W. L. & ADAO, D. E. (2008) Identification of the 18S-ribosomal-DNA genotypes of *Acanthamoeba* isolates from the Philippines. *Ann Trop Med Parasitol,* 102**,** 671-7.

ROCHA-AZEVEDO, B., JAMERSON, M., CABRAL, G. & MARCIANO-CABRAL, F. (2009a) *Acanthamoeba culbertsoni*: Analysis of amoebic

adhesion and invasion on extracellular matrix components collagen I and laminin-1. *Exp Parasitol*.

ROCHA-AZEVEDO, B., JAMERSON, M., CABRAL, G., SILVA-FILHO, F. & MARCIANO-CABRAL, F. (2009b) *Acanthamoeba* interaction with extracellular matrix glycoproteins: biological and biochemical characterization and role in cytotoxicity and invasiveness. *J Eukaryot Microbiol,* 56**,** 270-8.

RODRIGUEZ DE CUNA, C., KIERSZENBAUM, F. & WIRTH, J. J. (1991) Binding of the specific ligand to Fc receptors on *Trypanosoma cruzi* increases the infective capacity of the parasite. *Immunology,* 72**,** 114-20.

ROSENBERG, A. & MORGAN, M. (2001) Disseminated acanthamoebiasis presenting as lobular panniculitis with necrotizing vasculitis in a patient with AIDS. *J Cutan Pathol,* 28**,** 307-13.

RUMELT, S., COHEN, I., LEFLER, E. & REHANY, U. (2001) Corneal co-infection with *Scedosporium apiospermum* and *Acanthamoeba* after sewage-contaminated ocular injury. *Cornea,* 20**,** 112-6.

SACK, R. A., NUNES, I., BEATON, A. & MORRIS, C. (2001) Host-defense mechanism of the ocular surfaces. *Biosci Rep,* 21**,** 463-80.

SAID, N., SHOEIR, A., PANJWANI, N., GARATE, M. & CAO, Z. (2004) Local and systemic humoral immune response during acute and chronic *Acanthamoeba* keratitis in rabbits. *Curr Eye Res,* 29**,** 429-39.

SANTAGUIDA, S., JANIGRO, D., HOSSAIN, M., OBY, E., RAPP, E. & CUCULLO, L. (2006) Side by side comparison between dynamic versus static models of blood-brain. *Brain Res,* 1109**,** 1-13.

SARICA, F., TUFAN, K., CEKINMEZ, M., ERDOĞAN, B. & ALTINÖRS, M. (2009) A rare but fatal case of granulomatous amebic encephalitis with brain abscess: the first case reported from Turkey. *Turk Neurosurg,* 19**,** 256-9.

SCHLACHETZKI, F., ZHU, C. & PARDRIDGE, W. M. (2002) Expression of the neonatal Fc receptor (FcRn) at the blood-brain barrier. *J Neurochem,* 81**,** 203-6.

SCHNAPP, A. R., EICKHOFF, C. S., SCHARFSTEIN, J. & HOFT, D. F. (2002) Induction of B- and T-cell responses to cruzipain in the murine model of *Trypanosoma cruzi* infection. *Microbes Infect,* 4**,** 805-13.

SCHNEIDER, C. A., RASBAND, W. S. & ELICEIRI, K. W. (2012) NIH Image to ImageJ: 25 years of image analysis. *Nat Meth,* 9**,** 671-675.

SCHROEDER, J., BOOTON, G., HAY, J., NISZL, I., SEAL, D., MARKUS, M., FUERST, P. & BYERS, T. (2001) Use of subgenic 18S ribosomal DNA PCR and sequencing for genus and genotype identification of *Acanthamoeba* from humans with keratitis and from sewage sludge. *J Clin Microbiol,* 39**,** 1903-11.

SCHUSTER, F., HONARMAND, S., VISVESVARA, G. & GLASER, C. (2006) Detection of antibodies against free-living amoebae Balamuthia mandrillaris and *Acanthamoeba* species in a population of patients with encephalitis. *Clin Infect Dis,* 42**,** 1260-5.

SCHWARZWALD, H., SHAH, P., HICKS, J., LEVY, M., WAGNER, M. & KLINE, M. (2003) Disseminated *Acanthamoeba* infection in a human immunodeficiency virus-infected infant. *Pediatr Infect Dis J,* 22**,** 197-9.

SEDMAK, D. D., DAVIS, D. H., SINGH, U., VAN DE WINKEL, J. G. & ANDERSON, C. L. (1991) Expression of IgG Fc receptor antigens in placenta and on endothelial cells in humans. An immunohistochemical study. *Am J Pathol,* 138**,** 175-81.

SEIJO MARTINEZ, M., GONZALEZ-MEDIERO, G., SANTIAGO, P., RODRIGUEZ DE LOPE, A., DIZ, J., CONDE, C. & VISVESVARA, G. (2000) Granulomatous amebic encephalitis in a patient with AIDS: isolation of *Acanthamoeba* sp. Group II from brain tissue and successful treatment with sulfadiazine and fluconazole. *J Clin Microbiol,* 38**,** 3892-5.

SERRANO-LUNA, J. J., CERVANTES-SANDOVAL, I., CALDERÓN, J., NAVARRO-GARCÍA, F., TSUTSUMI, V. & SHIBAYAMA, M. (2006) Protease activities of *Acanthamoeba polyphaga* and *Acanthamoeba castellanii*. *Can J Microbiol,* 52**,** 16-23.

SEYDEL, K. B. & STANLEY, S. L., JR. (1998) *Entamoeba histolytica* induces host cell death in amebic liver abscess by a non-Fas-dependent, non-tumor necrosis factor alpha-dependent pathway of apoptosis. *Infect Immun,* 66**,** 2980-3.

SHENG, W., HUNG, C., HUANG, H., LIANG, S., CHENG, Y., JI, D. & CHANG, S. (2009) First case of granulomatous amebic encephalitis caused by *Acanthamoeba castellanii* in Taiwan. *Am J Trop Med Hyg,* 81**,** 277-9.

SHIN, H., CHO, M., KIM, H., LEE, M., PARK, S., SOHN, S. & IM, K. (2000) Apoptosis of primary-culture rat microglial cells induced by pathogenic *Acanthamoeba* spp. *Clin Diagn Lab Immunol,* 7**,** 510-4.

SHIN, H. J., CHO, M. S., JUNG, S. Y., KIM, H. I., PARK, S., SEO, J. H., YOO, J. C. & IM, K. I. (2001) Cytopathic changes in rat microglial cells induced by pathogenic *Acanthamoeba culbertsoni*: morphology and cytokine release. *Clin Diagn Lab Immunol,* 8**,** 837-40.

SIDDHARTHAN, V., KIM, Y. V., LIU, S. & KIM, K. S. (2007) Human astrocytes/astrocyte-conditioned medium and shear stress enhance the. *Brain Res,* 1147**,** 39-50.

SIDDIQUI, R., MATIN, A., WARHURST, D., STINS, M. & KHAN, N. A. (2007) Effect of antimicrobial compounds on *Balamuthia mandrillaris* encystment and human brain microvascular endothelial cell cytopathogenicity. *Antimicrob Agents Chemother,* 51**,** 4471-3.

SISSONS, J., ALSAM, S., GOLDSWORTHY, G., LIGHTFOOT, M., JARROLL, E. & KHAN, N. (2006a) Identification and properties of proteases from an *Acanthamoeba* isolate capable of producing granulomatous encephalitis. *BMC Microbiol,* 6**,** 42.

SISSONS, J., ALSAM, S., JAYASEKERA, S., KIM, K., STINS, M. & KHAN, N. (2004) *Acanthamoeba* induces cell-cycle arrest in host cells. *J Med Microbiol,* 53**,** 711-7.

SISSONS, J., ALSAM, S., STINS, M., RIVAS, A., MORALES, J., FAULL, J. & KHAN, N. (2006b) Use of in vitro assays to determine effects of human serum on biological characteristics of *Acanthamoeba castellanii*. *J Clin Microbiol,* 44**,** 2595-600.

SISSONS, J., KIM, K., STINS, M., JAYASEKERA, S., ALSAM, S. & KHAN, N. (2005) *Acanthamoeba castellanii* induces host cell death via

a phosphatidylinositol 3-kinase-dependent mechanism. *Infect Immun,* 73**,** 2704-8.

SLATER, C., SICKEL, J., VISVESVARA, G., PABICO, R. & GASPARI, A. (1994) Brief report: successful treatment of disseminated *Acanthamoeba* infection in an immunocompromised patient. *N Engl J Med,* 331**,** 85-7.

SLEDGE, C. R. & BING, D. H. (1973) Binding properties of the human complement protein Clq. *J Biol Chem,* 248**,** 2818-23.

SMITH, A. M., CARMONA, C., DOWD, A. J., MCGONIGLE, S., ACOSTA, D. & DALTON, J. P. (1994) Neutralization of the activity of a *Fasciola hepatica* cathepsin L proteinase by anti-cathepsin L antibodies. *Parasite Immunol,* 16**,** 325-8.

SMITH, A. M., DOWD, A. J., HEFFERNAN, M., ROBERTSON, C. D. & DALTON, J. P. (1993) *Fasciola hepatica*: a secreted cathepsin L-like proteinase cleaves host immunoglobulin. *Int J Parasitol,* 23**,** 977-83.

SOBUE, K., YAMAMOTO, N., YONEDA, K., HODGSON, M. E., YAMASHIRO, K., TSURUOKA, N., TSUDA, T., KATSUYA, H., MIURA, Y., ASAI, K. & KATO, T. (1999) Induction of blood-brain barrier properties in immortalized bovine brain. *Neurosci Res,* 35**,** 155-64.

SOHN, H. J., KIM, J. H., SHIN, M. H., SONG, K. J. & SHIN, H. J. (2010) The Nf-actin gene is an important factor for food-cup formation and cytotoxicity of pathogenic *Naegleria fowleri*. *Parasitol Res,* 106**,** 917-24.

SOMMER, U., COSTELLO, C. E., HAYES, G. R., BEACH, D. H., GILBERT, R. O., LUCAS, J. J. & SINGH, B. N. (2005) Identification of *Trichomonas vaginalis* cysteine proteases that induce apoptosis in human vaginal epithelial cells. *J Biol Chem,* 280**,** 23853-60.

STEHR-GREEN, J. K., BAILEY, T. M. & VISVESVARA, G. S. (1989) The epidemiology of *Acanthamoeba* keratitis in the United States. *Am J Ophthalmol,* 107**,** 331-6.

STEINBERG, J., GALINDO, R., KRAUS, E. & GHANEM, K. (2002) Disseminated acanthamebiasis in a renal transplant recipient with osteomyelitis and cutaneous lesions: case report and literature review. *Clin Infect Dis,* 35**,** e43-9.

STEWART, G., KIM, I., SHUPE, K., ALIZADEH, H., SILVANY, R., MCCULLEY, J. & NIEDERKORN, J. (1992) Chemotactic response of macrophages to *Acanthamoeba castellanii* antigen and antibody-dependent macrophage-mediated killing of the parasite. *J Parasitol,* 78**,** 849-55.

STEWART, G., SHUPE, K., KIM, I., SILVANY, R., ALIZADEH, H., MCCULLEY, J. & NIEDERKORN, J. (1994) Antibody-dependent neutrophil-mediated killing of *Acanthamoeba castellanii*. *Int J Parasitol,* 24**,** 739-42.

STILES, J., MEADE, J., KUCEROVA, Z., LYN, D., THOMPSON, W., ZAKERI, Z. & WHITTAKER, J. (2001) *Trypanosoma brucei* infection induces apoptosis and up-regulates neuroleukin expression in the cerebellum. *Ann Trop Med Parasitol,* 95**,** 797-810.

STILES, J., WHITTAKER, J., SARFO, B., THOMPSON, W., POWELL, M. & BOND, V. (2004) Trypanosome apoptotic factor mediates apoptosis

in human brain vascular endothelial cells. *Mol Biochem Parasitol,* 133**,** 229-40.

STINS, M. F., GILLES, F. & KIM, K. S. (1997) Selective expression of adhesion molecules on human brain microvascular endothelial cells. *J Neuroimmunol,* 76**,** 81-90.

STOTHARD, D., SCHROEDER-DIEDRICH, J., AWWAD, M., GAST, R., LEDEE, D., RODRIGUEZ-ZARAGOZA, S., DEAN, C., FUERST, P. & BYERS, T. (1998) The evolutionary history of the genus *Acanthamoeba* and the identification of eight new 18S rRNA gene sequence types. *J Eukaryot Microbiol,* 45**,** 45-54.

SULIMAN, H. S., APPLING, D. R. & ROBERTUS, J. D. (2007) The gene for cobalamin-independent methionine synthase is essential in *Candida albicans*: a potential antifungal target. *Arch Biochem Biophys,* 467**,** 218-26.

TANAKA, Y., SUGURI, S., HARADA, M., HAYABARA, T., SUZUMORI, K. & OHTA, N. (1994) *Acanthamoeba*-specific human T-cell clones isolated from healthy individuals. *Parasitol Res,* 80**,** 549-53.

TARLETON, R. L. & KEMP, W. M. (1981) Demonstration of IgG-Fc and C3 receptors on adult *Schistosoma mansoni*. *J Immunol,* 126**,** 379-84.

TAYLOR, W., PIDHERNEY, M., ALIZADEH, H. & NIEDERKORN, J. (1995) *In vitro* characterization of *Acanthamoeba castellanii* cytopathic effect. *J Parasitol,* 81**,** 603-9.

THOMPSON, P., KOWALSKI, R., SHANKS, R. & GORDON, Y. (2008) Validation of real-time PCR for laboratory diagnosis of *Acanthamoeba* keratitis. *J Clin Microbiol,* 46**,** 3232-6.

TIEN, S. & SHEU, M. (1999) Treatment of *Acanthamoeba* keratitis combined with fungal infection with polyhexamethylene biguanide. *Kaohsiung J Med Sci,* 15**,** 665-73.

TILAK, R., SINGH, R., WANI, I., PAREKH, A., PRAKASH, J. & USHA, U. (2008) An unusual case of *Acanthamoeba* peritonitis in a malnourished patient on continuous ambulatory peritoneal dialysis (CAPD). *J Infect Dev Ctries,* 2**,** 146-8.

TONEY, D. & MARCIANO-CABRAL, F. (1998) Resistance of *Acanthamoeba* species to complement lysis. *J Parasitol,* 84**,** 338-44.

TORPIER, G., CAPRON, A. & OUAISSI, M. A. (1979) Receptor for IgG(Fc) and human beta2-microglobulin on *S. mansoni* schistosomula. *Nature,* 278**,** 447-9.

TOURE-BALDE, A., SARTHOU, J. L., ARIBOT, G., MICHEL, P., TRAPE, J. F., ROGIER, C. & ROUSSILHON, C. (1996) *Plasmodium falciparum* induces apoptosis in human mononuclear cells. *Infect Immun,* 64**,** 744-50.

TRAN, V. Q., HERDMAN, D. S., TORIAN, B. E. & REED, S. L. (1998) The neutral cysteine proteinase of *Entamoeba histolytica* degrades IgG and prevents its binding. *J Infect Dis,* 177**,** 508-11.

TRIPATHI, A., SULLIVAN, D. & STINS, M. (2006) *Plasmodium falciparum*-infected erythrocytes increase intercellular adhesion molecule 1 expression on brain endothelium through NF-kappaB. *Infect Immun,* 74**,** 3262-70.

TRIPATHI, A. K., SULLIVAN, D. J. & STINS, M. F. (2007) *Plasmodium falciparum*-infected erythrocytes decrease the integrity of human

blood-brain barrier endothelial cell monolayers. *J Infect Dis,* 195**,** 942-50.

TSUKITA, S., FURUSE, M., ITOH, M., (1998) Molecular dissection of tight junctions: occludin and ZO-1. IN PARDRIDGE, W. M. (Ed.) *Introduction to the blood-brain barrier.* Cambridge, UK, Cambridge University Press.

TURNER, M., COCKERELL, E., BRERETON, H., BADENOCH, P., TEA, M., COSTER, D. & WILLIAMS, K. (2005) Antigens of selected *Acanthamoeba* species detected with monoclonal antibodies. *Int J Parasitol,* 35**,** 981-90.

USCHUPLICH, V., MILEUSNIC, D. & JOHNSON, M. (2004) Pathologic quiz case. Progressive fatal encephalopathy in an immunosuppressed patient with a history of discoid lupus erythematosus. Subacute granulomatous meningoencephalitis (*Acanthamoeba culbertsoni*). *Arch Pathol Lab Med,* 128**,** e109-11.

VAN KLINK, F., ALIZADEH, H., HE, Y., MELLON, J. A., SILVANY, R. E., MCCULLEY, J. P. & NIEDERKORN, J. Y. (1993) The role of contact lenses, trauma, and Langerhans cells in a Chinese hamster model of *Acanthamoeba* keratitis. *Invest Ophthalmol Vis Sci,* 34**,** 1937-44.

VAN KLINK, F., LEHER, H., JAGER, M., ALIZADEH, H., TAYLOR, W. & NIEDERKORN, J. (1997) Systemic immune response to *Acanthamoeba* keratitis in the Chinese hamster. *Ocul Immunol Inflamm,* 5**,** 235-44.

VAN KLINK, F., TAYLOR, W. M., ALIZADEH, H., JAGER, M. J., VAN ROOIJEN, N. & NIEDERKORN, J. Y. (1996) The role of macrophages in *Acanthamoeba* keratitis. *Invest Ophthalmol Vis Sci,* 37**,** 1271-81.

VERCAMMEN, M., EL BOUHDIDI, A., BEN MESSAOUD, A., DE MEUTER, F., BAZIN, H., DUBREMETZ, J. F. & CARLIER, Y. (1998) Identification and characterization of a Fc receptor activity on the *Toxoplasma gondii* tachyzoite. *Parasite Immunol,* 20**,** 37-47.

VERMEIRE, J. J., LANTZ, L. D. & CAFFREY, C. R. (2012) Cure of hookworm infection with a cysteine protease inhibitor. *PLoS Negl Trop Dis,* 6**,** e1680.

VILLAVEDRA, M., RAMPOLDI, C., CAROL, H., BAZ, A., BATTISTONI, J. J. & NIETO, A. (2001) Identification of circulating antigens, including an immunoglobulin binding protein, from *Toxoplasma gondii* tissue cyst and tachyzoites in murine toxoplasmosis. *Int J Parasitol,* 31**,** 21-8.

VINCENDEAU, P. & DAERON, M. (1989) *Trypanosoma musculi* co-express several receptors binding rodent IgM, IgE, and IgG subclasses. *J Immunol,* 142**,** 1702-9.

VISVESVARA, G., MIRRA, S., BRANDT, F., MOSS, D., MATHEWS, H. & MARTINEZ, A. (1983) Isolation of two strains of *Acanthamoeba castellanii* from human tissue and their pathogenicity and isoenzyme profiles. *J Clin Microbiol,* 18**,** 1405-12.

WALIA, R., MONTOYA, J., VISVESVERA, G., BOOTON, G. & DOYLE, R. (2007) A case of successful treatment of cutaneous *Acanthamoeba* infection in a lung transplant recipient. *Transpl Infect Dis,* 9**,** 51-4.

WALLNER, B., FANG, H., OHLSON, T., FREY-SKOTT, J. & ELOFSSON, A. (2004) Using evolutionary information for the query and target improves fold recognition. *Proteins,* 54**,** 342-50.

WALOCHNIK, J., OBWALLER, A., HALLER-SCHOBER, E. & ASPÖCK, H. (2001) Anti-*Acanthamoeba* IgG, IgM, and IgA immunoreactivities in correlation to strain pathogenicity. *Parasitol Res,* 87**,** 651-6.

WATSON, P. M., ANDERSON, J. M., VANLTALLIE, C. M. & DOCTROW, S. R. (1991) The tight-junction-specific protein ZO-1 is a component of the human and rat blood-brain barriers. *Neurosci Lett,* 129**,** 6-10.

WEEKERS, P. H. H., BODELIER, P. L. E., WIJEN, J. P. H. & VOGELS, G. D. (1993) Effects of grazing by the free-living soil amebas *Acanthamoeba castellanii*, *Acanthamoeba polyphaga*, and *Hartmanella vermiformis* on various bacteria. *Applied and Environmental Microbiology,* 59**,** 2317-2319.

WEI, S., MARCHES, F., BORVAK, J., ZOU, W., CHANNON, J., WHITE, M., RADKE, J., CESBRON-DELAUW, M. F. & CURIEL, T. J. (2002) *Toxoplasma gondii*-infected human myeloid dendritic cells induce T-lymphocyte dysfunction and contact-dependent apoptosis. *Infect Immun,* 70**,** 1750-60.

WHITEMAN, L. Y. & MARCIANO-CABRAL, F. (1987) Susceptibility of pathogenic and nonpathogenic *Naegleria* spp. to complement-mediated lysis. *Infect Immun,* 55**,** 2442-7.

WHITEMAN, L. Y. & MARCIANO-CABRAL, F. (1989) Resistance of highly pathogenic *Naegleria fowleri* amoebae to complement-mediated lysis. *Infect Immun,* 57**,** 3869-75.

WHO (2011) Global HIV/AIDS response. Epidemic update and health sector progress towards Universal Access. Progress Report 2011. World Health Organisation.

WILSON, N., HUANG, M., ANDERSON, W., BOND, V., POWELL, M., THOMPSON, W., ARMAH, H., ADJEI, A., GYASI, R., TETTEY, Y. & STILES, J. (2008) Soluble factors from *Plasmodium falciparum*-infected erythrocytes induce apoptosis in human brain vascular endothelial and neuroglia cells. *Mol Biochem Parasitol,* 162**,** 172-6.

WINCHESTER, K., MATHERS, W., SUTPHIN, J. & DALEY, T. (1995) Diagnosis of *Acanthamoeba* keratitis in vivo with confocal microscopy. *Cornea,* 14**,** 10-7.

YANG, Y. L., SERRANO, M. G., SHEORAN, A. S., MANQUE, P. A., BUCK, G. A. & WIDMER, G. (2009) Over-expression and localization of a host protein on the membrane of. *Mol Biochem Parasitol,* 168**,** 95-101.

YANG, Z., CAO, Z. & PANJWANI, N. (1997) Pathogenesis of *Acanthamoeba* keratitis: carbohydrate-mediated host-parasite interactions. *Infect Immun,* 65**,** 439-45.

YERA, H., ZAMFIR, O., BOURCIER, T., ANCELLE, T., BATELLIER, L., DUPOUY-CAMET, J. & CHAUMEIL, C. (2007) Comparison of PCR, microscopic examination and culture for the early diagnosis and characterization of *Acanthamoeba* isolates from ocular infections. *Eur J Clin Microbiol Infect Dis,* 26**,** 221-4.

ZHANG, R., BEHBEHANI, K. & LEVINE, B. D. (2009) Dynamic pressure-flow relationship of the cerebral circulation during acute increase in arterial pressure. *J Physiol,* 587**,** 2567-77.

ZHENG, X., UNO, T., GOTO, T., ZHANG, W., HILL, J. & OHASHI, Y. (2004) Pathogenic *Acanthamoeba* induces apoptosis of human corneal epithelial cells. *Jpn J Ophthalmol,* 48**,** 23-9.

Appendices

Appendix 1

Buffer preparations used in the study are given below.

1) Phosphate-Buffered Saline (PBS)

   1× PBS tablet

   To 500ml with dH_2O

2) PBS-Tween 20 (PBST)

   2× PBS tablets

   0.5ml Tween-20

   To 1L with dH_2O

3) Acetone / ethanol fixative

   100ml Acetone

   100ml 100% Ethanol

4) 4% Formaldehyde

   55ml 36.5% w/v Formaldehyde solution

   To 500ml with ddH_2O

5) 1M Tris Base pH 8.8

   18g $NH_2C(CH_2OH)_3$

   To 150ml with dH_2O

   Adjust to pH 8.8

6) 1M Glycine elution buffer

37.5g $C_2H_5NO_2$

To 500ml with dH_2O

Adjust to pH 3

7) Carbonate/bicarbonate coating buffer

3g Na_2CO_3

6g $NaHCO_3$

To 1L with dH_2O

Adjust to pH 9.6

8) 5% Bovine Serum Albumin

2.5g BSA

To 50ml with PBS

9) 2M Sulphuric Acid

55ml conc. H_2SO_4 (18M)

To 500ml with dH_2O

10) TGS blotting buffer

50ml 10× TGS blot buffer

200ml Methanol

To 1L with ddH_2O

11) SDS running buffer

50ml 20× SDS run buffer

To 1L with ddH_2O

12) Coomassie staining buffer

200ml Methanol

50ml Glacial Acetic acid

0.125g Coomassie Brilliant Blue

To 500ml with ddH_2O

13) Destaining buffer

200ml Methanol

50ml Glacial Acetic acid

To 500ml with ddH_2O

14) Silver staining fixing solution

100ml Ethanol

25ml Glacial Acetic acid

To 250ml with dH_2O

15) Silver staining sensitising solution

75ml Ethanol

10ml 5% w/v Sodium thiosulphate

17g Sodium acetate

1.25ml 25% w/v Glutardialdehyde

To 250ml with dH_2O

16) Silver staining silver solution

25ml 2.5% w/v Silver nitrate solution

To 250ml with dH_2O

17) Silver staining developing solution

6.25g Sodium carbonate

0.2ml 37% w/v Formaldehyde

To 250ml with dH_2O

18) Silver staining stop solution

3.65g EDTA-Na_2•$2H_2O$

To 250ml with dH_2O

19) Zymogram wash buffer

7.88g $NH_2C(CH_2OH)_3$ •HCl [Trizma HCl]

25g Triton X-100

To 1L with dH_2O

Adjust pH to 7.5

20) Zymogram developing buffer

7.88g $NH_2C(CH_2OH)_3$ •HCl [Trizma HCl]

1.1g $CaCl_2$

To 1L with dH_2O

Adjust pH to

21) Zymogram nonreducing sample buffer

2ml Glycerol

1ml 0.5M $NH_2C(CH_2OH)_3$ •HCl [Trizma HCl]

0.4ml 2-β-Mercaptoethanol

0.2ml 0.05% w/v Bromophenol blue

To 8ml with dH_2O

Appendix 2

Peptide identities from tandem MS sequencing obtained from searches against the NCBI n "ESTs others" dataset. Limited additional hits were seen within the amoebazoa and in other organisms. The best matches were found for the mitochondrial F1 complex ATP synthase in *Polysphondylium pallidum* (a slime mould), *Selaginella moellendorffii* (a vascular plant) and *Dictyostelium fasciculatum* (a social amoeba).

Band	Identity (Best matches)	BLAST identity	BLAST E-value
1	N/S	N/S	N/S
2/3	N/S	N/S	N/S
4	**Hypothetical protein** (Monosiga brevicollis)	30%	0.063
5	**Mitochondrial F1 complex ATP synthase** (Polysphondylium pallidum) (Dictyostelium fasciculatum **Hypothetical protein** (Selaginella moellendorffii)	 17% 20% 33% 34%	 1e-11 8e-10 3e-17 9e-17

Appendix 3

10 PfEMP1 variant sequences were retrieved from NCBI GenBank and aligned using SeaView version 4.4.1. As expected, and in accordance with reports of antigenic variation in PfEMP1, sequence variability was observed. The PfEMP1 variants were therefore used as individual tBLASTn queries against the *A. castellanii* genome.

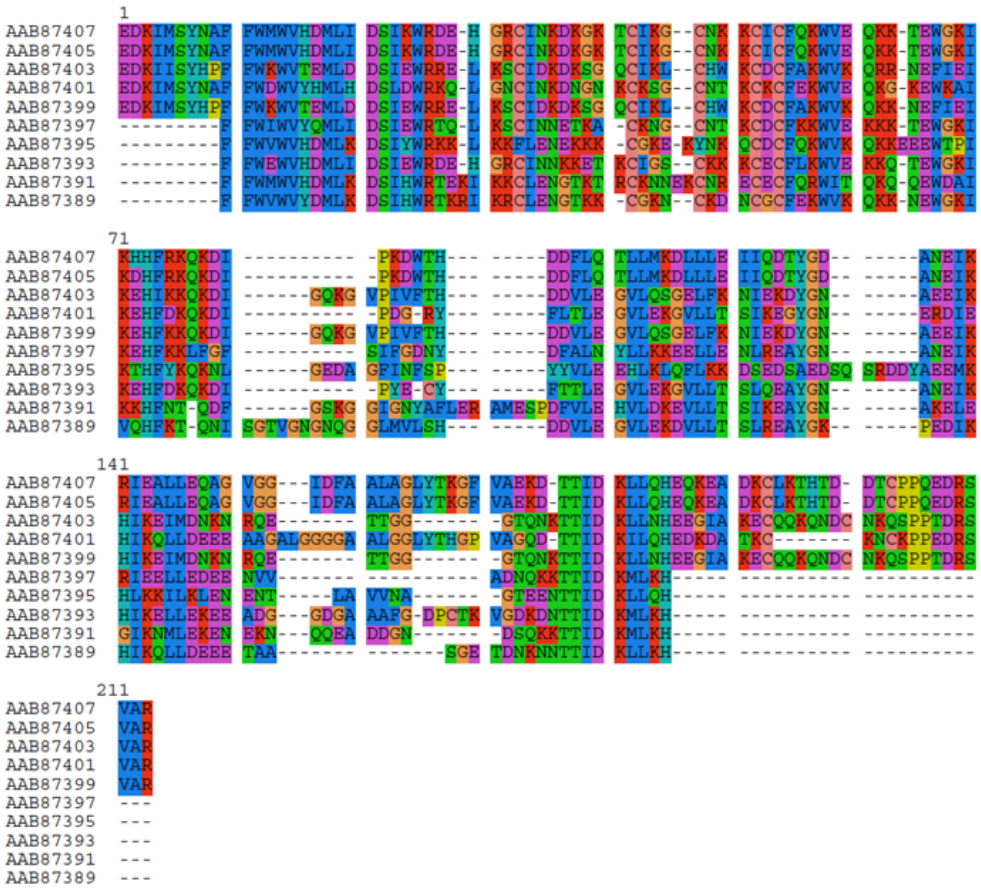

Accession	Query length	Match length	Coverage	E-value
AAB87407	178aa	41aa, 65aa	20%	0.19
AAB87405	178aa	41aa, 65aa	20%	0.19
AAB87403	174aa	46aa, 48aa	26%	0.004†
AAB87401	174aa	51aa	26%	0.90
AAB87399	174aa	114aa, 35aa	58%	0.17
AAB87397	129aa	16aa	12%	6.9
AAB87395	147aa	29aa, 39aa	18%	1.9
AAB87393	141aa	26aa, 39aa	18%	5.8
AAB87391	151aa	41aa	27%	1.7
AAB87389	142aa	59aa	37%	4.0

BLAST output for 10 PfEMP1 variants against *A. castellanii*. No significant alignments were seen for any variant examined. Peptide sequences were retrieved from the NCBI protein database and searched against the *A. castellanii* genome using the tBLASTn algorithm. Accession numbers, length of aligned regions, coverage and E-values for matches are shown for each search and the best match only is displayed. †The E-value for this match was significant but similarity was fragmented across several transcriptomic regions.

Appendix 4

Unfiltered reciprocal BLAST output for Fc binding protein sequences.

Query I.D.	Subject I.D.	% Ident.	alignment length	e-value
Acanthamoeba_Leishmania_Lmsp1_contig	Acanthamoeba_T.brucei_Lmsp1_contig	100	94	2.00E-54
Acanthamoeba_Leishmania_Lmsp1_contig	Acanthamoeba_T.cruzi_Lmsp1_contig	100	91	9.00E-53
Acanthamoeba_Leishmania_Lmsp1_contig	Acanthamoeba_Toxoplasma_beta_contig	31.58	19	0.51
Acanthamoeba_T.brucei_Lmsp1_contig	Acanthamoeba_T.cruzi_Lmsp1_contig	100	89	1.00E-51
Acanthamoeba_T.brucei_Lmsp1_contig	Acanthamoeba_Toxoplasma_beta_contig	31.58	19	0.5
Acanthamoeba_T.cruzi_Lmsp1_contig	Acanthamoeba_Toxoplasma_beta_contig	31.58	19	0.48
Acanthamoeba_Toxoplasma_beta_contig	Acanthamoeba_Schistosoma_paramyosin_contig	38.46	26	2.7
Chicken_FcR	Acanthamoeba_Schistosoma_paramyosin_contig	26.67	30	4
Chicken_FcR	Acanthamoeba_Toxoplasma_beta_contig	34.78	23	0.28
Chicken_FcR	Acanthamoeba_Toxoplasma_beta_contig	36.84	19	0.82
Chicken_FcR	Acanthamoeba_Toxoplasma_beta_contig	50	12	2.4
Chicken_FcR	Leishmania_major_Lmsp1	30.43	23	2.6
Chicken_FcR	Leishmania_major_Lmsp1	27.08	48	3.4
Chicken_FcR	Streptococcus_pyogenes_FcgR	25.64	39	0.64
Chicken_FcR	Streptococcus_pyogenes_FcgR	33.33	30	1.1
Chicken_FcR	Streptococcus_pyogenes_FcgR	33.33	18	4.2
Chicken_FcR	Toxoplasma_gondii_Beta	80	10	0.22
Chicken_FcR	Trypanosoma_brucei_Lmsp1	50	8	1.5
Chicken_FcR	Trypanosoma_cruzi_Lmsp1	50	8	3.5
Human_Fca_mR	Acanthamoeba_Leishmania_Lmsp1_contig	47.62	21	0.013
Human_Fca_mR	Acanthamoeba_Leishmania_Lmsp1_contig	29.17	24	0.25
Human_Fca_mR	Acanthamoeba_Schistosoma_paramyosin_contig	38.89	18	3.2
Human_Fca_mR	Acanthamoeba_Schistosoma_paramyosin_contig	33.33	27	4.1
Human_Fca_mR	Acanthamoeba_Schistosoma_paramyosin_contig	30.77	13	7
Human_Fca_mR	Acanthamoeba_Schistosoma_paramyosin_contig	33.33	18	9.2
Human_Fca_mR	Acanthamoeba_T.brucei_Lmsp1_contig	47.62	21	0.013
Human_Fca_mR	Acanthamoeba_T.brucei_Lmsp1_contig	29.17	24	0.24
Human_Fca_mR	Acanthamoeba_T.cruzi_Lmsp1_contig	47.62	21	0.012
Human_Fca_mR	Acanthamoeba_T.cruzi_Lmsp1_contig	29.17	24	0.23
Human_Fca_mR	Acanthamoeba_Toxoplasma_beta_contig	46.15	13	3.2
Human_Fca_mR	Acanthamoeba_Toxoplasma_beta_contig	38.46	13	4.2
Human_Fca_mR	Chicken_FcR	33.33	36	7.00E-04
Human_Fca_mR	Chicken_FcR	100	6	3.6
Human_Fca_mR	Human_FceR1	38.46	13	0.86
Human_Fca_mR	Human_FceR1	37.5	16	2.5
Human_Fca_mR	Human_FceR1	60	5	4.3
Human_Fca_mR	Human_FceR2	30.77	39	1

Query I.D.	Subject I.D.	% Ident.	alignment length	e-value
Human_Fca_mR	Human_FceR2	60	5	8.8
Human_Fca_mR	Human_FcgR1b	33.33	18	3.3
Human_Fca_mR	Human_FcgR1b	33.33	18	4.3
Human_Fca_mR	Human_FcgR2a	33.33	18	1.5
Human_Fca_mR	Human_FcgR2a	38.46	13	7.4
Human_Fca_mR	Human_FcgR2a	31.25	16	7.4
Human_Fca_mR	Human_FcgR2B	38.46	13	7.1
Human_Fca_mR	Human_FcgR3a	22.35	85	0.11
Human_Fca_mR	Human_FcgR3a	31.25	16	0.54
Human_Fca_mR	Human_FcgR3B	20.48	83	0.18
Human_Fca_mR	Human_FcgR3B	26.32	19	3.3
Human_Fca_mR	Leishmania_major_Lmsp1	58.82	17	0.24
Human_Fca_mR	Leishmania_major_Lmsp1	23.81	21	2.1
Human_Fca_mR	Leishmania_major_Lmsp1	26.32	19	3.5
Human_Fca_mR	Mouse_FcamR	48.62	436	5.00E-97
Human_Fca_mR	Mouse_FceR1	38.89	18	0.3
Human_Fca_mR	Mouse_FceR1	25.93	27	2.5
Human_Fca_mR	Mouse_FceR1	40	10	5.6
Human_Fca_mR	Mouse_FceR2	25	16	0.82
Human_Fca_mR	Mouse_FceR2	33.33	9	3.1
Human_Fca_mR	Mouse_FceR2	55.56	9	3.1
Human_Fca_mR	Mouse_FceR2	33.33	18	4.1
Human_Fca_mR	Mouse_FceR2	60	5	6.9
Human_Fca_mR	Mouse_FceR2	83.33	6	9
Human_Fca_mR	Mouse_FcgR1	23.81	21	0.35
Human_Fca_mR	Mouse_FcgR1	44.44	18	0.46
Human_Fca_mR	Mouse_FcgR1	25	16	8.7
Human_Fca_mR	Mouse_FcgR2b	45.45	11	1.5
Human_Fca_mR	Mouse_FcgR2b	40	25	2.5
Human_Fca_mR	Mouse_FcgR2b	57.14	7	4.3
Human_Fca_mR	Mouse_FcgR3	45.45	11	2.6
Human_Fca_mR	Mouse_FcgR3	46.15	13	3.4
Human_Fca_mR	Mouse_FcgR3	57.14	7	4.4
Human_Fca_mR	Mouse_FcgR4	21.74	161	0.42
Human_Fca_mR	Mouse_FcgR4	55.56	9	4.6
Human_Fca_mR	Mouse_FcgR4	26.32	19	6
Human_Fca_mR	Mouse_FcgR4	42.86	14	7.9
Human_Fca_mR	Oyster_FceR	37.5	16	6.9
Human_Fca_mR	Plasmodium_falciparum_PfEMP1	25	16	2.5
Human_Fca_mR	Plasmodium_falciparum_PfEMP1	23.53	17	9.4
Human_Fca_mR	Staphylococcus_aureus_ProteinA	36.84	19	4.1
Human_Fca_mR	Streptococcus_agalactiae_FcaR	22.09	86	0.043
Human_Fca_mR	Streptococcus_agalactiae_FcaR	34.48	29	1.1
Human_Fca_mR	Streptococcus_agalactiae_FcaR	21.88	32	3.1
Human_Fca_mR	Streptococcus_agalactiae_FcaR	27.27	22	4

Query I.D.	Subject I.D.	% Ident.	alignment length	e-value
Human_Fca_mR	Streptococcus_pyogenes_FcgR	22.97	74	3.3
Human_Fca_mR	Streptococcus_pyogenes_FcgR	35.29	17	9.6
Human_Fca_mR	Toxoplasma_gondii_Beta	28.57	28	1.2
Human_Fca_mR	Trypanosoma_brucei_Lmsp1	58.82	17	0.24
Human_Fca_mR	Trypanosoma_brucei_Lmsp1	62.5	8	2
Human_Fca_mR	Trypanosoma_cruzi_Lmsp1	58.82	17	0.25
Human_Fca_mR	Trypanosoma_cruzi_Lmsp1	24.24	33	2.1
Human_FcaR1	Acanthamoeba_Leishmania_Lmsp1_contig	31.25	16	3
Human_FcaR1	Acanthamoeba_Leishmania_Lmsp1_contig	26.67	15	8.8
Human_FcaR1	Acanthamoeba_Schistosoma_paramyosin_contig	31.58	19	4.1
Human_FcaR1	Acanthamoeba_T.brucei_Lmsp1_contig	31.25	16	3
Human_FcaR1	Acanthamoeba_T.brucei_Lmsp1_contig	26.67	15	8.6
Human_FcaR1	Acanthamoeba_T.cruzi_Lmsp1_contig	31.25	16	2.8
Human_FcaR1	Acanthamoeba_T.cruzi_Lmsp1_contig	26.67	15	8.3
Human_FcaR1	Acanthamoeba_Toxoplasma_beta_contig	46.67	15	0.51
Human_FcaR1	Acanthamoeba_Toxoplasma_beta_contig	54.55	11	0.67
Human_FcaR1	Acanthamoeba_Toxoplasma_beta_contig	26.92	26	2.5
Human_FcaR1	Acanthamoeba_Toxoplasma_beta_contig	36.36	22	2.5
Human_FcaR1	Acanthamoeba_Toxoplasma_beta_contig	29.41	17	3.3
Human_FcaR1	Acanthamoeba_Toxoplasma_beta_contig	57.14	7	5.6
Human_FcaR1	Chicken_FcR	30.27	185	5.00E-10
Human_FcaR1	Chicken_FcR	23.15	203	6.00E-05
Human_FcaR1	Chicken_FcR	24.66	219	5.00E-04
Human_FcaR1	Human_Fca_mR	36.67	30	1.3
Human_FcaR1	Human_FceR1	19.59	148	0.013
Human_FcaR1	Human_FceR1	27.03	37	0.016
Human_FcaR1	Human_FceR1	50	12	0.021
Human_FcaR1	Human_FceR2	45.45	11	4
Human_FcaR1	Human_FcgR1b	26.98	63	0.006
Human_FcaR1	Human_FcgR1b	22.22	54	0.049
Human_FcaR1	Human_FcgR1b	36.36	11	0.31
Human_FcaR1	Human_FcgR2a	24.24	66	1.00E-04
Human_FcaR1	Human_FcgR2a	24.27	103	0.029
Human_FcaR1	Human_FcgR2a	37.5	8	0.7
Human_FcaR1	Human_FcgR2a	12.9	31	7.8
Human_FcaR1	Human_FcgR2B	23.81	63	1.00E-04
Human_FcaR1	Human_FcgR2B	24.27	103	0.012
Human_FcaR1	Human_FcgR2B	27.27	55	0.035
Human_FcaR1	Human_FcgR2B	30	10	0.39
Human_FcaR1	Human_FcgR2B	12.9	31	7.4
Human_FcaR1	Human_FcgR3a	24.78	113	0.004
Human_FcaR1	Human_FcgR3a	19.28	83	0.19
Human_FcaR1	Human_FcgR3a	27.78	18	0.25
Human_FcaR1	Human_FcgR3B	25.23	111	7.00E-04
Human_FcaR1	Human_FcgR3B	20.48	83	0.049

Query I.D.	Subject I.D.	% Ident.	alignment length	e-value
Human_FcaR1	Human_FcgR3B	27.78	18	0.24
Human_FcaR1	Leishmania_major_Lmsp1	28.57	14	8.2
Human_FcaR1	Mouse_FcamR	53.33	15	0.96
Human_FcaR1	Mouse_FcamR	28.57	21	4.8
Human_FcaR1	Mouse_FcamR	57.14	7	6.2
Human_FcaR1	Mouse_FcamR	54.55	11	8.1
Human_FcaR1	Mouse_FceR1	37.5	24	0.01
Human_FcaR1	Mouse_FceR1	71.43	7	0.063
Human_FcaR1	Mouse_FceR1	36.36	11	0.41
Human_FcaR1	Mouse_FcgR1	27.59	58	0.002
Human_FcaR1	Mouse_FcgR1	23.77	122	0.043
Human_FcaR1	Mouse_FcgR2b	30.56	108	1.00E-06
Human_FcaR1	Mouse_FcgR2b	38.46	13	0.082
Human_FcaR1	Mouse_FcgR3	30.1	103	1.00E-05
Human_FcaR1	Mouse_FcgR3	50	8	0.19
Human_FcaR1	Mouse_FcgR3	36.36	11	0.71
Human_FcaR1	Mouse_FcgR4	31.82	44	1.00E-04
Human_FcaR1	Mouse_FcgR4	24.56	114	0.003
Human_FcaR1	Mouse_FcgR4	22.89	83	0.03
Human_FcaR1	Mouse_FcgR4	25	40	0.051
Human_FcaR1	Oyster_FceR	87.5	8	0.097
Human_FcaR1	Plasmodium_falciparum_PfEMP1	44.44	9	2
Human_FcaR1	Plasmodium_falciparum_PfEMP1	37.5	8	4.4
Human_FcaR1	Streptococcus_agalactiae_FcaR	26.67	90	1
Human_FcaR1	Toxoplasma_gondii_Beta	32	25	0.021
Human_FceR1	Acanthamoeba_Schistosoma_paramyosin_contig	41.67	12	1.2
Human_FceR1	Acanthamoeba_Schistosoma_paramyosin_contig	22.73	22	6.1
Human_FceR1	Chicken_FcR	24.81	133	7.00E-06
Human_FceR1	Chicken_FcR	37.5	48	4.00E-04
Human_FceR1	Chicken_FcR	26.03	73	0.003
Human_FceR1	Chicken_FcR	32.26	31	0.075
Human_FceR1	Chicken_FcR	24.43	131	0.64
Human_FceR1	Human_FceR2	27.78	18	2.7
Human_FceR1	Human_FcgR1b	43.33	150	1.00E-40
Human_FceR1	Human_FcgR1b	16.28	43	6.8
Human_FceR1	Human_FcgR2a	38.1	168	3.00E-36
Human_FceR1	Human_FcgR2a	30.61	49	0.004
Human_FceR1	Human_FcgR2B	38.69	168	1.00E-36
Human_FceR1	Human_FcgR2B	30.61	49	0.004
Human_FceR1	Human_FcgR3a	43.98	166	2.00E-39
Human_FceR1	Human_FcgR3B	43.98	166	4.00E-39
Human_FceR1	Leishmania_major_Lmsp1	37.5	8	4.2
Human_FceR1	Mouse_FcamR	60	5	4.1
Human_FceR1	Mouse_FceR1	52.22	180	1.00E-53
Human_FceR1	Mouse_FceR2	27.27	22	0.33

Query I.D.	Subject I.D.	% Ident.	alignment length	e-value
Human_FceR1	Mouse_FcgR1	43.37	166	6.00E-40
Human_FceR1	Mouse_FcgR1	23.61	144	9.00E-07
Human_FceR1	Mouse_FcgR1	32.76	58	9.00E-04
Human_FceR1	Mouse_FcgR2b	41.92	167	2.00E-38
Human_FceR1	Mouse_FcgR3	41.32	167	4.00E-38
Human_FceR1	Mouse_FcgR3	30	20	1.4
Human_FceR1	Mouse_FcgR4	41.32	167	7.00E-38
Human_FceR1	Mouse_FcgR4	66.67	6	0.38
Human_FceR1	Oyster_FceR	75	8	0.19
Human_FceR1	Oyster_FceR	39.29	28	2.1
Human_FceR1	Plasmodium_falciparum_PfEMP1	25.93	27	2.3
Human_FceR1	Schistosoma_mansoni_paramyosin	38.46	13	1.6
Human_FceR1	Schistosoma_mansoni_paramyosin	20.59	34	2.7
Human_FceR1	Schistosoma_mansoni_paramyosin	41.67	24	2.7
Human_FceR1	Streptococcus_agalactiae_FcaR	83.33	6	2.6
Human_FceR1	Streptococcus_agalactiae_FcaR	45.45	11	5.8
Human_FceR1	Streptococcus_agalactiae_FcaR	45.45	11	5.8
Human_FceR1	Streptococcus_agalactiae_FcaR	45.45	11	5.8
Human_FceR1	Streptococcus_agalactiae_FcaR	45.45	11	5.8
Human_FceR1	Streptococcus_agalactiae_FcaR	45.45	11	5.8
Human_FceR1	Streptococcus_agalactiae_FcaR	27.27	11	7.5
Human_FceR1	Taenia_solium_paramyosin	28.57	35	0.55
Human_FceR1	Taenia_solium_paramyosin	28.95	76	0.72
Human_FceR1	Taenia_solium_paramyosin	38.46	13	1.6
Human_FceR1	Toxoplasma_gondii_Beta	42.86	7	6.6
Human_FceR1	Trypanosoma_brucei_Lmsp1	28.13	32	1.1
Human_FceR1	Trypanosoma_cruzi_Lmsp1	30.43	23	0.51
Human_FceR1	Trypanosoma_cruzi_Lmsp1	71.43	7	1.9
Human_FceR2	Acanthamoeba_Leishmania_Lmsp1_contig	50	12	0.36
Human_FceR2	Acanthamoeba_T.brucei_Lmsp1_contig	50	12	0.35
Human_FceR2	Acanthamoeba_T.cruzi_Lmsp1_contig	50	12	0.34
Human_FceR2	Chicken_FcR	41.67	12	5
Human_FceR2	Chicken_FcR	30	20	8.5
Human_FceR2	Human_FcgR1b	26.79	56	0.94
Human_FceR2	Human_FcgR2a	80	5	3.6
Human_FceR2	Human_FcgR2B	41.67	12	2
Human_FceR2	Human_FcgR2B	80	5	3.4
Human_FceR2	Human_FcgR3a	31.82	22	2.9
Human_FceR2	Human_FcgR3B	31.82	22	2.8
Human_FceR2	Mouse_FcamR	40.54	37	0.12
Human_FceR2	Mouse_FcamR	30.43	46	0.16
Human_FceR2	Mouse_FcamR	36.84	19	0.77
Human_FceR2	Mouse_FcamR	25	20	5
Human_FceR2	Mouse_FceR1	20	40	3.5
Human_FceR2	Mouse_FceR2	52.13	282	2.00E-82

Query I.D.	Subject I.D.	% Ident.	alignment length	e-value
Human_FceR2	Mouse_FcgR1	23.73	59	0.84
Human_FceR2	Mouse_FcgR1	37.5	8	1.4
Human_FceR2	Mouse_FcgR2b	35.29	17	1.6
Human_FceR2	Mouse_FcgR3	35.29	17	1.6
Human_FceR2	Mouse_FcgR3	40	10	2.8
Human_FceR2	Mouse_FcgR3	38.46	13	8.1
Human_FceR2	Oyster_FceR	32.3	161	1.00E-25
Human_FceR2	Oyster_FceR	33.33	27	0.66
Human_FceR2	Schistosoma_mansoni_paramyosin	24.24	99	0.061
Human_FceR2	Schistosoma_mansoni_paramyosin	21.55	116	0.061
Human_FceR2	Schistosoma_mansoni_paramyosin	17.78	90	0.14
Human_FceR2	Schistosoma_mansoni_paramyosin	27.03	37	0.52
Human_FceR2	Schistosoma_mansoni_paramyosin	23.76	101	1.2
Human_FceR2	Schistosoma_mansoni_paramyosin	37.5	16	9.8
Human_FceR2	Streptococcus_agalactiae_FcaR	60	15	0.29
Human_FceR2	Streptococcus_agalactiae_FcaR	27.03	37	1.9
Human_FceR2	Streptococcus_agalactiae_FcaR	55.56	9	9.2
Human_FceR2	Streptococcus_pyogenes_FcgR	24.76	105	0.017
Human_FceR2	Streptococcus_pyogenes_FcgR	33.33	42	0.11
Human_FceR2	Streptococcus_pyogenes_FcgR	19.3	114	0.18
Human_FceR2	Streptococcus_pyogenes_FcgR	25.93	54	0.91
Human_FceR2	Taenia_solium_paramyosin	22.64	53	0.52
Human_FceR2	Taenia_solium_paramyosin	24.32	37	1.2
Human_FceR2	Taenia_solium_paramyosin	22.81	57	1.5
Human_FceR2	Taenia_solium_paramyosin	24.24	33	2
Human_FceR2	Taenia_solium_paramyosin	16.95	118	2.6
Human_FceR2	Trypanosoma_brucei_Lmsp1	50	8	1.7
Human_FcgR1b	Acanthamoeba_Schistosoma_paramyosin_contig	38.89	18	4.8
Human_FcgR1b	Chicken_FcR	25.84	178	6.00E-05
Human_FcgR1b	Chicken_FcR	24.34	152	0.009
Human_FcgR1b	Chicken_FcR	25	76	0.5
Human_FcgR1b	Chicken_FcR	33.33	12	9.4
Human_FcgR1b	Human_FcgR2a	49.01	151	1.00E-42
Human_FcgR1b	Human_FcgR2a	17.24	29	3.1
Human_FcgR1b	Human_FcgR2B	46.95	164	2.00E-42
Human_FcgR1b	Human_FcgR3a	44.07	177	3.00E-45
Human_FcgR1b	Human_FcgR3B	45.2	177	3.00E-46
Human_FcgR1b	Leishmania_major_Lmsp1	38.46	13	3.3
Human_FcgR1b	Leishmania_major_Lmsp1	50	8	3.3
Human_FcgR1b	Leishmania_major_Lmsp1	50	6	7.4
Human_FcgR1b	Mouse_FcamR	23.4	94	0.17
Human_FcgR1b	Mouse_FcamR	34.62	26	1.1
Human_FcgR1b	Mouse_FcamR	83.33	6	1.4
Human_FcgR1b	Mouse_FcamR	42.86	14	4.2
Human_FcgR1b	Mouse_FcamR	36.84	19	4.2

Query I.D.	Subject I.D.	% Ident.	alignment length	e-value
Human_FcgR1b	Mouse_FceR1	40.52	153	7.00E-34
Human_FcgR1b	Mouse_FceR1	20.41	49	1.4
Human_FcgR1b	Mouse_FceR2	38.89	18	0.74
Human_FcgR1b	Mouse_FcgR1	69.83	179	5.00E-72
Human_FcgR1b	Mouse_FcgR1	22.76	123	0.003
Human_FcgR1b	Mouse_FcgR1	31.48	54	0.003
Human_FcgR1b	Mouse_FcgR2b	45.35	172	2.00E-46
Human_FcgR1b	Mouse_FcgR3	42.93	184	5.00E-46
Human_FcgR1b	Mouse_FcgR4	45.73	164	5.00E-43
Human_FcgR1b	Oyster_FceR	37.5	16	1.2
Human_FcgR1b	Oyster_FceR	40	10	2.8
Human_FcgR1b	Staphylococcus_aureus_ProteinA	36.36	22	0.067
Human_FcgR1b	Staphylococcus_aureus_ProteinA	36.36	22	0.067
Human_FcgR1b	Streptococcus_agalactiae_FcaR	37.5	16	3.4
Human_FcgR1b	Streptococcus_pyogenes_FcgR	23.53	34	2.2
Human_FcgR1b	Taenia_solium_paramyosin	62.5	8	2.8
Human_FcgR2a	Acanthamoeba_Leishmania_Lmsp1_contig	60	10	0.71
Human_FcgR2a	Acanthamoeba_Leishmania_Lmsp1_contig	41.67	12	2.1
Human_FcgR2a	Acanthamoeba_T.brucei_Lmsp1_contig	60	10	0.7
Human_FcgR2a	Acanthamoeba_T.brucei_Lmsp1_contig	41.67	12	2
Human_FcgR2a	Acanthamoeba_T.cruzi_Lmsp1_contig	60	10	0.68
Human_FcgR2a	Acanthamoeba_T.cruzi_Lmsp1_contig	41.67	12	2
Human_FcgR2a	Chicken_FcR	24.44	90	8.00E-04
Human_FcgR2a	Chicken_FcR	29.63	108	0.003
Human_FcgR2a	Chicken_FcR	31.58	38	0.22
Human_FcgR2a	Chicken_FcR	31.25	16	0.29
Human_FcgR2a	Chicken_FcR	50	8	1.5
Human_FcgR2a	Chicken_FcR	23.81	21	2.5
Human_FcgR2a	Chicken_FcR	42.86	14	4.2
Human_FcgR2a	Human_FcgR2B	93.64	173	7.00E-101
Human_FcgR2a	Human_FcgR3a	51.5	167	2.00E-47
Human_FcgR2a	Human_FcgR3B	52.1	167	1.00E-48
Human_FcgR2a	Leishmania_major_Lmsp1	50	6	5.7
Human_FcgR2a	Mouse_FcamR	34.38	32	0.23
Human_FcgR2a	Mouse_FcamR	30.77	39	0.38
Human_FcgR2a	Mouse_FcamR	57.14	7	7.2
Human_FcgR2a	Mouse_FceR1	34.12	170	1.00E-27
Human_FcgR2a	Mouse_FceR2	35.71	14	0.75
Human_FcgR2a	Mouse_FceR2	26.47	34	2.8
Human_FcgR2a	Mouse_FcgR1	45.83	168	4.00E-41
Human_FcgR2a	Mouse_FcgR1	21.39	173	6.00E-05
Human_FcgR2a	Mouse_FcgR2b	62.71	177	1.00E-67
Human_FcgR2a	Mouse_FcgR3	61.02	177	8.00E-65
Human_FcgR2a	Mouse_FcgR3	37.5	24	0.004
Human_FcgR2a	Mouse_FcgR4	49.72	177	4.00E-48

Query I.D.	Subject I.D.	% Ident.	alignment length	e-value
Human_FcgR2a	Mouse_FcgR4	35.71	14	4.2
Human_FcgR2a	Oyster_FceR	50	8	8.1
Human_FcgR2a	Plasmodium_falciparum_PfEMP1	30	10	3
Human_FcgR2B	Acanthamoeba_Leishmania_Lmsp1_contig	50	10	1.5
Human_FcgR2B	Acanthamoeba_Leishmania_Lmsp1_contig	41.67	12	2
Human_FcgR2B	Acanthamoeba_Schistosoma_paramyosin_contig	22.95	61	2
Human_FcgR2B	Acanthamoeba_T.brucei_Lmsp1_contig	50	10	1.5
Human_FcgR2B	Acanthamoeba_T.brucei_Lmsp1_contig	41.67	12	1.9
Human_FcgR2B	Acanthamoeba_T.cruzi_Lmsp1_contig	50	10	1.4
Human_FcgR2B	Acanthamoeba_T.cruzi_Lmsp1_contig	41.67	12	1.9
Human_FcgR2B	Chicken_FcR	23.33	90	6.00E-04
Human_FcgR2B	Chicken_FcR	28.04	107	0.004
Human_FcgR2B	Chicken_FcR	23.33	60	0.16
Human_FcgR2B	Chicken_FcR	31.25	16	0.28
Human_FcgR2B	Chicken_FcR	45	20	0.62
Human_FcgR2B	Chicken_FcR	50	8	1.4
Human_FcgR2B	Chicken_FcR	23.81	21	1.8
Human_FcgR2B	Human_FcgR3a	50.3	167	3.00E-47
Human_FcgR2B	Human_FcgR3B	50.9	167	2.00E-48
Human_FcgR2B	Leishmania_major_Lmsp1	50	6	5.4
Human_FcgR2B	Mouse_FcamR	34.38	32	0.21
Human_FcgR2B	Mouse_FcamR	30.77	39	0.36
Human_FcgR2B	Mouse_FceR1	34.12	170	2.00E-27
Human_FcgR2B	Mouse_FceR2	35.71	14	0.71
Human_FcgR2B	Mouse_FceR2	26.47	34	2.7
Human_FcgR2B	Mouse_FcgR1	47.02	168	4.00E-42
Human_FcgR2B	Mouse_FcgR1	22.42	165	6.00E-05
Human_FcgR2B	Mouse_FcgR1	22.89	83	0.081
Human_FcgR2B	Mouse_FcgR2b	64.71	170	1.00E-67
Human_FcgR2B	Mouse_FcgR3	62.21	172	1.00E-64
Human_FcgR2B	Mouse_FcgR3	33.33	24	0.014
Human_FcgR2B	Mouse_FcgR4	50.59	170	4.00E-48
Human_FcgR2B	Mouse_FcgR4	50	10	4
Human_FcgR2B	Plasmodium_falciparum_PfEMP1	30	10	2.9
Human_FcgR2B	Trypanosoma_cruzi_Lmsp1	50	12	1.4
Human_FcgR3a	Acanthamoeba_Schistosoma_paramyosin_contig	30.43	23	1.7
Human_FcgR3a	Chicken_FcR	40	25	0.012
Human_FcgR3a	Chicken_FcR	41.18	17	0.062
Human_FcgR3a	Chicken_FcR	30	20	0.1
Human_FcgR3a	Chicken_FcR	29.03	31	0.18
Human_FcgR3a	Human_FcgR3B	97.28	184	1.00E-108
Human_FcgR3a	Leishmania_major_Lmsp1	31.58	19	0.7
Human_FcgR3a	Mouse_FcamR	24.42	86	0.31
Human_FcgR3a	Mouse_FceR1	36.69	169	7.00E-29
Human_FcgR3a	Mouse_FceR2	41.67	12	5

Query I.D.	Subject I.D.	% Ident.	alignment length	e-value
Human_FcgR3a	Mouse_FcgR1	44.09	186	2.00E-42
Human_FcgR3a	Mouse_FcgR1	23.18	151	0.002
Human_FcgR3a	Mouse_FcgR1	30.77	39	0.023
Human_FcgR3a	Mouse_FcgR2b	50.88	171	3.00E-51
Human_FcgR3a	Mouse_FcgR3	49.44	178	4.00E-51
Human_FcgR3a	Mouse_FcgR3	30	20	0.39
Human_FcgR3a	Mouse_FcgR4	67.86	168	1.00E-70
Human_FcgR3a	Mouse_FcgR4	50	10	9.9
Human_FcgR3a	Plasmodium_falciparum_PfEMP1	30	20	7.1
Human_FcgR3a	Streptococcus_agalactiae_FcaR	29.17	24	8.1
Human_FcgR3a	Streptococcus_agalactiae_FcaR	36.84	19	8.1
Human_FcgR3a	Toxoplasma_gondii_Beta	50	8	4.2
Human_FcgR3B	Chicken_FcR	40	25	0.009
Human_FcgR3B	Chicken_FcR	41.18	17	0.1
Human_FcgR3B	Chicken_FcR	25	44	0.22
Human_FcgR3B	Chicken_FcR	29.03	31	0.29
Human_FcgR3B	Chicken_FcR	25	20	0.38
Human_FcgR3B	Mouse_FcamR	62.5	8	2.5
Human_FcgR3B	Mouse_FceR1	36.09	169	3.00E-28
Human_FcgR3B	Mouse_FceR2	41.67	12	8.3
Human_FcgR3B	Mouse_FcgR1	45.83	168	5.00E-42
Human_FcgR3B	Mouse_FcgR1	22.45	147	2.00E-04
Human_FcgR3B	Mouse_FcgR1	30.77	39	0.038
Human_FcgR3B	Mouse_FcgR2b	51.46	171	6.00E-52
Human_FcgR3B	Mouse_FcgR3	50	178	8.00E-52
Human_FcgR3B	Mouse_FcgR3	30	20	0.37
Human_FcgR3B	Mouse_FcgR4	66.67	168	2.00E-69
Human_FcgR3B	Mouse_FcgR4	50	10	9.4
Human_FcgR3B	Plasmodium_falciparum_PfEMP1	30	20	6.7
Human_FcgR3B	Schistosoma_mansoni_paramyosin	27.03	37	2.2
Human_FcgR3B	Schistosoma_mansoni_paramyosin	35.29	17	2.8
Human_FcgR3B	Schistosoma_mansoni_paramyosin	21.43	28	8.2
Human_FcgR3B	Streptococcus_agalactiae_FcaR	24.24	33	4.5
Human_FcgR3B	Toxoplasma_gondii_Beta	50	8	4
Leishmania_major_Lmsp1	Acanthamoeba_Leishmania_Lmsp1_contig	55.91	93	7.00E-34
Leishmania_major_Lmsp1	Acanthamoeba_Schistosoma_paramyosin_contig	40	15	0.77
Leishmania_major_Lmsp1	Acanthamoeba_Schistosoma_paramyosin_contig	26.47	34	2.9
Leishmania_major_Lmsp1	Acanthamoeba_Schistosoma_paramyosin_contig	28.57	14	6.5
Leishmania_major_Lmsp1	Acanthamoeba_T.brucei_Lmsp1_contig	55.91	93	7.00E-34
Leishmania_major_Lmsp1	Acanthamoeba_T.cruzi_Lmsp1_contig	56.18	89	6.00E-33
Leishmania_major_Lmsp1	Acanthamoeba_Toxoplasma_beta_contig	26.32	19	5.4
Leishmania_major_Lmsp1	Plasmodium_falciparum_PfEMP1	33.33	12	4.2
Leishmania_major_Lmsp1	Trypanosoma_brucei_Lmsp1	82	150	5.00E-68
Leishmania_major_Lmsp1	Trypanosoma_cruzi_Lmsp1	84.25	127	4.00E-61
Mouse_FcamR	Acanthamoeba_T.brucei_Lmsp1_contig	25	24	7.6

Query I.D.	Subject I.D.	% Ident.	alignment length	e-value
Mouse_FcamR	Acanthamoeba_T.cruzi_Lmsp1_contig	21.43	14	9.5
Mouse_FcamR	Acanthamoeba_Toxoplasma_beta_contig	34.78	23	0.82
Mouse_FcamR	Chicken_FcR	40	30	0.7
Mouse_FcamR	Chicken_FcR	43.48	23	2
Mouse_FcamR	Chicken_FcR	25	16	7.8
Mouse_FcamR	Oyster_FceR	60	5	3.9
Mouse_FcamR	Schistosoma_mansoni_paramyosin	33.33	21	1.4
Mouse_FcamR	Schistosoma_mansoni_paramyosin	19.61	51	5.3
Mouse_FcamR	Staphylococcus_aureus_ProteinA	26.67	45	3
Mouse_FcamR	Streptococcus_agalactiae_FcaR	30.56	36	0.6
Mouse_FcamR	Streptococcus_agalactiae_FcaR	30.61	49	0.6
Mouse_FcamR	Streptococcus_agalactiae_FcaR	24.39	41	1.3
Mouse_FcamR	Streptococcus_agalactiae_FcaR	29.03	31	1.7
Mouse_FcamR	Streptococcus_agalactiae_FcaR	27.78	36	2.3
Mouse_FcamR	Streptococcus_agalactiae_FcaR	27.78	36	3.9
Mouse_FcamR	Streptococcus_agalactiae_FcaR	54.55	11	5
Mouse_FcamR	Streptococcus_agalactiae_FcaR	31.25	16	6.6
Mouse_FcamR	Streptococcus_agalactiae_FcaR	25.56	90	6.6
Mouse_FcamR	Streptococcus_agalactiae_FcaR	26.09	23	8.6
Mouse_FcamR	Streptococcus_pyogenes_FcgR	24.56	57	0.099
Mouse_FcamR	Streptococcus_pyogenes_FcgR	31.82	22	0.64
Mouse_FcamR	Streptococcus_pyogenes_FcgR	100	6	2.4
Mouse_FcamR	Streptococcus_pyogenes_FcgR	60	10	3.2
Mouse_FcamR	Streptococcus_pyogenes_FcgR	23.91	46	9.3
Mouse_FcamR	Taenia_solium_paramyosin	25.45	55	0.48
Mouse_FcamR	Taenia_solium_paramyosin	35	20	1.4
Mouse_FcamR	Toxoplasma_gondii_Beta	24.07	54	1.9
Mouse_FcamR	Toxoplasma_gondii_Beta	44.44	18	2.5
Mouse_FcamR	Toxoplasma_gondii_Beta	62.5	8	9.5
Mouse_FcamR	Toxoplasma_gondii_Beta	66.67	6	9.5
Mouse_FcamR	Toxoplasma_gondii_Beta	66.67	6	9.5
Mouse_FcamR	Toxoplasma_gondii_Beta	66.67	6	9.5
Mouse_FcamR	Trypanosoma_cruzi_Lmsp1	44.44	9	1.6
Mouse_FcamR	Trypanosoma_cruzi_Lmsp1	100	5	2
Mouse_FceR1	Acanthamoeba_Leishmania_Lmsp1_contig	50	8	2.7
Mouse_FceR1	Acanthamoeba_T.brucei_Lmsp1_contig	50	8	2.6
Mouse_FceR1	Acanthamoeba_T.cruzi_Lmsp1_contig	50	8	2.5
Mouse_FceR1	Chicken_FcR	27.08	48	0.026
Mouse_FceR1	Chicken_FcR	60	10	0.076
Mouse_FceR1	Chicken_FcR	40	20	0.099
Mouse_FceR1	Chicken_FcR	33.33	15	0.64
Mouse_FceR1	Chicken_FcR	66.67	6	1.9
Mouse_FceR1	Chicken_FcR	44.44	9	7.1
Mouse_FceR1	Mouse_FceR2	20.45	44	3.6
Mouse_FceR1	Oyster_FceR	55.56	9	0.72

Query I.D.	Subject I.D.	% Ident.	alignment length	e-value
Mouse_FceR1	Plasmodium_falciparum_PfEMP1	26.67	15	5.1
Mouse_FceR1	Schistosoma_mansoni_paramyosin	45.45	11	2.8
Mouse_FceR1	Schistosoma_mansoni_paramyosin	26.47	34	3.6
Mouse_FceR1	Schistosoma_mansoni_paramyosin	33.33	18	8
Mouse_FceR1	Streptococcus_agalactiae_FcaR	33.33	21	1.2
Mouse_FceR1	Taenia_solium_paramyosin	37.5	16	0.95
Mouse_FceR1	Taenia_solium_paramyosin	23.53	34	1.6
Mouse_FceR1	Taenia_solium_paramyosin	50	10	4.7
Mouse_FceR1	Trypanosoma_cruzi_Lmsp1	30.43	23	9.7
Mouse_FceR2	Leishmania_major_Lmsp1	50	12	0.21
Mouse_FceR2	Mouse_FcamR	50	18	0.46
Mouse_FceR2	Mouse_FcamR	25	16	1.3
Mouse_FceR2	Mouse_FcamR	33.33	9	6.7
Mouse_FceR2	Mouse_FcamR	41.67	12	6.7
Mouse_FceR2	Mouse_FcamR	42.86	7	8.7
Mouse_FceR2	Oyster_FceR	31.68	161	9.00E-19
Mouse_FceR2	Oyster_FceR	33.33	6	9.8
Mouse_FceR2	Plasmodium_falciparum_PfEMP1	66.67	6	0.42
Mouse_FceR2	Plasmodium_falciparum_PfEMP1	38.89	18	2.7
Mouse_FceR2	Schistosoma_mansoni_paramyosin	23.13	134	5.00E-05
Mouse_FceR2	Schistosoma_mansoni_paramyosin	20.45	132	3.00E-04
Mouse_FceR2	Schistosoma_mansoni_paramyosin	23.64	110	4.00E-04
Mouse_FceR2	Schistosoma_mansoni_paramyosin	21.84	87	0.048
Mouse_FceR2	Staphylococcus_aureus_ProteinA	25.81	124	0.006
Mouse_FceR2	Staphylococcus_aureus_ProteinA	18.52	108	0.69
Mouse_FceR2	Streptococcus_agalactiae_FcaR	21.77	124	0.001
Mouse_FceR2	Streptococcus_agalactiae_FcaR	21.6	125	0.016
Mouse_FceR2	Streptococcus_agalactiae_FcaR	27.69	65	0.17
Mouse_FceR2	Streptococcus_agalactiae_FcaR	38.1	21	0.66
Mouse_FceR2	Streptococcus_agalactiae_FcaR	30	20	1.1
Mouse_FceR2	Streptococcus_agalactiae_FcaR	25	24	9.5
Mouse_FceR2	Streptococcus_pyogenes_FcgR	23.13	134	1.00E-05
Mouse_FceR2	Streptococcus_pyogenes_FcgR	19.64	112	1.00E-05
Mouse_FceR2	Streptococcus_pyogenes_FcgR	26.05	119	0.029
Mouse_FceR2	Streptococcus_pyogenes_FcgR	80	5	4.7
Mouse_FceR2	Taenia_solium_paramyosin	22.33	103	3.00E-04
Mouse_FceR2	Taenia_solium_paramyosin	17.45	149	9.00E-04
Mouse_FceR2	Taenia_solium_paramyosin	20	105	0.01
Mouse_FceR2	Taenia_solium_paramyosin	17.43	109	0.028
Mouse_FceR2	Taenia_solium_paramyosin	20.16	124	0.028
Mouse_FceR2	Taenia_solium_paramyosin	19.53	128	0.18
Mouse_FceR2	Taenia_solium_paramyosin	13.33	60	0.7
Mouse_FceR2	Toxoplasma_gondii_Beta	46.15	13	0.43
Mouse_FceR2	Trypanosoma_brucei_Lmsp1	50	12	0.27
Mouse_FcgR1	Acanthamoeba_Leishmania_Lmsp1_contig	50	8	6.8

Query I.D.	Subject I.D.	% Ident.	alignment length	e-value
Mouse_FcgR1	Acanthamoeba_Leishmania_Lmsp1_contig	42.86	7	8.9
Mouse_FcgR1	Acanthamoeba_Schistosoma_paramyosin_contig	46.15	13	9.6
Mouse_FcgR1	Acanthamoeba_T.brucei_Lmsp1_contig	50	8	6.6
Mouse_FcgR1	Acanthamoeba_T.brucei_Lmsp1_contig	42.86	7	8.6
Mouse_FcgR1	Acanthamoeba_T.cruzi_Lmsp1_contig	50	8	6.4
Mouse_FcgR1	Acanthamoeba_T.cruzi_Lmsp1_contig	42.86	7	8.3
Mouse_FcgR1	Chicken_FcR	27.38	84	1.00E-04
Mouse_FcgR1	Chicken_FcR	21.85	238	0.001
Mouse_FcgR1	Chicken_FcR	29.87	77	0.004
Mouse_FcgR1	Chicken_FcR	24.84	161	0.069
Mouse_FcgR1	Chicken_FcR	28.57	28	1.3
Mouse_FcgR1	Leishmania_major_Lmsp1	71.43	7	3.8
Mouse_FcgR1	Leishmania_major_Lmsp1	50	8	8.4
Mouse_FcgR1	Mouse_FcamR	30.3	33	0.041
Mouse_FcgR1	Mouse_FcamR	26.32	19	1.7
Mouse_FcgR1	Mouse_FcamR	31.25	16	2.9
Mouse_FcgR1	Mouse_FcamR	66.67	6	2.9
Mouse_FcgR1	Mouse_FceR1	42.35	170	5.00E-37
Mouse_FcgR1	Mouse_FceR1	24.05	158	7.00E-04
Mouse_FcgR1	Mouse_FceR1	26.76	71	0.004
Mouse_FcgR1	Mouse_FceR2	50	10	2.5
Mouse_FcgR1	Mouse_FcgR2b	46.71	167	2.00E-44
Mouse_FcgR1	Mouse_FcgR2b	28.65	178	4.00E-11
Mouse_FcgR1	Mouse_FcgR2b	33.33	15	0.71
Mouse_FcgR1	Mouse_FcgR2b	41.67	12	0.93
Mouse_FcgR1	Mouse_FcgR3	46.51	172	4.00E-45
Mouse_FcgR1	Mouse_FcgR3	24.5	151	1.00E-08
Mouse_FcgR1	Mouse_FcgR3	28.57	56	0.066
Mouse_FcgR1	Mouse_FcgR3	26.09	23	0.73
Mouse_FcgR1	Mouse_FcgR4	41.57	166	2.00E-37
Mouse_FcgR1	Mouse_FcgR4	25.5	149	4.00E-06
Mouse_FcgR1	Mouse_FcgR4	38.1	21	0.04
Mouse_FcgR1	Oyster_FceR	29.17	24	1.9
Mouse_FcgR1	Schistosoma_mansoni_paramyosin	38.1	21	4.4
Mouse_FcgR1	Staphylococcus_aureus_ProteinA	36.36	22	1.1
Mouse_FcgR1	Staphylococcus_aureus_ProteinA	36.36	22	1.1
Mouse_FcgR1	Streptococcus_agalactiae_FcaR	30	30	3.2
Mouse_FcgR1	Streptococcus_agalactiae_FcaR	45.45	11	3.2
Mouse_FcgR1	Streptococcus_agalactiae_FcaR	66.67	6	5.4
Mouse_FcgR1	Streptococcus_agalactiae_FcaR	29.41	17	7
Mouse_FcgR1	Streptococcus_pyogenes_FcgR	30.43	23	2.6
Mouse_FcgR1	Streptococcus_pyogenes_FcgR	35.71	14	5.9
Mouse_FcgR1	Taenia_solium_paramyosin	35	20	3.4
Mouse_FcgR1	Taenia_solium_paramyosin	40	15	5.7
Mouse_FcgR1	Taenia_solium_paramyosin	46.15	13	7.5

Query I.D.	Subject I.D.	% Ident.	alignment length	e-value
Mouse_FcgR1	Toxoplasma_gondii_Beta	66.67	6	7.9
Mouse_FcgR1	Trypanosoma_cruzi_Lmsp1	30	20	6.6
Mouse_FcgR2b	Acanthamoeba_Schistosoma_paramyosin_contig	26.15	65	0.19
Mouse_FcgR2b	Chicken_FcR	27.59	87	8.00E-04
Mouse_FcgR2b	Chicken_FcR	20.61	165	0.02
Mouse_FcgR2b	Chicken_FcR	26.42	106	0.026
Mouse_FcgR2b	Chicken_FcR	33.33	27	7.1
Mouse_FcgR2b	Leishmania_major_Lmsp1	44.44	9	4.3
Mouse_FcgR2b	Mouse_FcamR	25	80	0.058
Mouse_FcgR2b	Mouse_FcamR	43.48	23	0.13
Mouse_FcgR2b	Mouse_FceR1	39.64	169	2.00E-32
Mouse_FcgR2b	Mouse_FceR2	22.5	40	0.56
Mouse_FcgR2b	Mouse_FceR2	40	15	8.1
Mouse_FcgR2b	Mouse_FcgR3	92.66	177	1.00E-100
Mouse_FcgR2b	Mouse_FcgR3	30	20	0.13
Mouse_FcgR2b	Mouse_FcgR4	45.81	179	4.00E-45
Mouse_FcgR2b	Mouse_FcgR4	66.67	6	0.49
Mouse_FcgR2b	Mouse_FcgR4	35.71	14	3.2
Mouse_FcgR2b	Oyster_FceR	42.86	21	0.94
Mouse_FcgR2b	Oyster_FceR	50	8	4.7
Mouse_FcgR2b	Plasmodium_falciparum_PfEMP1	45.45	11	0.27
Mouse_FcgR2b	Staphylococcus_aureus_ProteinA	36.84	19	1.3
Mouse_FcgR2b	Staphylococcus_aureus_ProteinA	28.57	21	8.1
Mouse_FcgR2b	Staphylococcus_aureus_ProteinA	28.57	21	8.1
Mouse_FcgR2b	Streptococcus_pyogenes_FcgR	25	28	2.9
Mouse_FcgR2b	Streptococcus_pyogenes_FcgR	46.15	13	4.9
Mouse_FcgR3	Chicken_FcR	29.23	65	0.007
Mouse_FcgR3	Chicken_FcR	25.71	140	0.009
Mouse_FcgR3	Chicken_FcR	20.75	106	0.012
Mouse_FcgR3	Chicken_FcR	23.08	65	0.5
Mouse_FcgR3	Mouse_FcamR	36.67	30	0.17
Mouse_FcgR3	Mouse_FcamR	28.24	85	0.23
Mouse_FcgR3	Mouse_FceR1	40.12	172	2.00E-33
Mouse_FcgR3	Mouse_FceR2	22.5	40	0.75
Mouse_FcgR3	Mouse_FceR2	40	15	8.3
Mouse_FcgR3	Mouse_FcgR4	46.59	176	3.00E-46
Mouse_FcgR3	Mouse_FcgR4	30	20	0.23
Mouse_FcgR3	Mouse_FcgR4	66.67	6	0.5
Mouse_FcgR3	Mouse_FcgR4	35.71	14	3.3
Mouse_FcgR3	Oyster_FceR	50	8	4.8
Mouse_FcgR3	Plasmodium_falciparum_PfEMP1	45.45	11	0.12
Mouse_FcgR3	Staphylococcus_aureus_ProteinA	36.84	19	2.2
Mouse_FcgR3	Streptococcus_agalactiae_FcaR	50	8	5.9
Mouse_FcgR3	Streptococcus_pyogenes_FcgR	30	30	2.3
Mouse_FcgR3	Streptococcus_pyogenes_FcgR	46.15	13	3.9

Query I.D.	Subject I.D.	% Ident.	alignment length	e-value
Mouse_FcgR4	Chicken_FcR	44	25	0.013
Mouse_FcgR4	Chicken_FcR	20.54	112	0.028
Mouse_FcgR4	Chicken_FcR	32.26	31	0.081
Mouse_FcgR4	Chicken_FcR	32.14	28	0.11
Mouse_FcgR4	Mouse_FcamR	36.36	22	0.24
Mouse_FcgR4	Mouse_FcamR	75	8	0.9
Mouse_FcgR4	Mouse_FcamR	62.5	8	3.4
Mouse_FcgR4	Mouse_FceR1	40.48	168	4.00E-32
Mouse_FcgR4	Mouse_FceR2	37.5	16	3.9
Mouse_FcgR4	Oyster_FceR	33.33	15	5
Mouse_FcgR4	Plasmodium_falciparum_PfEMP1	38.46	13	3.1
Mouse_FcgR4	Plasmodium_falciparum_PfEMP1	40	15	3.1
Mouse_FcgR4	Schistosoma_mansoni_paramyosin	45.45	11	6.7
Mouse_FcgR4	Schistosoma_mansoni_paramyosin	83.33	6	6.7
Mouse_FcgR4	Schistosoma_mansoni_paramyosin	50	10	8.8
Mouse_FcgR4	Streptococcus_agalactiae_FcaR	54.55	11	6.3
Mouse_FcgR4	Toxoplasma_gondii_Beta	25.53	47	1.1
Mouse_FcgR4	Toxoplasma_gondii_Beta	31.58	19	9.3
Oyster_FceR	Acanthamoeba_Leishmania_Lmsp1_contig	55.56	9	0.8
Oyster_FceR	Acanthamoeba_Schistosoma_paramyosin_contig	56.25	16	0.062
Oyster_FceR	Acanthamoeba_Schistosoma_paramyosin_contig	26.92	26	2.6
Oyster_FceR	Acanthamoeba_Schistosoma_paramyosin_contig	38.89	18	5.8
Oyster_FceR	Acanthamoeba_Schistosoma_paramyosin_contig	71.43	7	5.8
Oyster_FceR	Acanthamoeba_T.brucei_Lmsp1_contig	55.56	9	0.78
Oyster_FceR	Acanthamoeba_Toxoplasma_beta_contig	45.45	11	7.8
Oyster_FceR	Chicken_FcR	29.41	17	1.3
Oyster_FceR	Chicken_FcR	19.64	56	2.3
Oyster_FceR	Leishmania_major_Lmsp1	50	10	3.8
Oyster_FceR	Plasmodium_falciparum_PfEMP1	40	25	0.017
Oyster_FceR	Plasmodium_falciparum_PfEMP1	40	15	0.022
Oyster_FceR	Plasmodium_falciparum_PfEMP1	66.67	6	3.5
Oyster_FceR	Staphylococcus_aureus_ProteinA	20.51	39	1.5
Oyster_FceR	Staphylococcus_aureus_ProteinA	35.71	14	1.5
Oyster_FceR	Staphylococcus_aureus_ProteinA	17.95	39	7.6
Oyster_FceR	Staphylococcus_aureus_ProteinA	17.95	39	9.9
Oyster_FceR	Streptococcus_agalactiae_FcaR	33.33	33	0.66
Oyster_FceR	Streptococcus_agalactiae_FcaR	34.15	41	1.9
Oyster_FceR	Streptococcus_agalactiae_FcaR	71.43	7	3.3
Oyster_FceR	Streptococcus_agalactiae_FcaR	33.33	15	9.5
Oyster_FceR	Streptococcus_pyogenes_FcgR	29.17	24	0.55
Oyster_FceR	Streptococcus_pyogenes_FcgR	75	8	2.7
Oyster_FceR	Trypanosoma_brucei_Lmsp1	50	8	3.8
Oyster_FceR	Trypanosoma_brucei_Lmsp1	50	10	6.5
Oyster_FceR	Trypanosoma_cruzi_Lmsp1	50	10	6.7
Oyster_FceR	Trypanosoma_cruzi_Lmsp1	29.41	17	8.7

Query I.D.	Subject I.D.	% Ident.	alignment length	e-value
Schistosoma_mansoni_paramyosin	Acanthamoeba_Leishmania_Lmsp1_contig	71.43	7	2.2
Schistosoma_mansoni_paramyosin	Acanthamoeba_Leishmania_Lmsp1_contig	38.46	13	6.5
Schistosoma_mansoni_paramyosin	Acanthamoeba_T.brucei_Lmsp1_contig	71.43	7	2.2
Schistosoma_mansoni_paramyosin	Acanthamoeba_T.brucei_Lmsp1_contig	38.46	13	6.4
Schistosoma_mansoni_paramyosin	Acanthamoeba_T.cruzi_Lmsp1_contig	71.43	7	2.1
Schistosoma_mansoni_paramyosin	Acanthamoeba_T.cruzi_Lmsp1_contig	38.46	13	6.1
Schistosoma_mansoni_paramyosin	Acanthamoeba_Toxoplasma_beta_contig	27.27	33	2.1
Schistosoma_mansoni_paramyosin	Leishmania_major_Lmsp1	71.43	7	2.3
Schistosoma_mansoni_paramyosin	Plasmodium_falciparum_PfEMP1	30.77	26	3.5
Schistosoma_mansoni_paramyosin	Plasmodium_falciparum_PfEMP1	50	12	3.5
Schistosoma_mansoni_paramyosin	Staphylococcus_aureus_ProteinA	26.14	153	4.00E-05
Schistosoma_mansoni_paramyosin	Staphylococcus_aureus_ProteinA	19.32	88	0.19
Schistosoma_mansoni_paramyosin	Staphylococcus_aureus_ProteinA	21.3	108	0.93
Schistosoma_mansoni_paramyosin	Staphylococcus_aureus_ProteinA	28.57	35	4.6
Schistosoma_mansoni_paramyosin	Staphylococcus_aureus_ProteinA	30.43	23	6
Schistosoma_mansoni_paramyosin	Staphylococcus_aureus_ProteinA	50	10	6
Staphylococcus_aureus_ProteinA	Acanthamoeba_Toxoplasma_beta_contig	32.5	40	0.065
Staphylococcus_aureus_ProteinA	Acanthamoeba_Toxoplasma_beta_contig	22.38	143	0.084
Staphylococcus_aureus_ProteinA	Acanthamoeba_Toxoplasma_beta_contig	30	40	0.32
Staphylococcus_aureus_ProteinA	Acanthamoeba_Toxoplasma_beta_contig	29.17	24	1.6
Staphylococcus_aureus_ProteinA	Acanthamoeba_Toxoplasma_beta_contig	23.08	26	2.7
Staphylococcus_aureus_ProteinA	Acanthamoeba_Toxoplasma_beta_contig	66.67	6	4.6
Staphylococcus_aureus_ProteinA	Acanthamoeba_Toxoplasma_beta_contig	23.08	26	6
Streptococcus_agalactiae_FcaR	Acanthamoeba_Leishmania_Lmsp1_contig	44.44	9	2.7
Streptococcus_agalactiae_FcaR	Acanthamoeba_Leishmania_Lmsp1_contig	22.5	80	2.7
Streptococcus_agalactiae_FcaR	Acanthamoeba_Leishmania_Lmsp1_contig	26.92	26	4.6
Streptococcus_agalactiae_FcaR	Acanthamoeba_Leishmania_Lmsp1_contig	42.11	19	6.1
Streptococcus_agalactiae_FcaR	Acanthamoeba_Schistosoma_paramyosin_contig	33.33	24	5.8
Streptococcus_agalactiae_FcaR	Acanthamoeba_T.brucei_Lmsp1_contig	44.44	9	2.6
Streptococcus_agalactiae_FcaR	Acanthamoeba_T.brucei_Lmsp1_contig	22.5	80	2.6
Streptococcus_agalactiae_FcaR	Acanthamoeba_T.brucei_Lmsp1_contig	26.92	26	4.5
Streptococcus_agalactiae_FcaR	Acanthamoeba_T.brucei_Lmsp1_contig	42.11	19	5.9
Streptococcus_agalactiae_FcaR	Acanthamoeba_T.cruzi_Lmsp1_contig	44.44	9	2.5
Streptococcus_agalactiae_FcaR	Acanthamoeba_T.cruzi_Lmsp1_contig	22.86	70	3.3
Streptococcus_agalactiae_FcaR	Acanthamoeba_T.cruzi_Lmsp1_contig	26.92	26	4.3
Streptococcus_agalactiae_FcaR	Acanthamoeba_T.cruzi_Lmsp1_contig	42.11	19	5.6
Streptococcus_agalactiae_FcaR	Acanthamoeba_Toxoplasma_beta_contig	42.86	28	0.012
Streptococcus_agalactiae_FcaR	Acanthamoeba_Toxoplasma_beta_contig	40.54	37	0.047
Streptococcus_agalactiae_FcaR	Acanthamoeba_Toxoplasma_beta_contig	39.13	23	0.4
Streptococcus_agalactiae_FcaR	Acanthamoeba_Toxoplasma_beta_contig	24.53	53	0.52
Streptococcus_agalactiae_FcaR	Acanthamoeba_Toxoplasma_beta_contig	32.26	31	0.68
Streptococcus_agalactiae_FcaR	Acanthamoeba_Toxoplasma_beta_contig	53.85	13	0.68
Streptococcus_agalactiae_FcaR	Acanthamoeba_Toxoplasma_beta_contig	29.63	27	1.2
Streptococcus_agalactiae_FcaR	Acanthamoeba_Toxoplasma_beta_contig	25.93	27	2
Streptococcus_agalactiae_FcaR	Acanthamoeba_Toxoplasma_beta_contig	26.92	26	2

Query I.D.	Subject I.D.	% Ident.	alignment length	e-value
Streptococcus_agalactiae_FcaR	Acanthamoeba_Toxoplasma_beta_contig	20	45	2
Streptococcus_agalactiae_FcaR	Acanthamoeba_Toxoplasma_beta_contig	46.15	13	2
Streptococcus_agalactiae_FcaR	Acanthamoeba_Toxoplasma_beta_contig	32	25	2.6
Streptococcus_agalactiae_FcaR	Acanthamoeba_Toxoplasma_beta_contig	20	65	3.4
Streptococcus_agalactiae_FcaR	Acanthamoeba_Toxoplasma_beta_contig	29.63	27	4.4
Streptococcus_agalactiae_FcaR	Acanthamoeba_Toxoplasma_beta_contig	42.11	19	4.4
Streptococcus_agalactiae_FcaR	Acanthamoeba_Toxoplasma_beta_contig	25	24	9.8
Streptococcus_agalactiae_FcaR	Leishmania_major_Lmsp1	27.27	33	2.7
Streptococcus_agalactiae_FcaR	Plasmodium_falciparum_PfEMP1	27.16	81	0.047
Streptococcus_agalactiae_FcaR	Plasmodium_falciparum_PfEMP1	37.5	16	0.3
Streptococcus_agalactiae_FcaR	Plasmodium_falciparum_PfEMP1	25.93	27	5.7
Streptococcus_agalactiae_FcaR	Schistosoma_mansoni_paramyosin	22.19	311	8.00E-10
Streptococcus_agalactiae_FcaR	Schistosoma_mansoni_paramyosin	19.81	631	2.00E-08
Streptococcus_agalactiae_FcaR	Schistosoma_mansoni_paramyosin	17.75	355	2.00E-07
Streptococcus_agalactiae_FcaR	Schistosoma_mansoni_paramyosin	19.13	345	1.00E-06
Streptococcus_agalactiae_FcaR	Schistosoma_mansoni_paramyosin	19.5	241	4.00E-06
Streptococcus_agalactiae_FcaR	Schistosoma_mansoni_paramyosin	19.57	138	0.01
Streptococcus_agalactiae_FcaR	Schistosoma_mansoni_paramyosin	25	48	0.14
Streptococcus_agalactiae_FcaR	Schistosoma_mansoni_paramyosin	22.58	31	7.8
Streptococcus_agalactiae_FcaR	Staphylococcus_aureus_ProteinA	17.68	198	8.00E-04
Streptococcus_agalactiae_FcaR	Staphylococcus_aureus_ProteinA	17.71	192	0.1
Streptococcus_agalactiae_FcaR	Staphylococcus_aureus_ProteinA	30.77	52	0.39
Streptococcus_agalactiae_FcaR	Staphylococcus_aureus_ProteinA	23.08	65	0.67
Streptococcus_agalactiae_FcaR	Staphylococcus_aureus_ProteinA	28.85	52	0.88
Streptococcus_agalactiae_FcaR	Staphylococcus_aureus_ProteinA	28.85	52	1.1
Streptococcus_agalactiae_FcaR	Staphylococcus_aureus_ProteinA	25.58	43	3.3
Streptococcus_agalactiae_FcaR	Staphylococcus_aureus_ProteinA	24.53	53	3.3
Streptococcus_agalactiae_FcaR	Streptococcus_pyogenes_FcgR	19.14	324	9.00E-07
Streptococcus_agalactiae_FcaR	Streptococcus_pyogenes_FcgR	21.68	309	7.00E-06
Streptococcus_agalactiae_FcaR	Streptococcus_pyogenes_FcgR	18.36	207	7.00E-06
Streptococcus_agalactiae_FcaR	Streptococcus_pyogenes_FcgR	20.19	322	1.00E-04
Streptococcus_agalactiae_FcaR	Streptococcus_pyogenes_FcgR	23.58	229	0.038
Streptococcus_agalactiae_FcaR	Streptococcus_pyogenes_FcgR	23.08	26	7.8
Streptococcus_agalactiae_FcaR	Taenia_solium_paramyosin	20.72	613	2.00E-08
Streptococcus_agalactiae_FcaR	Taenia_solium_paramyosin	16.22	333	6.00E-06
Streptococcus_agalactiae_FcaR	Taenia_solium_paramyosin	17.56	450	7.00E-06
Streptococcus_agalactiae_FcaR	Taenia_solium_paramyosin	18.91	497	1.00E-04
Streptococcus_agalactiae_FcaR	Taenia_solium_paramyosin	16.38	574	9.00E-04
Streptococcus_agalactiae_FcaR	Taenia_solium_paramyosin	28.57	63	0.006
Streptococcus_agalactiae_FcaR	Taenia_solium_paramyosin	25	76	0.19
Streptococcus_agalactiae_FcaR	Toxoplasma_gondii_Beta	36.07	122	5.00E-28
Streptococcus_agalactiae_FcaR	Toxoplasma_gondii_Beta	35.25	122	5.00E-28
Streptococcus_agalactiae_FcaR	Toxoplasma_gondii_Beta	36.13	119	9.00E-28
Streptococcus_agalactiae_FcaR	Toxoplasma_gondii_Beta	33.61	122	2.00E-27
Streptococcus_agalactiae_FcaR	Toxoplasma_gondii_Beta	31.41	156	2.00E-27

Query I.D.	Subject I.D.	% Ident.	alignment length	e-value
Streptococcus_agalactiae_FcaR	Toxoplasma_gondii_Beta	36.13	119	3.00E-27
Streptococcus_agalactiae_FcaR	Toxoplasma_gondii_Beta	33.61	122	3.00E-27
Streptococcus_agalactiae_FcaR	Toxoplasma_gondii_Beta	33.61	122	3.00E-27
Streptococcus_agalactiae_FcaR	Toxoplasma_gondii_Beta	30.14	146	2.00E-26
Streptococcus_agalactiae_FcaR	Toxoplasma_gondii_Beta	28.76	153	2.00E-25
Streptococcus_agalactiae_FcaR	Toxoplasma_gondii_Beta	31.5	127	3.00E-25
Streptococcus_agalactiae_FcaR	Toxoplasma_gondii_Beta	24.39	246	3.00E-20
Streptococcus_agalactiae_FcaR	Toxoplasma_gondii_Beta	22.5	80	0.003
Streptococcus_agalactiae_FcaR	Toxoplasma_gondii_Beta	28.57	35	0.19
Streptococcus_agalactiae_FcaR	Toxoplasma_gondii_Beta	24.32	37	1.2
Streptococcus_agalactiae_FcaR	Toxoplasma_gondii_Beta	19.3	57	1.6
Streptococcus_agalactiae_FcaR	Toxoplasma_gondii_Beta	26.47	34	1.6
Streptococcus_agalactiae_FcaR	Toxoplasma_gondii_Beta	22.22	36	3.6
Streptococcus_agalactiae_FcaR	Trypanosoma_brucei_Lmsp1	34.62	26	0.25
Streptococcus_agalactiae_FcaR	Trypanosoma_brucei_Lmsp1	28.95	38	3.6
Streptococcus_agalactiae_FcaR	Trypanosoma_cruzi_Lmsp1	26.83	41	2.2
Streptococcus_pyogenes_FcgR	Acanthamoeba_Schistosoma_paramyosin_contig	41.67	12	3.6
Streptococcus_pyogenes_FcgR	Acanthamoeba_Schistosoma_paramyosin_contig	29.73	37	4.7
Streptococcus_pyogenes_FcgR	Schistosoma_mansoni_paramyosin	25.43	173	4.00E-11
Streptococcus_pyogenes_FcgR	Schistosoma_mansoni_paramyosin	26.09	184	2.00E-10
Streptococcus_pyogenes_FcgR	Schistosoma_mansoni_paramyosin	26.84	231	5.00E-10
Streptococcus_pyogenes_FcgR	Schistosoma_mansoni_paramyosin	25.62	203	3.00E-09
Streptococcus_pyogenes_FcgR	Schistosoma_mansoni_paramyosin	26.92	182	5.00E-08
Streptococcus_pyogenes_FcgR	Schistosoma_mansoni_paramyosin	22.09	172	2.00E-06
Streptococcus_pyogenes_FcgR	Schistosoma_mansoni_paramyosin	24.83	149	3.00E-06
Streptococcus_pyogenes_FcgR	Schistosoma_mansoni_paramyosin	21.89	169	6.00E-04
Streptococcus_pyogenes_FcgR	Schistosoma_mansoni_paramyosin	21.23	146	0.005
Streptococcus_pyogenes_FcgR	Staphylococcus_aureus_ProteinA	23.5	183	0.003
Streptococcus_pyogenes_FcgR	Staphylococcus_aureus_ProteinA	22.86	140	0.066
Streptococcus_pyogenes_FcgR	Staphylococcus_aureus_ProteinA	31.25	32	1.2
Streptococcus_pyogenes_FcgR	Staphylococcus_aureus_ProteinA	40	15	2.8
Streptococcus_pyogenes_FcgR	Staphylococcus_aureus_ProteinA	62.5	8	3.6
Streptococcus_pyogenes_FcgR	Staphylococcus_aureus_ProteinA	62.5	8	3.6
Streptococcus_pyogenes_FcgR	Taenia_solium_paramyosin	25.15	167	1.00E-12
Streptococcus_pyogenes_FcgR	Taenia_solium_paramyosin	24.47	237	1.00E-10
Streptococcus_pyogenes_FcgR	Taenia_solium_paramyosin	23.14	242	3.00E-09
Streptococcus_pyogenes_FcgR	Taenia_solium_paramyosin	26.28	156	6.00E-09
Streptococcus_pyogenes_FcgR	Taenia_solium_paramyosin	25.15	167	2.00E-08
Streptococcus_pyogenes_FcgR	Taenia_solium_paramyosin	22.18	275	4.00E-08
Streptococcus_pyogenes_FcgR	Taenia_solium_paramyosin	25.71	175	1.00E-07
Streptococcus_pyogenes_FcgR	Taenia_solium_paramyosin	23.43	175	7.00E-07
Streptococcus_pyogenes_FcgR	Taenia_solium_paramyosin	25.58	172	3.00E-06
Streptococcus_pyogenes_FcgR	Taenia_solium_paramyosin	21.98	182	5.00E-06
Streptococcus_pyogenes_FcgR	Taenia_solium_paramyosin	21.13	194	0.052
Streptococcus_pyogenes_FcgR	Toxoplasma_gondii_Beta	50	8	2.3

Query I.D.	Subject I.D.	% Ident.	alignment length	e-value
Streptococcus_pyogenes_FcgR	Trypanosoma_brucei_Lmsp1	47.06	17	0.019
Streptococcus_pyogenes_FcgR	Trypanosoma_brucei_Lmsp1	83.33	6	2.4
Streptococcus_pyogenes_FcgR	Trypanosoma_brucei_Lmsp1	40	15	6.9
Streptococcus_pyogenes_FcgR	Trypanosoma_brucei_Lmsp1	40	15	9
Taenia_solium_paramyosin	Acanthamoeba_Schistosoma_paramyosin_contig	25.93	54	2.7
Taenia_solium_paramyosin	Acanthamoeba_Toxoplasma_beta_contig	28.57	35	0.55
Taenia_solium_paramyosin	Acanthamoeba_Toxoplasma_beta_contig	26.47	34	3.6
Taenia_solium_paramyosin	Acanthamoeba_Toxoplasma_beta_contig	25	16	6.1
Taenia_solium_paramyosin	Plasmodium_falciparum_PfEMP1	22.5	40	2.1
Taenia_solium_paramyosin	Plasmodium_falciparum_PfEMP1	50	12	3.5
Taenia_solium_paramyosin	Schistosoma_mansoni_paramyosin	72.19	791	0
Taenia_solium_paramyosin	Schistosoma_mansoni_paramyosin	22.04	608	3.00E-30
Taenia_solium_paramyosin	Schistosoma_mansoni_paramyosin	22.4	308	1.00E-13
Taenia_solium_paramyosin	Schistosoma_mansoni_paramyosin	20.69	174	2.00E-05
Taenia_solium_paramyosin	Staphylococcus_aureus_ProteinA	31.82	22	6
Toxoplasma_gondii_Beta	Acanthamoeba_Leishmania_Lmsp1_contig	32	25	1.5
Toxoplasma_gondii_Beta	Acanthamoeba_Leishmania_Lmsp1_contig	35.71	14	2
Toxoplasma_gondii_Beta	Acanthamoeba_Leishmania_Lmsp1_contig	28.57	14	3.3
Toxoplasma_gondii_Beta	Acanthamoeba_Leishmania_Lmsp1_contig	28.57	14	3.3
Toxoplasma_gondii_Beta	Acanthamoeba_Leishmania_Lmsp1_contig	28.57	14	3.3
Toxoplasma_gondii_Beta	Acanthamoeba_Schistosoma_paramyosin_contig	24	25	2.2
Toxoplasma_gondii_Beta	Acanthamoeba_T.brucei_Lmsp1_contig	32	25	1.5
Toxoplasma_gondii_Beta	Acanthamoeba_T.brucei_Lmsp1_contig	35.71	14	1.9
Toxoplasma_gondii_Beta	Acanthamoeba_T.brucei_Lmsp1_contig	28.57	14	3.3
Toxoplasma_gondii_Beta	Acanthamoeba_T.brucei_Lmsp1_contig	28.57	14	3.3
Toxoplasma_gondii_Beta	Acanthamoeba_T.brucei_Lmsp1_contig	28.57	14	3.3
Toxoplasma_gondii_Beta	Acanthamoeba_T.cruzi_Lmsp1_contig	32	25	1.4
Toxoplasma_gondii_Beta	Acanthamoeba_T.cruzi_Lmsp1_contig	35.71	14	1.8
Toxoplasma_gondii_Beta	Acanthamoeba_T.cruzi_Lmsp1_contig	28.57	14	3.1
Toxoplasma_gondii_Beta	Acanthamoeba_T.cruzi_Lmsp1_contig	28.57	14	3.1
Toxoplasma_gondii_Beta	Acanthamoeba_T.cruzi_Lmsp1_contig	28.57	14	3.1
Toxoplasma_gondii_Beta	Acanthamoeba_Toxoplasma_beta_contig	18.95	190	1.00E-06
Toxoplasma_gondii_Beta	Acanthamoeba_Toxoplasma_beta_contig	21.89	169	2.00E-06
Toxoplasma_gondii_Beta	Acanthamoeba_Toxoplasma_beta_contig	27.06	85	6.00E-06
Toxoplasma_gondii_Beta	Acanthamoeba_Toxoplasma_beta_contig	29.41	68	8.00E-06
Toxoplasma_gondii_Beta	Acanthamoeba_Toxoplasma_beta_contig	27.66	94	8.00E-06
Toxoplasma_gondii_Beta	Acanthamoeba_Toxoplasma_beta_contig	35	40	2.00E-04
Toxoplasma_gondii_Beta	Acanthamoeba_Toxoplasma_beta_contig	20	135	3.00E-04
Toxoplasma_gondii_Beta	Acanthamoeba_Toxoplasma_beta_contig	33.33	30	0.008
Toxoplasma_gondii_Beta	Acanthamoeba_Toxoplasma_beta_contig	29.63	27	0.024
Toxoplasma_gondii_Beta	Acanthamoeba_Toxoplasma_beta_contig	20.47	127	0.053
Toxoplasma_gondii_Beta	Staphylococcus_aureus_ProteinA	27.85	79	0.067
Toxoplasma_gondii_Beta	Staphylococcus_aureus_ProteinA	33.33	48	0.088
Toxoplasma_gondii_Beta	Staphylococcus_aureus_ProteinA	34.78	23	0.088
Toxoplasma_gondii_Beta	Staphylococcus_aureus_ProteinA	21.98	91	0.11

Query I.D.	Subject I.D.	% Ident.	alignment length	e-value
Toxoplasma_gondii_Beta	Staphylococcus_aureus_ProteinA	21.18	85	0.2
Toxoplasma_gondii_Beta	Staphylococcus_aureus_ProteinA	22.64	106	0.2
Toxoplasma_gondii_Beta	Staphylococcus_aureus_ProteinA	20.41	147	1.3
Trypanosoma_brucei_Lmsp1	Acanthamoeba_Leishmania_Lmsp1_contig	54.84	93	4.00E-28
Trypanosoma_brucei_Lmsp1	Acanthamoeba_T.brucei_Lmsp1_contig	54.84	93	4.00E-28
Trypanosoma_brucei_Lmsp1	Acanthamoeba_T.cruzi_Lmsp1_contig	55.06	89	3.00E-27
Trypanosoma_brucei_Lmsp1	Staphylococcus_aureus_ProteinA	29.41	17	8.6
Trypanosoma_brucei_Lmsp1	Toxoplasma_gondii_Beta	28	25	9.3
Trypanosoma_cruzi_Lmsp1	Acanthamoeba_Leishmania_Lmsp1_contig	52.81	89	6.00E-23
Trypanosoma_cruzi_Lmsp1	Acanthamoeba_T.brucei_Lmsp1_contig	52.81	89	5.00E-23
Trypanosoma_cruzi_Lmsp1	Acanthamoeba_T.cruzi_Lmsp1_contig	52.81	89	5.00E-23
Trypanosoma_cruzi_Lmsp1	Plasmodium_falciparum_PfEMP1	40	10	4.3
Trypanosoma_cruzi_Lmsp1	Staphylococcus_aureus_ProteinA	27.27	22	1
Trypanosoma_cruzi_Lmsp1	Trypanosoma_brucei_Lmsp1	88.98	127	1.00E-52

Appendix 5

Human IgG Heavy chain (BAA37168.1)

QVQLQESGGGLVQPGGSLRLSCAASGFTVSGNYMTWVRQAPGKGLE
WVSVVYSGGSTFYADSVKGRFTISRDISKNTLYLQMNSLRPEDTALYY
CATSYERWGQGTLVTVSSASTKGPSVFPLAPSSKSTSGGTAALGCLVK
DYFPEPVTVSWNSGALTSGVHTFPAVLQSSGLYSLSSVVTVPSSSLGTQ
TYICNVNHKPSNTKVDKTVERK

Human IgG Light chain (CAA42227.1)

MASFPLLLTLLTHCAGSWAQSVLTQPPSASGTPGQRVTISCSGSNSNIG
GNTVNWYQQLPGTAPKLLIYSNNQRPSGVPDRFSGSKSGTSASLAISGL
QSEDEAAYYCAAWDDSLNGHVLFGGGTKLTVLGQPKAAPSVTLFPPS
SEEL

Predicted cleavage residues present in human IgG heavy and light chain for chymotrypsin-like (green) and elastase-like (red) serine proteases. Immunoglobulin peptide sequence was retrieved from NCBI GenBank and manually analysed using a standard text editor.

Appendix 6

An *A. castellanii* transcriptomic sequence showed significant alignment with *L. major* Lmsp1, a gene from the nucleoside diphosphate kinase protein superfamily. A conserved domain search of this matching sequence revealed conservation with NDPk group 1.